BuMines OFR 138-83
PB83-238758

COLLEGE OF EARTH AND MINERAL SCIENCES

REMOVAL OF PYRITE FROM COAL BY HEAP LEACHING

by

L. M. Cathles and K. J. Breen

Pennsylvania Mining and Mineral Resources Research Institute
The Pennsylvania State University
University Park, PA 16802

FINAL REPORT

on

Research Grants G5105007, G5115007, and G1115427

Submitted to: Bureau of Mines, U.S. Department of the Interior,
Division of Technical Services and Research

June 1983

Bureau of Mines Open File Report 138-83

The Pennsylvania State University

University Park, Pennsylvania

THE PENNSYLVANIA STATE UNIVERSITY

College of Earth and Mineral Sciences

UNDERGRADUATE PROGRAMS OF STUDY

Ceramic Science and Engineering, Earth Sciences, Fuel Science, Geography, Geosciences, Metallurgy, Meteorology, Mineral Economics, Mining Engineering, Petroleum and Natural Gas Engineering, and Polymer Science.

GRADUATE PROGRAMS AND FIELDS OF RESEARCH

Ceramic Science, Fuel Science, Geochemistry and Mineralogy, Geography, Geology, Geophysics, Metallurgy, Meteorology, Mineral Economics, Mineral Processing, Mining Engineering, Petroleum and Natural Gas Engineering, and Polymer Science.

UNIVERSITY-WIDE INTERDISCIPLINARY GRADUATE PROGRAMS INVOLVING E&MS FACULTY AND STUDENTS

Earth Sciences, Ecology, Environmental Pollution Control Engineering, Mineral Engineering Management, Operations Research, Regional Planning, and Solid State Science.

ASSOCIATE DEGREE PROGRAMS

Metallurgical Engineering Technology and Mining Technology.

INTERDISCIPLINARY RESEARCH GROUPS WITHIN THE COLLEGE

Coal Research Section, Mineral Conservation Section, Ore Deposits Research Section, and Mining and Mineral Resources Research Institute.

ANALYTICAL AND STRUCTURE STUDIES

Classical chemical analysis of metals and silicate and carbonate rocks; X-ray crystallography; electron microscopy and diffraction; electron microprobe analysis; atomic absorption analysis; spectrochemical analysis.

U.Ed. 9-725

REPORT DOCUMENTATION PAGE	1. REPORT NO. BuMines OFR 138-83	2.	3. Recipient's Accession No. PB83 238758
4. Title and Subtitle: Removal of Pyrite From Coal by Heap Leaching			5. Report Date: June 1983
7. Author(s): L. M. Cathles and K. J. Breen			8. Performing Organization Rept. No.
9. Performing Organization Name and Address: Pennsylvania Mining and Mineral Resources Research Institute, The Pennsylvania State University, University Park, PA 16802			10. Project/Task/Work Unit No.
			11. Contract(C) or Grant(G) No. (C) G5105007 (G) G5115007 G1115427
12. Sponsoring Organization Name and Address: Office of Surface Mining, Bureau of Mines, U.S. Department of the Interior, Washington, DC 20241			13. Type of Report & Period Covered: University grant, 9/30/79 - 12/31/82
			14.

15. Supplementary Notes

Approved for release July 6, 1983.

16. Abstract (Limit: 200 words)

The feasibility of leaching pyrite from coal heaps is analyzed by adapting a model of the heap-leaching process developed in the copper industry. Parameters in the model are first determined through literature review and direct measurement. The model is then used to predict how coal fragments will leach in reaction kettles containing ferric sulfate solution, in columns through which air is circulated, and in actual heaps. Model parameters are verified and refined by kettle and column experiments. The model is then used to determine the optimum heap size and operating procedures. Eight-foot heaps of 1/4-inch coal fragments leach best. The average rate of application of flush solutions should be less than 0.01 gal/ft^2 hr. It should be possible to leach more than 90% of the finely disseminated pyrite from the coal in 9 months, provided the flush solutions are recirculated. Removal of pyrite from coal utilizing such a process is economically attractive. A heap-leaching operation capable of depyritizing 1 million tons of coal per year has a positive net present value at discount rates up to 16% (base case) to 33% (best case).

17. Document Analysis a. Descriptors

Mining

Heap leach modeling
Coal desulfurization
Pyrite oxidation
Coal oxidation
Column leaching
Acid mine drainage
Desulfurization economics

b. Identifiers/Open-Ended Terms

c. COSATI Field/Group: 08I

18. Availability Statement	19. Security Class (This Report)	21. No. of Pages
Release unlimited by NTIS.	Unclassified	287
	20. Security Class (This Page) Unclassified	22. Price

DISCLAIMER

The views and conclusions contained in this document are those of the authors and should not be interpreted as necessarily representing the official policies or recommendations of the Interior Department's Bureau of Mines or the U.S. Government.

REMOVAL OF PYRITE FROM COAL BY HEAP LEACHING

by

L. M. Cathles, Adjunct Professor
K. J. Breen, Graduate Student
Department of Geosciences
Mineral Conservation Section
The Pennsylvania State University
University Park, PA 16802

June 1983

Final Report on a three-year project funded by the U.S. Department of the Interior, Bureau of Mines, Division of Technical Services and Research under Grants G5105007, G5115007, and G1115427.

ACKNOWLEDGMENTS

The authors would like to thank the faculty, staff, and students of The Pennsylvania State University who have contributed to this research.

Funding for initiation and final wrap-up of this project was provided by the Mineral Conservation Section at Penn State. The effort, support, and interest of Dr. A. W. Rose, Director of the Mineral Conservation Section, is gratefully acknowledged.

The Coal Research Section provided technical support throughout the course of this research. Dr. William Spackman and Dr. Alan Davis were particularly generous, both with their time and with the Coal Research Section's laboratory and sample bank facilities. Dr. K. W. Kuehn and D. F. Bensley performed the rapid-scan pyrite analyses. R. Carson, R. Copenhaver, D. Eckley, and R. Williams offered expertise in and assistance with coal sample preparation for the experimental and petrographic studies. Ruth and Don Krebs provided expert illustrative and photographic print work, respectively.

Special thanks are extended to the staff of the Mineral Constitution Lab, particularly N. H. Suhr, H. Gong, J. Bodkin, and J. DeVine, for providing analytical support and for numerous instructive discussions on coal analysis and aqueous solution analyses.

We are also extremely grateful to L. E. Eary, B. Goss, A. J. Macleod, and J. Specht, all Geosciences students who made contributions to the experimental and computer modeling aspects of this research.

The Geosciences Department provided support for report preparation, including the services of Rob Texter, who is responsible for the majority of the illustrations that appear in this report.

Useful discussions were held concerning potential application of the heap leaching technology with Dr. P.T. Luckie and with George Dragonir and the staff at Rochester and Pittsburgh Coal Co., Indiana, Pa., and Mr. Alan Walker and his staff at the Bradford Coal Co., Bigler, Pa. Dr. John A. Campbell, the Peabody Coal Co., and Kerr-McGee Coal Corp. supplied the coal samples used in this study. Advice, background information, and encouragement from John throughout the project were especially valuable and are gratefully acknowledged.

Margaret Biggers, Janice Bellis, and Colleen Wingard are acknowledged for their diligence in typing this report.

Last but not least, the support for most of the research was provided by the Office of Surface Mining of the U.S. Department of the Interior through Penn State's Mineral Research Institute, headed by Dr. Z. T. Bieniawski. All officials of the Office of Surface Mining were extremely cooperative and helpful in accomodating the shifts that occurred in the course of this research and, particularly, in facilitating the purchase of the equipment used in the finally successful execution of the kettle experiments. We would like to thank the Office of Surface Mining and Dick Bieniawski for providing the priviledge of carrying out this research.

TABLE OF CONTENTS

APPENDICES

LIST OF FIGURES

LIST OF TABLES

LIST OF PHOTOGRAPHIC PLATES

I. INTRODUCTION

EPA New Source Performance Standards presently require removal of at least 70% of the sulfur from all coal burned by plants where construction was initiated after September 18, 1978. As old plants are replaced, sulfur will need to be increasingly removed from even low sulfur coal. The law is unlikely to change. The recent recognition of the destructive impact of "acid" rain on forests and fish thousands of miles from industrial centers or power plants underscores the need to control SO_2 emissions. SO_2 is converted to acid (H_2SO_4) in the upper atmosphere. Canadians are becoming increasingly concerned over the acidification of their northern lakes by acid rain.

At the same time, world energy shortages and cartel actions mandate that the U.S. strive for the maximum environmentally acceptable energy self-sufficiency. This produces strong pressures to utilize our coal resources. We thus face the following dilemma: we need to burn increasing quantities of coal, but it is very important that SO_2 emissions to the atmosphere by this burning be kept to a minimum.

SO_2 emissions can be reduced by removing pyrite from coal by mechanical beneficiation or by scrubbing SO_2 from the flue gas. Flue gas scrubbing is expensive, and mechanical beneficiation will work only on pyrite blebs a few hundred microns in size. The overall objective of our work is to determine through literature review, laboratory experiments and modeling if the fine-grained pyrite present in many coals can be economically removed by heap leaching technology. The fine-grained pyrite cannot be removed by mechanical cleaning techniques, although vat leaching techniques have been developed that operate at $\sim$ 100°C.

The potential economic incentive for an inexpensive depyritization technology is high. Kennecott workers have published an estimate that at least 35 billion tons of coal contain low enough organic sulfur levels that they could meet EPA standards of 1.2 lbs SO_2/million B.t.u. if depyritized (Sareen et al., 1977). Most of this coal is in the Appalachian region; this economically depressed area would be most benefited by the development of an efficient and economic depyritization process. If we assume low sulfur coal is worth $10/ton more than high sulfur coal, a viable depyritization process would increase the value of our nation's coal resources by $350 billion

dollars, minus the cost of depyritization. The potential economic benefit is thus large. The social benefit of breathing SO_2 and SO_4^{2-} free air is equally significant but more difficult to quantify.

The heap leaching we address in this report is an alternative to the "Meyers" (TRW Inc.) process of depyritizing coal by vat treatment with ferric sulfate at 90-130°C. It is also an alternate to the Kennecott "LOL" process where pyrite is leached with oxygen at 100-130°C and 300 psi pressure. Both Kennecott and TRW have amassed substantial literature (Hamersma et al., 1974, 1976, 1977; Meyers, 1977; Meyers et al., 1972; Sareen et al., 1977; Van Nice et al., 1977; Tyler, 1975) to show that depyritization of coal can have substantial beneficial impact on environmental problems attendant to coal combustion and can, in many cases, produce coal in compliance with new strict environmental standards (1.2 lb $SO_2/10^6$ BTU). The main requirement is that most of the sulfur in the coal be present as pyrite, not as organic sulfur. TRW and Kennecott have shown that this is the case in enough instances that a process for removing pyrite can be of great significance. TRW has also shown that crushing and washing alone is not effective; some leaching is necessary (see Meyers, in Tyler, 1975). The heap leaching process would utilize natural air convection and leaching processes and be substantially less expensive (in terms of dollars and energy) than the TRW or Kennecott processes which involve substantial equipment, heating of the coal to 90-130°C, and in the case of the TRW process, heating of a portion of the process stream to 430°C.

Recently, a model of the heap leaching of copper from low-grade industrial waste dumps has been developed that includes the basic physical and chemical processes of heap leaching, such as air convection, heat balance, temperature-dependent mixed oxidation kinetics, and bacterial catalysis (Cathles and Apps, 1975; Cathles, 1979; Cathles and Schlitt, 1980). The copper heap leaching model has been shown to successfully predict the leaching of test dumps (Cathles and Apps, 1975). The model has been successfully tested against leaching characteristics of a very large scale column (40' high, 10' diameter, containing 170 tons of waste) designed and operated for that purpose (Cathles, 1979; Cathles et al., 1977; Murr et al., 1977; Cathles and Murr, 1980).

In this study, the successfully tested copper heap leaching model is modified to describe the heap leaching of pyrite from coal. The basic

parameters required by the model are first deduced from existing literature or determined experimentally. The validity of the resulting model is then tested by carrying out two different kinds of laboratory experiments: (1) the leaching of pyrite from coal fragments immersed in ferric sulfate solution in reaction kettles, and (2) the leaching of pyrite from coal fragments in constant temperature columns subject to the counter-current upflow of air and periodic downflow of flush solution. The doubly calibrated heap leaching model is then used to predict how coal heaps of realistic size will leach under actual field conditions. These predictions form the basis for an economic evaluation of the heap leaching coal depyritization process.

In the following pages, we show it is possible to develop a model of the coal depyritization process that describes the leaching of fragments in a laboratory reaction kettle, as well as the leaching of coal in a leach column. By using the model, we can predict how much larger heaps of coal should leach, and determine the optimum heap size and operating procedures. The multi-tiered process of first predicting leaching from basic principles and fundamental parameters, then testing the model against the results of kettle experiments, and finally, testing it against the results of column experiments, gives confidence in the model. Sensitivity analysis of model parameters allows optimum dump design and operating procedures to be identified. It would take many, many years to determine them through the trial and error process of heap construction and operation. The economic analysis indicates that if optimally designed and operated heaps leach as predicted, heap leaching is an economically attractive method of depyritizing coal.

The study reported here may appear straightforward. In fact, the complex coal leaching process resisted quantification at nearly every turn, and new approaches had to be developed in several instances. These approaches should have utility outside the particular hydrometallurgical problem reported here. In what follows, we will first present the model of coal depyritization by heap leaching, then determine the basic physical and chemical parameters from the literature or by direct measurement, and then test the predictions of the resulting model by comparing the prediction against the results of kettle and column experiments. Finally, we use the tested model to predict the leaching of coal heaps under realistic field conditions and assess how economically attractive such heaps might be. Experimental and technical details will be reported in detail in appendices. The text will be restricted to the essentials of the model, its testing, and its implications.

II. A PHYSICAL AND CHEMICAL MODEL OF THE DEPYRITIZATION OF COAL BY HEAP LEACHING

A. General Overview

Figure 1 gives an overview of the heap leaching process. Coal is piled in a heap and water applied intermittently to the pile with a sprinkler system. The applied solutions migrate down through the heap and flush out iron salts produced in the intervening period by oxidation of pyrite in the coal. The leach or flush solutions are collected, treated to remove or regenerate the iron added, and eventually returned to the heap in the next flush.

Within the heap, another important process operates: air convects up through the heap and supplies the oxygen required to oxidize and leach the pyrite in the coal. Pyrite can be solubilized and removed from the coal only after it has been oxidized. Oxidation at useful industrial rates requires air convection. Recognition of the importance of air convection in copper sulfide waste dumps was the key to understanding that process (Cathles and Apps, 1975).

Figure 2 shows the pyrite leaching process in more detail. We know from our experience in copper sulfide waste dumps that the following processes or steps are involved in the leaching process: (1) Oxygen dissolves in capillary water, coating the coal fragments. (2) Ubiquitous bacteria (Thiobacillus ferrooxidans) catalyze the oxidation of Fe^{2+} to Fe^{3+}, utilizing this dissolved oxygen. (3) The Fe^{3+} diffuses into the coal fragment and reacts with pyrite (FeS_2) to produce solid elemental sulfur (S^o), dissolved sulfate (SO_4^{2-}), and ferrous iron (Fe^{2+}). The precise stoichiometry of the leaching reaction in the coal matrix is one of the things we must determine in this study.

If the rate of oxidation of pyrite by Fe^{3+} is rapid with respect to the rate at which Fe^{3+} can diffuse into the coal through water-filled pores, there will be a fairly sharp transition between the part of the coal fragment that is leaching and the part that remains unleached. With time, this zone of active leaching will migrate into the coal fragment, leaving behind a "leached rim" through which the Fe^{3+} oxidant must migrate. This leached rim is shown in Figure 2 by the absence of pyrite blebs. Hydrometallurgists refer to the model where a growing leached rim surrounds a diminishing core of unleached material as a "shrinking core model." A major breakthrough in

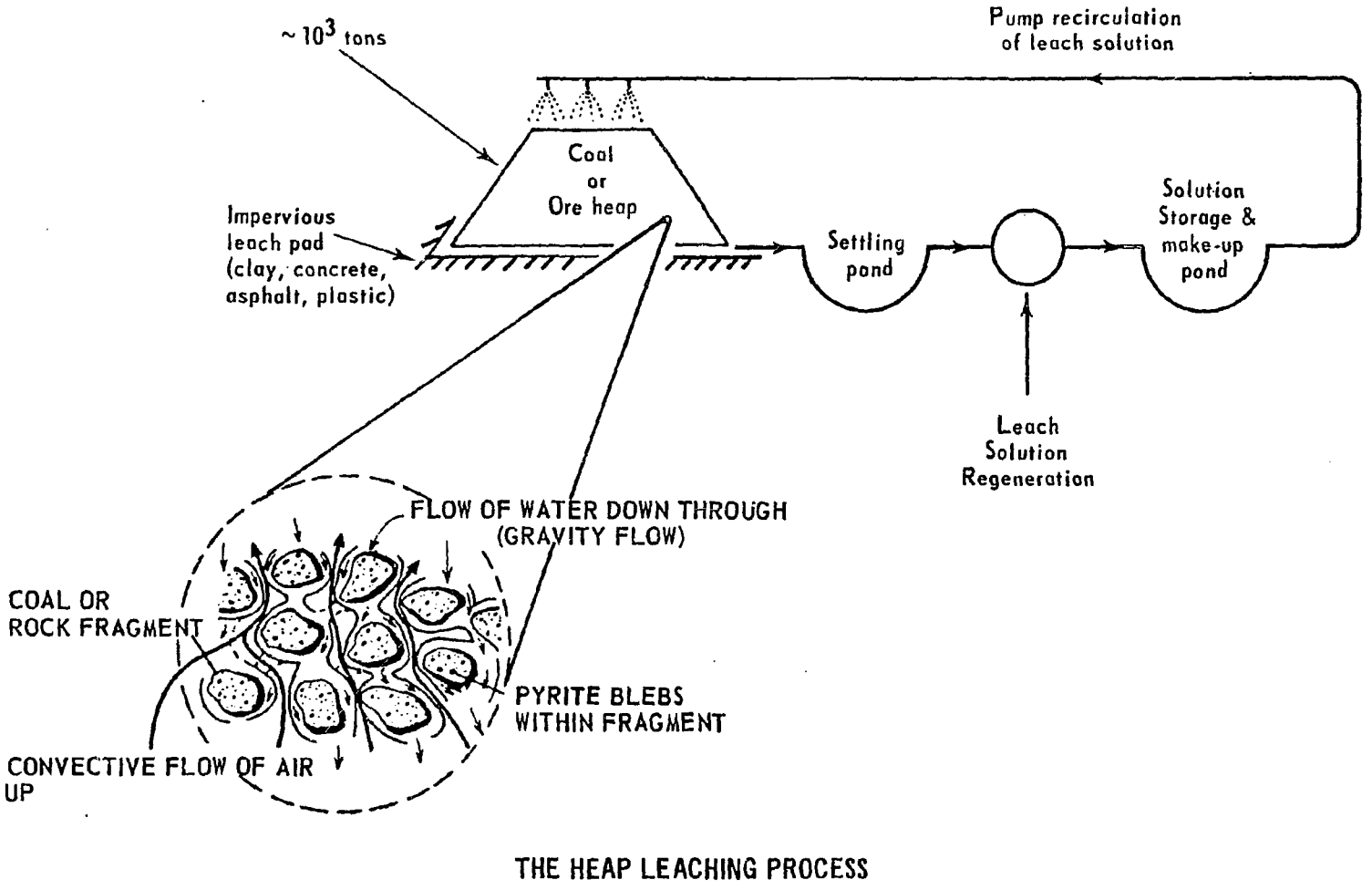

Figure 1 Schematic flow chart of depyritization of coal by heap leaching

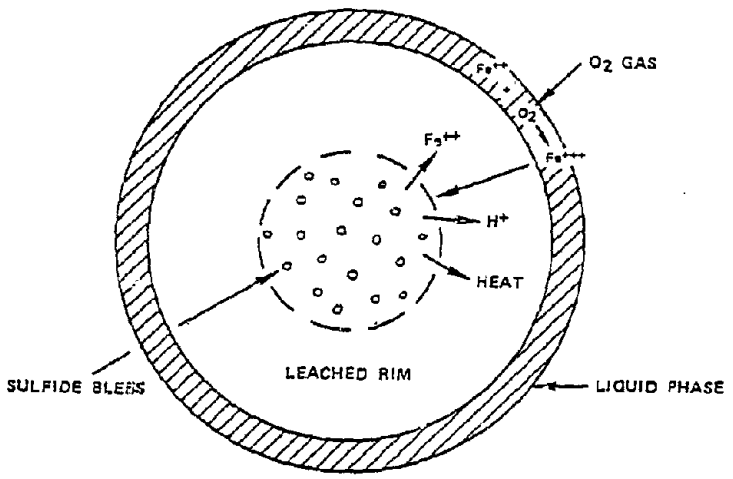

Figure 2 Details of the leaching of finely disseminated pyrite from a coal fragment

characterizing the kinetics of copper sulfide leaching was the demonstration of the applicability of the shrinking core model and the prediction, and then discovery of leached rims around rock fragments in the dumps. This study shows the shrinking core model is also valid for the description of the leaching of coal fragments in a heap. Leached rims are found on coal fragments in our experiments just as they are found on rock fragments in copper sulfide leach experiments and in copper industry leach dumps. Actually, we formulate our shrinking core model in such a fashion that the leach rate is controlled by both the chemical rate of oxidation of the pyrite and the diffusion of oxidant to the pyrite through the coal. Such a model is called a "mixed kinetic shrinking core model." The relative magnitudes of the kinetic terms in this model indicate whether a leached rim is expected to form. Thus, the observation of leached rims on coal particles indicates the relative rates of pyrite oxidation and oxidant diffusion.

The permeability of the coal heap will depend on the size of the coal fragments in the heap. We use the Blake-Kozeny equation as a crude measure of this relationship. Air convects up through the heap driven by the following buoyant forces: (1) the removal of oxygen, a heavy air component, by pyrite and coal oxidation, (2) the addition of water vapor, a light component of air, by the water-saturated coal fragments in the heap, and (3) by the heating of the air by the exothermic pyrite and coal oxidation reactions. The heating of the heap can be modeled by quantifying the rate of pyrite oxidation and the convective (water and air) and conductive losses of heat from the heap.

The elements of our model for the heap leaching of coal are thus (1) a mixed kinetic shrinking core model (including bacterial catalysis) that describes the rate of extraction of pyrite from the coal fragments that are contacted by oxygenated air, (2) a heat balance model that gives the temperature of the heap as it leaches, and (3) a momentum balance model that describes how air convects through the heap to supply oxygen for the leaching process. With the exception of coal oxidation, these are precisely the same elements that have been successfully used to characterize the leaching of copper from waste dumps, and the reader is referred to publications describing those models for details of the brief discussion given below (Cathles and Apps, 1975; Cathles, 1979; Cathles and Schlitt, 1980).

B. The Mathematical Model

As discussed in Cathles and Schlitt (1980), the mixed kinetic shrinking core model describes the rate of leaching in terms of the rate of change of the fraction of pyrite remaining unoxidized within the coal fragment, X_{py}:

$$\frac{\partial X_{py}}{\partial t} = \frac{-3X_{py}^{2/3}B(T)H([O_2])}{6\tau_D X_{py}^{1/3}(1-X_{py}^{1/3}) + \tau_C} \tag{1}$$

$H([O_2])$ is the heavy-side step function and has the value of 1.0 for oxygen concentrations in air, $[O_2]$, greater than zero, and is zero if the oxygen concentration is zero. $B(T)$ accounts for the bacterial catalysis of sulfide leaching. Thiobacillus ferrooxidans become sick above temperatures of 55°C or so, T_{sick}, and cease to function at some higher temperature T_{kill}. $B(T)$ is defined as follows:

$$\begin{aligned} B(T) &= 1.0 && T < T_{sick} \\ B(T) &= \frac{T_{kill}-T}{T_{kill}-T_{sick}} && T_{sick} < T < T_{kill} \\ B(T) &= 0.0 && T_{kill} < T \ . \end{aligned} \tag{2}$$

For discussion of the necessity and appropriateness of this function, see Cathles (1979), Cathles and Murr (1980), and Cathles and Schlitt (1980).

τ_D is the time required to leach the coal fragment completely if diffusion were the sole rate-limiting process; τ_C is the same if the chemical rate of oxidation of the pyrite were the sole limiting process. As discussed by Cathles and Apps (1975), both can be derived from more fundamental parameters:

$$\tau_C = \frac{Ka}{k_{ox}a_{sulf}^{R}\delta[ox]} \tag{3}$$

$$\tau_D = \frac{a^2K}{6[ox]D_E} \tag{4}$$

where

$$\delta = \sqrt{D_E / k_{ox} a^R_{sulf}} \quad . \tag{5}$$

In the above equations, K is the oxidant required to leach pyrite from a unit volume of coal, a is the radius of the coal fragment (assumed spherical), k_{ox} is the first order rate constant for the oxidation of pyrite by the oxidant (Fe^{3+}), a^R_{sulf} is the surface area of disseminated pyrite per unit volume of coal, and D_E is the effective diffusion constant for oxidant (Fe^{3+}) through the coal matrix.

The skin depth, δ, is the distance into an unleached coal fragment that the oxidant concentration falls to 0.368, its initial value. The skin depth, δ, thus provides a direct measure of the thickness of the zone of active leaching within the coal fragment. From (3), (4), and (5), it can be seen that τ_C and τ_D provide a measure of the thickness of the active leaching zone relative to the coal fragment:

$$\frac{\delta}{a} = \frac{\tau_C}{6\tau_D} \tag{6}$$

Both τ_C and τ_D are given temperature dependencies:

$$\tau = \tau_o \exp(E^*/293.R - E^*/R(273+T)) \tag{7}$$

E^* is the activation energy in calories per mole, and R is the gas constant. τ_o is the leach time at 20°C. Because equation (3) contains δ, the proper activation energy for τ_C is half the sum of the activation energy for diffusion and chemical reaction $1/2(E^*_C + E^*_D)$.

The rate of oxidation of coal is described by a different kind of equation, the general form of which we have determined from a literature study described in Appendix A. In this case, X_c is the mass fraction of coal oxidized (rather than pyrite unoxidized), and:

$$\frac{\partial X_c}{\partial t} = k_c (\overline{RSP})^{5/4} X_c^{-1/4} \; H([O_2]) \tag{8}$$

$H([O_2])$ has the same meaning as in (1). k_c is a constant characterizing the oxidation rate of a particular coal. X_c starts at a value X_{co} so (8) remains finite.

The dimensionless terms in (8) have the form:

$$\bar{R} = \exp\left(\frac{E^*}{R}\left(\frac{1}{298} - \frac{1}{273 + T}\right)\right)$$

$$\bar{S} = \frac{1.09}{2a}\left(1 - e^{-4.34a}\right) \qquad (9)$$

$$\bar{P} = [O_2]/[O_2]_{STP}$$

Note that the reference temperature in this case is 25°C rather than 20°C.

Equation (1) and (8) describe the kinetics of pyrite and coal oxidation, respectively. Heat and oxygen mass balance relations may be written if the rate of consumption of oxygen, R_{O_2}, and the rate of production of heat, R_A, within the dump are known. Both are simply related to the oxidation rates of pyrite and coal:

$$R_{O_2} = \rho_{coal}\,(1-\phi)\left(-Q_{py}\,G_{py}\,\frac{\partial X_{py}}{\partial t} + Q_c\,\frac{\partial X_c}{\partial t}\right) \qquad (10)$$

$$R_A = \rho_{coal}\,(1-\phi)\left(-A_{py}\,G_{py}\,\frac{\partial X_{py}}{\partial t} + A_c\,\frac{\partial X_c}{\partial t}\right) \qquad (11)$$

R_{O_2} is the rate of consumption of oxygen per unit volume of heap, and R_A is the rate of production of heat per unit volume. ρ_{coal} is the density of coal, ϕ the inter-coal-fragment porosity of the heap, Q_{py}, the grams of O_2 consumed per gram of pyrite oxidized, Q_c the same for coal, A_{py} the calories produced per gram of pyrite oxidized, A_c the same for coal, and G_{py} is the weight fraction pyrite in the coal.

Oxygen concentration can be determined by following a parcel of air along a streamline from where the air first enters the coal heap:

$$[O_2] = [O_2]_{Ambient} - \int_{streamline} \frac{ds}{v} R_{O_2} \qquad (12)$$

v is the Darcy velocity of the air (see Cathles and Schlitt, 1980).

Once $[O_2]$ is known within the heap by solving (12), the energy balance equation may be solved, and the temperature of the oxidizing coal heap a time Δt later determined. The pertinent one-dimensional energy equation (eg. Cathles and Apps, 1975) is:

$$\rho_T C_T \frac{\partial T}{\partial t} = -(\rho_w C_w v_w + \rho_a C_a v_a)\frac{\partial T}{\partial z} + R_A + K_T \frac{\partial^2 T}{\partial z^2} \qquad (13)$$

Here ρ_T, C_T, and K_T are the density, heat capacity, and thermal conductivity of the heap as a whole, ρ_w, C_w, and v_w the density, heat capacity, and Darcy velocity of water applied to the heap, and ρ_a, C_a, and v_a the same for air traveling through the dump.

If air convects through the heap (i.e. it is not forced through with a blower) the one-dimensional air flow through the heap may be described:

$$v_a = \frac{k_{ave}}{\mu_a} \frac{\Delta P}{H} \tag{14}$$

H is the height of the heap, μ_a is the viscosity of air (= 1.9×10^{-4} poise), and k_{ave} the average permeability of a vertical section through the heap. ΔP is the pressure drop across the heap:

$$\Delta P = \int_o^H \Delta \rho_a g dz \tag{15}$$

$\Delta \rho_a$ is the difference in density of air inside and outside the heap. If we assume the air inside the heap is saturated with water vapor, we can derive expressions for the heat capacity of the air and its density to complete (13) and (14) above (Cathles and Schlitt, 1980):

$$C_a = .24 + \frac{514620}{\rho_a T} \exp\left(-5220.9/(T + 273)\right) \quad ,$$

$$\frac{\rho_a}{\rho_{ao}} = 1 - 3.66 \times 10^{-3} (T-20) + 2.83 \times 10^{-2} (1 - [O_2]) + 4.7093 \times 10^5 \exp(-5220.9/(T + 273)). \tag{16}$$

Finally the permeability of the coal heap can be related, at least approximately to the size of the coal fragments in the heap and the inter-fragment porosity of the heap, ϕ, by the Blake-Kozeny Equation (Bird et al. 1960, p199):

$$k_{ave} = \frac{(2a)^2 \phi^3}{150 (1-\phi)^2} \tag{17}$$

The equations above represent a complete model of the heap leaching process that can be solved so as to predict the leach history of any heap by finite difference techniques (Cathles and Apps, 1975; Cathles, 1979) once the values of the various parameters in the model are known.

C. Direct Determination of Basic Model Parameters

Parameters in the model of the previous section fall naturally into three categories: First there are parameters that depend on the way in which the coal is prepared or the coal heap operated. These parameters include the average size of coal fragments in the heap, the inter-fragment porosity of the heap, and the rate at which water is applied. Second are parameters that depend on the type of coal being leached. Different coals will have different amounts of disseminated pyrite with a different size distribution and consequently the pyrite surface area per unit volume will vary in various coals. Ionic diffusion will be easier in some coals than in others; indeed the effective diffusion constant of the coal is expected to be the single most important factor in determining the rate at which disseminated pyrite can be leached. Some coals may decrepitate as they leach. Substantial pyrite removal may be possible in the preparation steps for coals that contain coarse fracture filling (cleat) pyrite as well as coarse-grained disseminated pyrite. Finally, there is a group of parameters that should be relatively constant from one coal to another such as density, thermal conductivity, heat capacity, the kinetic constants describing oxidation of pyrite and coal, the activation energies of these kinetic constants, the heat released per gram of coal or pyrite oxidized, and the oxygen required to oxidize a gram of pyrite or coal. In this section we review the literature to determine the last set of parameters and describe measurements or experiments we have carried out to determine the second set. The first set we treat as variables in the heap leaching model since they are subject to direct operator or design control.

1. Literature Determination of Constants Describing General Coal Properties

The parameters that are not expected to vary greatly between coals can usefully be extracted from the literature. This is done in Table 1. The entries in the table are for the most part self explanatory, but some discussion of the stoichiometry of the leach reaction and values of k_{ox} is useful.

The oxidation of pyrite by Fe^{3+} can be written in a general form that allows the products of the reaction to be variable proportions of HSO_4^- and S^o:

$$FeS_2 + (2 + 12X)Fe(III) + (8X)H_2O \rightarrow (3 + 12X)Fe(II) + (14X)H^+ + (2X)HSO_4^- + 2(1-X)S^o \quad . \tag{18}$$

If X in this equation is 1.0, pyrite oxidizes entirely to HSO_4^- ; if X = 0.0, pyrite oxidizes entirely to S^o. The reaction is written in terms of HSO_4^- because at low pH this species is expected to be more abundant than SO_4^- (Barnes et al., 1966, show the pK(25°C) of HSO_4^- is 1.97). The notation Fe(III) and Fe(II) indicate the total concentration of ferric and ferrous iron in solution. The various complexes of iron are ignored.

Hamersma et al. (1973) have indicated an X value of 0.6 is appropriate for the Meyers process of coal depyritization. A literature review of other studies (see Table 1 of Appendix D) indicates that this value is fairly generality appropriate, although different studies show quite a spread of X values. We adopt X = 0.6 with the caution that this will need to be verified.

Much of the stoichiometric data in Table 1 comes from equation (18). For example, 4 moles of Fe(III) are equivalent to one mole of O_2, and the atomic weight of pyrite is 119 grams and O_2 32 grams. With this in mind, the value of Q_{py} can be read from equation (18). The heat released by pyrite oxidation, A_{py}, is calculated from the enthalpy of reaction (18) as discussed in Cathles and Apps (1975).

There has been considerable debate in the literature over whether rate expressions for the oxidation of pyrite should be written in terms of free Fe^{3+} or the total ferric iron in solution, Fe(III). Sasmojo (1969) has shown that complexes of ferric iron are less reactive than free Fe^{3+}, but Amell and Langmuir (1978) argue that surface charge means complexed ferric species will have more intimate access to the leaching surface. Most workers

Parameter	Description	Value	Units	Basis or Reference
Q_c	grams O_2 consumed per gram; coal oxidized	2.67	-	$C + O_2 \rightarrow CO_2$; atomic weight of C is 12, O_2 is 32, $32 \div 12 = 2.67$
k_{ox}	First order rate constant describing pyrite oxidation	10^{-6} to 10^{-7}	cm/sec	The oxidation dependence of pyrite is probably zero not first order in total ferric iron concentration under realistic heap condition. Nonetheless a pseudo-first order rate constant can be defined as shown in Figure 3.
E^*_C	Activation energy for pyrite oxidation	20,000	cal/mole	Mathews and Robins (1972)
D'	Diffusion constant of Fe(III) in 1N H_2SO_4	$5.2 \pm 0.3 \times 10^{-6}$	cm^2/sec	Tobias and Nobe (1975)
E^*_D	Activation energy for diffusion of oxidant through the coal matrix	5,000	cal/mole	Lasaga (1981, p. 34)
k_c	Constant characterizing the rate of oxidation of coal	3.5×10^{-11}	sec^{-1}	Appendix A
X_{co}	Starting value of fraction coal oxidized	1.12×10^{-4}	$\frac{\text{g coal oxidized}}{\text{g coal}}$	required to keep equation (8) finite
E^*	Activation energy for coal oxidation	12,000	cal/mole	Sondreal and Ellman (1974) Schmidt and Elder (1940)

Table 1. Values of constants describing properties of coal that should be reasonably similar for different coals.

Parameter	Definition	Value	Unit	Basis or Reference
ρ_{coal}	Density of coal	1.6 ± 0.15	g/cc	Ten measurements of density of dry Illinois #6 coal performed for this study
$\rho_{coal}\ C_{coal}$	Heat capacity per unit volume of coal	0.41 to 0.44	$\frac{cal}{cm^3 - °C}$	Divide thermal conductivity by thermal diffusivity Badzioch et al. (1964)
$\rho_T C_T$	Heat capacity per unit volume of heap	0.34	$cal/cm^3-°C$	Assumes 20% bulk heap porosity and 0.42 $cal/cm^3-°C$ for ρ_{coal} C_{coal}
K_T	Bulk thermal conductivity of heap	5.2×10^{-4}	cal/cm -sec-°C	Thermal conductivity of coal is about $6.0 \pm .5 \times 10^{-4}$ cal/cm-sec-°C (Badzioch et al., 1964). Air has a thermal conductivity of 2.4×10^{-4}. Assuming $\phi = 0.2$, K has value indicated.
A_{py}	Calories released when 1 gram pyrite is oxidized	2900 Q_{py}	$\frac{cal}{g}$	Consideration of enthalpy of leach reaction
Q_{py}	grams O_2 consumed in oxidizing 1 gram pyrite	0.133(1 + 6x)	-	Stoichiometry of pyrite leaching (see text)
X	Stoichiometric variable; if X=1 the product of pyrite oxidation is entirely HSO_4^-, if = 0 entirely S^o	~0.6		
A_c	Calories released per gram; coal oxidized	6440	$\frac{cal}{g}$	Assumes 11,500 Btu/lb for coal

Table 1 (continued)

have used Fe(III) as the basis for kinetic expressions (this is the case for all curves shown in Figure 3). The diffusion rate of Fe(III) into coal fragments to the sites of pyrite oxidation will certainly be controlled by the total ferric iron concentration. Thus formulation of the oxidation kinetic model in terms of Fe(III) will be consistent with the diffusion transport model. For this reason and also because kinetic studies available in the literature are couched in terms of Fe(III), we will use rate expressions involving Fe(III). Figure 3 shows the appropriate range of k_{ox}, under heap leaching conditions is 10^{-6} to 10^{-7}. The units of k_{ox} are cm/sec; the rate of destruction of Fe(III) at the pyrite surface is given by k_{ox} times the total ferric iron concentration, Fe(III).

Figure 3 shows the rate of pyrite oxidation is approximately zero order in Fe(III). k_{ox} decreases as Fe(III) increases so that the rate of leaching depends only very weakly on Fe(III). This means that it is not critical that we know the ferric iron concentration in the pore solutions of the heap or columns. The rate constant can be determined in experiments where the iron concentration is known and then used for the columns and heaps. Because of the approximate zero order dependence of the leaching, the rate of pyrite oxidation will be correct even if the concentration of Fe(III) in the columns and heaps is quite different.

2. Measurement of Parameters Specific to the Coals used in this Study

Early in the study, four barrels of Illinois Basin (#6 seam) and a barrel of Wyoming coal were obtained from the Peabody Coal Company and Kerr McGee, respectively. Analysis for the forms of sulfur was made on representative samples, and the results appear in Table 2. Generally, Illinois #6 coal contains about 2% pyritic sulfur, and the Wyoming coal about 0.13%.

The Illinois coal contains both coarse fracture-filling cleat pyrite, and disseminated pyrite. As shown in Table 3, the disseminated pyrite retained in the coal matrix after a float-sink preparation is fine-grained, roughly two-thirds being less than 10 μm in diamater. The Wyoming coal pyrite is also fine-grained and disseminated throughout the coal. The fact that pyrite in the Illinois and the Wyoming coal exists in the very small size range indicates it will be easy to leach but very hard to remove from the coal by conventional washing methods.

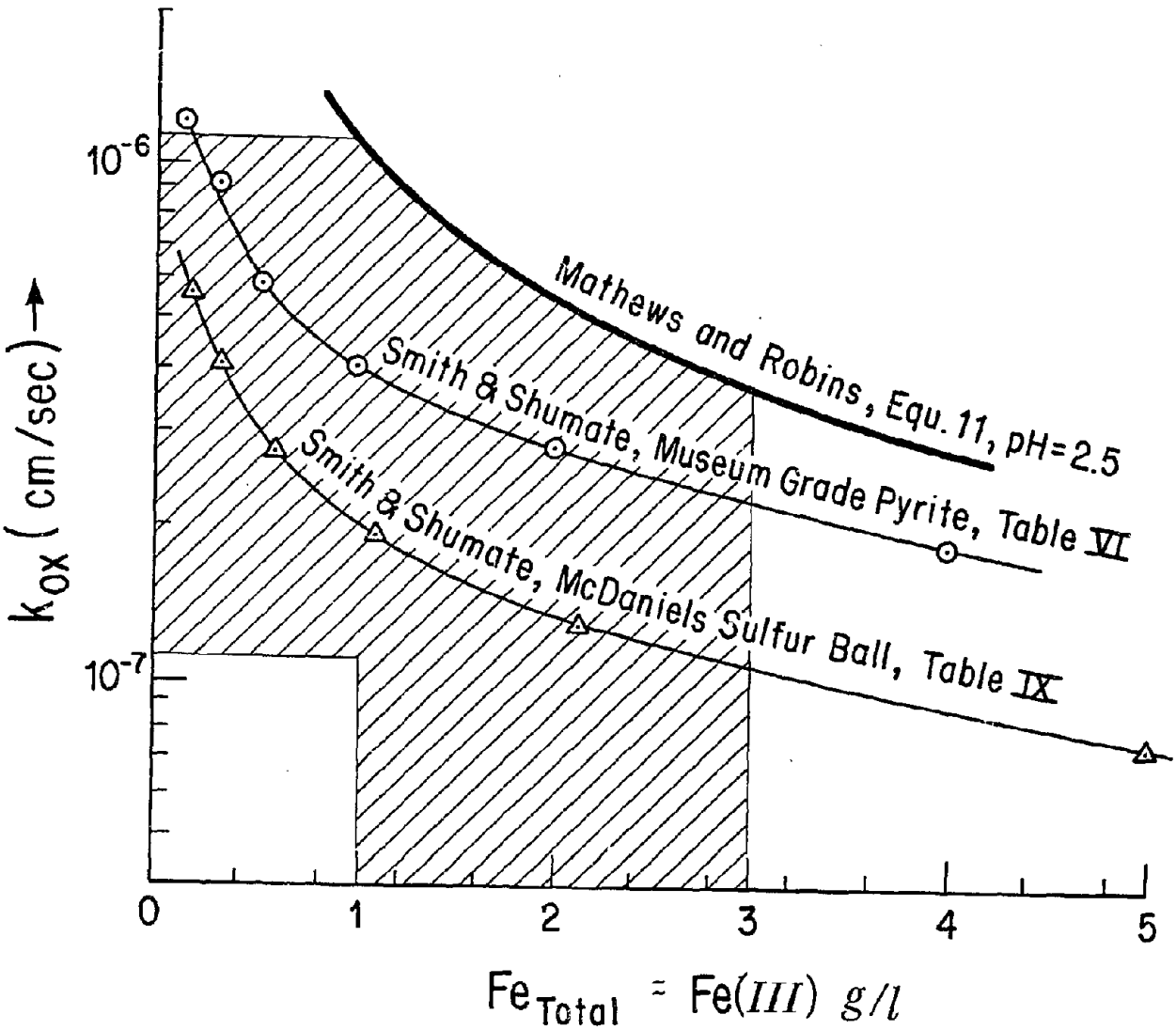

Figure 3. Kinetic data for the oxidation of pyrite by Fe^{3+} is to our knowledge available from only two sources: Smith and Shumate (1970), and Mathews and Robins (1972). In Smith and Shumate's work, we calculate (using methods described in Addendum 2 to Appendix D) that 80% of the total iron in solution is present in the ferric state. We assume this was also true for Mathews and Robins work, but cannot verify this because they do not report Eh. The curves show a close to zero order dependence of pyrite oxidation on Fe(III) concentration. A first order rate constant, k_{ox}, which when multiplied by total ferric iron concentration would give the rate of consumption of ferric iron per unit pyrite surface area, is plotted on the ordinate scale. The figure shows the "first" order rate constant appropriate for describing the rate of pyrite oxidation under expected heap leaching condition shaded area is between 10^{-6} and 10^{-7} cm/sec.

	Sulfate S%	Pyrite S%	Organic S%	Total S%
Illinois, Seam #6				
River King Pit 3	.17	2.39	2.16	4.72
River King Pit 6	.23	2.38	1.98	4.59
Baldwin Mine	.15	1.81	1.70	3.66
Marissa Mine	.12	1.81	2.04	3.97
Wyoming				
Jacobs Ranch Mine	0.02	0.13	0.48	0.63

Table 2. Forms-of-sulfur analyses of the as-received, run-of-mine coals used in this study

	Percent disseminated pyrite with radius:		
	<5μm	<10μm	<20μm
Illinois #6			
Baldwin Mine	71%	81%	
	74%	87%	
Marissa Mine	60%	67%	
	50%	73%	
River King Pit 3	66%	75%	
	62%	79%	
River King Pit 6	48%	69%	
	48%	72%	
Wyoming			
Jacobs Ranch Mine			91%
			77%

Table 3. Size distribution of pyrite disseminated in coals used in this study. Size distribution was measured using an automated microscopic method developed at Penn State and described by Kuehn (1979).

The as-received coal was prepared for analysis and experiments as described in the flow charts of Figure 4a-c. The coal was hand picked to remove clay and massive pyrite chunks, then crushed, passed through a 2.8 specific gravity, Certigrave, organic liquid float-sink separation to remove the cleat and chunk pyrite, and then washed and split into several size fractions. The effect of the float-sink separation on pyrite content can be seen in Table 4. It shows the pyrite content of the Illinois #6 River King Mine Pit #3 coal was reduced from 2.39% to about 1.2%. This provides a measure of the sulfur removal that might be achieved by mechanical coal cleaning processes. More information on the characteristics of the Illinois #6 River King Pit #3 coal, used in all our experiments (except one column test that used Wyoming coal), is given in Table 5

The parameters for which we seek values in this section are listed in Table 6. The surface area of disseminated pyrite per unit volume of coal was directly measured by an automated Rapid Scan Microscopic technique developed at The Pennsylvania State University and described by Kuehn (1979). The technique rapidly collects data on the total length of pyrite encountered in the scan and the number of pyrite blebs encountered. This data allows the surface area of pyrite per cm^3 of coal to be computed as well as the mean diameter of sulfide blebs in the coal. The values of a^R_{sulf} for various coal size fractions are given in Table 4.

As commented in the caption of Table 4, the weight percent pyrite calculated assuming a pyrite density of 5 g/cc is about half the weight percent pyrite indicated by the forms of sulfur analysis. The discrepancy is caused by the tail on the bleb size distribution curve. For example Appendix B shows that for the +0.85mm - 2.00mm size fraction, 10 volume percent of the pyrite occurs in blebs greater than 36 μm in diameter even though the average bleb size is 7.4 μm.

The surface area of pyrite in the coal was also measured by gas adsorption techniques (Appendix B). This approach suggests $a^R_{sulf} = 235\ cm^{-1}$. Much of the disseminated pyrite in Illinois #6 coal is characteristically spongy in morphology. For this reason, and also because diffusion will smooth the irregular shapes of pyrite blebs to some extent from the point of view of leaching kinetics, the full gas adsorption measure of a^R_{sulf} is too large. A reasonable estimate of pyrite surface area per unit volume of coal is 30 to 100 cm^{-1} as shown in Table 6.

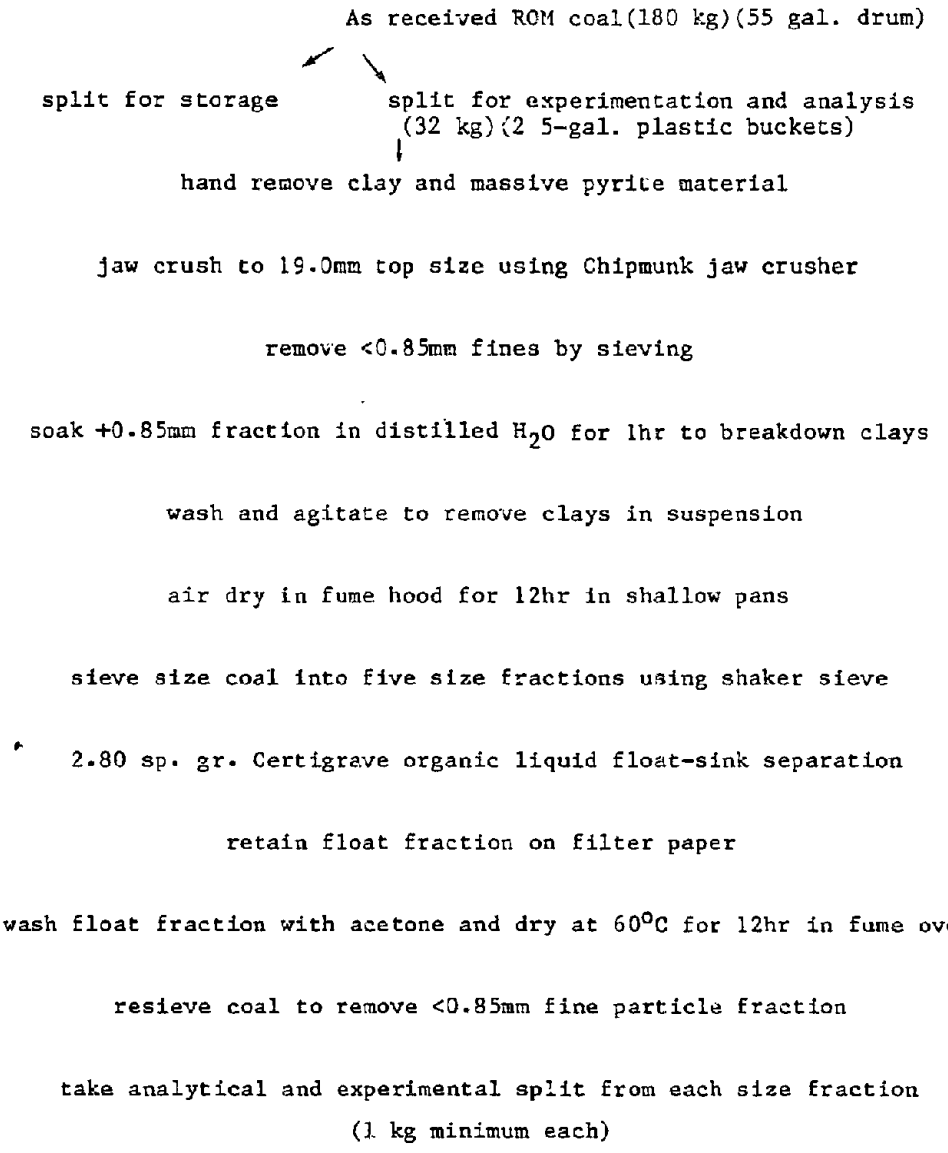

Figure 4a

Coal Sample Preparation Flow Chart

Experiment split (1 kg)

↓

removal of pyrite bearing fusinite macerals

hand remove macroscopic calcite, quartz, and clay particles

soak 15 min. in 1M HCl to remove carbonate fines

distilled H_2O rinse till effluent $AgNO_3$ check for Cl^- negative

air dry for 24hr

store under nitrogen in sealed plastic or glass containers

split out experimental fractions, (10g), and store under nitrogen until used for experimentation

prior to experimental run, vacuum impregnate coal for 45 min. in 1% H_2SO_4 solution to displace air from pore spaces

commence experimental run

Figure 4b

Experimental Size Fraction Split Preparation Scheme

Analytical Split (1 kg)

↓

removal of pyrite bearing fusinite macerals

grind to -0.85mm size using rotating plate grinder

● SPLIT #1 for petrographic pellet preparation (500 g)

↙ ↘

rapid-scan microscopy (50 g) microscopic analysis

● SPLIT #2 for chemical analyses* (200 g)

↓

grind to -100mesh (mortar&pestle)

Split #2A (10g) for High Temperature Ash (HTA)

Heat in muffle furnace overnight (750°C)

SPLIT #2B (5g) for forms of sulfur analysis

SPLIT #2C (10g) for Low Temperature Ash (LTA)

heat at 105°C for ~30 min.

ash at ~180°C until constant weight established

grind to -200 mesh (mortar&pestle)

quantitative x-ray diffraction analysis

*Standard analytical scheme used at The Pennsylvania State University Mineral Constitution Laboratory.

Figure 4c

Analytical Scheme for Size Fraction Splits

Illinois #6 River King Mine, Pit #3, High Volatile B Bituminous Coal

Calorific value: 14337 Mmmf Btu/lb

Sulfur content (weight % dry basis):

					Rapid Scan Microscopy Data						
	Pyrite S	Sulfate S	Organic S	Total S	Volume % py	mean py diameter	Calculated pyrite surface area cm^2/cm^3 coal	Number of scans	% moisture	% LTA	%HTA
Run of mine	2.39	0.17	2.16	4.72							
<2.80 g/cc float fraction											
2mm x .85mm	1.37 ± 0.03	0.26 ± 0.01	2.13	3.76 ± 0.05	0.51 ± 0.09	7.4 ± 0.3	41 ± 23%	3	3.10	--	--
3.15mm x 2mm	1.30	0.24	2.31	3.85	0.52 ± 0.05	8.1 ± 0.4	38 ± 14%	5	3.38	--	9.44
9.5mm x 3.15mm	1.15	0.21	2.19	3.55	0.38 ± 0.04	7.8 ± 0.3	29 ± 16%	3	3.77	13.1	11.10
12.5mm x 9.5mm	0.99	0.20	2.42	3.61	0.26 ± 0.02	6.9 ± 0.4	23 ± 14%	3	3.33	11.4	9.63
19mm x 12.5mm	1.01	0.18	2.64	3.83	0.34 ± 0.03	7.0 ± 0.4	29 ± 15%	4	2.15	10.8	9.11
Average ± Std Deviation	1.16 ± 0.17				0.40 ± 0.11		32 ± 7.5				

Table 4. Characteristics of Illinois #6 River King Pit #3 coal that has been subject to a 2.8 specific gravity float and sized. Note 1.19% pyrite is removed in the sink fraction. This provides a rough measure of the pyrite beneficiation possible with mechanical coal cleaning processes. The Rapid Scan Microscopy data are described in Appendix B. Each scan is 80 cm long and encounters 163 to 327 sulfide blebs. Taking $\rho_{py} = 5.0$ and $\rho_{coal} = 1.6$, the average 0.40 vol % py corresponds to 1.18 wt % pyrite, which is considerably less than the 2.16 wt % pyrite indicated by forms of sulfur analysis. This discrepancy reflects the small population of substantially larger pyrite blebs (cleat pyrite) within the coal (i.e., the tail of the size distribution; see Appendix B).

Table 5 Selected Chemical and Physical Characteristics of Illinois #6 Coal from River King Pit #3 That Was Used in Column Leach Studies (before leaching)

Column Experiment No.	Coal I.D. and (size fraction)	%* Moisture	% Ash (HTA)	Forms of Sulfur Analysis (%) Pyritic S	Sulfate S	Organic S	Total S	Percent Iron in Coal Calc. from % Fe_2O_3 in HTA	Percent Pyrite Calc. from % Iron in Coal	Percent Pyrite Calc. from % Pyritic S	Calorific Value Btu/lb Dry Basis	Mmmf Btu/lb**	dmmf Btu/lb***
1	Wyoming Subbit. (+20 mesh - 3/4 in.)	21.80	5.48	0.13	0.02	0.48	0.63	0.3	0.7	0.24	11955	9805	12674
2	Illinois #6 (+20 mesh - 3/4 in.)	2.93	13.85	0.85	0.40	2.42	3.67	1.7	3.6	1.6	12086	13213	14336
3	Illinois #6 (+20 mesh - 3/4 in.)	2.93	13.85	0.85	0.40	2.42	3.67	1.7	3.6	1.6	12086	13213	14336
4	Illinois #6 (+20 mesh - 1/4 in.)	3.74	11.53	0.79	0.37	2.43	3.59	1.4	3.0	1.5	12190	12830	14035

ASH ANALYSIS

Wt. Percent

	SiO_2	Al_2O_3	TiO_2	Fe_2O_3	MgO	CaO	MnO	Na_2O	K_2O	P_2O_5	SO_3	Totals
Illinois #6	52.8	21.1	0.93	17.3	1.16	1.97	0.025	0.81	2.15			98.25
Wyoming	26.6	14.3	1.20	8.05	4.49	25.1	0.029	0.42	0.20	0.50	19.5	100.49

ppm in Ash

	Ba	Be	Cr	Cu	Ni	Rb	Sr	V	Zn	Zr
Illinois #6	410		170	70	95		200	170	210	160
Wyoming	3150	7	5	160	90	10	2050	210	570	220

*All percents by weight on a dry basis (except moisture)

**Mmmf = [Btu/lb moist coal - 50 (g total S/100 g moist coal)] ÷ [100 -(1.08 (g ash/100 g moist coal) + 0.55 (g total S/100 g moist coal))] x 100

***dmmf = [Btu/lb dry coal -50(g total S/100 g dry coal)] ÷ [100-(1.08(g ash/100 g dry coal) + 0.55 (g total S/100 g dry coal))] x 100

Parameter	Definition	Value	Units	Comments
a^R_{sulf}	Pyrite surface area per unit volume of coal	30 to 100	cm^{-1}	For Illinois #6 coal; main uncertainty is spongy nature of pyrite. See Table 4 and Appendix B.
D_E	Effective diffusion constant for Fe(III) through the coal macerals	$7.5 \pm 8 \times 10^{-8}$	cm^2/sec	See discussion in text and Appendix C.
G_{py}	Grams of pyrite per gram of coal	$\sim .02$	--	See caption to Table 4.
K	Grams Fe^{3+} required to leach pyrite from 1 cm^3 coal	$0.47\ \rho_{coal} G_{py} (2+12X)$	$\frac{g\ Fe^{3+}}{cm^3\ coal\ leached}$	Equation 18; 0.47 is ratio of atomic weight of iron to that of pyrite.

Table 6. Values of constants describing properties of coal from Illinois #6 seam taken from River King Pit #3 of the Peabody Coal Company

For pyrite grade, G_{py}, we take the average weight percent pyritic sulfur and convert to weight percent pyrite as shown in the caption to Table 4. A disseminated pyrite grade of 2% is reasonable for Illinois #6 coal from the River King Pit #3. Similarly, K, the grams/Fe^{3+} required to leach pyrite from one cm^3 of coal can be easily calculated from equation (18), G_{py}, and ρ_{coal}, as shown in Table 6.

The effective diffusion constant of the coal matrix, D_E, can be estimated from the connected porosity of the coal, the diffusion constant for Fe^{3+} in water (given in Table 1), and the tortuosity of the coal pores, as indicated in equation (19) below. D_E can, with great difficulty, also be measured directly.

$$D_E = \frac{\phi_c D'}{T} \tag{19}$$

Eight water imbibition measurements of the connected porosity, ϕ_c, of Illinois #6 coal were made using techniques similar to those of Dabbous et al. (1974) as described in Appendix C. The connected porosity of the coal is 7.2 ± 0.7%. The tortuosity of the pores, T, is difficult to measure, but might be estimated by measuring the "formation factor" of the coal (Worthington, 1975; Katsube, 1981). We have found from past experience that a tortuosity of 5.0 is often appropriate (e.g. Cathles and Apps, 1975). Using these values and the iron diffusion constant in Table 1, equation (19) gives $D_E = 7.5 \times 10^{-8}$ cm^2/sec. The uncertainty in this estimate comes mainly from T and is at least 100%.

Considerable effort was invested in an attempt to measure D_E directly using a Garrels-type diffusion cell (see Garrels et al., 1949). Wafers of coal 1.5 to 4.5 mm thick were prepared and placed between two reservoirs: one containing KCl solution and the other distilled water. The problem was that the wafers showed an extreme tendency to crack. The cracks were not always visually apparent. Out of 50 measurements made on Illinois #6 coal wafers, we are confident the data from only three reflect the effective diffusional porosity of the coal. These three measurements give $D_E = 9.8 \times 10^{-7}$, 7.5×10^{-8}, and 5.6×10^{-8}. The measurements agree well with the estimation of D_E from imbibition techniques cited above. Considerably more success was obtained in measuring D_E of the Wyoming coal. The reader is

referred to Appendix C for a complete description of the techniques applied and the results.

3. Predicted Reaction Skin Depth, δ, and Leach Times, τ_C and τ_D

The parameter values in Tables 1 and 6 can be used in equations (3), (4), (5), and (7) to calculate the time required to leach pyrite from coal fragments of different sizes at various temperatures, and to estimate the reaction skin depth, δ. The results appear in Table 7. Figure 5 shows the predictions of the shrinking core model in general terms. If, at a particular temperature the total leach time, $\tau_C + \tau_D$, is known, Figure 5 allows determination of the fraction pyrite oxidized and leached at intermediate times. This figure is particularly useful in interpreting leach experiments, as we shall see in later sections.

Two important predictions can be drawn from Figure 5 and Table 7: First, especially at higher temperatures the rate of leaching should be diffusion controlled and leach rims should be observed on partially leached coal fragments. This is indicated by calculated values of δ of a millimeter or less (Table 7). Secondly, Figure 5 and Table 7 show it should be possible to leach a substantial fraction of the disseminated pyrite from coal fragments in less than a year if the heap temperatures are greater than 40°C and the coal fragments are <1/2 inch in dimension (a = 0.64 cm).

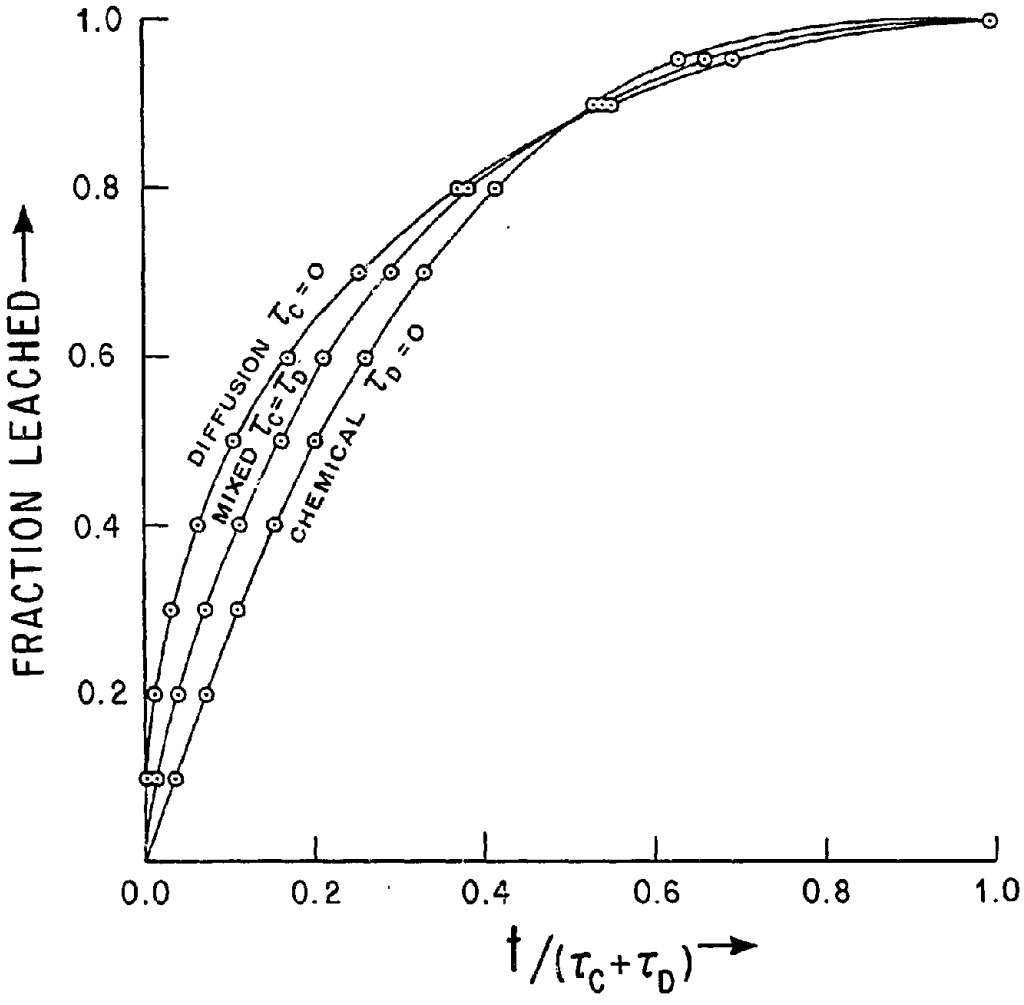

Figure 5. The integrated form of equation (1) assuming $B(T) = H([O_2]) = 1.0$ is useful in evaluating experimental leach results in terms of τ_C and τ_D. When $t = \tau_C + \tau_D$, pyrite is entirely leached from the coal. Appropriate values of $\tau_C + \tau_D$ can be read from Table 7 for various size coal fragments and temperatures.

	a^R_{sulf} = 30 cm^{-1}		a^R_{sulf} = 100 cm^{-1}	
	20°C	40°C	20°C	40°C
δ(μm)	1580	308	866	169
τ_c(mo)	109 a	28 a	33 a	8.4 a
τ_D(mo)	116 a^2	67 a^2	116 a^2	67 a^2
$\tau_c + \tau_D$ for a = 0.64		45.4 mo		32.8 mo

Table 7. Reaction skin depth and leach times at 20°C and 40°C calculated from the parameters in Tables 1 and 6, and equations (3), (4), and (5). k_{ox} is taken to be 10^{-7} cm/sec, a value at the low end of its range (see Table 1). The stoichiometric X factor is taken as 0.6. The oxidant concentration [ox] is taken equal to 10^{-3} g Fe(III)/cm^3. The leach times are given in terms of a, the radius of the coal fragments in the heap.

D. Model Verification and Parameter Calibration by Kettle Leaching Experiments

The predictions of the previous section were first verified by leaching carefully selected and sized samples of coal in kettles in which the ferric iron concentration of the leach solutions was accurately controlled and atmospheric oxygen excluded. A great deal of effort was devoted to perfecting the kettle leaching technique. What seemed at first a simple approach turned out to be complicated by the complex chemistry of the coal. At first, we thought the leaching of pyrite could be monitored by additions of SO_4^{2-} to ferric chloride leach solutions. Acid soluble sulfate phases in the coal, such as gypsum, anhydrite, jarosite, and melanterite (Davis, 1982; Bladh, 1982), contributed enough SO_4^{2-} that inference of pyrite leaching through increases in solution sulfate concentration was impossible, even ignoring the stoichiometric complication that some of the pyrite sulfur is likely to remain in the coal as S^o. Finally, an Eh-pH-stat technique was developed in which both the Eh and pH of the leaching solutions are maintained at fixed values by automatic titration of base and H_2O_2 into a ferric sulfate solution. The pyrite oxidation is monitored by keeping track of the amount of H_2O_2 added. The technique was shown to work very well. The H_2O_2 reacts quickly with the leach solution to increment the ferric iron level; H_2O_2 does not react with the coal. The technique and its justification are described in detail in Appendix D. We consider development of this technique and demonstration of its validity to be one of the more important contributions of this study.

Illinois #6 coal was treated, handpicked, and sized into five fractions that contained only finely disseminated pyrite. Carbonates (which could affect pH and require acid titration) were removed by soaking the coal in 1 M HCL for 15 minutes. Ten-gram charges of the coal were then washed and prepared for introduction to the leach kettle.

Typically, the products of pyrite oxidation were allowed to build up in the leach solution of the kettle for 20 to 40 hours; after this, the solution in the kettle was replaced. The rate of consumption of Fe(III) was determined from the rate of addition of H_2O_2 required to keep the Eh of the solution constant. As discussed in appendix D, one mole of H_2O_2 oxidizes two moles of ferrous to ferric iron.

The average rate of ferric iron consumption can be determined for each batch, and the drop in rate for successive batches plotted versus time, as shown in Figure 6. The trend of the points in Figure 6 is characteristic of all the coal samples leached. Leaching begins with a rapid reaction rate and rapidly declines to a more slowly changing but steadily decreasing rate. We assign the term "fast" to the portion of Figure 6 where the rate of reaction is rapidly changing. The more gradual sloping portion of Figure 6 is referred to as the "slow" or "tail" segment of a sample's leaching history. Fast leaching is characteristic of fresh samples having no prior leaching history.

1. The Temperature Dependence of Leaching

The temperature dependence of leaching was determined both at the start of leaching in the "fast" part (Figure 6) of fresh (unreacted) sample splits and as a function of time as leaching took place. The results are shown in Figures 7 and 8. Figure 7 shows an activation energy of 20.8 ± 2.5 kcal/mole adequately describes the temperature dependence of the first stages of leaching. In the early stages of leaching, the leach rate is controlled by the chemical kinetics of the oxidation reaction of pyrite, and the activation energy is appropriate for the temperature dependence of k_{ox}, which we have characterized in Table 1 by E_C^*. The activation energy in Figure 7 confirms the 20 kcal/mole activation energy determined from the literature and listed in Table 1.

Figure 8 shows the overall activation energy decreases as leaching takes place. The leach rate declines as leaching takes place as shown by the solid line through the 40°C points. More rapid leaching results if the temperature is increased; less rapid if the temperature is decreased. Arrows on the figure show the activation energy indicated by the observed changes in rate. The drop in activation energy with leaching (time) suggests, and is consistent with, the development of a leached rim around the coal fragments. Aqueous diffusion has an activation energy of 5 kcal/mole; the activation energy of the mixed diffusion and chemical oxidation should be between 20 and 5 kcal/mole and decrease as the leaching progresses and the kinetics are more dominated by diffusion, as observed.

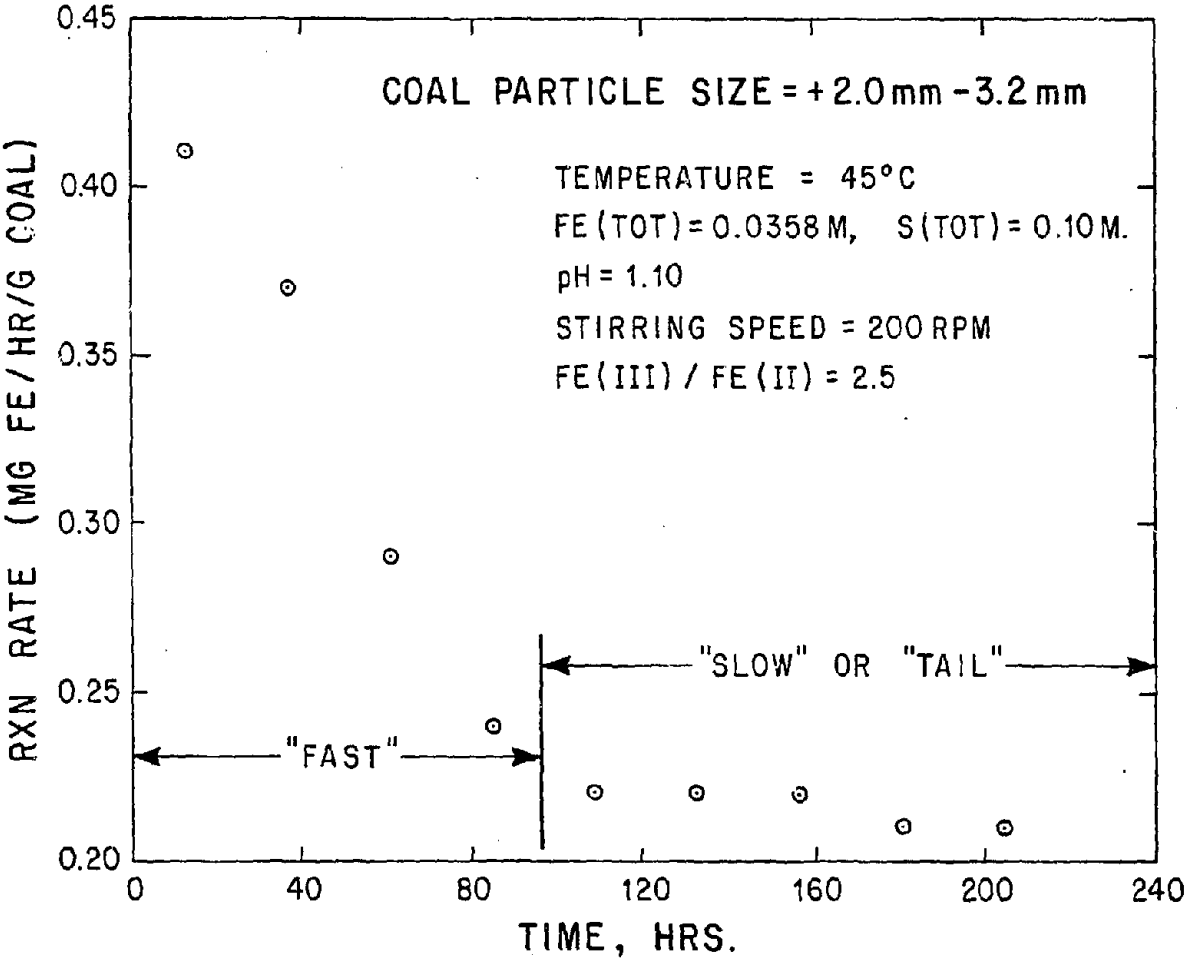

Figure 6 . Reaction rate plotted as a function of total leach time. Experimental points are plotted at the middle of the time block (typically 30 hrs.) required for each batch run.

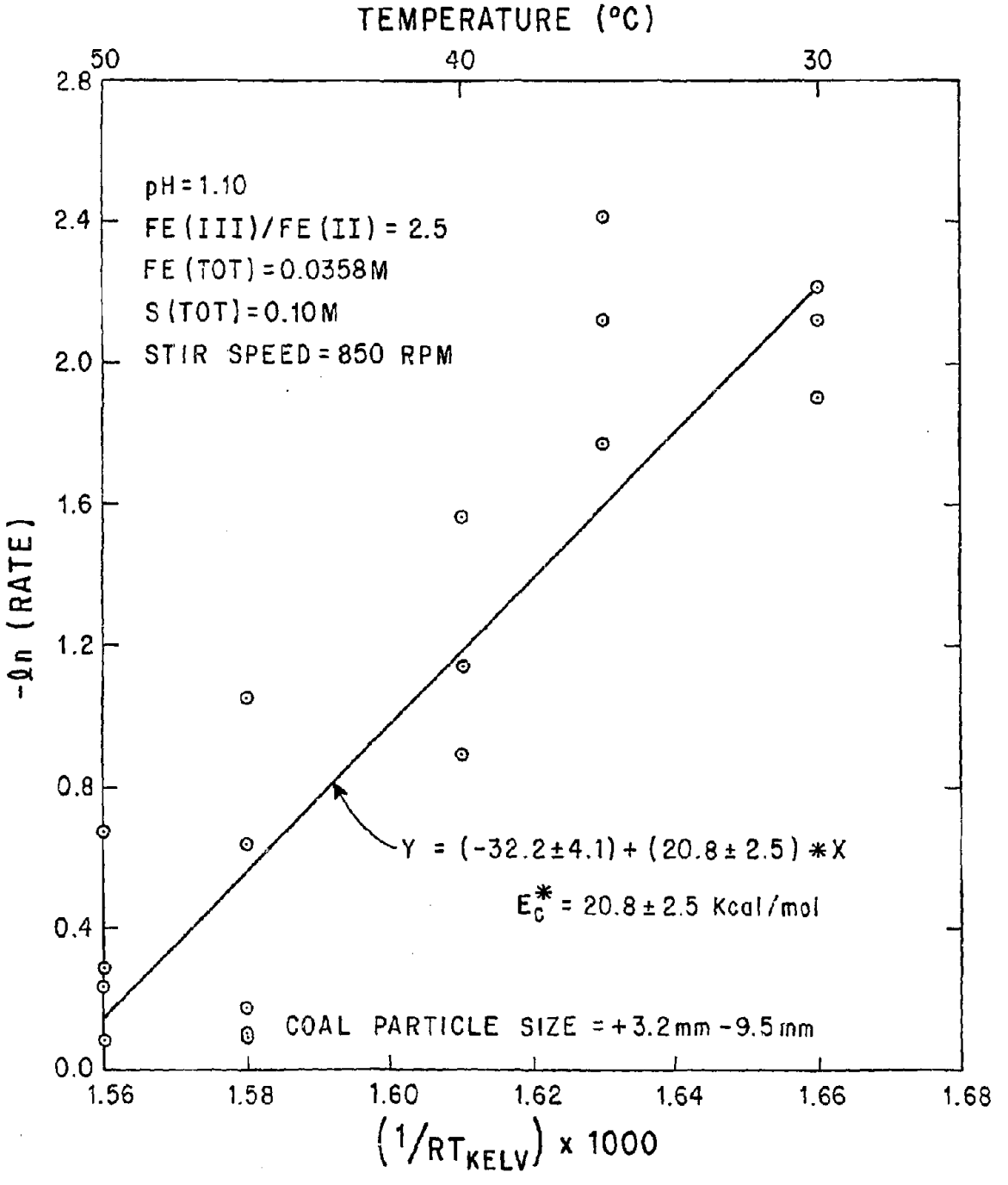

Figure 7 . Arrhenius plot showing the reaction rate (mg Fe(III)/hr/g coal) as a function of temperature. The data points each represent a separate fresh coal sample and rate determination. The solid line represents a least squares fit of data. The correlation coefficient equals 89%.

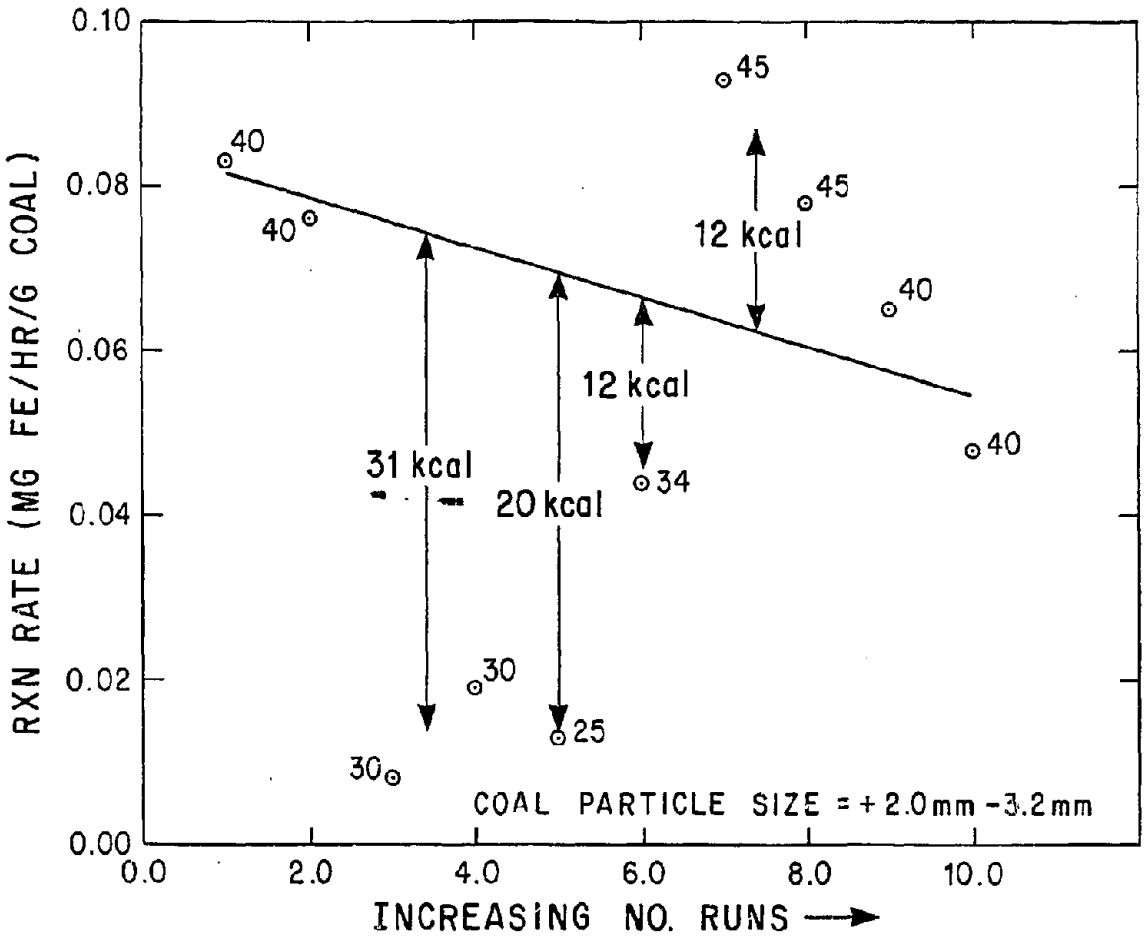

Figure 8. Reaction rate is plotted as a function of time. The temperature of the leaching was varied as leaching progressed. The arrows compare the rate of leaching at various temperatures to the rate that would have obtained if the temperature of the kettle had been 40°C. The numbers in the arrows give the activation energy suggested by the change in rate and temperature. The activation energies decrease with time from ∿20 kcal/mole toward 5 kcal/mole as suggested by the shrinking core model.

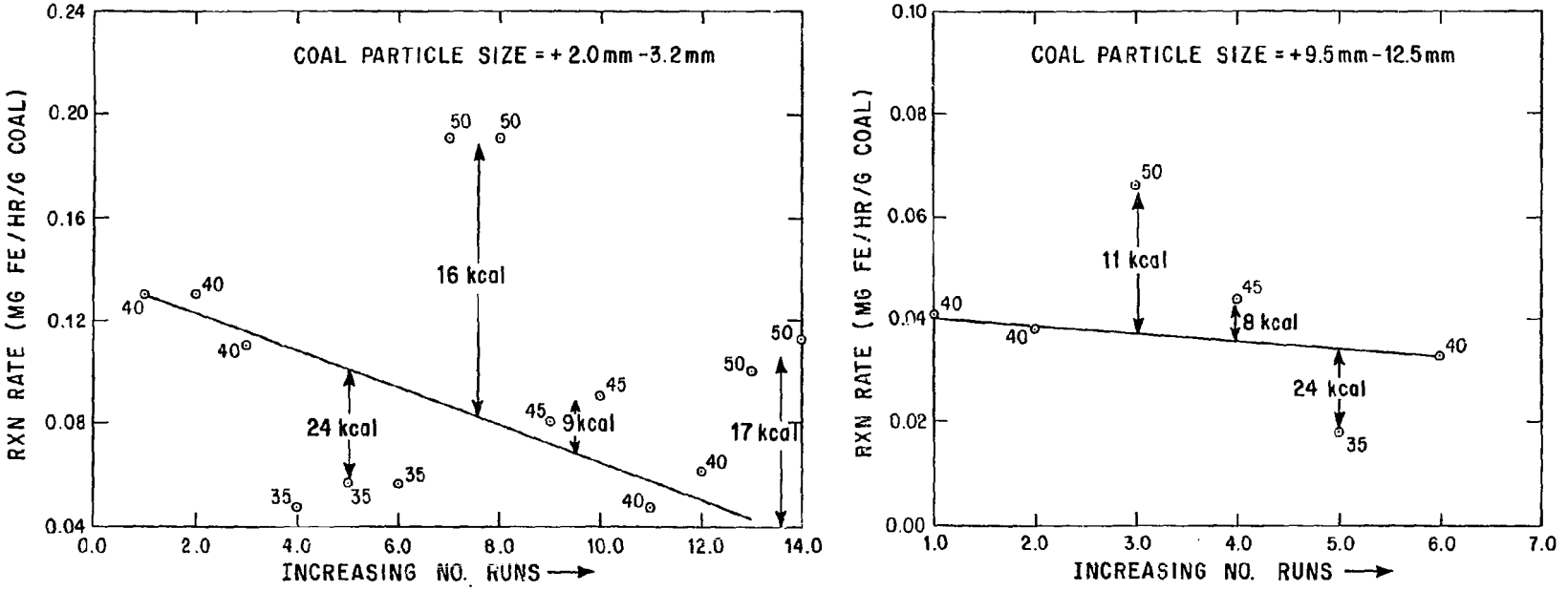

Figure 8 (continued)

2. The Stoichiometry of Pyrite Oxidation

The stoichiometry of pyrite oxidation can be determined from the consumption of H_2O_2 and the decrease in pyrite before and after leaching and (independently) from the increase in organic sulfur after leaching. Sulfur analyses of four kettle charges, before and after leaching, are shown in Table 8. Generally, about 60% of the pyritic sulfur in the charges was leached in 200-400 hours at 40°C, a decrease of 0.76 weight percent. The organic sulfur content, on the other hand, increased about 0.3 weight percent.

Equation (18) and the fact one mole of H_2O_2 oxidized two moles of ferrous iron to ferric indicates (1 + 6X) moles of pyrite will be oxidized per mole of H_2O_2 consumed. Table 9 lists the moles of pyrite oxidized for each sample of Table 8, the moles of H_2O_2 consumed in the process, and the stoichiometric X value calculated from the above stoichiometry. The X so calculated is 0.68 ± 0.25, which is consistent with the value of 0.6 determined in studies by other workers (Table 1).

It should be pointed out that although Meyers (1977) proposed an effective stoichiometry of X = 0.6 for coal depyritization by ferric sulfate, he also showed that at the 102°C temperatures of his process, ferric iron reacts with the coal matrix. The excess ferric iron reduction was 0.3 ± 0.2 g Fe^{3+}/g coal (Meyers, 1977, p. 112). We have investigated the possibility that ferric iron could be consumed by oxidation of the organic material in the coal matrix. Stumm and Morgan (1970, p. 536)discuss the ability of organic substances, especially those that contain hydroxy and/or carboxyl functional groups, to reduce aqueous ferric iron to ferrous iron. Carboxyl groups are known to be absent in the High Volatile B bituminous coal used here (Given, 1979). We have observed more organics in ferric sulfate leach solutions than in "blank" sulfuric acid solutions we have interacted with the coal. The increase in organic content of the leach solutions is not sufficient to affect the stoichiometric X determinations, however.

The stoichiometry of pyrite oxidation in the kettles can also be estimated from the increase in organic sulfur. In the forms of sulfur analysis, sulfate sulfur is determined from gravimetric analyses of the sulfur solubilized by a hydrochloric acid leach. Pyritic sulfur is determined from nitric acid soluble iron levels in the coal sample leachate. Total sulfur is a result of iodometric titration of SO_2(g) evolved from combustion

Table 8

Sulfur Forms Analysis of Four Kettle Runs

Run	Size Fraction (mm)	Run Duration (hrs)	Temp °C	Fe(III) g/l	pH	Mass Coal Reacted (g)	Initial Pyritic Sulfur[a]	Final Pyritic Sulfur	Initial Sulfate Sulfur	Final Sulfate Sulfur	Initial Organic Sulfur[*]	Final Organic Sulfur[*]	Initial Total Sulfur	Final Total Sulfur
A	2.00 x 3.2	540	45[c]	1.4	1.10	12.22	1.30 ± 0.03[b]	0.45 ± 0.03	0.24 ± 0.01	0.31 ± 0.01	2.31 ± 0.16	2.55 ± 0.28	3.85 ± 0.05	3.31 ± 0.05
B	1.2 x 9.50	357	40	1.4	1.25	10.06	1.15 ± 0.03	0.46 ± 0.03	0.21 ± 0.01	0.18 ± 0.01	2.19 ± 0.20	2.68 ± 0.38	3.55 ± 0.05	3.32 ± 0.05
C	0.85 x 2.00	323	40[d]	1.4	1.10	10.00	1.37 ± 0.03	0.80 ± 0.03	0.26 ± 0.01	0.24 ± 0.01	2.13 ± 0.15	2.45 ± 0.22	3.76 ± 0.05	3.49 ± 0.05
D	2.00 x 3.2	404	40	1.4	1.25	10.00	1.30 ± 0.03	0.39 ± 0.03	0.24 ± 0.01	0.26 ± 0.01	2.31 ± 0.16	2.46 ± 0.32	3.85 ± 0.05	3.11 ± 0.05

[a] All sulfur values are percent on a dry weight basis.

[b] Forms of sulfur analysis er estimated as one-half max. allowable by ASTM proc. #D2492 (1981).

[*] Note: error for organic sulfur is a summation of the errors for pyritic, sulfate, and total S.

[c] 45°C for 200 hr, then variable between 35 and 50°C.

[d] 40°C for 100 hr, then variable between 35 and 50°C.

Table 9

Summary of Leach Reaction Stoichiometry Analysis

Run I.D.	Figure Notation	Moles Pyrite Oxidized	Moles H_2O_2 Consumed	Corresponding[a] X Value (Fig.)	Moles S^o Generated[b]	X Value Computed[c] from S^o Generated
2.00 X 3.17 GR	A	1.62×10^{-3} ± 9%	8.36×10^{-3} ± 2%	0.7 ± 11%	0.92×10^{-3} ± 18%	0.7 ± 27%
3.17 X 9.50 SF	B	1.08×10^{-3} ± 10%	3.57×10^{-3} ± 2%	0.4 ± 12%	1.54×10^{-3} ± 23%	0.3 ± 33%
0.85 X 2.00 SF	C	0.89×10^{-3} ± 6%	6.37×10^{-3} ± 2%	1.0 ± 8%	1.00×10^{-3} ± 16%	0.4 ± 22%
2.00 X 3.17 TCTC	D	1.42×10^{-3} ± 10%	6.26×10^{-3} ± 2%	0.6 ± 12%	0.47×10^{-3} ± 20%	0.8 ± 30%

[a] Moles py oxi = (2/2 + 12X) moles H_2O_2 consumed.

[b] Assuming organic sulfur increases due to elemental sulfur generation.

[c] 2(1-X) = moles S^o generated per mole pyrite oxidized.

of a split of the coal sample. Organic sulfur is determined by the difference between total sulfur and the sum of pyritic and sulfate sulfur. Organic sulfur is therefore all sulfur not soluble in hydrochloric or nitric acid. Elemental sulfur is not soluble in either of these acids and is the postulated cause of the organic sulfur increases.

If the increase in organic sulfur is attributed to S^o, the amount of pyrite oxidized and the fact 2(1-X) moles of S^o should be generated per mole of pyrite oxidized can be used to determine X. This is done in the last column of Table 9. The column shows a mean X value of 0.55 ± 0.24, which is consistent with both the previous estimates.

3. Determination of k_{ox} and D_E

Figure 9 shows the leach history of Runs B and D (see Table 8) deduced from Fe(III) consumption data assuming $X = 0.6 \pm 0.1$. The curves are clearly similar in form to those expected in Figure 5. In Run D, the iron consumption data indicate about 68% of the pyrite is leached in 400 days (Table 8 suggests 70% leaching). Figure 5 shows 70% leaching can be achieved in 0.23 ($\tau_C + \tau_D$) if the leaching is diffusion controlled. On this basis, we would estimate a leach time ($\tau_C + \tau_D$) of 400 hours/0.23 or 2.3 months. A similar estimate made for Run B is 360 hours/0.035 or 13.8 months. These estimates agree very well with the predicted values for the two runs of 2.2 and 9.4 months respectively (Table 10), taking $a^R_{sulf} = 100\ cm^{-1}$.

A comparison of the predicted and observed leaching parameters that takes account of the shape of the observed curves of Figure 9 as well as the total pyrite leached is shown in Table 10. The observed τ_C and τ_D values of Table 10 were obtained by fitting the kettle data to the shrinking core model using a non-linear least squares technique. The advantage of this approach is that values for both τ_C and τ_D are obtained. The values so obtained clearly show the rate of leaching is controlled by diffusion (τ_D is greater than τ_C). This conclusion can be and was verified by various graphical curve analyses. The shape of the leaching curve clearly indicates diffusion control.

Diffusion control requires formation of leached rims. The leached coal fragments were examined and leached rims were indeed found. An example is shown in Plate 1. The thickness of the transition zone between the leached rim and the unleached core in Plate 1 is about 650 μm in both

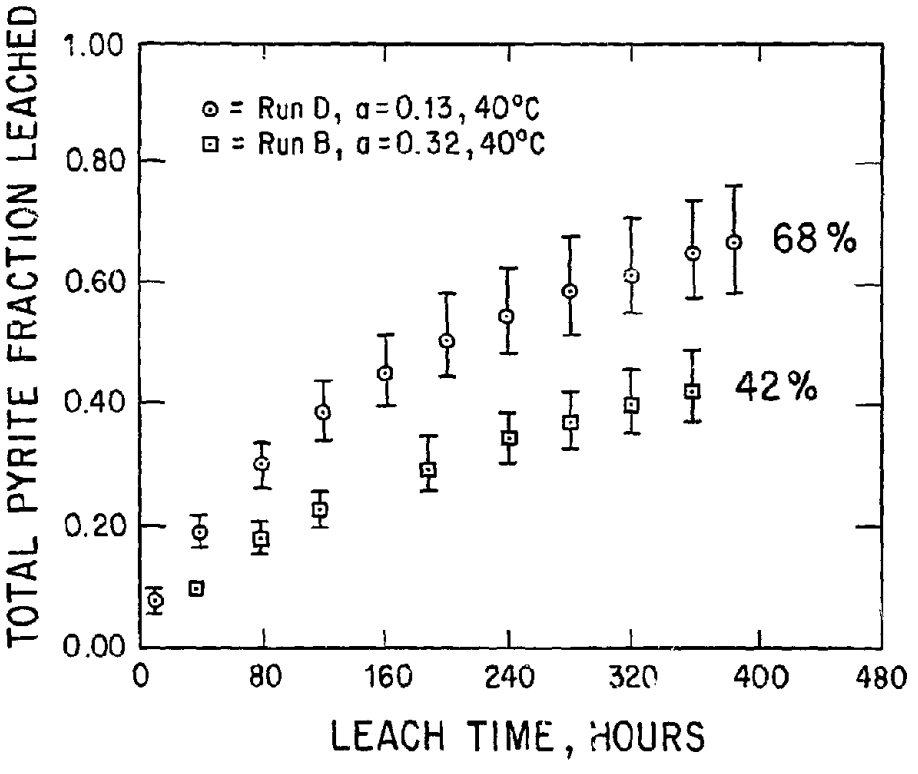

Figure 9 Leach histories of two kettle runs

Run	a	Predicted τ_C	Observed (Least Squares) τ_C	Predicted τ_D	Observed (Least Squares) τ_D
B	0.32	8.9 to 2.7	.9 1.0 1.1	6.9	2.8 4.0 5.5
D	0.13	3.6 to 1.1	.4 .3 .3	1.1	1.1 1.8 2.7

Table 10. Leach parameters at 40°C predicted from Table 7 are compared to the curves in Figure 9 which represent best fits to the shrinking core model using a least squares non-linear fitting technique (APL Statistical Library, 1979). The two values for τ_C are for a^R_{SULF}= 30 and 100 cm^{-1}.

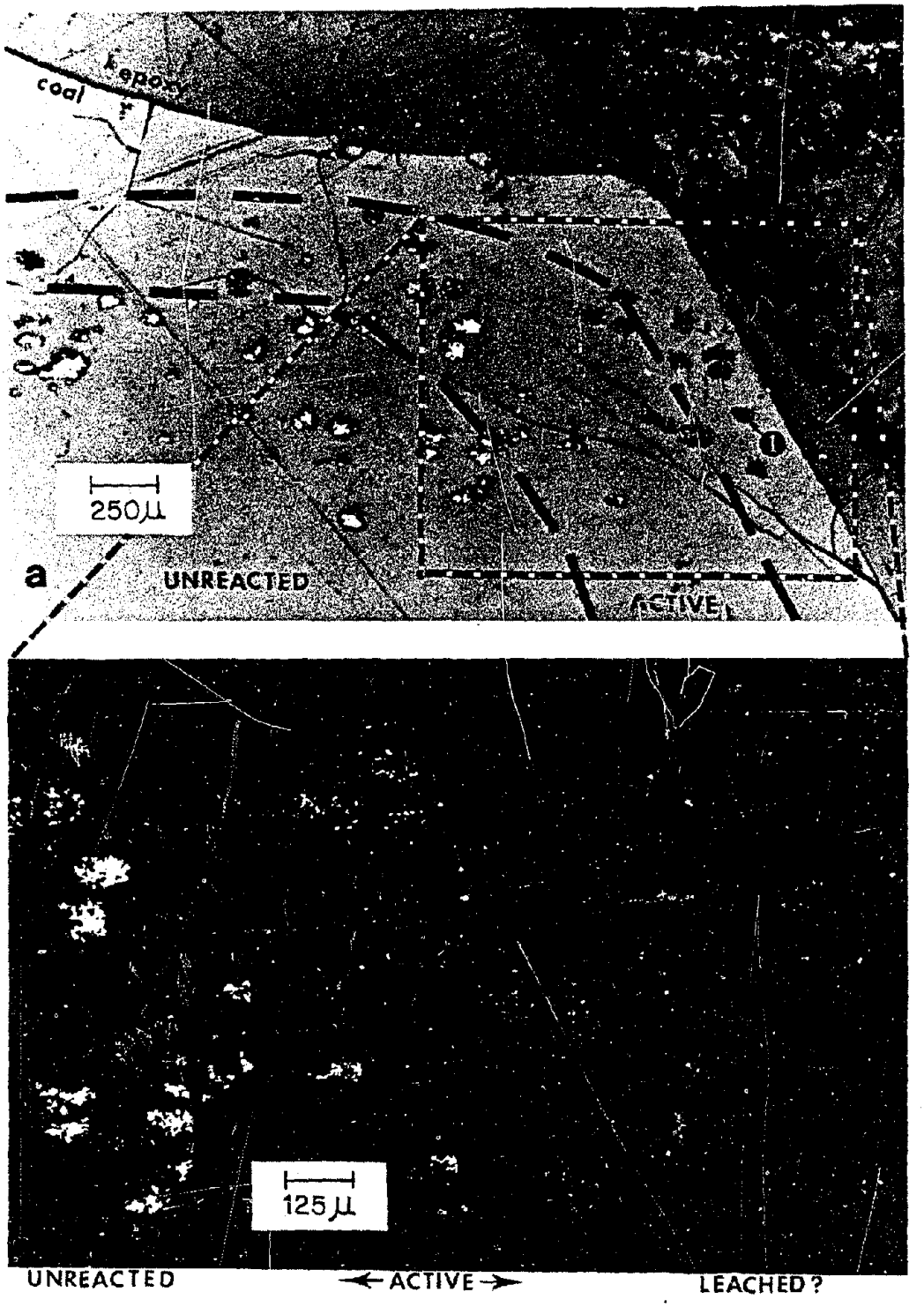

Plate 1 Rimming phenomena observed within coal leached in the kettle apparatus. Three zones or stages of leaching are evident. Circle 1 denotes a void space containing evidence of remnant (unleached) pyrite.

cases. The transition zone width will be about 2δ, so this observed width is in excellent agreement with the predicted δ value of 169 to 308 μm at 40°C (Table 7).

Finally we can use the observed δ value of 325 μm, a τ_C value of 1.0 mo., and τ_D value of 4.0 mo for the larger size fraction leached (the 0.7 mm δ value makes utilization of the smaller size fraction data questionable) to calculate D_E and k_{ox} from equations (3) and (6). We assume K=0.14 and $a^R_{sulf} = 30$, $[O_x] = 1.4 \times 10^{-3}$. The results, extrapolated back to 20°C, are: $D_E = 8.7 \times 10^{-8}$ and $k_{ox} = 1.5 \times 10^{-6}$. These values are in excellent agreement with those inferred from the literature of 7.5×10^{-8} and 10^{-6} to 10^{-7} respectively (Table 1 and 4).

4. Summary and Conclusions.

The kettle experiments confirm the activation energies, rate constants, and reaction stoichiometry deduced from the literature in the previous section. k_{ox} seems to be on the high end of the range we identified from the literature. $a^R_{sulf} = 100\ cm^{-1}$ appears preferable to $30\ cm^{-1}$. Leached rims were observed as it was predicted they should be and the width of the transition zone between leached and unleached coal is about the thickness predicted. The kettle experiments provide excellent confirmation of the shrinking core leaching model.

E. Model Verification and Parameter Calibration by Column Leaching Experiment.

Four 356-422 day column leaching experiments were carried out to further test the shrinking core heap leaching model. Plexiglass columns (three inch ID) were wrapped with copper tubing and maintained at constant temperature by passing water from a thermal bath through the tubing (see Figure 10). The columns were charged with about 2.5 kg of coal, and the coal was leached by passing air at a measured rate up through the column. The leach products were periodically flushed from the columns with batches of acidified water. The cumulative oxygen extracted and iron produced by the column was monitored, as was temperature at several locations along the column. Complete details of the operation are given in Appendix E.

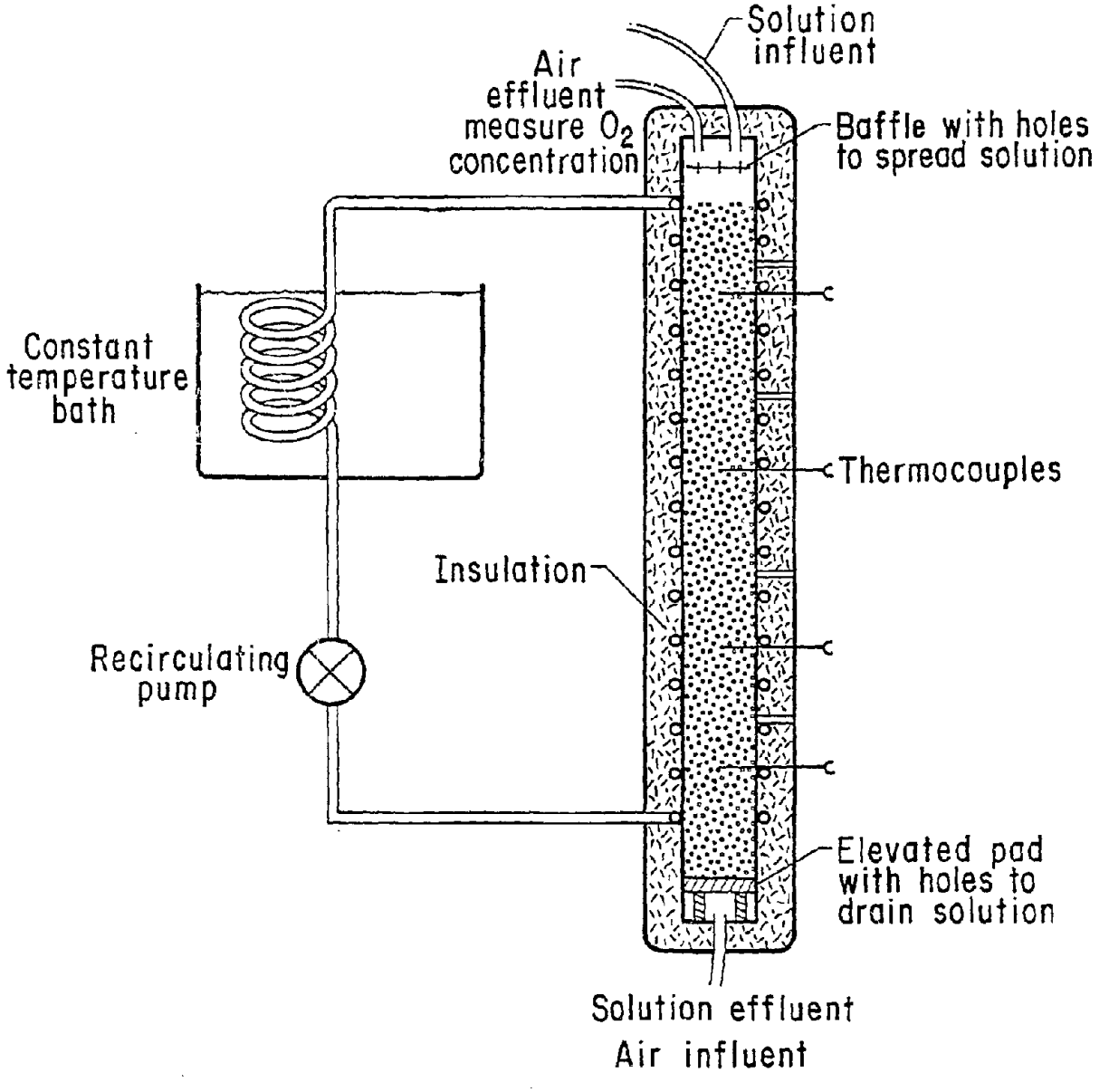

Figure 10 Schematic drawing of a constant temperature leach column. Flush solutions are applied to the top of the column, air is input at the base. Constant temperature is maintained by a constant temperature bath and tubing wrapped around the insulated column. Temperature is measured along the column. Oxygen concentration is measured in the air effluent from the top of the column.

Data on the columns and on the results of leaching are summarized in Tables 11-14. Plots of the fraction of total iron removed as a function of time for the four columns is given in Figure 11. Figure 11 shows that, as expected, the leaching is faster for smaller coal fragments and higher leaching temperature. The Wyoming coal in Column 1 leaches rapidly, as might be expected from its very low pyrite content (see Table 11, and note in equations (3) and (4) that τ_C and τ_D contain the variable K which increases linearly with pyrite content as shown in Table 6). The slow startup time of Column 1 may be related to retention of iron in the organic structure of the Wyoming coal.

It can be seen from Table 11 that a rather large discrepancy exists between the pyrite content estimated from total iron in the HTA and the pyrite content determined from a forms-of-sulfur analysis for pyritic sulfur. The reason for this discrepancy is not clear, since mineralogic analyses of the low-temperature ash consistently only detected pyrite, quartz and calcite, and showed no evidence for the presence of iron-containing mineral phases other than pyrite (FeS_2). A possible explanation is that the coal contains a considerable amount of organically-bound iron.

The post-mortem analyses reported in Table 13 were obtained in the following fashion: Following the completion of a column experiment, the apparatus was dismantled, and the packed bed of coal was removed from the Plexiglass column in an aluminum coring tube so as to preserve the spatial distribution, both lateral and vertical, of the coal particles within the leach column. The core tube was sealed air-tight, and inlet/outlet tubing was attached so that an inert atmosphere of nitrogen gas could be passed through the coal within the core tube. The nitrogen served to prevent coal oxidation and also to enhance moisture removal. The entire core assembly was placed in a large oven and dried for approximately 40 hours at a temperature of 60°C.

After drying, the core tube was divided into five vertical sections, each approximately 6-8 inches in length. The coal contained in each section was sampled for chemical analysis by a micro-channel sampling technique that yielded approximately 50 grams of coal from each section. The coal remaining in the core tube was prepared for microscopic analysis. Each

Table 11. Selected Chemical and Physical Characteristics of Coal Used in Column Leach Studies (Before Leaching)

Column Experiment No.	Coal I.D. and (size fraction)	%* Moisture	% Ash (HTA)	Forms of Sulfur Analysis (%) Pyritic S	Sulfate S	Organic S	Total S	Percent Iron in Coal Calc. from % Fe_2O_3 in HTA	Percent Pyrite Calc. from % Iron in Coal	Percent Pyrite Calc. from % Pyritic S	Calorific Value Btu/lb Dry Basis	Mmmf Btu/lb**	dmmf Btu/lb***
1	Wyoming Subbit. (+20 mesh - 3/4 in.)	21.80	5.48	0.13	0.02	0.48	0.63	0.3	0.7	0.24	11955	9805	12674
2	Illinois #6 (+20 mesh - 3/4 in.)	2.93	13.85	0.85	0.40	2.42	3.67	1.7	3.6	1.6	12086	13213	14336
3	Illinois #6 (+20 mesh - 3/4 in.)	2.93	13.85	0.85	0.40	2.42	3.67	1.7	3.6	1.6	12086	13213	14336
4	Illinois #6 (+20 mesh - 1/4 in.)	3.74	11.53	0.79	0.37	2.43	3.59	1.4	3.0	1.5	12190	12830	14035

ASH ANALYSIS

Wt. Percent

	SiO_2	Al_2O_3	TiO_2	Fe_2O_3	MgO	CaO	MnO	Na_2O	K_2O	P_2O_5	SO_3	Totals
Illinois #6	52.8	21.1	0.93	17.3	1.16	1.97	0.025	0.81	2.15			98.25
Wyoming	26.6	14.3	1.20	8.05	4.49	25.1	0.029	0.42	0.30	0.50	19.5	100.49

ppm in Ash

	Ba	Be	Cr	Cu	Ni	Rb	Sr	V	Zn	Zr
Illinois #6	410		170	70	95		200	170	210	160
Wyoming	3150	7	5	160	90	10	2050	210	570	220

*All percents by weight on a dry basis (except moisture)

**Mmmf = [Btu/lb moist coal - 50 (g total S/100 g moist coal)] ÷ [100 - (1.08 (g ash/100 g moist coal) + 0.55 (g total S/100 g moist coal))] x 100

***dmmf = [Btu/lb dry coal -50(g total S/100 g dry coal)] ÷ [100-(1.08(g ash/100 g dry coal) + 0.55 (g total S/100 g dry coal))] x 100

Table 12

OPERATIONAL PARAMETERS FOR COLUMN LEACHING EXPERIMENTS

Column Experiment #	^{O}C Temperature	Total Leach Time (days)	Leachate Compcsition/pH	Coal Mass (Kg)	Solution Flush Rate ml/day	Darcy Air Flow Rate (cm/s)	Interblock Porosity**
1	35	365	HCl/1.5	2.18	500	0.0011-0.0015	--
2	35	422	HCl/1.5	2.46	500	0.0011-0.0015	57%
3	50	376	*H_2SO_4/1.5	2.66	1000	0.0011-0.0015	56%
4	50	379	*H_2SO_4/1.5	2.61	1000	0.0011-0.0015	56%

*Bacterial innoculation with Thiobacillus ferrooxidans ATCC #13661. (Supplied by Prof. R.W. Stone, Microbiology Dept., Penn State University.)

**Interblock porosity = $1 - \left(\left(\frac{\text{mass coal}}{\rho \text{ coal}} \right) \div \frac{\text{column}}{\text{volume}} \right)$; column volume = 3600 cm^3

Table 13. Chemical Analyses of Coal Samples After Leaching in the Column Apparatus

	Sample I.D.	% Moisture*	% Ash (HTA)	Forms of Sulfur (%) Pyritic S	Sulfate S	Organic S	Total S	% Pyrite Calc. from % Pyritic S	Calorific Value (BTU/lb) Dry Basis	Mmmf	dmmf
Column 1	WY 1-6 (top)	7.03	--	--	--	--	--	--	12092	--	--
	WY 2-6	7.03	2.32	0.05	0.01	0.42	0.48	0.094	12006	11440	12324
	WY 3-6	5.41	--	--	--	--	--	--	12047	--	--
	WY 4-6	5.29	3.83	0.02	0.00	0.45	0.47	0.038	11988	11850	12515
	WY 5-6	6.67	--	--	--	--	--	--	12094	--	--
	WY 6-6	5.99	2.42	0.03	0.00	0.43	0.46	0.056	12227	11815	12568
	WY 7-6 (bot)	5.34	--	--	--	--	--	--	11934	--	--
Column 2	2-1 (top)	2.08	10.5	0.68±0.03	0.06±0.01	2.42	3.16±0.05	1.28	12596	14015	14313
	2-2	1.78	8.84	0.65	0.05	2.50	3.20	1.22	12710	13897	14149
	2-3	1.99	9.16	0.51	0.05	2.53	3.09	0.96	12630	13854	14135
	2-4	1.59	9.70	0.52	0.04	2.51	3.07	0.98	12530	13872	14096
	2-5 (bot)	1.89	9.42	0.49	0.05	2.51	3.05	0.92	12592	14193	14466
Column 3	3-1 (bot)	3.86	7.16	0.45	0.17	2.62	3.24	0.84	12778	13402	13940
	3-2	5.14	7.84	0.87	0.19	2.60	3.66	1.63	12518	13074	13782
	3-3	5.42	7.75	0.54	0.19	2.60	3.33	1.01	12514	13005	13750
	3-4	2.79	7.28	0.38	0.19	2.65	3.22	0.71	12564	13337	13720
	3-5 (top)	4.15	7.62	0.37	0.28	2.55	3.20	0.69	12702	13358	13936
Column 4	4-1 (top)	1.27	10.7	0.20	0.22	2.46	2.88	0.38	12028	13501	13675
	4-2	0.89	11.2	0.17	0.22	2.39	2.78	0.32	12774	14494	14624
	4-3	1.12	11.0	0.18	0.20	2.38	2.76	0.34	12878	14540	14711
	4-4	1.16	9.98	0.15	0.19	2.43	2.77	0.28	12079	13457	13615
	4-5 (bot)	0.44	12.5	0.20	0.16	2.45	2.81	0.38	12168	14088	14150

* dried at 60°C under nitrogen for 40 h.

Table 14 Percent Change in Chemical Characteristics of Coal Leached in the Column Apparatus

Sample I.D.	Ash HTA	Pyrite Content	Organic Sulfur	Total Sulfur	Calorific Value (BTU/lb) dry basis	Mmmf	dmmf
Column 1							
WY 2-6	-57.7	-61.5	-12.5	-24.8	+0.4	+16.7	-2.8
WY 4-6	-30.1	-84.6	- 6.3	-25.4	+0.3	+20.9	-1.3
WY 6-6	-55.8	-76.9	-10.4	-27.0	+2.3	+20.5	-0.8
		-74.3± 11.8					
Column 2							
2-1	-24.2	-20.0	0.0	-13.9	+4.2	+ 6.0	-0.2
2-2	-36.2	-23.5	+ 3.3	-12.8	+5.2	+ 5.2	-1.3
2-3	-33.9	-40.0	+ 4.5	-15.8	+4.7	+ 4.9	-1.4
2-4	-30.0	-38.8	+ 3.7	-16.3	+3.7	+ 5.0	-1.7
2-5	-32.0	-42.4	+ 3.7	-16.9	+4.2	+ 7.4	+0.9
		-32.9± 10.4					
Column 3							
3-1	-48.3	-47.0	+ 8.3	-11.7	+5.7	+ 1.4	-2.8
3-2	-43.4	+ 2.4	+ 7.4	- 0.3	+3.6	- 1.0	-3.9
3-3	-44.0	-36.4	+ 7.4	- 9.3	+3.5	- 1.6	-4.1
3-4	-47.4	-55.3	+ 9.5	-12.3	+4.0	+ 0.9	-4.3
3-5	-45.0	-56.5	+ 5.4	-12.8	+5.1	+ 1.1	-2.8
		-38.6± 24.3					
Column 4							
4-1	- 7.2	-74.7	+ 1.2	-19.8	-1.3	+ 5.2	-2.6
4-2	- 2.9	-78.5	- 1.6	-22.6	+4.8	+13.0	+4.2
4-3	- 4.6	-77.2	- 2.1	-23.1	+5.6	+13.3	+4.8
4-4	-13.4	-81.0	0.0	-22.8	-0.9	+ 4.9	-3.0
4-5	+ 8.4	-74.7	+ 0.1	-21.7	-0.2	+ 9.8	+0.8
		-77.2± 2.7					

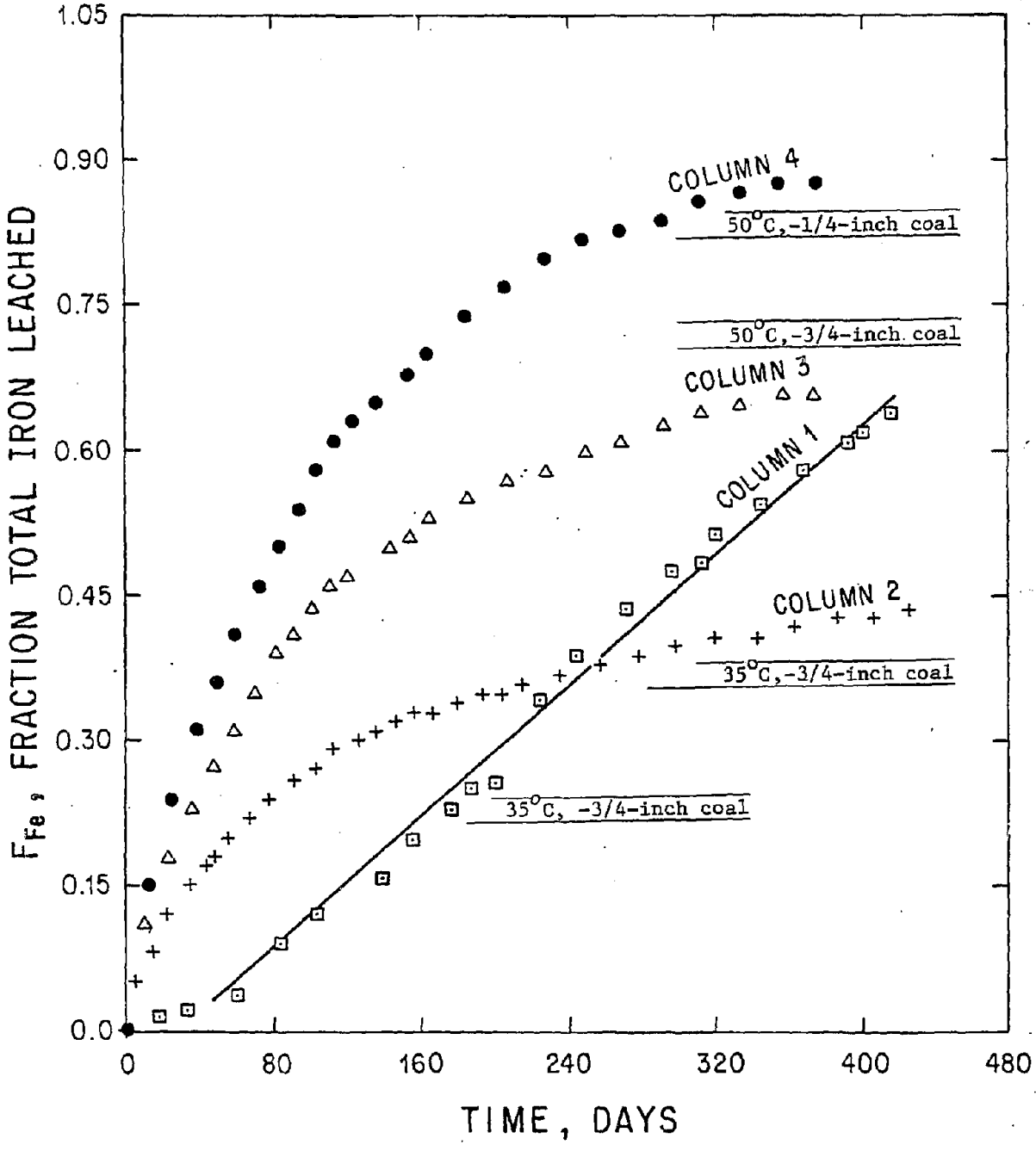

Figure 11 Iron extraction histories for coals leached in extended-duration column experiments. Total iron in solution effluents from the leach columns are ratioed against total iron in the unleached coal (from HTA analysis) to estimate fractional iron removal.

50-gram coal sample was crushed to the appropriate size range for chemical analysis.

Changes in the chemical characteristics of the coal before and after column leaching are most easily interpreted by using Table 14 that reports the effects of leaching on a percent change basis. A minus sign indicates a net decrease and a plus sign a net increase after leaching.

1. The Stoichiometry of Leaching

As in the kettle experiments, the stoichiometry of leaching can be determined from the increase in organic sulfur and the decrease in pyritic sulfur. Note, however that the fate of organic sulfur varies in the four column experiments (Table 14). The Wyoming coal loses organic sulfur, columns 2 and 3 gain organic sulfur, and column 4 shows no change. Table 15 interprets the results for columns 2 to 4. Columns 2 and 3 indicate a stoichiometric X value of 0.6 ± 0.2.

2. Determination of k_{ox} and D_E

τ_C and τ_D can be determined from the shape of the leach curves if we assume the form of the iron fraction leached vs. time curves (Figure 11) reflect the form of the fraction pyrite leached vs. time curves. It is clear from Table 14 that the fraction iron leached does not accurately reflect the fraction pyrite leached. This is shown also in Figure 12 where pyrite leach curves (heavy dash) have been constructed such that they pass through the total pyrite extracted points and have a similar form to the iron leach curves. The pyrite recovery (dashed curves) lie distinctly below the iron recovery data. The pyrite recovery curves are analyzed in two ways: (1) by the non-linear curve fitting technique used in the kettle experiments, and (2) by simulating the column leach experiments using the finite difference model described and used in the next section.

Shrinking core model curves, fit for two different values of τ_C by a least squares iterative technique to the iron recovery data, are shown in Figure 13. The values of τ_C and τ_D obtained by this fit are corrected for the difference between the iron and pyrite recovery curves by increasing both by the ratio of the total leach time to the leach time at which the

Table 15 Summary of Stoichiometry Analysis of Chemical Data from Column Leaching Experiments

Column	Coal Mass Reacted (kg)	Initial g FeS_2	Final g FeS_2	Moles FeS_2 leached	Initial g Organic S (n = 1)	Final g Organic S (n = 5)	Moles S° generated	Moles S° Generation Predicted by Setting X = 0.6 in Eqn.	X Computed[a] from sulfur balance
2	2.46	39.4±0.8	26.3±4.1	0.11±0.02	59.5±4.1	61.8±0.7	0.072±0.006	0.088±0.016	0.67±26%
3	2.66	42.6±0.8	21.6±4.0	0.175±0.037	64.4±4.5	69.2±1.0	0.150±0.013	0.140±0.029	0.57±29%
4	2.61	39.2±0.8	8.9±1.0	0.25±0.03	63.4±4.7	63.2±1.0	---	0.20±0.03	∿1.0

[a] 2(1-X) = moles S° generated per mole pyrite leached

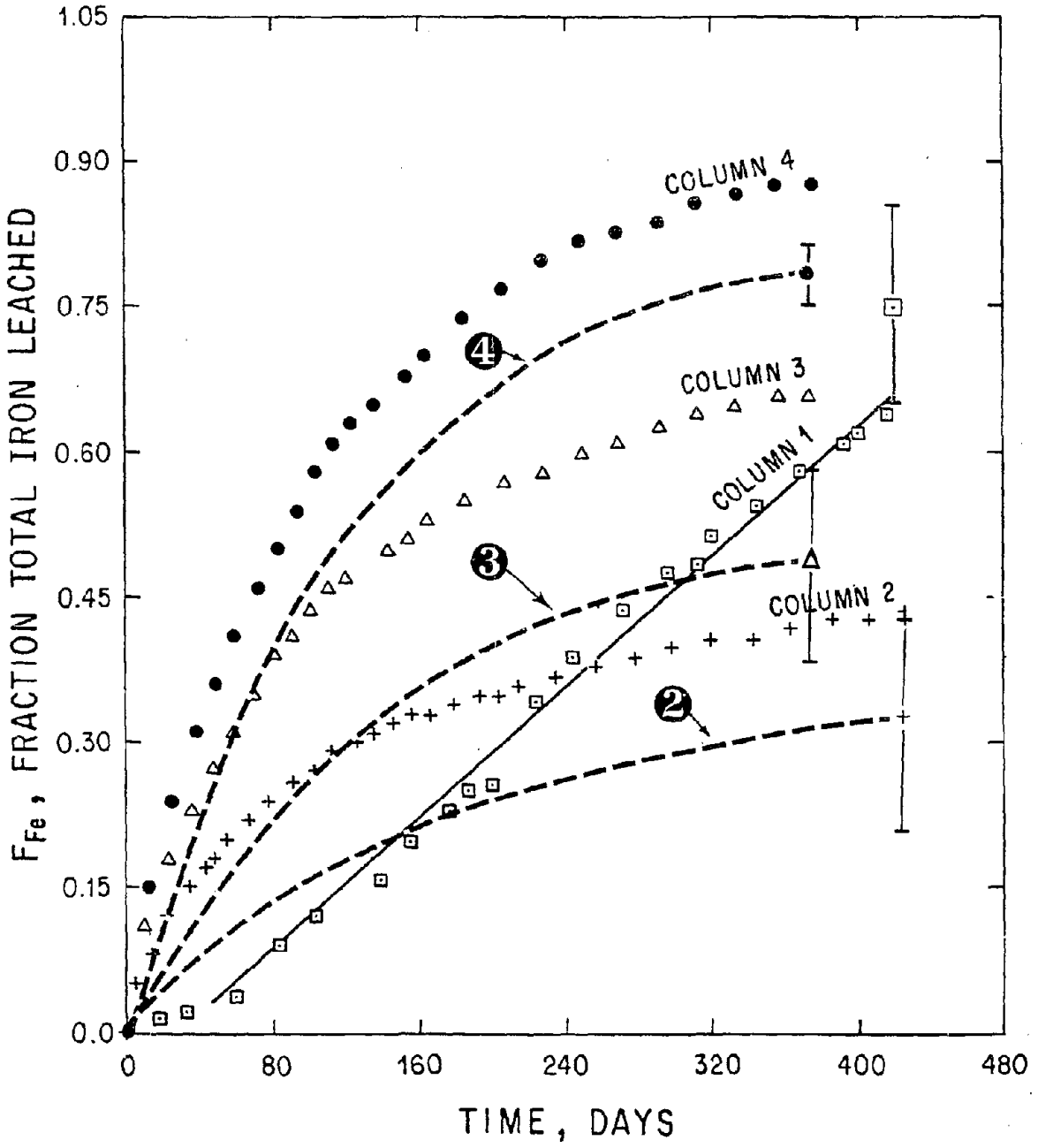

Figure 12 Iron extraction histories from the column experiments compared with analytical estimates of pyrite extraction (data points with error brackets). Dashed lines are pyrite leach histories estimated by assuming a pyrite removal curve similar in form to the iron removal curve.

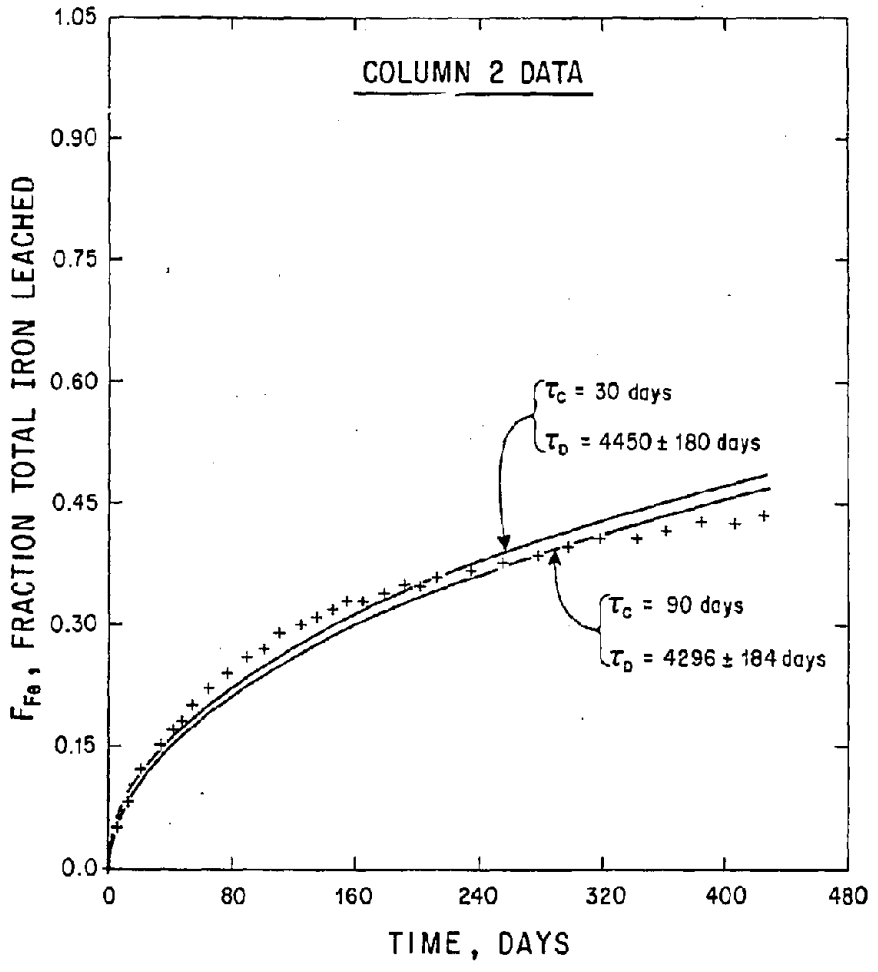

Figure 13 Estimates of τ_C and τ_D and the corresponding leach history curves obtained by non-linear data fitting of fractional iron data to the integrated form of equation (1).

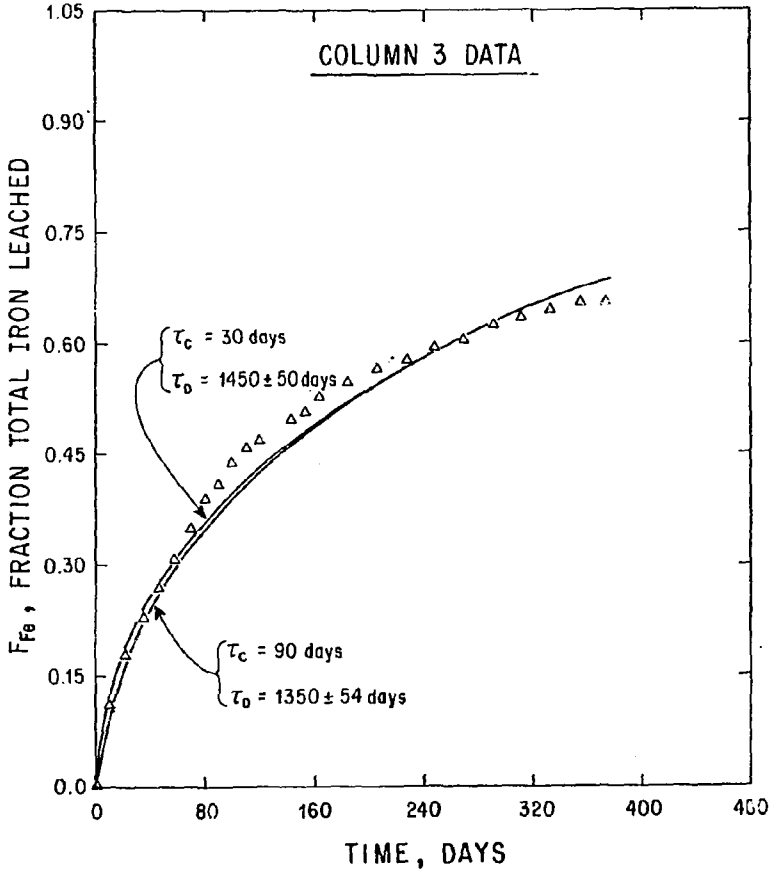

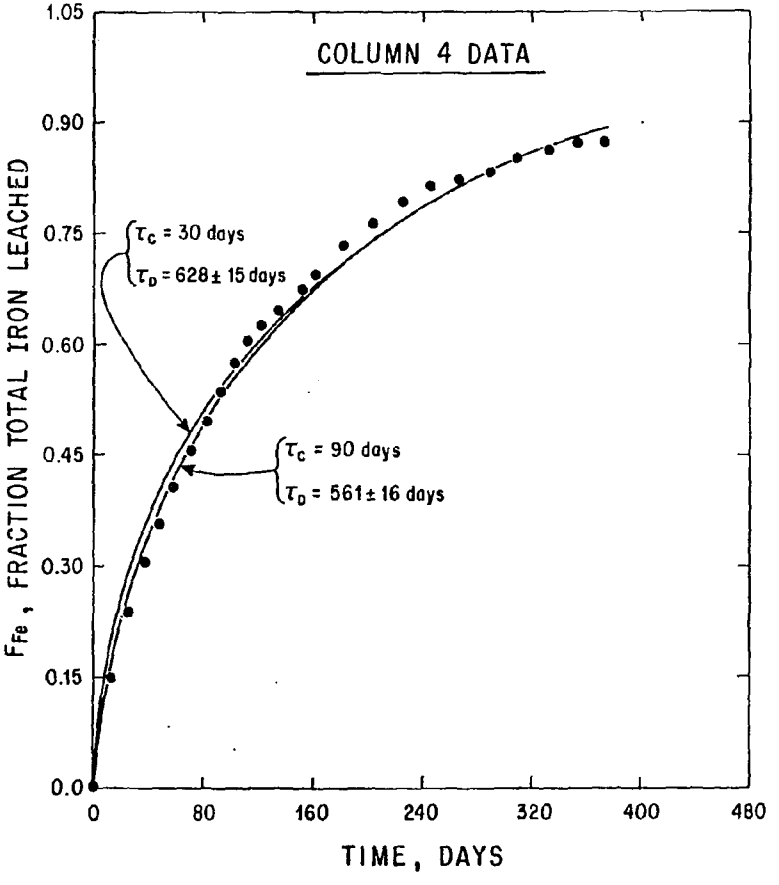

Figure 13 (continued)

iron recovery would equal the ultimate pyrite recovery. This factor for columns 2, 3, and 4 is: 2.63, 2.77, and 3.00 respectively. The resulting values of τ_C and τ_D are given in Table 16 and compared to the value range predicted by Table 7, adjusted to the proper temperature. Table 16 shows the observed and predicted values of τ_C are in reasonable agreement. This is not particularly meaningful because the values of τ_C are only very weakly constrained by the diffusion-dominated leach curves. On the other hand the τ_D values are well constrained by the observed curves, and the observed values are about an order of magnitude bigger than expected.

The bigger-than-expected values of τ_D could be due to a lower-than-expected iron concentration in the columns. The iron level is not important for the chemical kinetics of pyrite oxidation, since, as noted earlier, this reaction is approximately zero order in Fe(III). Ferric Iron concentration will control the flux of Fe(III) into the coal fragments through leached rims, however (see equation 4). Lower-than-expected (< 1 g/l) ferric iron concentrations will produce proportionately higher-than-expected τ_D values.

Figure 14 shows a fit of the finite difference model to the column leaching results. Good fits between observed and predicted curves are obtained with $k_{ox} = 3.3 \times 10^{-6}$ cm/sec (the mid point of the literature review range), and $D_E = 1.0 \times 10^{-8}$ cm^2/sec (a factor of 7.5 below the preferred value). These models assume $a^R_{SULF} = 30$ cm^{-1}.

3. Coal Oxidation

Figure 15 compares the observed drop in oxygen concentration of air passing through the columns to that which would be predicted from the observed iron in the effluent assuming the effluent iron came from pyrite leaching, and assuming various X factors. The observed oxygen concentration in the air exiting the columns is generally less than would be expected for X = 0.6. This could be due to oxygen consumption by coal oxidation or due to leaching of some of the non-pyritic iron in the column. We know substantial iron is leached from non-pyritic phases in the column because the pyrite oxidation inferred from the fraction of total iron leached is greater than the actual coal oxidation. Thus Figure 15 is of no use in estimating coal oxidation, except to suggest it is small.

	Observed	Predicted (a^R_{sulf} = 100 to 30 cm^{-1})
Column 2 35°C a=0.64cm	τ_C = 2.6 to 6.9 mo	7.5 to 25 mo
	τ_D = 378 mo	31.3 mo
Column 3 50°C a=0.64cm	τ_C = 2.8 to 8.3 mo	2.9 to 9.6 mo
	τ_D = 130 mo	21.5 mo
Column 4 50°C a=0.32cm	τ_C = 3 to 9 mo	1.4 to 4.8 mo
	τ_D = 60.8 mo	5.4 mo

Table 16. Curve fit values of τ_C and τ_D from Figure 13 are corrected to reflect pyrite rather than iron leaching and compared to the predicted values from Table 7 (adjusted for column temperature). τ_C values are poorly constrained because leaching is strongly diffusion controlled. Nevertheless, τ_C values agree reasonably with the predicted values. Observed τ_D values, on the other hand, are well constrained by the data and are about an order of magnitude bigger than predicted. This suggests iron levels in the column may be ~0.1 g/l rather than ~1.0 g/l. See text for discussion.

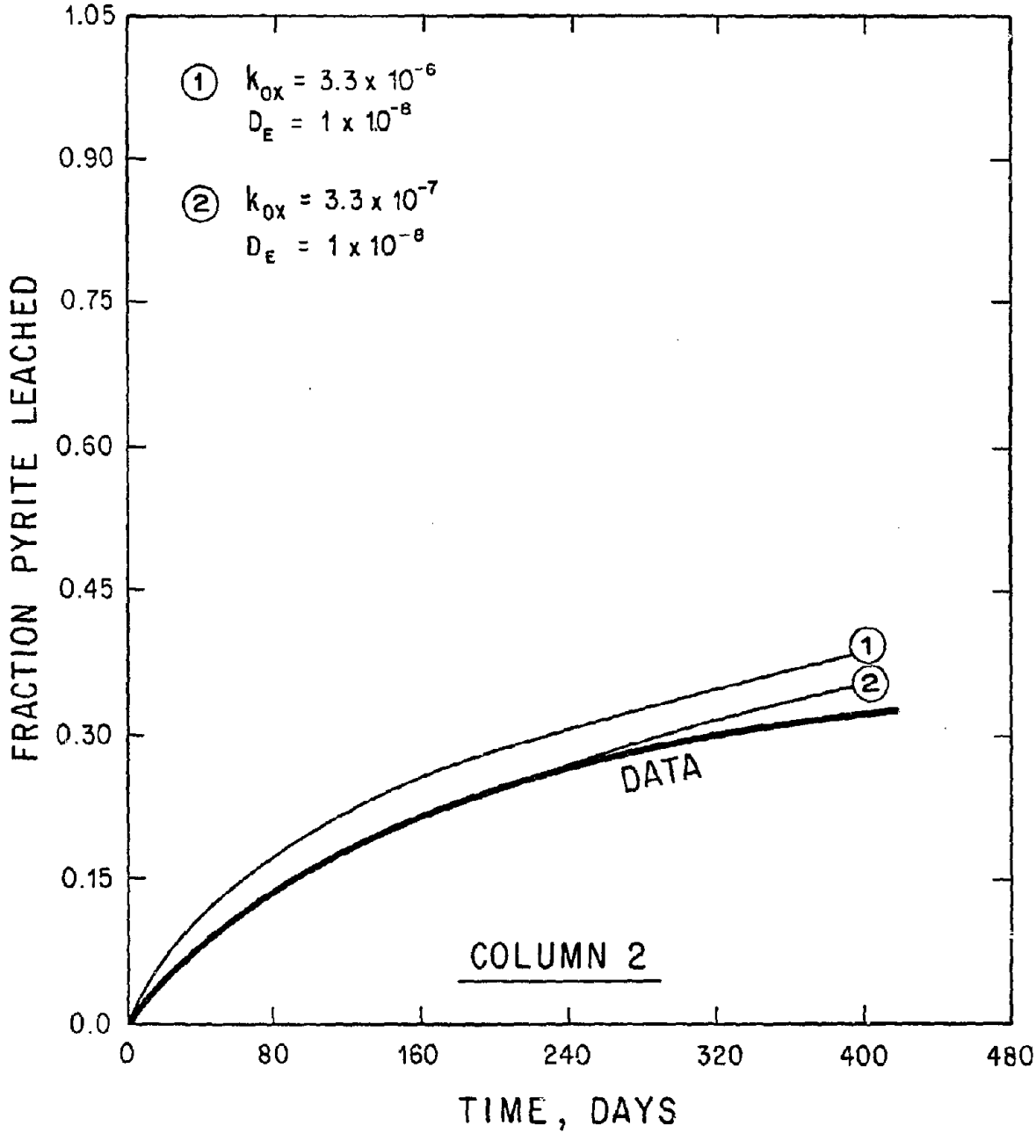

Figure 14 Finite difference models of the column leaching data agree well with the observed results if k_{ox} = 3.3 x 10^{-6} and D_E = 1.0 x 10^{-8}.

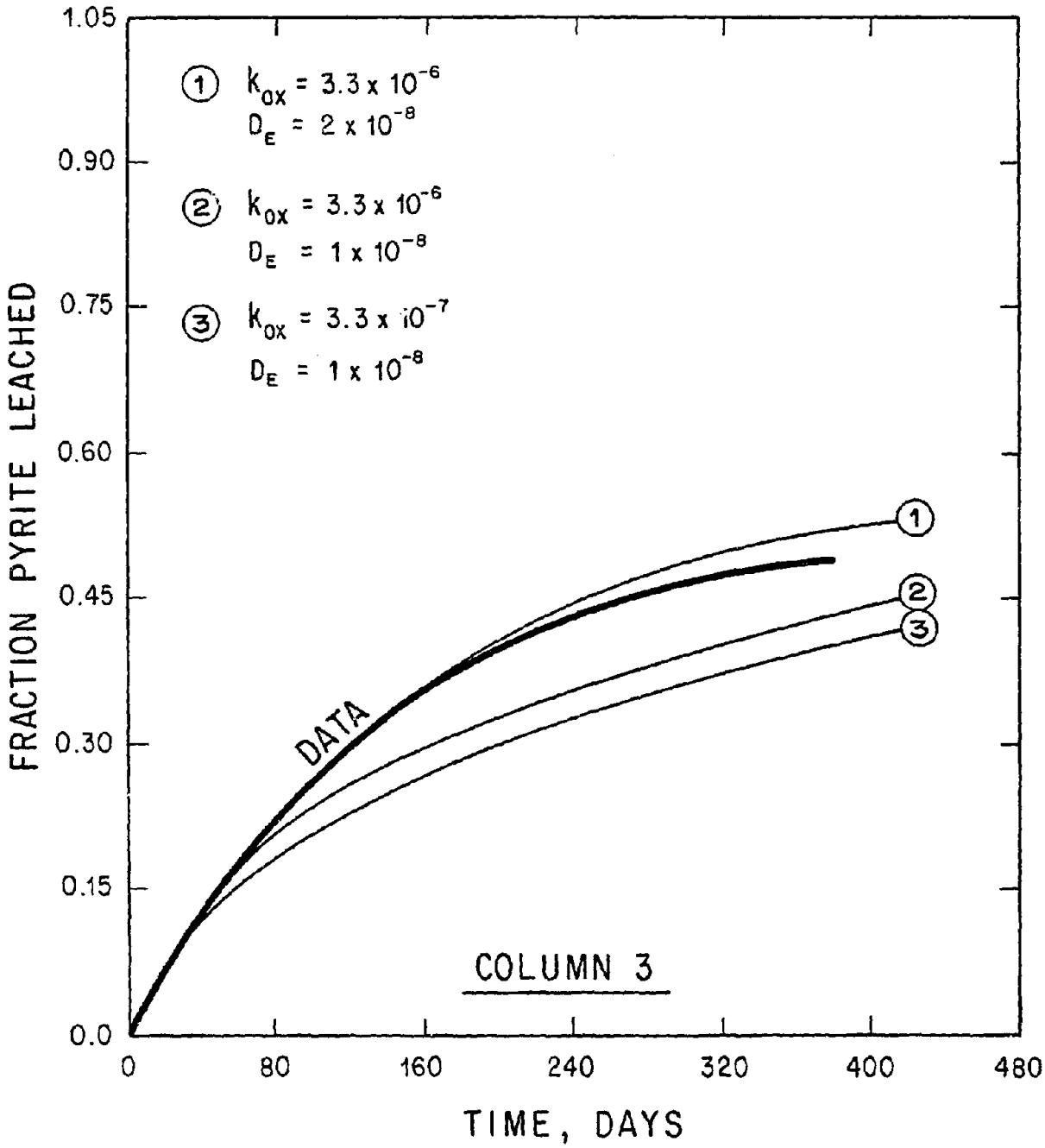

Figure 14 (continued)

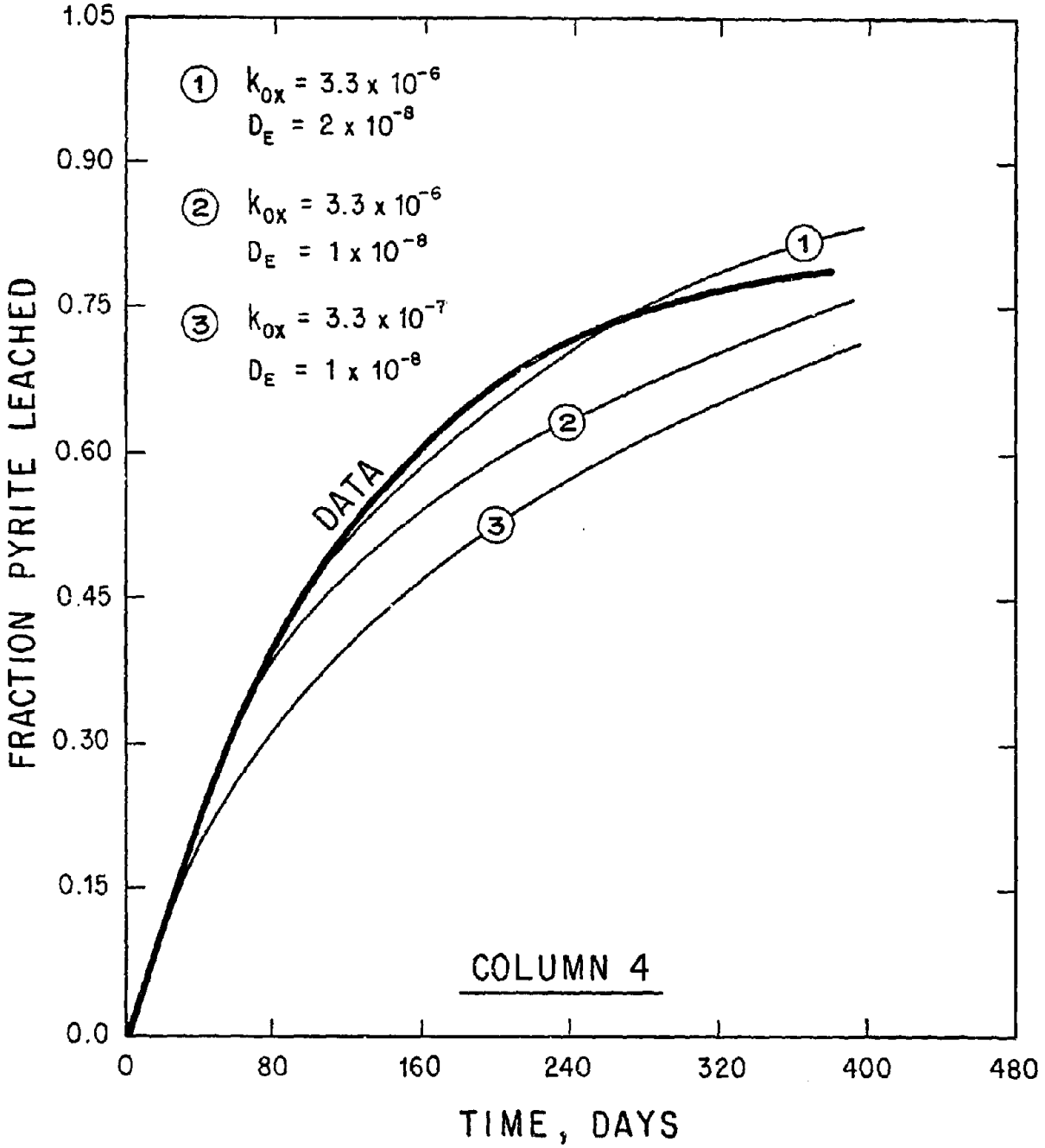

Figure 14 (continued)

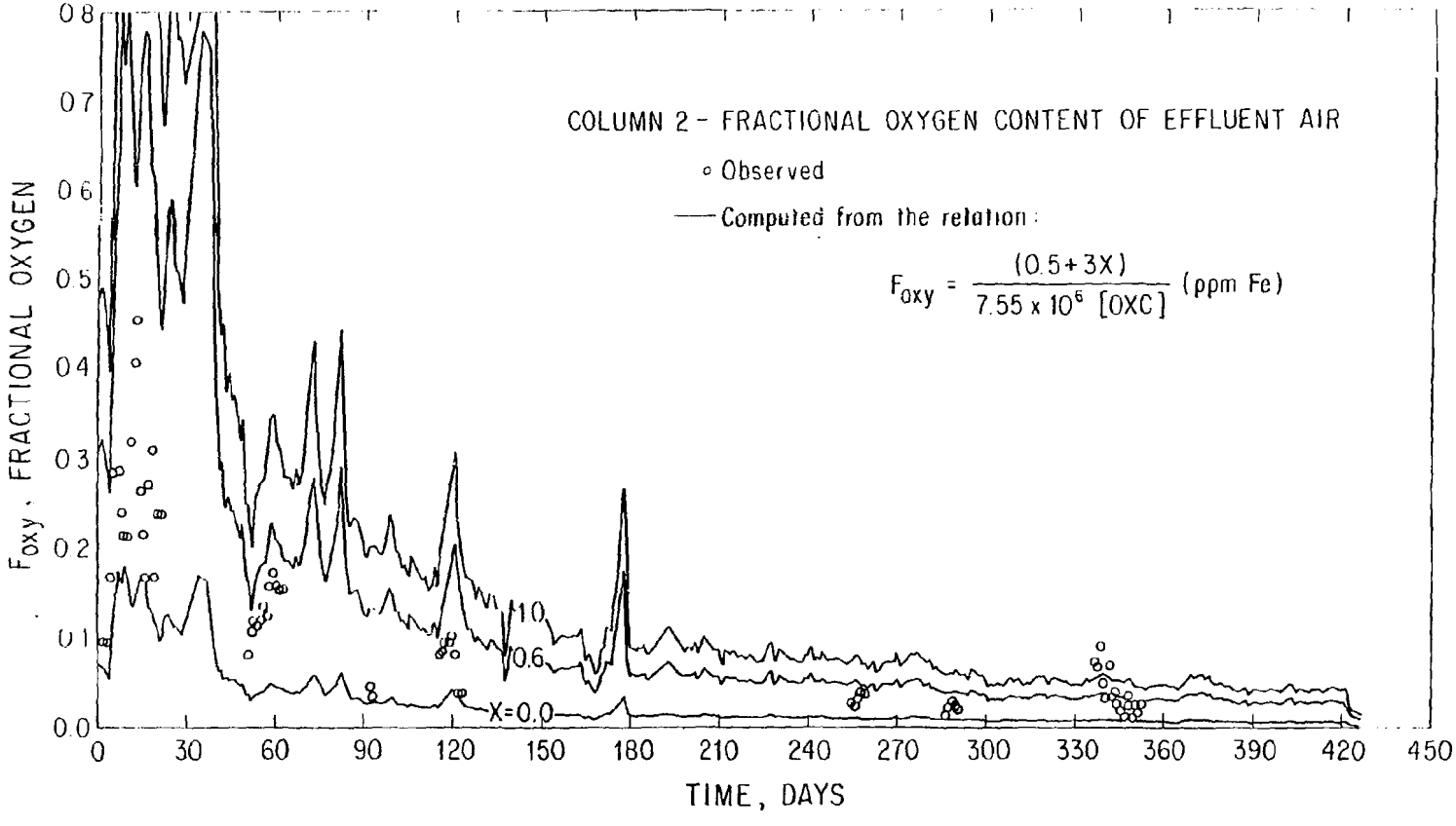

Figure 15 Stoichiometric predictions of effluent oxygen content computed from observed iron effluent data are compared with observed oxygen levels in effluent air for values of the stoichiometric X coefficient. [OXC] is the oxygen concentration in air effluent from the column in units of g O_2/cm^3. (ppm Fe) is the iron concentration in the flush effluent in ppm.

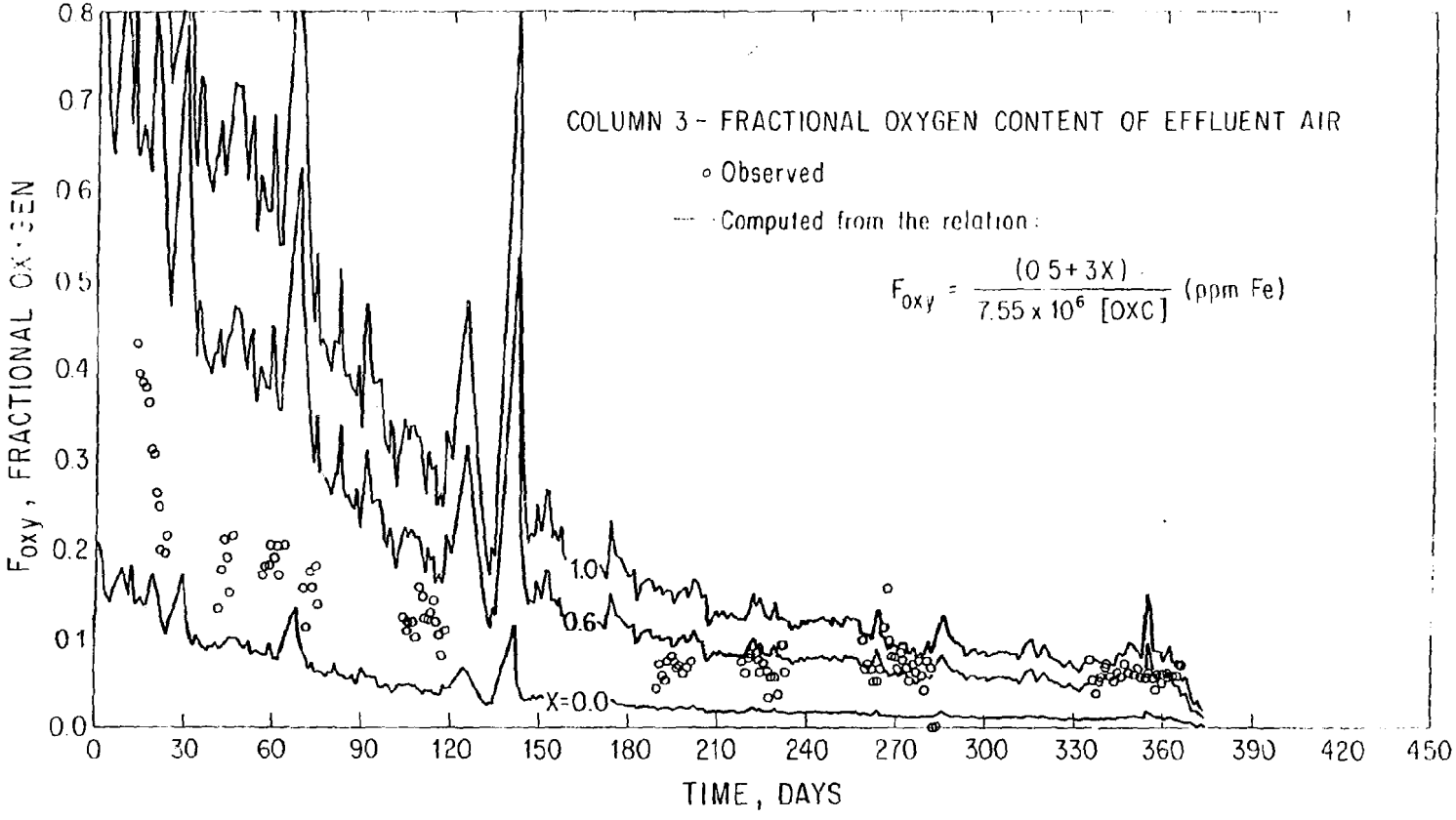

Figure 15 (continued)

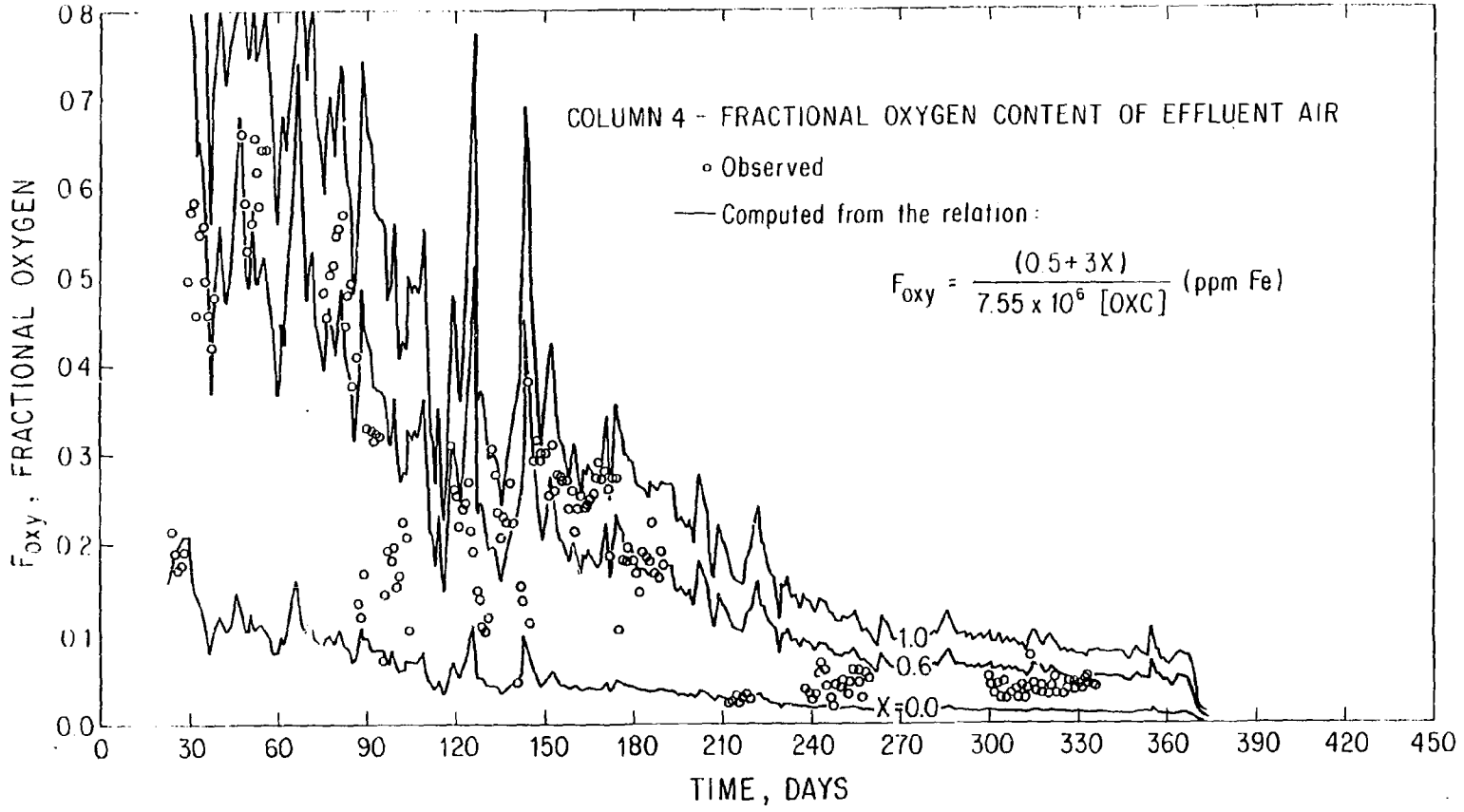

Figure 15 (continued)

Table 14 shows the calorific value of the coal actually increases as the result of leaching if computed on a Mmmf or Dry Basis. The Dmmf calorific value of the coal decreased slightly for most columns but increased for column 4. The increase in dmmf C.V. of Column 4 is physically impossible; the increase reflects the inaccuracy of the Btu determinations (Meyers, 1977. p. 111).

Literature review indicated we could expect about 2.5% coal oxidation of 3/8" coal particles at 50°C in a year (see appendix A). This translates to 3.2% oxidation of ¼" coal particles in one year at 50°C. The value of k_c used in this calculation was 3.5×10^{-11} sec^{-1}. Figure 15 shows less than 10% depletion of oxygen in the air passed through column 4 after a year of leaching. Table 17 shows the calculated oxygen depletion for Column 4 after 1 year for various coal oxidation rate constants. Depletions less than 10% require k_c values less than about 1×10^{-12} sec^{-1}. In the calculations that follow we use a value of 1.1×10^{-12} sec^{-1}. This gives a 0.17% coal oxidation for column 4, which is reasonable in light of the negligible measured Btu degradation of the coal (see Table 14).

Table 19 gives the best-fitting parameters for modeling of the column leach experiments.

4. The Distribution and Significance of Leached Rims

After sampling for chemical analysis as described in the preceeding section the entire packed bed of coal was cast with a plastic resin.[1] The core tube was coated with an aerosol releasing agent that facilitated its removal after the resin had set. The column was then cut into one-inch sections. Twenty of these sections from each column were polished on one side (surface area about 25 cm^2). For each polished block, one hundred coal fragments were examined microscopically and the fragments were classified as shown in the flow diagram of Figure 16. The distribution of totally leached, rimmed, voided, and unleached fragments is shown by the histograms in Figure 17. The types of leached rims are illustrated in Plate 2. The second photograph in Plate 2 illustrates the fact that the classification is not unique for any fragment. A fragment can appear unleached, rimmed, or totally leached depending on how it is sectioned.

[1]The Castolite Company, Woodstock, IL 60098

Coal Oxidation Constant, k_c (sec^{-1})	Oxygen Depletion of effluent air Column 4 predicted	Fraction Pyrite Leached	% coal oxidized
1.1×10^{-14}	4%	0.75	0.0029
1.1×10^{-13}	4%	0.75	0.025
1.1×10^{-12}	8%	0.75	0.17
1.1×10^{-11}	31%	0.75	0.96

Table 17 . Predicted oxygen depletion in the effluent air from Column 4 (after one year of leaching) for the best fitting model, and different values of k_c.

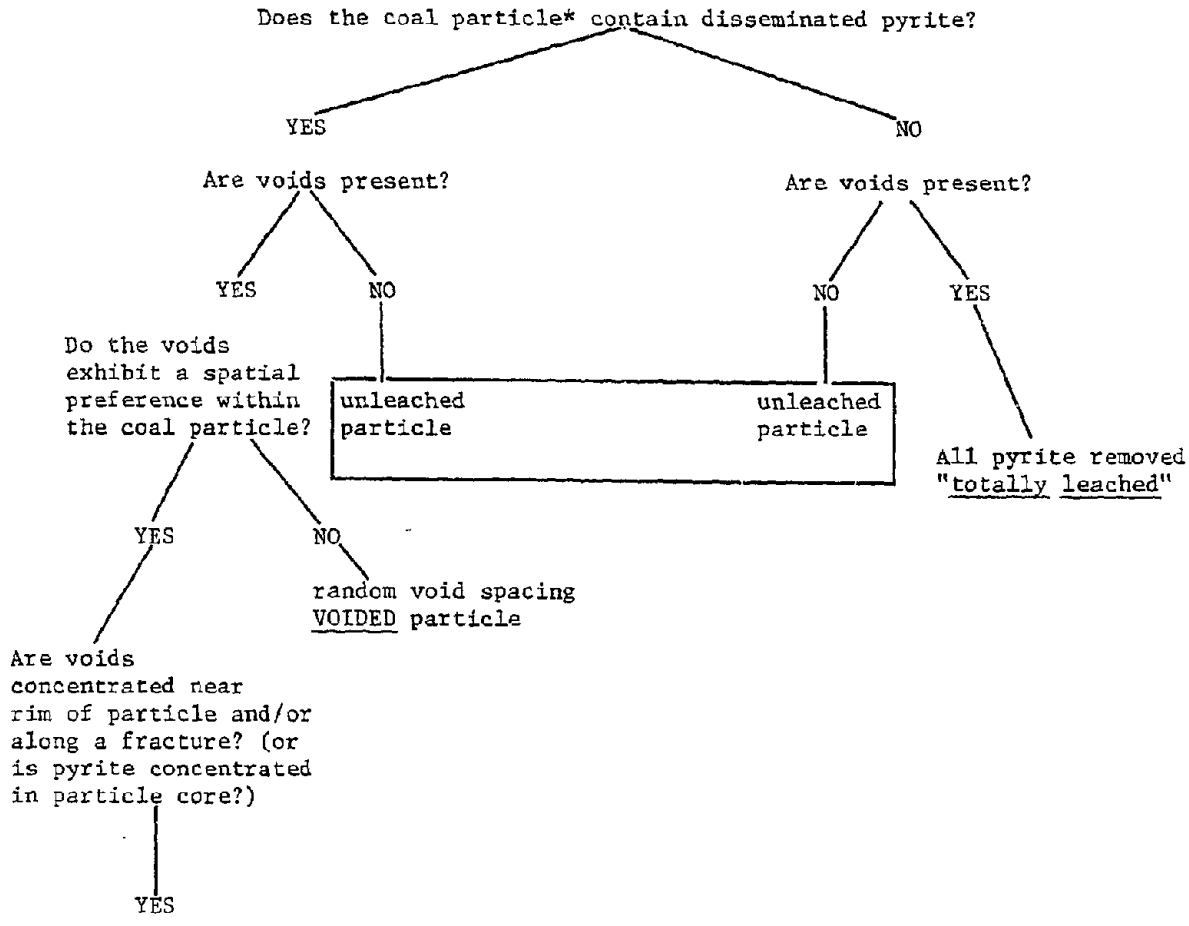

1. Measure thickness (width) of leached rim.
2. Measure thickness (width) of reaction zone.

* Particle refers to a sectioned coal fragment in the plane of the polished block surface. For each polished block, 100 coal particles were examined.

Figure 16 Classification Flow Chart Used for Microscopic Examination of Coal Particles Leached in the Column Apparatus.

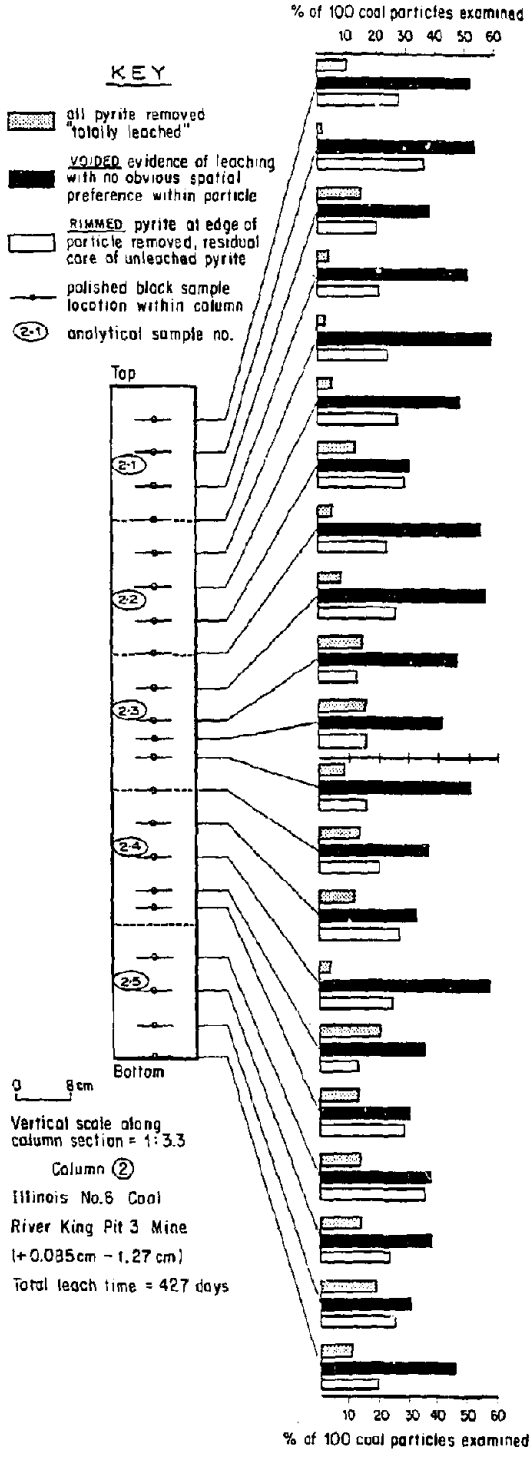

Figure 17a Frequency histograms of morphologic leaching types observed on polished coal samples taken from various levels within the coal column.

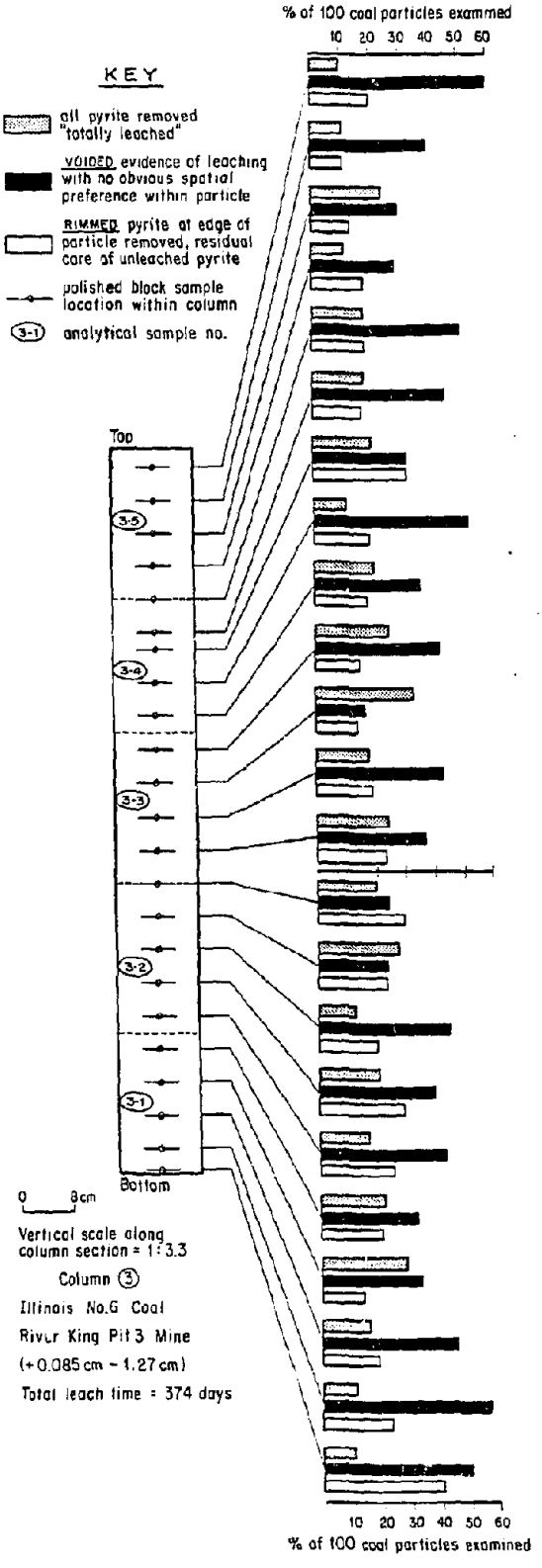

Figure 17b (continued)

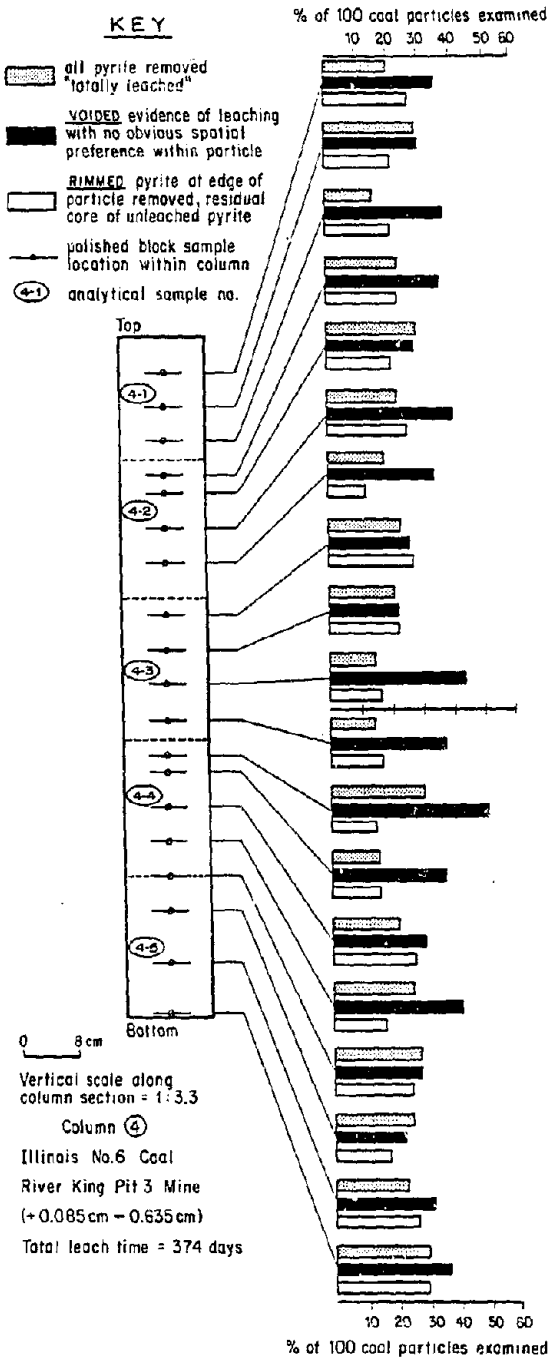

Figure 17c (continued)

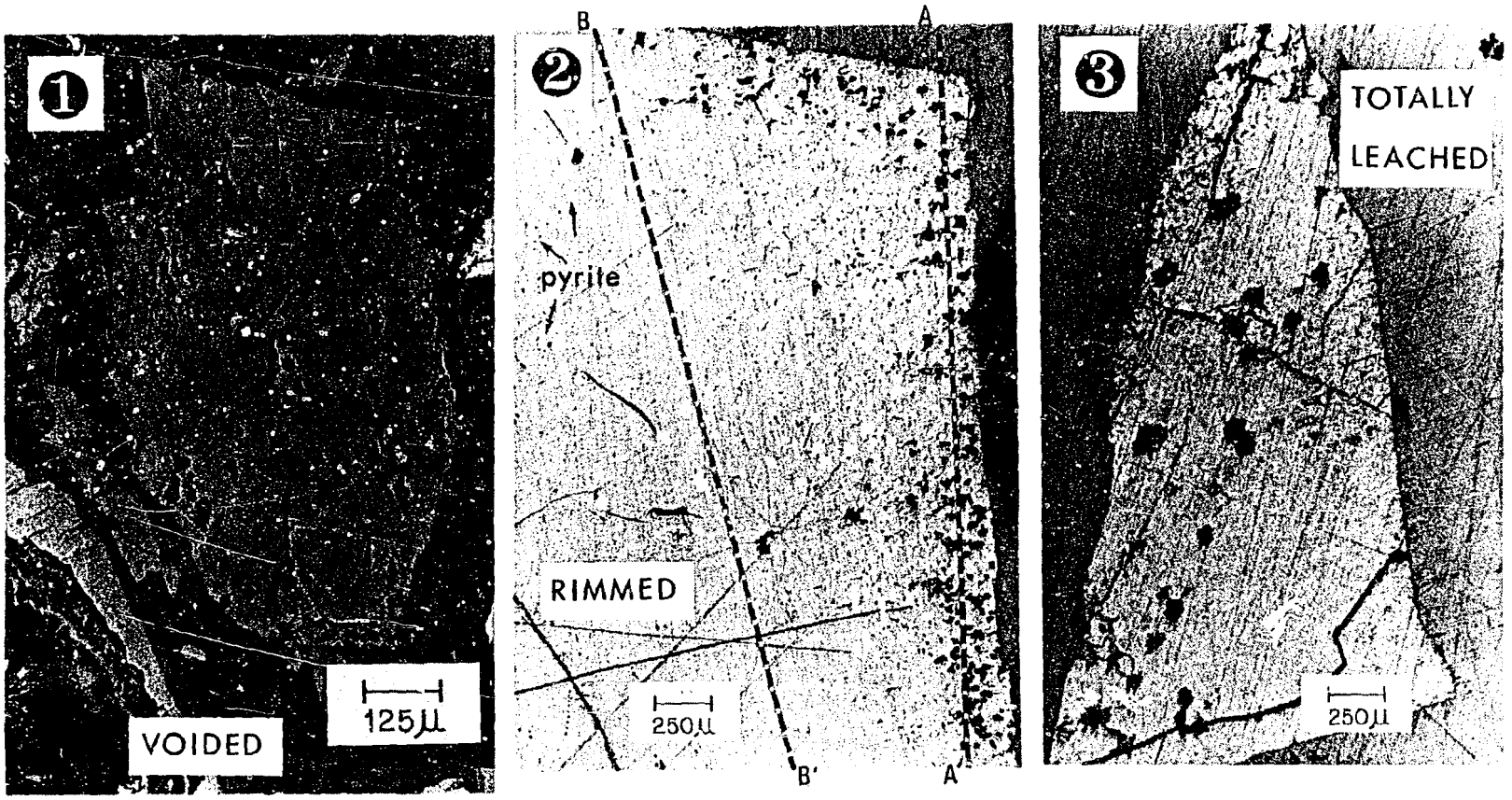

Plate 2 The three characteristic types of leaching morphologies: 1. voided, 2. rimmed, 3. totally leached.

The principle conclusions reached from petrographic analysis of the leached coal particles in the columns were:

(1) The columns were leached evenly along their length. Figure 17 indicates the proportion of rim types does not change along the columns.

(2) The percentage of fragments classified as "totally leached" increases from Column 1 to Column 2 to Column 3. This trend is consistent with that expected on the basis of temperature and fragment size.

(3) Rimming is a common phenomena. Columns 2, 3 and 4 contain 23%, 21% and 22% rimmed fragments, respectively.

(4) Leached rims are often of uniform thickness around a coal fragment. There is no evidence of diffusional anisotropy in the coal in many fragments (see Plate 3). On the other hand, the voided pattern may reflect inhomogeneities in D_E within other coal fragments.

(5) A variant of the uniform leached rim occurs when the pyrite is concentrated in certain bedding layers in the coal. The bedding-defined leached rim is still quite uniform. The nature of the pyrite in the bedding (euhedral or framboidal) does not influence the nature of the rim (see Plate 4a, b).

(6) The thickness of the actively leaching zone does not depend on the morphology of the pyrite (see Plate 5a, b).

(7) The thickness of leached rims vary from 100 to 500 μm in all three columns (see Figure 18).

(8) The thickness of active leaching zones varies from 50 to 150 μm (see Figure 19).

(9) Fractures in the coal can allow leaching of fragment interiors. (see Plate 6a, b).

Table 18 shows the observed leached rim thicknesses suggest k_{ox} and a^R_{sulf} are on the high side of their range of values, and D_E on the low end of its range (i.e. less than 1×10^{-8} cm^2/sec). The thick leaching zone observed on the column fragments is consistent with the slow observed leaching of the columns compared to the kettles. Pyrite oxidation is zero order in Fe(III). The diffusive flux of Fe(III) into the coal is proportional to the concentration of Fe(III) surrounding the coal fragments, however. Thus equation (5) should really have a term [Ox], in the numerator and denomenator. The denomenator product, [Ox] k_{ox} is a constant (the pyrite reaction is zero order). Therefore δ is proportional to the square root of

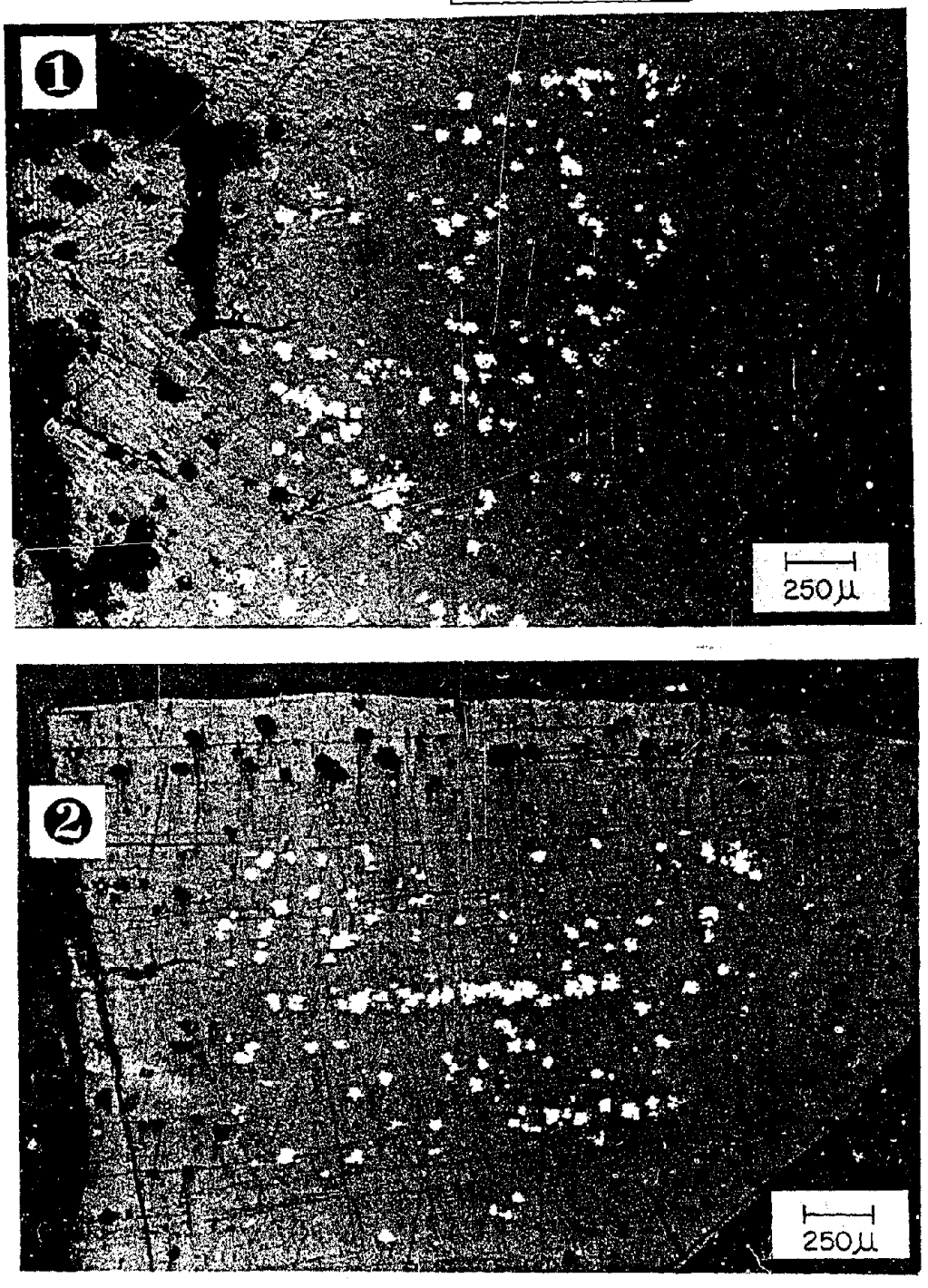

Plate 3 Lozenge or doughnut-shaped symmetric leached rims formed in: 1. homogeneous vitrinite matrix, 2. banded vitrinite matrix. The coal was leached in Column 4.

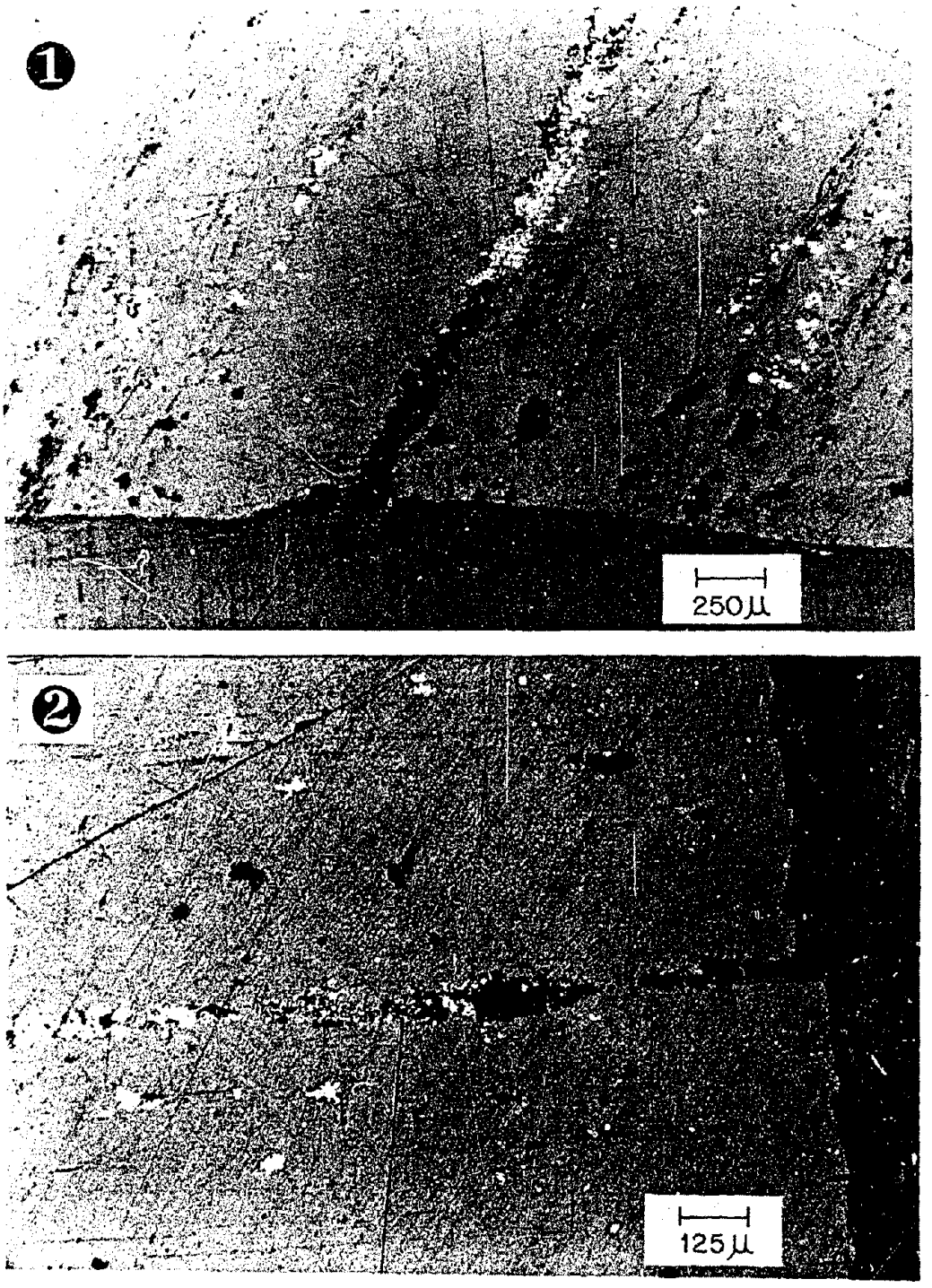

Plate 4a Leaching morphologies characteristic of pyritic material concentrated in bands or along bedding planes in the coal matrix. These examples show concentrations of fine-grained pyrite aggregates (non-framboidal). 1. Coal leached in Column 3, 2. Coal leached in Column 4.

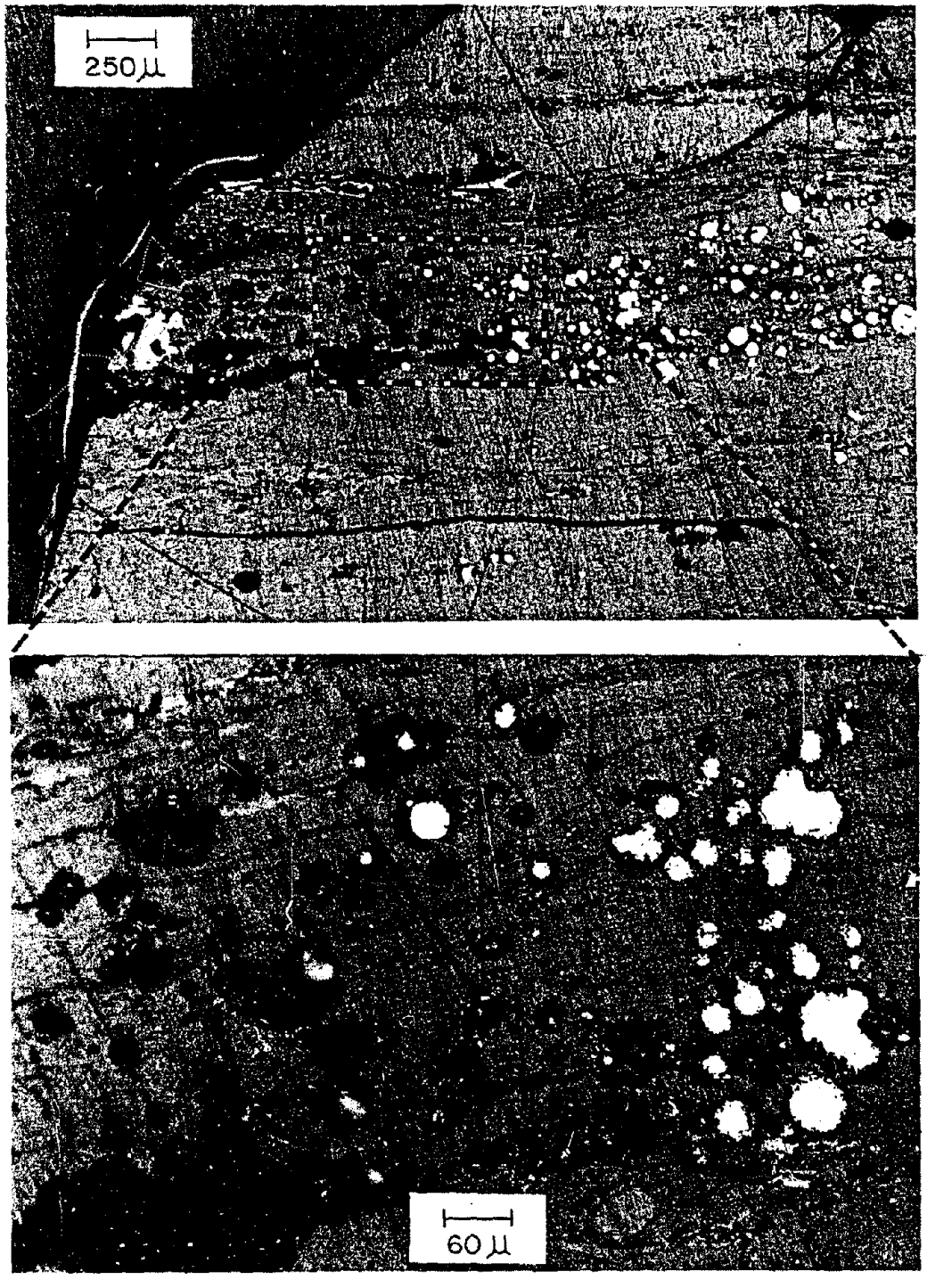

Plate 4b Leaching morphologies characteristic of pyritic material concentrated in bands or along bedding planes in the coal matrix. This example shows fine-grained framboidal pyrite aggregates disseminated in coal that was leached in Column 4.

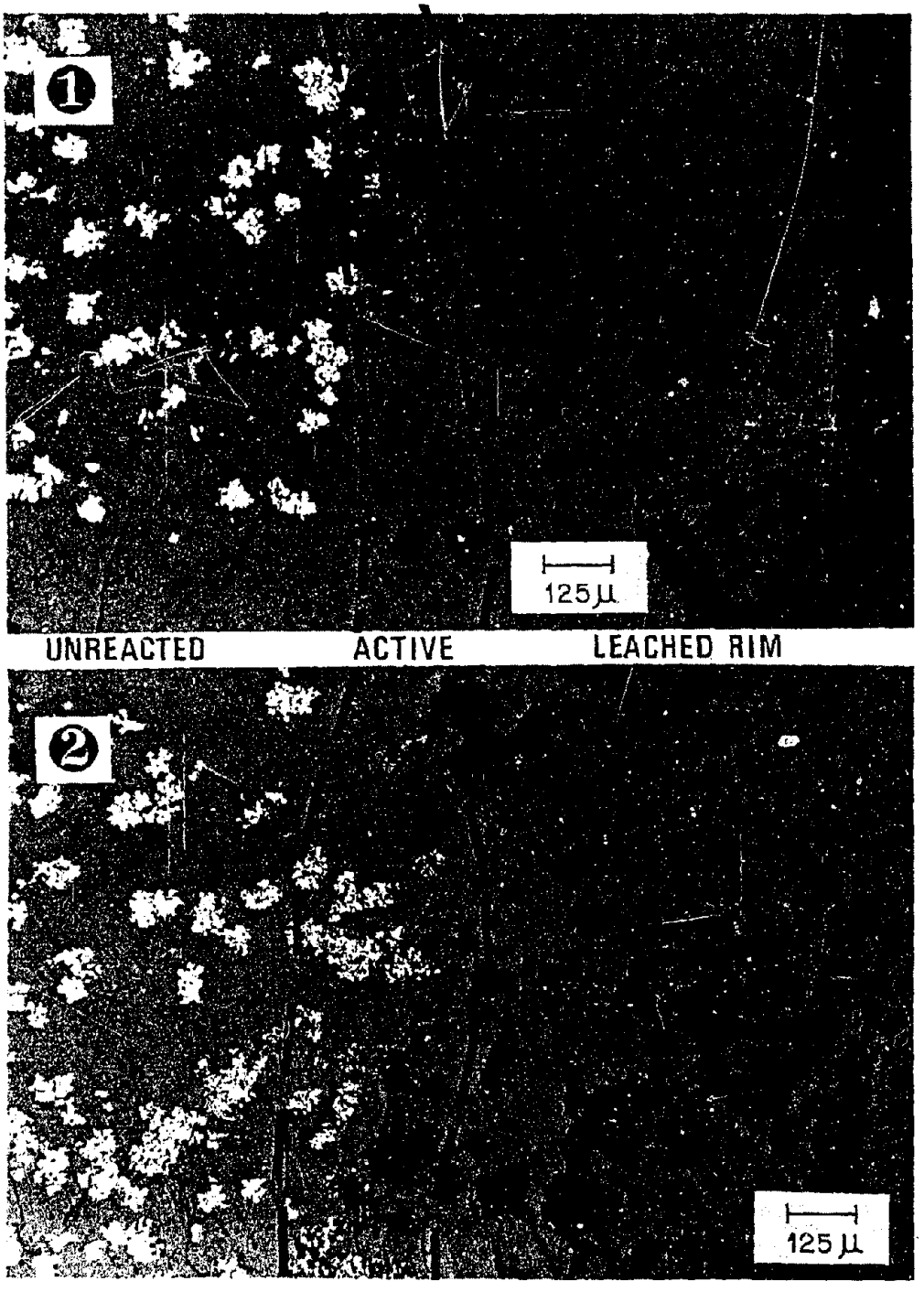

Plate 5a Rimmed edges of coal particles that illustrate the three characteristic zones of leaching. Both examples 1. and 2. were leached in Column 4.

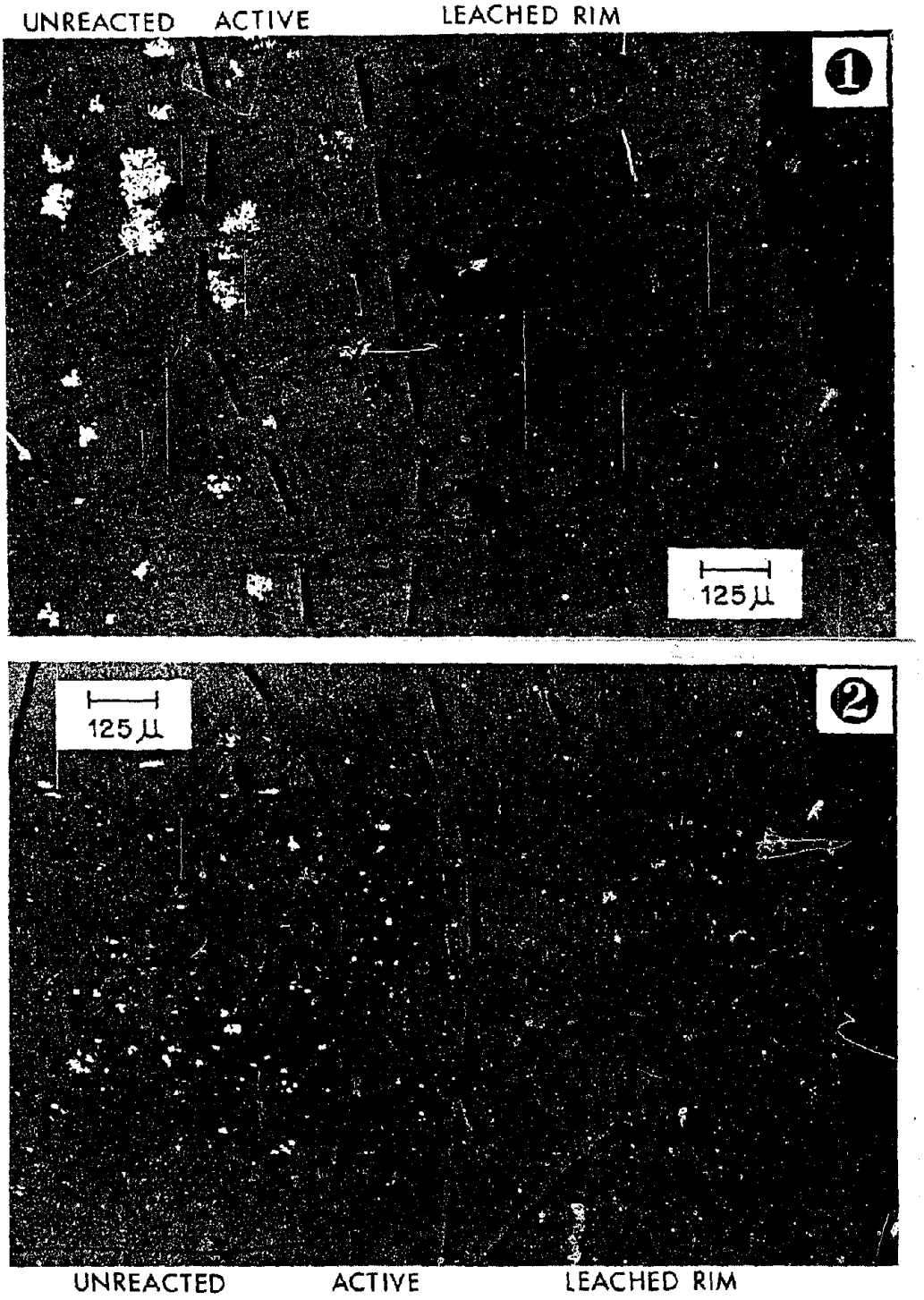

Plate 5b Rimmed edges of coal particles that illustrate the three characteristic zones of leaching and non-selective leaching of different pyrite morphologies. 1. mossy pyrite crystal aggregates, 2. fine-grained euhedral pyrite. Both examples are from Column 4.

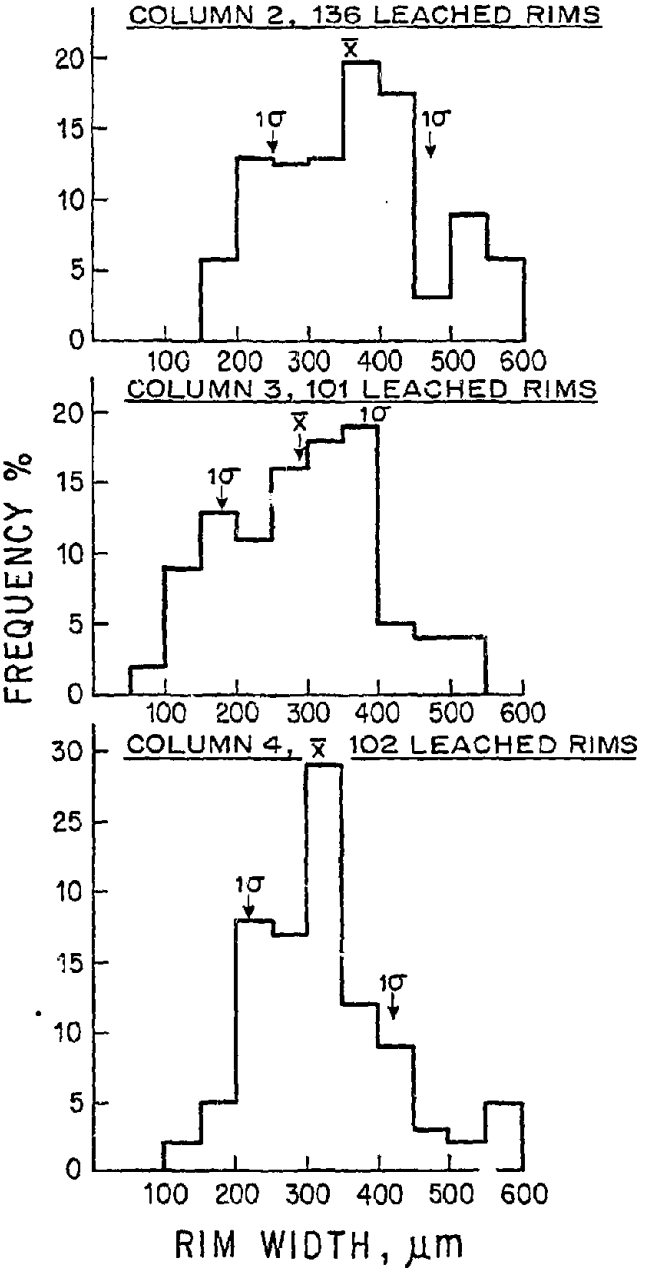

Figure 18 Thickness of leached rims on coal fragments from the three Illinois coal columns

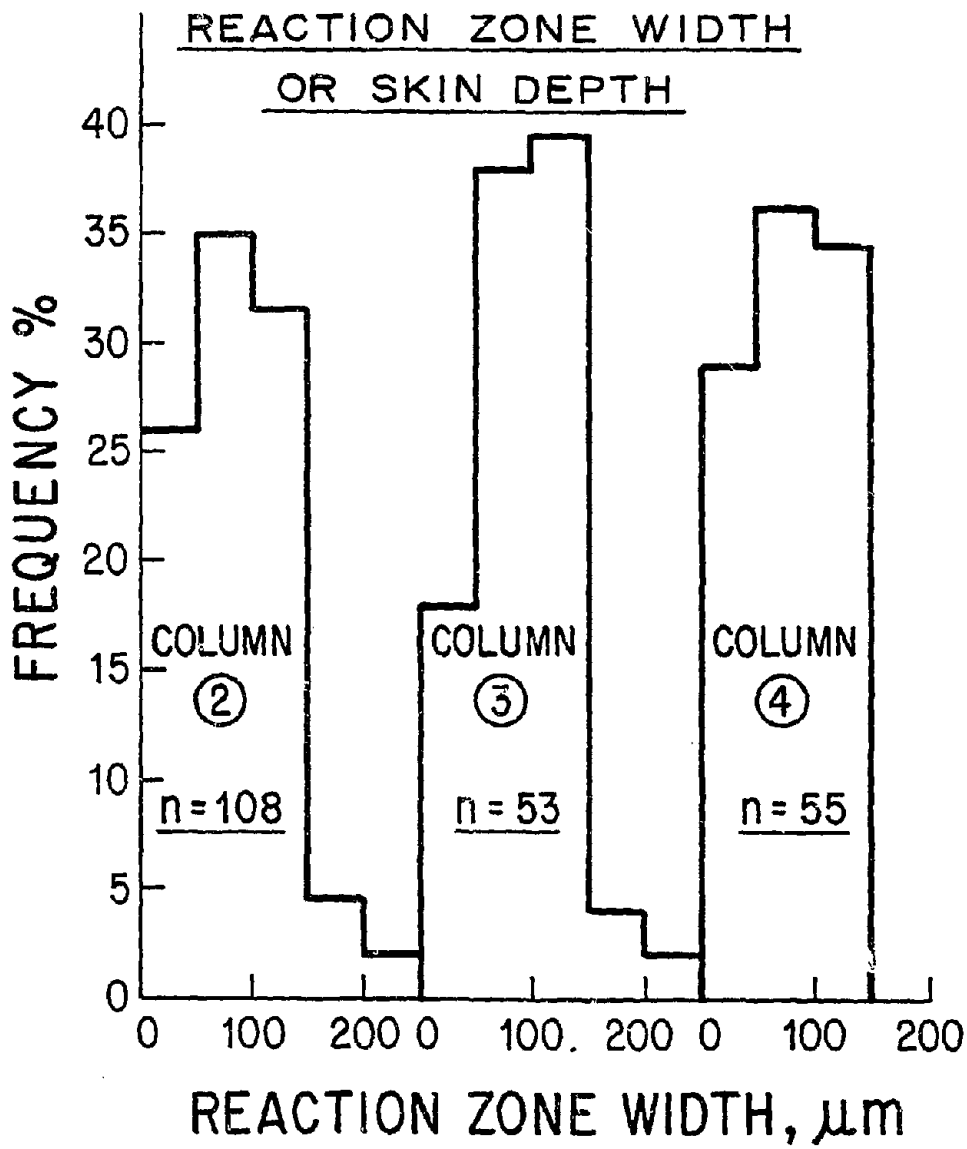

Figure 19 Frequency histograms for width of the zone of active chemical leaching as measured on Illinois #6 coal particles leached in the column apparatus

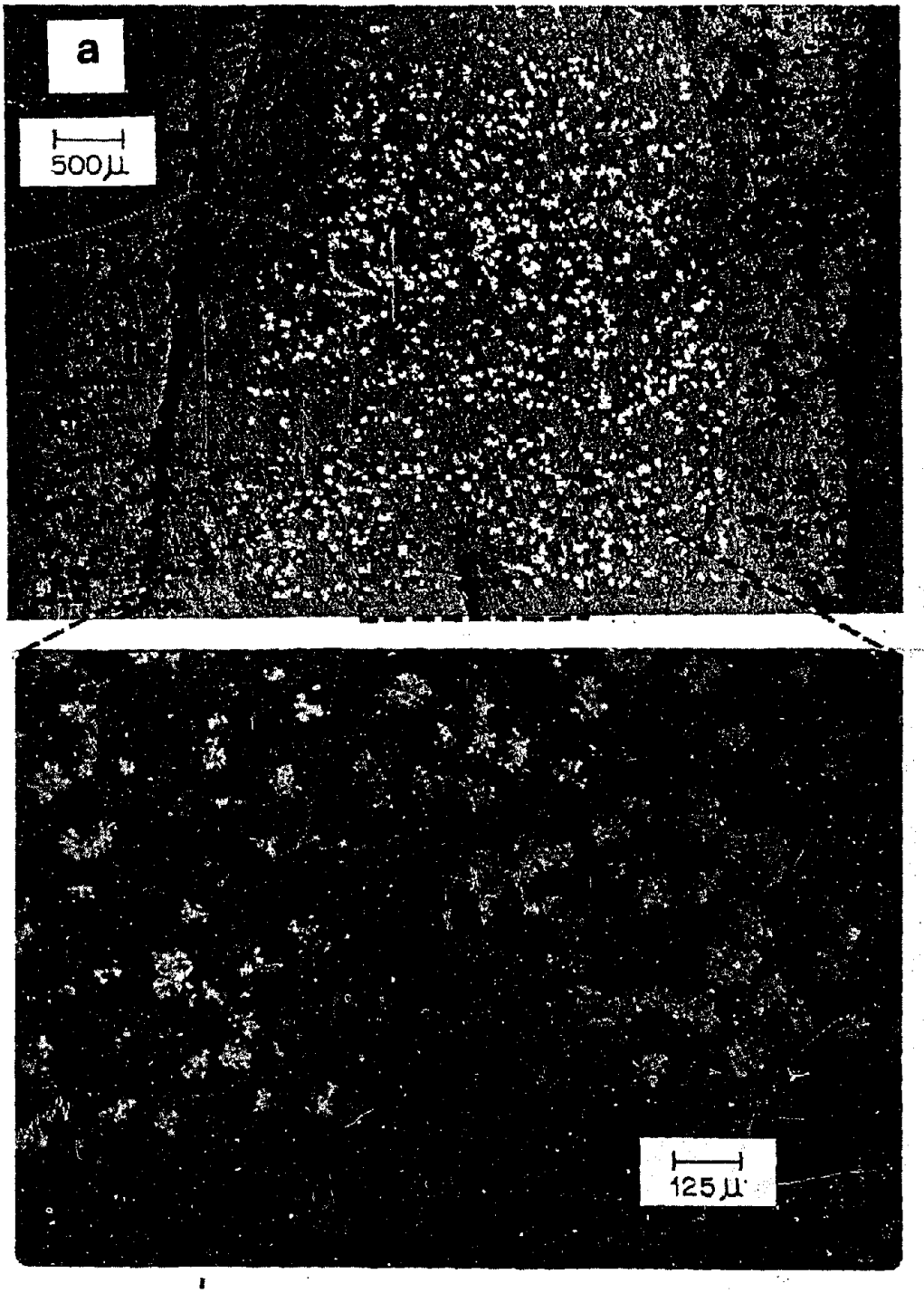

Plate 6a Coal particle containing abundant disseminated pyrite that occurs as mossy or flowery crystal aggregates. Leaching is controlled by the formation of a symmetric leached rim and by leaching along a fracture in the coal matrix (see enlarged portion of photomicrograph). This coal particle was leached in Column 4.

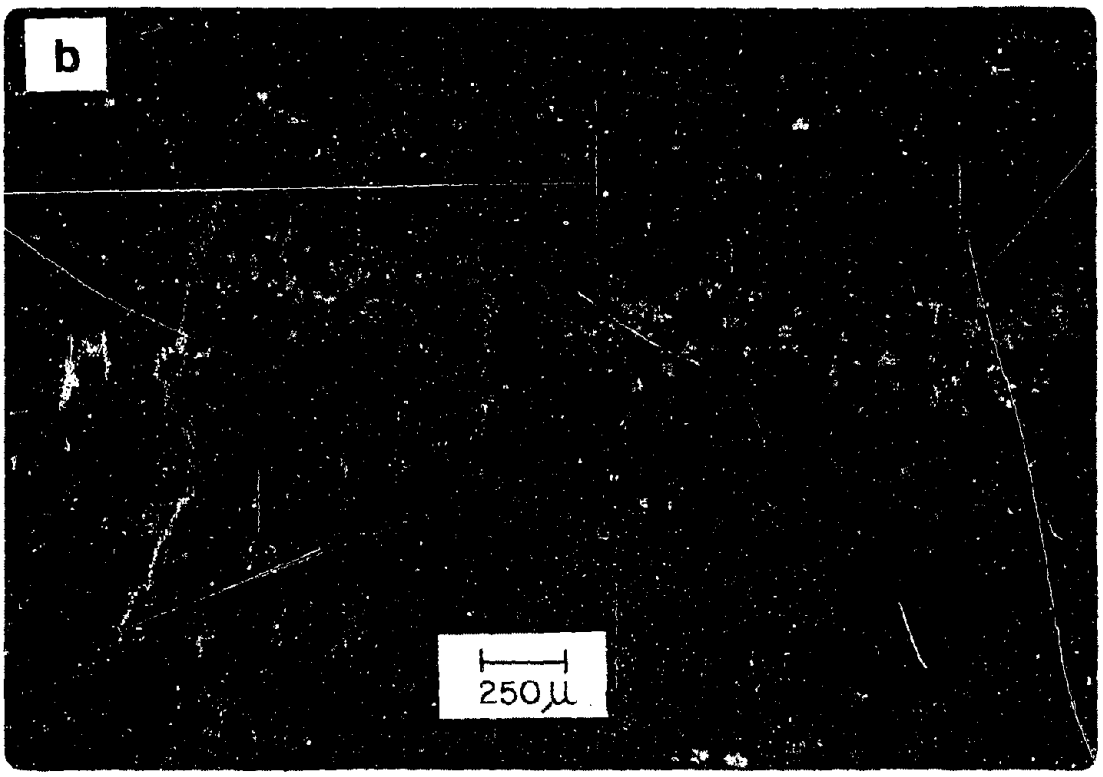

Plate 6b Example of fracture-controlled leaching of pyrite at the core of an otherwise unleached coal particle. Coal leached in Column 2.

T[°C]	Leached Rim Thickness, 2δ $k_{ox} = 10^{-7}$	$k_{ox} = 10^{-6}$
35	422 μm	204 μm
50	204 μm	61 μm

Table 18. Calculated 2δ values assuming $D_E = 1 \times 10^{-8}$ cm^2/sec, $k_{ox} = 10^{-7}$ or 10^{-6} cm/sec, $a^R_{sulf} = 100$, $\delta = \sqrt{D_E / k_{ox} a^R_{sulf}}$.

Fe(III). The value of D_E determined from the rate of leaching of the columns and the thicker active leaching zone is consistent with a ferric iron concentration in the columns 7.5 times less than in the kettle experiments (or 0.18 g/l rather than 1.4 g/l Fe(III), see Table 8). The lower concentration of Fe(III) in the columns is reasonable since the columns were flushed with acidified water that contained no iron.

The lack of dependence of leached rim formation on pyrite type is important and a direct reflection of diffusion control. Under diffusion control, it is the effective diffusional porosity of the coal and the concentration of Fe(III) in the columns that controls the rate of leaching, not the morphology or trace element chemistry of the pyrite. Framboidal pyrite will not leach faster than euhedral pyrite because the rate of leaching of both is controlled by the diffusional characteristics of the coal.

Reasons for the voided pattern are not clear. It may be that there are two kinds of coal from a leaching point of view: In one, the shrinking core model is entirely appropriate and leached rims develop with time. In the other, inhomogeneities in the diffusional properties of the coal cause an erratic pattern of leaching (voided morphology). So long as the rate of leaching in these fragments is diffusion controlled the leach rate should decline in a fashion similar to the shrinking core predictions, however. In this view the voided pattern is a reflection of inhomogeneities (due to fractures or bands of high D_E in the coal) of the effective diffusion constant in the coal matrix. The path of oxidant diffusion is difficult to recognize but diffusion still controls the leach rate.

Figure 17 indicated that about 25% of the fragments are unleached. If this is not an artifact of the sampling, it raises the possibility the ultimate removal of pyrite may be less than 100% (because some of the coal fragments will not leach).

5. Summary and Conclusions

The column leach tests generally confirm the shrinking core leach model developed and calibrated from literature studies, basic physical measurements, and the kettle experiments. The kettle experiments confirmed the appropriateness of the temperature dependence of the model ($E_C^* = 20{,}000$ cal/mole, and $E_D^* = 5000$ cal/mole), the measured effective diffusion constant

(D_E = 7.5 x 10^{-8} cm^2/sec), and the stoichiometric leach constant (X = 0.6). The kettle experiments suggested a^R_{sulf} and k_{ox} are at the high end of their measured and literature-suggested ranges (a^R_{sulf} = 100 cm^{-1}, k_{ox} = 1.5 x 10^{-6} cm/sec). Leached rims on coal fragments from the kettle experiments confirmed diffusion control of the leaching process. The column results confirm diffusion control: leach rims are present on a significant fraction of the coal fragments. The column experiments weakly confirm the appropriateness of the stoichiometric constant and temperature dependence of leaching.

The columns leached much more slowly than expected on the basis of the kettle experiments, however. The increased leach time is due to τ_D values an order of magnitude bigger than expected. This is illustrated by the leach behavior of Column 4 compared to kettle Run B. These two experiments employed the same size fraction coal (¼ inch) and were run at similar temperatures (50° and 40° respectively). Table 10 shows τ_D was predicted to be about 6.9 months for the kettle run, and was determined by analysis of the leach results of that run to be about 4.0 months. The temperature adjustment from 40 and 50°C for an activation energy of 5000 calories/mole is 1.28, so a value of 6.9/1.28 or 5.4 months was anticipated for τ_D of Column 4. Table 16 shows the observed τ_D was in fact about 61 months. This analysis used a time-axis-shift to convert iron leaching to pyrite leaching. Direct analysis of the pyrite leach curves using a finite difference model of the column leaching confirmed that D_E is about an order of magnitude smaller than the value estimated from the connected porosity, a few direct measurements, and the kettle experiments. The much smaller thickness of the active leaching zones in the column experiments (50 to 150 μm vs. ~650 μm for the kettle experiments) suggests $D_E[ox]$ is smaller than anticipated and $k_{ox}[ox]$ = const. A simple explanation of both observations is that the ferric iron concentration in the columns, that were flushed twice daily with acidified water containing no iron, was a factor of 7.5 less than the 1.4 g/l Fe(III) concentrations in the kettle experiments. The lower ferric iron concentration would explain both the slower leaching of the columns and the thicker active leaching zones in the coal fragments from the column experiments. This inference suggests the columns could have been leached much more rapidly had the iron-rich effluent solutions been recirculated rather than using fresh water for each flush.

The shrinking core model parameters that successfully simulate the column leaching results and that we shall use to predict the leaching of pyrite from coal heaps are summarized in Table 19. The rate of leaching implied by these parameters is very conservative since we take no credit for the much faster leaching that should result from the recycling of iron-rich effluent solutions back through the heap as would be done in any industrial process.

F. Predicted Performance of Coal Heaps

Now that appropriate values of the model parameters have been determined, the mathmatical model presented in section II-B may be used to predict how coal heaps will leach. These predictions are made by converting the mathematical model to finite difference form. The heap is divided into 150 layers and the model equations solved using an implicit finite difference method as described by Cathles and Apps (1975) (see also Appendix F). The heap leaching model of necessity contains several parameters not used thus far: Ambient temperature varies in a yearly cycle. This affects the temperature of the dump and the rate of pyrite leaching. The yearly temperature cycle is taken into account in the model. The average ambient temperature is assumed to vary between 72°F in the hottest summer month and 20°F in the coldest winter month. This is appropriate for the coal areas of Pennsylvania. Application of flush water to the heap is important in controlling heap temperature. Cooling by applied flush solutions is accounted for. The rate of air convection through the heap is controlled by the permeability and temperature of the heap. We calculate permeability from the Blake-Kozeny equation (equation 17). This permeability is certainly too large since account is not taken of fines in the coal heap. It may very well be that air will have to be blown through real field heaps; the heap permeability may not be sufficient for natural convection to provide an adequate supply of oxygen. Finally, real coal heaps will tend to heat up to temperatures above those optimum for bacterial conversion of Fe^{2+} to Fe^{3+}; the bacterial term in equation (2) must be included in the model as work on copper leach dumps so compellingly indicates. As in the copper leaching case we adopt values of $T_{sick} = 55°C$ and $T_{kill} = 65°C$ in our modeling. Heaps were not permitted to get hotter than 90°C. The

D_E	Effective diffusional porosity of coal	1×10^{-8} cm^2/sec
$k_{ox}a^R_{sulf}$	Product of first order rate constant and surface area of pyrite per unit volume of coal	10^{-4} sec^{-1}
X	Stoichiometric constant	0.6
k_c	Constant characterizing the rate of of oxidation of coal	10^{-12} sec^{-1}
E^*_C	Activation energy for pyrite oxidation	20,000 cal/mole
E^*_D	Activation energy for diffusion of oxidant through the coal matrix	5,000 cal/mole
E^*	Activation energy of coal oxidation	12,000 cal/mole

Table 19. Parameter values used to simulate column and heap leaching.

disseminated pyrite content of the heaps was assumed to be 1.7 Wt % (or 0.91% pyritic sulfur). To take into account the expected benefits of solution recirculation (higher iron levels) we calculate heap performance for both $D_E = 0.75 \times 10^{-7}$ and 0.10×10^{-7} cm^2/sec.

The predicted leaching of dumps of various heights operated under various average irrigation rates are given for two different size fractions of coal in Figure 20. Coal companies we have contacted indicate that 9 months is the longest period which coal could be inventoried, so the figures show the predicted disseminated pyrite removal in 9 months. Heap operation is assumed to begin in June.

Figure 20 shows the extraction of dissiminated pyrite from a heap is strongly dependent on the height of the heap and irrigation rate. The problem is really that of regulating temperature within the heap. If the heap gets too hot, bacteria cease to regenerate Fe(III) within the heap and the leaching rate is diminished. Temperature in heaps less than 15 ft in height can be most effectively regulated in the optimum range. Heaps less than 5 to 8 ft in height cool too much in winter. Coal fragment size also exerts a very important control on leach rate. Heaps about 11 ft in height constructed of ½ inch coal fragments will leach in an optimum fashion, for $D_E = 0.1 \times 10^{-7}$ cm^2/sec (single pass solution flush). Heaps 8 ft in height (¼" coal) will leach best for recirculated solution.

Table 20 shows the history of leaching of the better-performing dumps. Winter cooling of the 5 ft coal heap containing 1/4" particles is evident. The extra iron added to the recirculated flush solutions must be removed before the solution is recirculated to the heap (see Figure 1).

Table 21 summarizes the process steps involved in depyritizing coal by heap leaching. A power plant burning a million tons of coal per year can reduce the sulfur content of the coal burned by about 57% if heap leaching is employed in conjunction with conventional coal cleaning. We assume the plant uses Illinois #6 coal that contains 4.7% total sulfur. The processes summarized in Table 21 would reduce the sulfur content of the coal to about 2.8%.

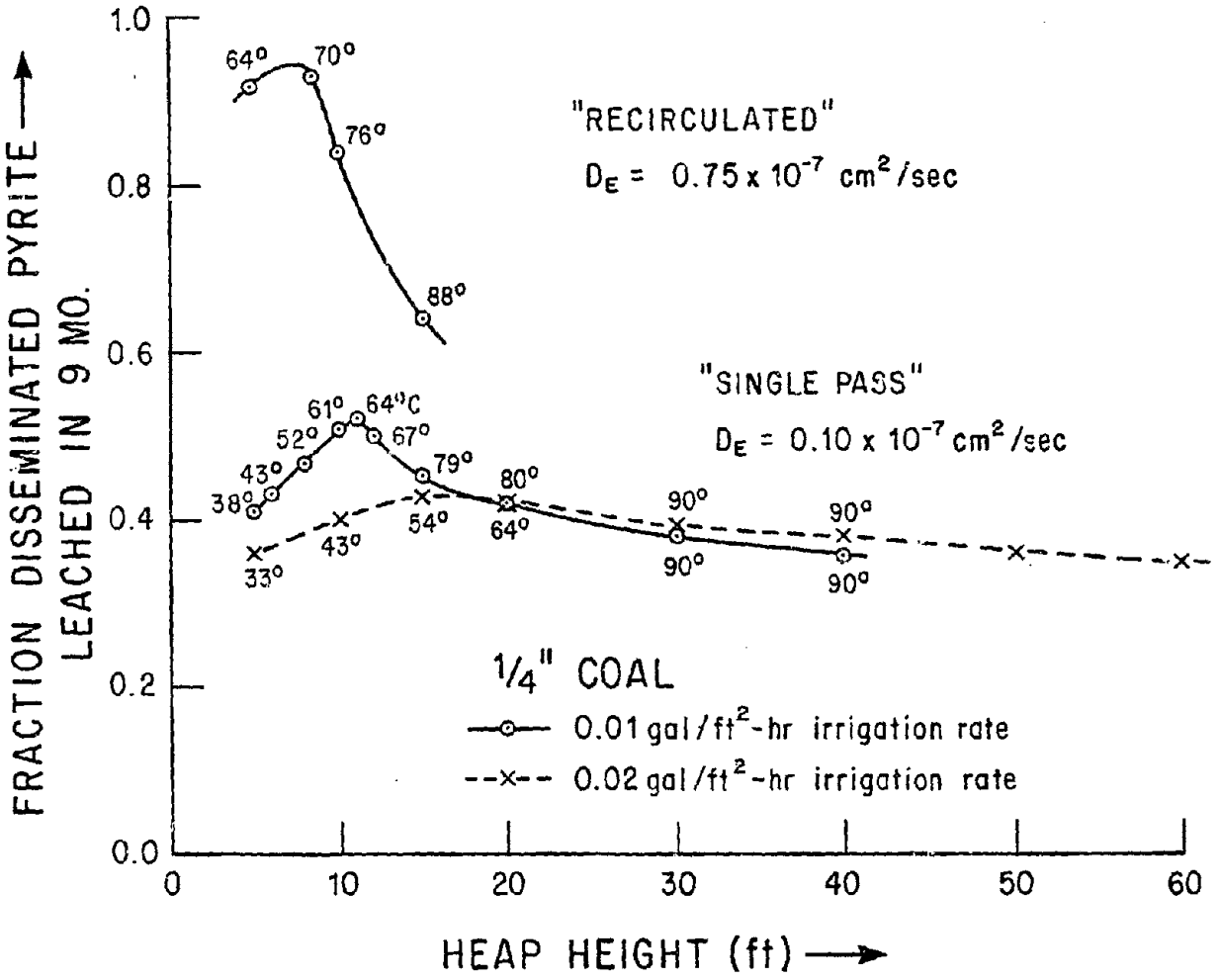

Figure 20a Fraction coal pyrite leached in 9 months as a function of heap height, irrigation rate, and iron levels in the flush solution (simulated through D_E). Recirculated solutions are assumed to have Fe(III) loadings of about 1 g/l. Maximum temperature attained by the heaps in the 9 months of leaching are shown along the curves.

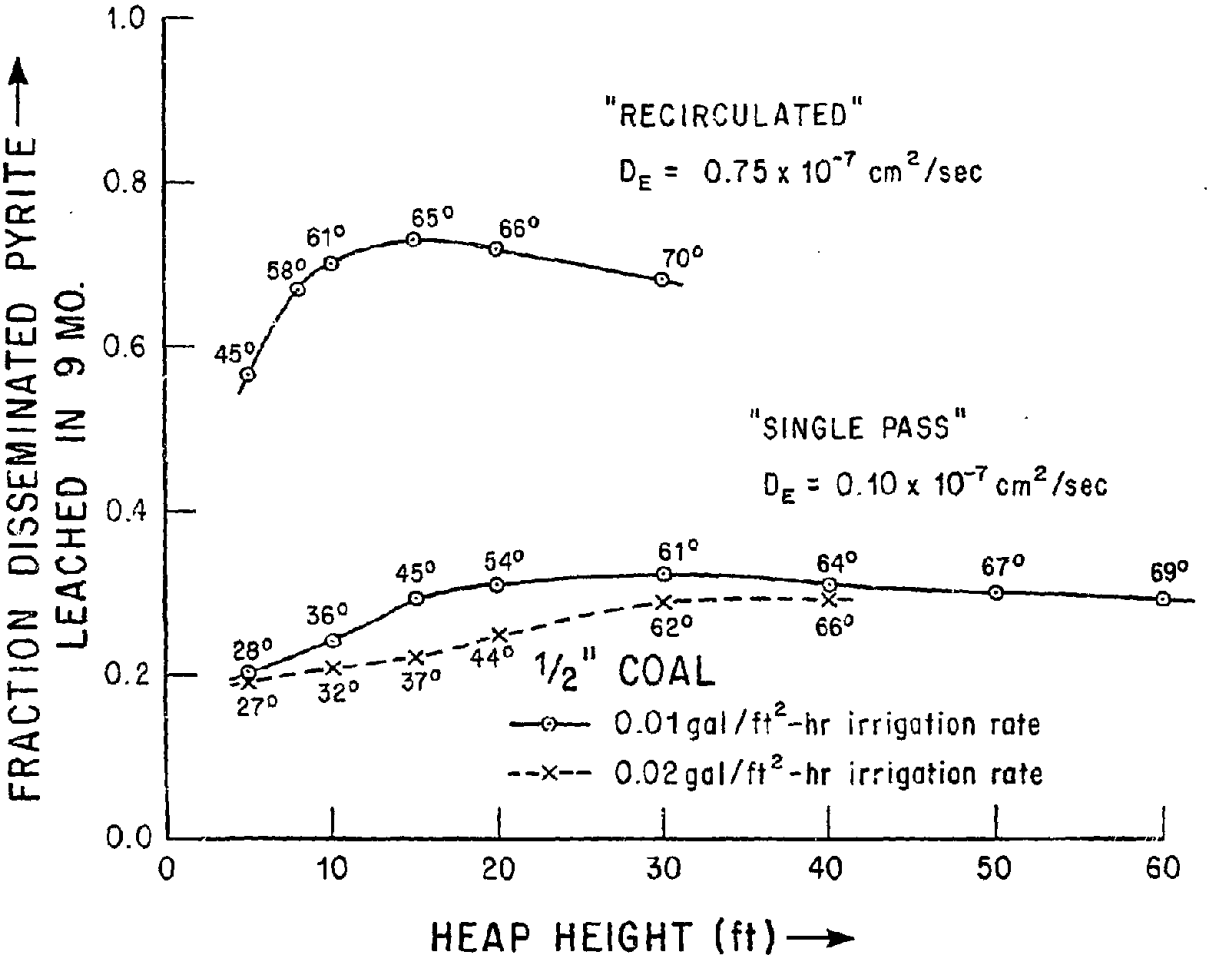

Figure 20b Same as 20a but for 1/2-inch rather than 1/4-inch coal

	11 foot heap ¼ inch coal $D_E = 0.1 \times 10^{-7}$				5 foot heap ¼ inch coal $D_E = 0.75 \times 10^{-7}$				8 foot heap ¼ inch coal $D_E = 0.75 \times 10^{-7}$				15 foot heap ½ inch coal $D_E = 0.75 \times 10^{-7}$			
Month	Fxp	T_{max}	ΔFe g/ℓ	Pxc	Fxp	T_{max}	ΔFe g/ℓ	Pxc	Fxp	T_{max}	ΔFe g/ℓ	Pxc	Fxp	T_{max}	ΔFe g/ℓ	Pxc
July	0.097	38°	20	.0014	0.39	63°	17	.0085	0.2	60	43	.0026	0.23	54	37	.0036
Aug	0.23	51	13	.0091	0.58	62	9.0	.039	0.46	70	8.3	.039	0.36	64	14	.021
Sept	0.31	61	8.2	.023	0.72	58	7.6	.056	0.53	69	6.6	.072	0.44	62	14	.033
Oct	0.36	64	5.1	.044	0.82	44	3.6	.066	0.61	65	7.3	.100	0.51	58	12	.043
Nov	0.40	63	4.4	.064	0.87	23	1.5	.068	0.70	64	7.7	.120	0.58	54	9.5	.049
Dec	0.43	61	4.3	.080	0.89	9	0.9	.069	0.78	62	7.4	.140	0.63	49	7.2	.054
Jan	0.46	58	4.2	.090	0.90	3	0.7	.069	0.85	58	6.4	.150	0.66	46	5.9	.058
Feb	0.50	53	3.4	.098	0.91	2	0.6	.070	0.91	47	3.1	.160	0.70	43	5.0	.061
Mar	0.52	42	2.5	.100	0.92	7	0.7	.070	0.93	32	1.6	.160	0.73	41	4.5	.064
12 mo	0.57	22	2.1	.110									0.80	42	3.8	.072
22.7 mo	0.69	17	1.2	.110									0.93	23	1.0	.094

Table 20 Leach history of the better-performing heaps. Fxp is the fraction pyrite leached, T_{max} is the maximum temperature in the heap at the time indicated, ΔFe is the iron added to the flush solutions in grams per liter, Pxc is the precent coal oxidized. The average flush rate is 0.01 gal/ft^2-hr, $k_{ox}a^R_{sulf} = 10^{-4}$ sec^{-1}, and $k_c = 1.07 \times 10^{-12}$ sec^{-1} in all cases.

	Process Step	Basis
I.	Mine 10^6 tons ofcoal with 4.7% total sulfur and 2.4% pyritic sulfur.	Table 4
II.	Size to 1/4" and remove cleat pyrite by mechanical means; coal now contains 0.91% disseminated pyritic sulfur (or 1.7% pyrite).	Estimate of mechanical benefication based on column analyses, see Table 11.
III.	Pile coal in 8 ft heaps. If the pile porosity is 20%, the coal will occupy a 3.2×10^5 m^2.	
IV.	Circulate water through the heap. At 0.01 gal/ft^2-hr (1.8×10^{-3} gal/m^2-min), a solution recirculation rate of 657 gpm is required.	
V.	Remove $FeSO_4$ added by pyrite oxidation and leaching from the heap effluent. If 92% of the disseminated pyrite is leached, the average $FeSO_4$ added to the flush solutions will be 32 g/l and 39,500 tons of $FeSO_4$ must be dispcsed of.	
VI.	After treatment, coal that initially contained 4.7% sulfur will contain 2.35% sulfur (0.07% pyritic and 2.28% non-pyritic).	We assume S^o is oxidized to SO_4^{2-} and removed from heap.

Table 21 Process Elements of Depyritization of Coal by Heap Leaching

III. THE ECONOMICS OF DEPYRITIZATION OF COAL BY HEAP LEACHING*

A. Introduction

In this section we estimate the cost benefit of depyritizing coal by heap leaching assuming an 8' coal heap will leach as predicted in Table 20 and assuming the predicted benefits of recirculation of the solutions applied at an average rate of 0.01 gal/ft^2-hr are realized (ie. that $D_E = 0.75 \times 10^{-7}$). The reader should realize that our objectives here are very limited and many economic questions remain unaddressed and unanswered. Our main interest is to provide some basis for assessing whether or not further research on coal depyritization by heap leaching is warranted. If the process looks as though it could be economically attractive, then funding of further research in this area would be desirable. It should be also pointed out that the next stages of research will be considerably more expensive because the next steps will almost certainly entail construction and operation of a test heap.

Our analysis is one of incremental cash flow. We assume heaps will be constructed and operated at the electric generating facility, although the process could be carried out at or near the mine. The incremental analysis considers the net costs and benefits of leaching local high-sulfur coal rather than buying non-local low-sulfur coal. The incremental analysis considers the extra costs and benefits associated with the use of leached high-sulfur as opposed to transported low-sulfur coal. We consider the case (shown in Table 21) of a moderate size facility that consumes one million tons of coal per year. Twenty years is chosen for the life of the project; there is no salvage at the end of 20 years. The inventory in the leach heap is used to reduce the amount of high-sulfur coal purchased in the final year.

The difference in cost between distant low-sulfur and local high-sulfur coal (delivered to the site) is treated as a variable in the analysis. Base case values of $40/ton (delivered) for low-sulfur coal and $30/ton (delivered) for high-sulfur coal appear reasonable (U.S. Dept. of Energy, 1982).

---

*The economic analysis was carried out by Mr. William T. Barton, a Ph.D. candidate in the Mineral Economics Department, College of Earth and Mineral Sciences, The Pennsylvania State University.

Other assumptions made in the analysis are:

(1) No inflation; the analysis was done in 1983$.

(2) The first major category in a cash flow is typically labeled 'Revenue'. In this incremental analysis, the comparable category labeled 'Net Savings' is calculated as follows:

[Price(low-S) * Quantity(low-S)]
- [Price(high-S) * Quantity(high-S)]

(3) The normal 30-60 day coal inventory for utilities is neglected. The presence of leach heap inventory should reduce (maybe eliminate) this inventory which would reduce costs and thus increase net cash flow.

(4) Specific cost assumptions not obvious from the cash flow in Table -22 are as follows:

(a) Coarse circuit cleaning costs are $1.70/ton.

(b) Salaries and overhead are assumed for 4 laborers and 2 professionals.

(c) Although recycling occurs, it is assumed that water replacement costs are $0.01/kgal of total water used yearly.

(d) A cost of $0.005/gal is assumed for water treatment.

(e) The amount of iron sulfate removed will vary depending on the residence time, irrigation rate, and heap characteristics. A sludge removal cost of $10/ton is assumed.

(5) All capital expenditures are assumed to occur in year one.

(a) Cost of land occupied by leaching operations will be site specific, and may equal zero if land is available with zero opportunity cost. For the base case it is assumed that land costs are $5000/acre.

(b) Liner construction for the leach pad is assumed to cost $\$5/ft^2$.

(c) The cost of drilling 5-10 wells for environmental monitoring of errant heap effluent is included.

(d) No salvage value is assumed for any capital item.

(6) All capital items except for land are depreciated using the Accelerated Cost Recovery System assuming ten year lives.

(7) Tax was calculated on the 'Net Before Tax' at a 46% corporate tax rate.

In our analysis, all net cash flows are discounted to calculate net present value (NPV), using a range of discount rates from 0-35% inclusive at 1% increments. Under conditions of certainty, the decision maker should

evaluate the net present value at the risk-free discount rate (the rate on government securities is an acceptable proxy), and accept the investment if,

$$NPV > = 0$$

If one is choosing between mutually exclusive investment alternatives, the investment with the highest non-negative NPV should be accepted. In practice, decision makers often use discount rates other than the risk-free rate (usually higher), such as a corporate 'hurdle' rate determined by previous investment performance, a weighted average cost of capital, or the rate that makes the NPV exactly equal to zero (internal rate of return - IRR). Other decision criteria, such as payback, while popular are theoretically suspect.

Uncertainty is handled in the paper through sensitivity analysis.

B. Results

The results of the economic analysis are summarized in Figures 21-23. Figure 21 shows the effects of the price of low sulfur coal ($35, $49, $45/ton) for a fixed $30/ton price for high-sulfur coal. Figure 22 shows the impact of capital and operating costs (up 40% or down 15%) of the leach process. And Figure 23 compares the best (highest cost low-sulfur coal, least capital and lowest operating cost plant), base, and worst cases. The analysis shows the most important factor is the price differential between competing coals.

The results of the economic analysis are encouraging. The leach process is profitable for the base and best cases at interest rates of 16% and 33% respectively. The rough analysis indicates, we believe, that heap leaching could prove an economically attractive depyritization technology.

C. Discussion

In our analysis we consider 9 months of leaching. Table 20 indicates the leach rate drops strongly with time and that much of the benefit of leaching can be realized in much shorter periods (particularly for smaller dumps). We do not consider these time/benefit tradeoffs. We also lump the benefits of heap depyritization in the analysis. Table 22 shows the operating cost of conventional cleaning is about 43% of the total operating cost; Table 21 suggests conventional cleaning removes 62% of the pyritic sulfur while heap

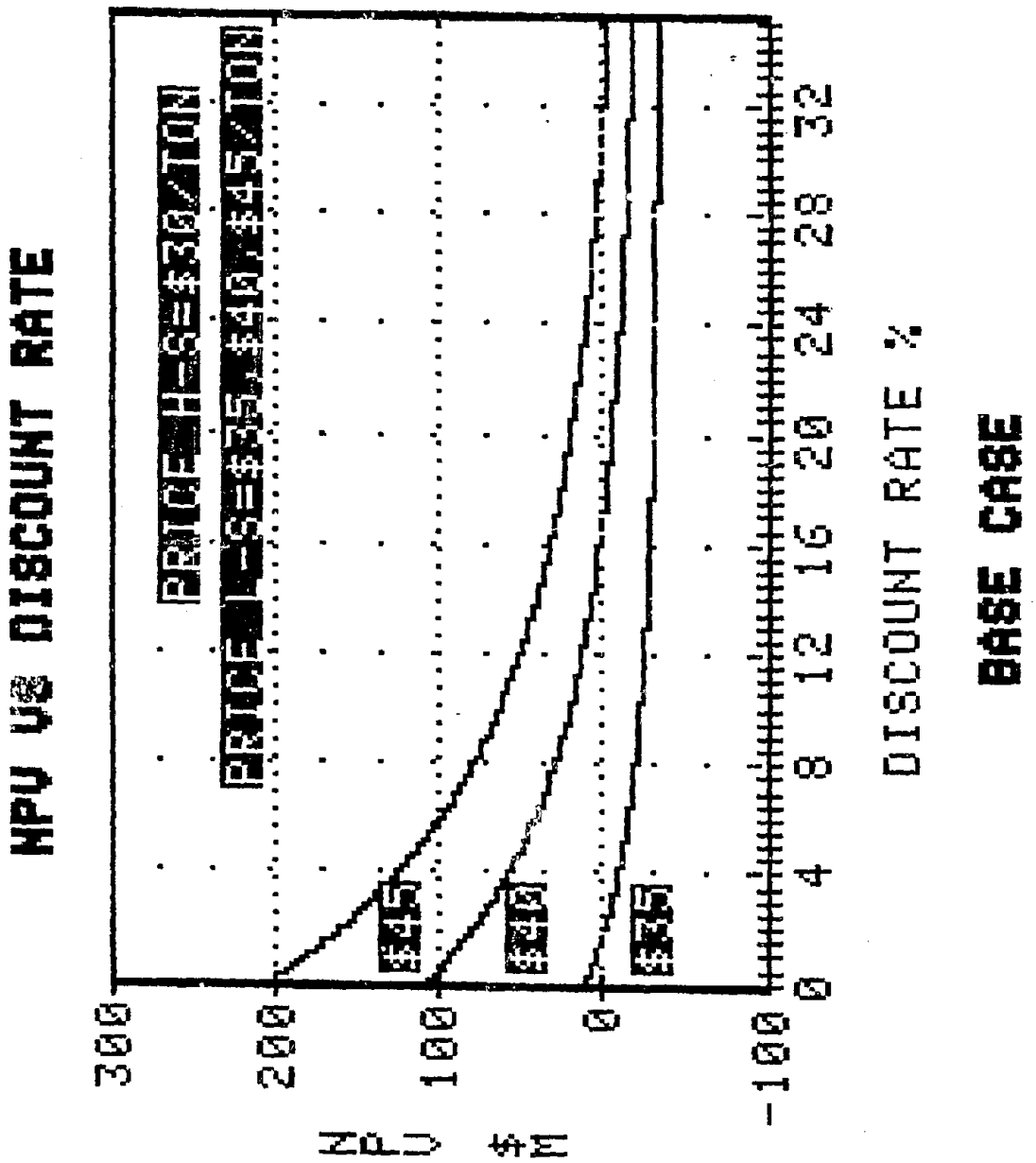

Figure 21 The effect of low sulfur coal price on the net present value of a heap leaching coal depyritization facility

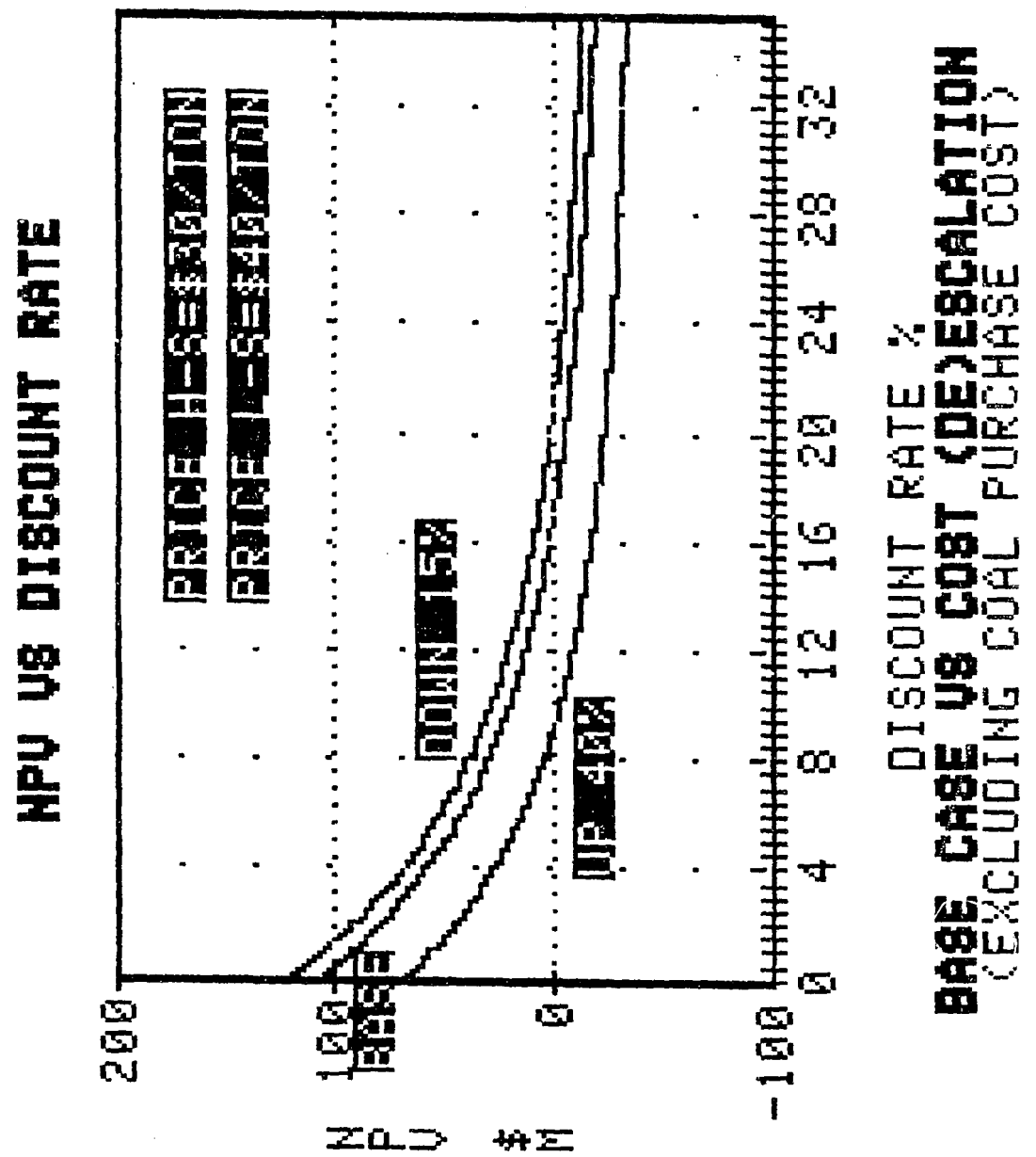

Figure 22 The effect on NPV of varying capital and operating costs

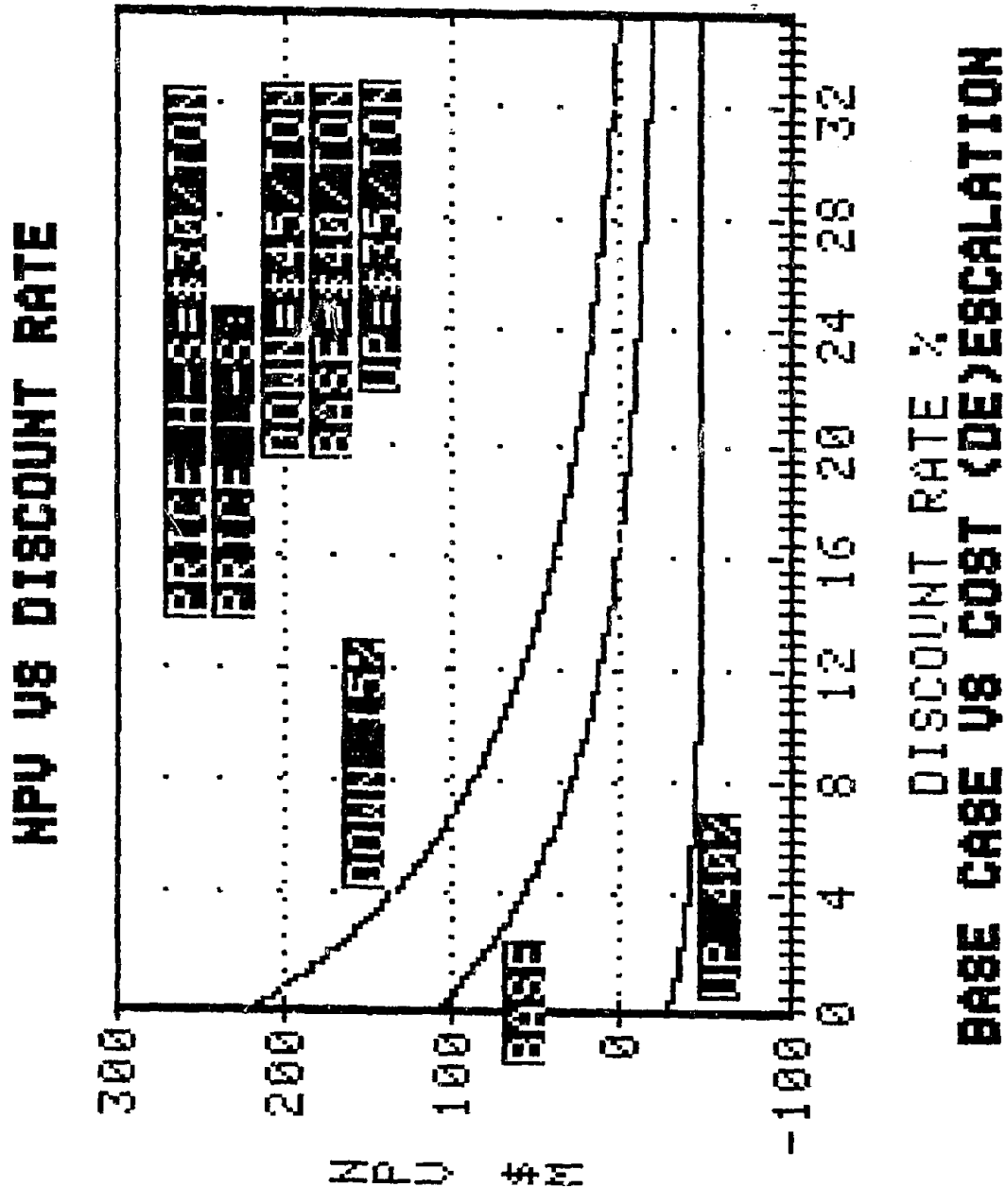

Figure 23 Comparison of best, base and worst cases

Table 22 The Base Economic Calculation

YEAR	1	2	3	4	5	6
BENEFIT(SAVINGS FROM COAL PURCHASE):						
LO-S OPTION						
QUANTITY TON	1000000	1000000	1000000	1000000	1000000	1000000
COST $	40000000	40000000	40000000	40000000	40000000	40000000
LEACH HI-S OPTION						
QUANTITY L-S TON	750000	0	0	0	0	0
QUANTITY H-S TON	1000000	1000000	1000000	1000000	1000000	1000000
COST $	60000000	30000000	30000000	30000000	30000000	30000000
SAVING $	-2E7	10000000	10000000	10000000	10000000	10000000
OPERATING COST(EXC. COAL PURCHASE):						
MECHANICAL CLEAN	1700000	1700000	1700000	1700000	1700000	1700000
LABOR	300000	100000	100000	100000	100000	100000
MONITORING	6000	6000	6000	6000	6000	6000
WATER	2854.536	2854.536	2854.536	2854.536	2854.536	2854.536
WATER TREATMENT	1427268.	1427268.	1427268.	1427268.	1427268.	1427268.
SLUDGE REMOVAL	399347.8	399347.8	399347.8	399347.8	399347.8	399347.8
RECLAMATION						
MISCELLANEOUS	100000	100000	100000	100000	100000	100000
TOTAL OPER COST	3935470.	3735470.	3735470.	3735470.	3735470.	3735470.
OPERATING INCOME	-2.394E7	6264530.	6264530.	6264530.	6264530.	6264530.
DEPRECIATION	1818149.	3181761.	2727224.	2272686.	2272686.	2272686.
NET BEFORE TAX	-2.575E7	3082769.	3537306.	3991843.	3991843.	3991843.
TAX @46%	-1.185E7					
+DEPRECIATION	1818149.	3181761.	2727224.	2272686.	2272686.	2272686.
NET AFTER TAX	-1.209E7	6264530.	6264530.	6264530.	6264530.	6264530.
CAPITAL EXPENDITURES:						
LAND	748072.2					
LINER	16293014					
TREATMENT PLANT	2000000					
IRRIGATION SYSTEM	300000					
HANDLING EQUIP	200000					
CRUSHER	100000					
PREP PLANT	5000000					
MONITOR WELLS	30000					
TOTAL CAPITAL EXP	24671086	0	0	0	0	0
NET CASH FLOW	-3.676E7	6264530.	6264530.	6264530.	6264530.	6264530.

BASE CASE

7	8	9	10	11	12	13
1000000	1000000	1000000	1000000	1000000	1000000	1000000
40000000	40000000	40000000	40000000	40000000	40000000	40000000
0	0	0	0	0	0	0
1000000	1000000	1000000	1000000	1000000	1000000	1000000
30000000	30000000	30000000	30000000	30000000	30000000	30000000
10000000	10000000	10000000	10000000	10000000	10000000	10000000
1700000	1700000	1700000	1700000	1700000	1700000	1700000
100000	100000	100000	100000	100000	100000	100000
6000	6000	6000	6000	6000	6000	6000
2854.536	2854.536	2854.536	2854.536	2854.536	2854.536	2854.536
1427268.	1427268.	1427268.	1427268.	1427268.	1427268.	1427268.
399347.8	399347.8	399347.8	399347.8	399347.8	399347.8	399347.8
100000	100000	100000	100000	100000	100000	100000
3735470.	3735470.	3735470.	3735470.	3735470.	3735470.	3735470.
6264530.	6264530.	6264530.	6264530.	6264530.	6264530.	6264530.
2045418.	2045418.	2045418.	2045418.			
4219112.	4219112.	4219112.	4219112.	6264530.	6264530.	6264530.
2045418.	2045418.	2045418.	2045418.	0	0	0
6264530.	6264530.	6264530.	6264530.	6264530.	6264530.	6264530.

0	0	0	0	0	0	0
6264530.	6264530.	6264530.	6264530.	6264530.	6264530.	6264530.

BASE CASE

14	15	16	17	18	19	20
1000000	1000000	1000000	1000000	1000000	1000000	1000000
40000000	40000000	40000000	40000000	40000000	40000000	40000000
0	0	0	0	0	0	0
1000000	1000000	1000000	1000000	1000000	1000000	250000
30000000	30000000	30000000	30000000	30000000	30000000	7500000
10000000	10000000	10000000	10000000	10000000	10000000	32500000
1700000	1700000	1700000	1700000	1700000	1700000	425000
100000	100000	100000	100000	100000	100000	100000
6000	6000	6000	6000	6000	6000	6000
2854.536	2854.536	2854.536	2854.536	2854.536	2854.536	713.6340
1427268.	1427268.	1427268.	1427268.	1427268.	1427268.	1427268.
399347.8	399347.8	399347.8	399347.8	399347.8	399347.8	399347.8
						1000000
100000	100000	100000	100000	100000	100000	100000
3735470.	3735470.	3735470.	3735470.	3735470.	3735470.	3458329.
6264530.	6264530.	6264530.	6264530.	6264530.	6264530.	29041671
6264530.	6264530.	6264530.	6264530.	6264530.	6264530.	29041671
0	0	0	0	0	0	0
6264530.	6264530.	6264530.	6264530.	6264530.	6264530.	29041671

0	0	0	0	0	0	0
6264530.	6264530.	6264530.	6264530.	6264530.	6264530.	29041671

leaching removes an additional 35%. Conventional cleaning could drop the sulfur content from 4.77% to 3.3%; heap leaching drops it to 2.4% (see Table 21). The benefit of 2.4% vs. 3.3 or 4.7% coal is likely to depend on factors specific to individual coal users. It is outside the scope of this report and our competance to assess such individual factors. The analysis may serve as a base from which others can start local evaluations.

IV. SUMMARY, CONCLUSIONS, AND RECOMMENDATIONS

A theoretical model of copper dump leaching has been adopted to describe the leaching of pyrite from coal. Model parameters were first determined from the published literature, supplemented where necessary by direct measurement (Table 1, Table 6 and Table 7). The predicted coal leaching was then checked by a carefully designed kettle experiment in which both Eh and pH were held constant by automatic titration. The kettle experiments confirmed the literature-determined activation energies describing the leaching process and the leaching stoichiometry, and refined the literature estimates of the chemical rate of pyrite oxidation ($k_{ox}\, a^{R}_{sulf}$ was shown to lie on the high end of the estimated range). Leached rims were observed around the leached coal fragments as it was predicted they should be, and the thickness of the active leaching zone was about 650 μm, a value close to that predicted.

The heap leaching model was further calibrated and tested by carrying out four column leach experiments each of over a year duration. The columns leached about an order of magnitude more slowly than would be expected on the basis of direct extrapolation from the kettle experiments and theoretical predictions, and the thickness of the actively leaching zone was much smaller (50 to 150 μm) than in the kettle experiments (650 μm). On the other hand leached rims were still present and the stoichiometry and the chemical rate of pyrite oxidation were similar to that in the kettle experiments. The explanation for the differences between the column and kettle experiments lies in the fact the columns were flushed twice daily with acidified water containing no iron. The average ferric iron level in the columns was evidently about 0.1 g/l Fe(III) as opposed to about 1.0 g/l Fe(III) in the kettle experiments. Because the rate of pyrite leaching is independent of Fe(III) concentration (i.e. the reaction is zero order in Fe(III)) the lower total ferric iron concentration does not affect the chemical rate of oxidation of

the pyrite in the coal but does proportionately affect the rate of Fe(III) diffusion into the coal fragments. The rate of leaching was reduced by an order of magnitude because the concentration difference during Fe(III) diffusion into the coal fragments was decreased tenfold. For the same reason, the thickness of the active leaching zone was reduced by the square root of ten. The thickness of the active leaching zone is inversely proportional to the square root of the Fe(III) concentration of the solutions surrounding the coal fragments. The columns would have leached much faster had the flush solutions been recirculated (ie. had the flush solutions contained a gram per liter rather than 0.1 gram per liter iron).

A finite difference model of the heap leaching process was then used to predict the way in which heaps of practical size will leach and to determine the optimum heap thickness and operating procedures. It was found that the rate of leaching depends strongly on the height of the heap, and is most rapid for heaps 5 to 15 feet high. The rate of leaching is most rapid for low rates of average solution application (see Figure 20). The experiments and theoretical developments we have carried out suggest an eight foot heap of -¼" coal fragments can be leached of 93% of its finely disseminated pyrite in 9 months (Table 20).

An incremental cost/benefit analysis indicates that if the 8' heaps indeed leach as predicted, the heap leaching depyritization process has a positive net present value for discount rates up to 16% (base case) and 33% (best case).

We conclude that depyritization of coal by heap leaching is both technically and economically feasible and that it is worth testing and evaluating the process further.

The next step is to verify that recirculation of flush solutions will indeed enhance the leach rate of columns as predicted. Assuming this is born out, the next step would be to construct an eight foot coal heap and determine if it leaches as predicted. Perhaps the biggest uncertainty in operating such a heap is the permeability of the heap. It may very well be that fines will cause the permeability of the heap to be low enough that natural air convection will be inadequate to oxygenate the heap. If this is the case, air may have to be blown through the heap, or heaps may have to be constructed of coarser coal fragments. Economic analyses should guide

the development efforts, and ultimately must become specific enough to be capable of indicating whether heap leaching techniques should be adopted by a particular user.

REFERENCES

Amell, A.R., and Langmuir, D. (1978) Factors influencing the solution rate of uranium dioxide under conditions applicable to in-situ leaching. Final Rept. to U.S. Bureau of Mines, Washington, D.C., contract no. H0272019, 124 p.

American Society for Testing and Materials (1981) 1981 Annual Book of ASTM Standards, Part 26, Easton, MD, 840 p.

APL Statistical Library (1979) Non-linear Least Squares with Constrained Marquardt Algorithm. Penn State University Computation Center. Available from: J. Prins, Advanced Logic Products, Poughkeepsie, New York.

Badzioch, S., Gregory, D.R., and Field, M.A. (1964) Investigation of The Temperature Variation of The Thermal Conductivity and Thermal Diffusivity of Coal. Fuel, 43, 267-280.

Barnes, H.L., Helgeson, H.C., and Ellis, A.J. (1966) Ionization constants in aqueous solutions. In Handbook of Physical Constants revised edition. Clark, S.P. (editor), Geological Society of America Memoir 97, 402-413.

Bird, R.B., Stewart, W.E., and Lightfoot, E.N. (1960) Transport Phenomena. J.C. Wiley and Sons, New York, 780 p.

Bladh, K.W. (1982) The formation of goethite, jarosite, and alunite during the weathering of sulfide-bearing felsic rocks. Econ. Geol. 77, 176-184.

Cathles, L.M. (1979) Predictive Capabilities of a Finite Difference Model of Copper Leaching in Low Grade Industrial Sulfide Waste Dumps, Mathematical Geology, 11 #2, 175-191.

Cathles. L.M. and Apps, J.A. (1975) A model of the dump leaching process that incorporates oxygen balance, heat balance, and air convection. Metallurgical Transactions B. 6B, 617-624.

Cathles. L.M., and Murr, L.E. (1980) Evaluation of an experiment involving large column leaching of low grade copper sulfide waste: a critical test of a model of the waste leaching process: In W.J. Schlitt, ed., Leaching and Recovering Copper from as-mined materials, AIME Inc., 29-48.

Cathles, L.M., and Schlitt, W.J. (1980) A Model of the Dump Leaching Process That Incorporates Oxygen Balance, Heat Balance, and Two Dimensional Air Convection: In W.J. Schlitt, ed., Leaching and Recovering Copper from as-mined materials, AIME Inc., 9-28.

Cathles, L.M., Reese, D.A., and Murr, L.E. (1977) Dump Leaching - Theory Experiment, and Practice. Proceedings of American Nuclear Conference, CONF-770440, NTIS, U.S. Dept. Commerce, Springfield, VA.

Garrels, R.M., Dreyer, R.M., and Howland, A.L. (1949) Diffusion of ions through intergranular spaces in water-saturated rocks, Geol. Soc. Am. Bull. 60, 1809-1828.

Given, P.H. (1979) The organic chemistry of coal macerals. Written communication in F.Sc. 597 from Dr. R.G. Jenkins, Fuel Science Dept., The Pennsylvania State University.

Hamersma, J.W., Kraft, M.L., Koutsoukos, E.P., and Meyers, R.A. (1973) Chemical removal of pyritic sulfur from coal. In Advances in Chemistry Series, No. 127, American Chemical Society, Washington D.C., 68-80.

Hamersma, J.W., Kraft, M.L., Kendrick, W.P. and Meyers, R.A. (1974) Chemical Desulfurization of Coal to Meet Pollution Control Standards. Am. Chem. Soc. Div. Fuel Chem. Prepr. 19, #2, 33-42.

Hamersma, J.W., Kraft, M.L., Koutsoukos, E.P. and Meyers, R.A. (1976) Chemical Removal of Pyritic Sulfur from Coal: Am. Chem. Soc. Div. Fuel Chem. Prepr. 17, #2, 1-14.

Hamersma, J.W., Kraft, M.L., and Meyers, R.A. (1977) Applicability of the Meyers process for desulfurization of U.S. coal (a survey of 35 coals). Chapter 11, In Coal Desulfurization: Chemical and Physical Methods, ACS Symposium, Series 64, American Chemical Soc. Washington, D.C., 143-152.

Katsube, T.J. (1981) Pore structure and pore parameters that control radionuclide transport in crystalline rocks. Proc. Tech. Prog., International Powder and Bulk Solids Handling and Processing, Rosemont, IL, May 12-14, 394-409.

Kuehn, K.W. (1979) An automated microscopical method for the characterization of pyrite in coal. Unpublished M.S. paper, The Pennsylvania State University, University Park, PA.

Lasaga, A.C. (1981) Rate laws of chemical reactions, Chap. 1, in: Kinetics of Geochemical Processes, Mineralogical Society of America, Reviews in Mineralogy, vol. 8, 1-67.

Mathews, C.T., and Robins, R.G. (1972) The Oxidation of Iron Disulfide by Ferric Sulphate, Australian Chemical Engineering, Aug. 1972, 21-25.

Meyers, R.A. (1977) Coal Desulfurization, Marcel Dekker Inc., New York, 254 p.

Murr, L.E., Cathles, L.M., Reese, D.A., Hiskey, J.B., Popp, P.J., Brierley, J.A., Bloss, D., Berry, U.K., Schlitt, W.J. and Hsu, P.C. (1977) Chemical, Biological and Metallurgical Aspects of Large Scale Column Leaching Experiments for Solution Mining and In-Situ Leaching: In-Situ, 1 #3.

Sareen, S.S., Giberti, R.A., Irminger, P.F. and Petrovic, L.T. (1977) The use of oxygen/water for removal of sulfur from coals. AICHE Symp. Ser. 73, #165, 183-189.

Sasmojo, S. (1969) Oxidation kinetics of pyritic materials in aqueous media. Unpublished Ph.D. Thesis, Ohio State University.

Schmidt, L.D. and Elder, J.L. (1940) Atmospheric Oxidation of Coal at Moderate Temperatures. Industr. Engng. Chem., 32, 249.

Smith, E.E. and Shumate, K.S. (1970) The sulfide to sulfate reaction. Water Pollution Control Research Series 14010 FPS 02/70 U.S. Dept. of the Interior, Federal Water Quality Administration, 115 p.

Sondreal, E.A. and Ellman, R.C. (1974) Laboratory determination of factors affecting storage of North Dakota lignite. U.S. Bureau of Mines Rept. of Inv. 7887, Washington, D.C.

Stumm, W. and Morgan, J.J. (1970) Aquatic Chemistry, Wiley-Interscience, New York, p. 596.

Tobias, R.F., and Nobe, K. (1975) Electrochemical behavior of rotating iron disks; Effect of Fe(III), Jour. of Electrochem. Soc., 122(1), 65-69.

Tyler, W.S. Inc., (1975) Coal Technology, Proceedings of conferences in Pittsburgh, Charleston, St. Louis, and Denver, copyright W.S. Tyler, Inc.

Van Nice, L.J., Santy, J.J., Koutsoukos, E.P., Orsine, R.A. and Meyers, R.A. (1977) Coal Desulfurization Test Plant Status - July 1977: in Am. Chem. Soc. Symp. Ser. 64, T.D. Wheelock (ed.), Washington, D.C., 153-163.

U.S. Department of Energy (1982) Cost and Quality of Fuels for Electric Utility Plants, available from: Energy Information Administration, Forrestal Bldg., Washington, DC 20585.

Worthington, P.F. (1975) Quantitative geophysical investigations of granular aquifers. In: Geophysical Surveys, vol. 2, D. Reidel, Dordrecht, pp. 313-366.

APPENDICES

A. The Rate of Oxidation of Coal
B. Determination of a^{R}_{sulf}; Rapid-Scan Microscopy and Pyrite Surface Areas
C. Determination of D_E, The Effective Diffusion Constant of Coal
D. Experimental Kettle Leaching of Coal
E. Experimental Column Leaching of Coal
F. Description of the Finite Difference Computer Model of Coal Heap Leaching

Appendix A The Rate of Oxidation of Coal

An expression suitable for our purposes can be extracted from the combined work of Schmidt and Elder (1940) and Sondreal and Ellman (1974). Schmidt and Elder showed the low temperature (< 100°C) oxidation of coal slows with time porportionately to the inverse of time to the one fifth power. Sondreal and Ellman (1974) investigated the effects of temperature, size distribution, oxygen concentration in the air, and moisture content of air on the rate of coal oxidation. Since we assume the air in the coal heap is water saturated, we need not consider the effects of air moisture content below saturation.

The fraction coal oxidation, X_c, can be expressed (Schmidt and Elder):

$$X_c = k_c' \, \bar{R}\bar{S}\bar{P} \, t^{+0.8} \quad . \tag{A-1}$$

The rate of coal oxidation is the differentiated form of this expression:

$$\frac{\partial X_c}{\partial t} = 0.8 \, k_c' \, \bar{R}\bar{S}\bar{P} \, t^{-0.2} \quad . \tag{A-2}$$

Because coal oxidation can be interrupted within the heap if a portion of the heap is oxygen starved, it is better to regulate the rate of coal oxidation with X_c than time. Using (A-1) to eliminate t in (A-2) we obtain:

$$\frac{\partial X_c}{\partial t} = 0.8 \, (k_c' \, \bar{R}\bar{S}\bar{P})^{5/4} \, X_c^{-1/4}, \quad \text{or}$$

$$\frac{\partial X_c}{\partial t} = k_c \, (\bar{R}\bar{S}\bar{P})^{5/4} \, X_c^{-1/4} \quad . \tag{A-3}$$

$\bar{R}$, $\bar{S}$, and $\bar{P}$ give the temperature, size and oxygen concentration dependence of the coal oxitation and are defined by equations (9) in the text. These dependencies are taken from Sondreal and Ellman and refer to base conditions of 25°C and 0.375 inch diameter (0.48 cm radius) coal fragments.

The available data on the rate of coal oxidation appears quite consistent. Schmidt and Elder quote oxidation rate constants which, when converted to our base conditions of 25°C and 0.375 inch diameter coal fragments, yields a k_c value of 3.6×10^{-11} sec^{-1} for Pittsburgh coal and a value of 3.3×10^{-11} sec^{-1} for Lower Kittanning coal. When applied to equation (A-1) this indicates an expected coal oxidation of 0.5% at 25°C after 1 year, and 2.5%

after 1 year at 50°C. The Btu degradation of the coal is, of course, the same as the fraction of coal oxidized.

APPENDIX A References

Schmidt, L. D. and Elder, J. L., 1940. Atmospheric Oxidation of Coal at Moderate Temperatures: Industr. Engng. Chem., 32, p. 249.

Soudreal, E. A. and Ellman, R. C., 1974, Laboratory Determination of Factors affecting Storage of North Dakota Lignite. U.S. Bureau of Mines Rept. of Inv. 7887, Washington, D.C.

APPENDIX B Determination of a^R_{SULF}

A. Rapid-Scan Microscopic Determination of a^R_{SULF}

Introduction

Rapid-scan microscopy (Kuehn, 1979), an automated microscopical method for characterization of pyrite in coal, was used to determine the size distribution of pyrite blebs, to obtain the mean pyrite particle diameter, and to estimate the volume percent pyrite in the five coal size fractions used for experimentation.

Sample Preparation and Instrumental Settings

Petrographic pellets were prepared by the technical staff of the Coal Research Section at The Pennsylvania State University. The standard pellet preparation procedure used is described by Eckley and Williams in a Technical Note available from the Coal Research Section. Three to five scans were performed on each pellet, using the instrumental settings and scan parameters listed below:

Photomultiplier Spot Size in Microns: 2.

Total Number of Points Sampled: 400000.

Total Length of Scan in Millimeters: 800.

Stage Drive Speed in Microns/Second: 800.

Size of Discontinuity to be Bridged in Microns: 20.

Number of Pyrite Particles Encountered: n

Scan Results and Derivation of a^R_{SULF} from Rapid scan estimates of Volume Percent Pyrite and Mean Pyrite Particle Diameter

Pyrite particle size data generated by the rapid-scan technique (data included at end of this section) show cumulative percentages of pyrite chord lengths skewed heavily toward small sizes. Chord is a geometrical term

defined in this context to represent the scan length between edges of a pyrite grain. Chord size is analogous to pyrite diameter along a particular scan traverse line. Assuming the mean particle diameter taken from a log-normalized data set represents a spherical pyrite bleb or grain, the mean bleb diameter and pyrite volume in the sample may be combined to calculate a^R_{SULF}. The geometrically- based derivation of a^R_{SULF} is given below:

It is easy to show that if d is the average pyrite bleb diameter,

$$a^R_{sulf} = \frac{6}{d} \quad \frac{\text{chord length}}{\text{total scan length}}$$

$$d = \frac{\text{chord length}}{\text{number of sulfide blebs encountered in scan}}$$

The following table contains the pyrite diameter and volume data from the rapid-scen analyses, as well as the computed values of a^R_{SULF}. The errors

associated with a^{R}_{SULF} represent the cumulative error in both the volume and the diameter estimates.

Table B-1 . Pyrite Data Obtained by Rapid Scan Microscopy

coal particle size fraction (+mm -mm)	volume % pyrite (cm^3 py / cm^3 coal)	mean particle diameter (x 10^4 cm)	calculated surface area (cm^2 py/cm^3 coal)	no. of scans made
+0.85 -2.00	0.51±0.09	7.39±0.33	41±23%	3
+2.00 -3.20	0.52±0.05	8.12±0.36	38±14%	5
+3.20 -9.50	0.38±0.04	7.83±0.35	29±16%	3
+9.50 -12.5	0.26±0.02	6.91±0.40	23±14%	3
+12.5 -19.0	0.34±0.03	7.01±0.39	29±15%	4

Errors listed represent values computed at 95% confidence interval.

Table B-2

Rapid-Scan Microscopy Data

for

Five Size Fractions of Illinois #6

Coal (River King Pit 3) Before Leaching

(Samples physically cleaned as described in the experimental section of this report.)

Table B-2 (cont.)

Coal Particle Size = +0.85 mm -2.00 mm

n = 252		n = 327		n = 260	
CHORD SIZE(UM)	CUM %	CHORD SIZE(UM)	CUM %	CHORD SIZE(UM)	CUM %
2	15.77	2	24.16	2	21.43
4	37.69	4	45.57	4	40.87
6	51.54	6	60.24	6	53.97
8	60.77	8	66.06	8	58.73
10	66.15	10	70.03	10	66.67
12	69.62	12	74.01	12	71.83
14	75.00	14	77.37	14	77.38
16	77.31	16	78.59	16	81.75
18	79.62	18	80.43	18	86.11
20	82.31	20	81.96	20	88.49
22	83.85	22	83.79	22	89.29
24	96.15	24	84.71	24	90.08
26	86.54	26	85.63	26	90.87
28	88.08	28	87.16	28	92.06
30	88.85	30	88.07	30	92.46
32	89.23	32	89.60	32	93.25
34	90.38	34	90.21	34	93.65
36	90.77	36	91.44	44	94.05
38	91.15	38	92.05	48	94.44
40	91.54	40	92.35	52	94.84
42	92.69	44	92.66	54	95.24
44	93.08	46	94.19	56	96.03
48	93.46	48	94.50	62	96.43
50	93.85	50	96.33	66	96.83
52	94.23	60	96.64	72	97.22

Table B-2 (cont.)

+0.85 -2.00 mm continued

n = 252		n = 327		n = 260	
CHORD SIZE(UM)	CUM %	CHORD SIZE(UM)	CUM %	CHORD SIZE(UM)	CUM %
54	94.62	74	96.94	74	97.62
56	95.00	76	97.25	104	98.41
60	95.38	82	97.55	114	98.81
62	96.15	86	98.17	156	99.21
64	96.54	88	98.47	170	99.60
74	96.92	100	98.78	194	100.00
76	97.31	128	99.08	194	100.00
78	97.69	168	99.39		
98	98.08	232	99.69		
104	98.85	280	100.00		
146	99.23				
148	99.62				
154	100.00				

Table B-2 (cont.)

Coal Particle Size = +2.00 mm -3.2 mm

n = 297		n = 283		n = 297		n = 231		n = 227	
CHORD SIZE(UM)	CUM %	CHORD SIZE(UM)	CUM %	CHORD SIZE(UM)	CUM %	CHORD SIZE(UM)	CUM %	CHORD SIZE(UM)	CUM %
2	23.57	2	18.37	2	17.85	2	21.65	2	13.66
4	41.75	4	35.69	4	40.07	4	41.13	4	30.40
6	55.22	6	50.88	6	53.54	6	54.98	6	46.26
8	63.30	8	58.30	8	62.29	8	60.61	8	54.63
10	67.00	10	63.25	10	66.67	10	64.87	10	63.00
12	70.03	12	66.43	12	71.04	12	70.56	12	68.28
14	73.40	14	72.44	14	75.08	14	73.16	14	73.57
16	76.77	16	75.27	16	77.10	16	74.89	16	76.65
18	79.12	18	77.39	18	79.80	18	78.35	18	77.97
20	79.80	20	79.15	20	81.48	20	79.22	20	80.62
22	80.47	22	82.69	22	82.15	22	80.95	22	82.38
24	82.15	24	84.45	24	83.16	24	82.25	24	84.14
26	83.16	26	85.16	26	84.51	26	83.55	26	85.02
28	83.84	28	86.57	28	86.53	32	84.45	28	88.11
30	84.51	30	86.93	30	88.22	34	87.01	30	90.31
32	86.53	32	87.63	32	89.90	36	87.45	32	91.19
34	87.21	34	89.05	34	90.24	38	87.88	34	92.95
36	87.54	36	89.40	36	91.25	42	88.74	38	93.39
38	88.55	38	89.75	38	91.58	44	89.18	40	93.83
40	89.23	40	90.46	40	91.92	46	89.61	44	94.71
42	89.90	42	91.17	42	92.93	48	90.61	48	95.15
44	90.24	44	91.87	46	93.60	50	92.21	54	96.04
46	90.57	46	92.23	52	94.28	54	92.64	68	96.48
48	91.58	48	93.99	58	94.61	56	93.07	70	96.92
50	92.26	50	94.35	68	95.29	60	93.51	72	97.36
54	92.59	54	94.70	74	95.62	64	93.94	78	98.24
56	93.27	58	95.05	78	95.96	66	94.37	110	98.68
60	93.60	70	95.41	82	96.30	70	95.24	144	99.12

Table B-2 (cont.)

+2.00 mm -3.2 mm continued

n = 297		n = 283		n = 297		n = 231		n = 227	
CHORD SIZE(UM)	CUM %	CHORD SIZE(UM)	CUM %	CHORD SIZE(UM)	CUM %	CHORD SIZE(UM)	CUM %	CHORD SIZE(UM)	CUM %
62	93.94	72	95.76	84	96.63	72	96.67	148	99.56
64	94.61	74	96.11	92	96.97	74	96.10	166	100.00
66	95.29	78	96.47	94	97.31	84	96.67		
70	95.62	80	96.82	102	97.64	88	97.40		
72	95.96	84	97.17	108	97.98	128	97.84		
76	96.30	100	97.53	116	98.32	140	98.27		
78	96.63	108	98.23	124	98.65	204	99.13		
86	96.97	112	98.59	138	98.99	312	99.57		
88	97.31	118	98.94	210	99.33	334	100.00		
90	97.64	150	99.29	302	99.66				
102	97.98	168	99.65	306	100.00				
114	98.32	180	100.00						
126	98.65								
134	98.99								
140	99.33								
200	99.66								
244	100.00								

Table B-2 (cont.)

Coal Particle Size = +3.2 mm -9.5 mm

n = 218		n = 170		n = 262	
CHORD SIZE(UM)	CUM %	CHORD SIZE(UM)	CUM %	CHORD SIZE(UM)	CUM %
2	15.60	2	11.76	2	19.85
4	35.32	4	27.06	4	49.62
6	50.92	6	41.18	6	63.74
8	60.65	8	55.29	8	70.61
10	66.51	10	62.94	10	74.43
12	72.48	12	71.76	12	79.77
14	76.15	14	74.12	14	83.21
16	77.98	16	78.82	16	86.88
18	79.82	18	81.76	18	87.02
20	81.19	20	82.94	20	88.55
22	82.11	22	84.71	22	91.22
24	83.03	24	85.88	26	92.37
26	83.49	26	87.65	28	93.13
28	84.86	28	88.82	30	93.89
30	85.32	30	89.41	34	94.66
32	86.70	32	90.00	38	95.42
34	87.16	34	90.59	44	95.80
36	88.53	38	91.76	48	96.56
38	88.99	40	92.35	52	96.95
40	89.91	48	92.94	58	97.71
42	91.74	52	94.12	60	98.47
44	92.66	60	94.71	68	98.85
46	93.12	70	95.88	112	99.24
48	94.04	76	96.47	134	99.62
50	94.50	86	97.06	136	100.00
54	94.95	92	97.65		

Table B-2 (cont.)

+3.2 mm -9.5 mm continued

n = 218		n = 170	
CHORD SIZE(UM)	CUM %	CHORD SIZE(UM)	CUM %
68	95.41	96	98.24
76	95.87	102	98.82
82	96.33	152	99.41
84	97.25	188	100.00
88	98.17		
112	99.08		
156	99.54		
180	100.00		

Table B-2 (cont.)

Coal Particle Size = +9.5 mm -12.5 mm

n = 163		n = 163		n = 165	
CHORD SIZE(UM)	CUM %	CHORD SIZE(UM)	CUM %	CHORD SIZE(UM)	CUM %
2	20.86	2	14.11	2	26.06
4	47.24	4	39.88	4	44.24
6	56.44	6	52.76	6	55.76
8	63.19	8	62.58	8	60.61
10	68.71	10	68.71	10	69.70
12	76.69	12	74.23	12	76.36
14	80.98	14	77.91	14	81.21
16	82.82	16	80.37	16	84.85
18	84.05	18	82.21	18	86.67
20	85.28	20	84.05	20	89.09
22	87.73	22	88.34	22	89.70
24	88.96	26	90.18	24	90.30
26	89.57	28	91.41	28	92.73
28	90.18	34	93.87	30	93.33
30	90.80	38	94.48	32	94.55
32	91.41	40	95.09	34	95.15
34	92.02	48	95.71	36	95.76
36	93.25	52	96.93	40	96.67
40	94.48	64	98.16	44	98.18
46	95.71	74	98.77	54	99.39
50	96.32	126	99.39	140	100.00
54	96.93	132	100.00		
56	98.16				
88	98.77				
98	99.39				
134	100.00				

Table B-2 (cont.)

Coal Particle Size = +12.5 mm -19.0 mm

n = 146		n = 168		n = 213		n = 158	
CHORD SIZE(UM)	CUM %	CHORD SIZE(UM)	CUM %	CHORD SIZE(UM)	CUM %	CHORD SIZE(UM)	CUM %
2	16.44	2	20.24	2	24.41	2	13.92
4	33.56	4	40.48	4	49.30	4	29.11
6	47.26	6	58.33	6	61.97	6	39.87
8	58.90	8	79.05	8	69.01	8	54.43
10	64.38	10	76.19	10	75.59	10	64.56
12	71.92	12	80.95	12	77.93	12	71.52
14	73.97	14	81.55	14	81.22	14	76.58
16	78.08	16	85.12	16	84.51	16	79.11
18	80.14	18	85.71	18	85.92	18	81.65
20	82.88	20	86.90	20	86.85	20	85.44
22	84.25	24	88.10	22	88.26	22	86.08
24	85.62	26	88.69	24	90.61	24	89.24
28	86.30	28	89.88	26	92.96	26	89.87
32	87.67	30	90.48	32	93.43	30	91.77
34	89.04	32	91.07	34	94.84	32	93.67
38	89.73	34	91.67	42	95.77	38	94.30
42	92.47	36	93.86	44	96.24	40	94.94
44	93.84	40	94.05	46	96.71	44	95.57
46	94.52	42	95.83	48	97.18	48	96.20
48	95.21	52	97.01	50	98.12	54	96.84
52	95.89	56	97.62	52	98.59	56	97.47
54	96.58	62	98.21	54	99.06	102	98.10
60	97.26	66	98.81	58	99.53	122	98.73
82	97.95	102	99.40	112	100.00	126	100.00
94	98.63	156	100.00				
104	99.32						
116	100.00						

B. BET Determination of Pyrite Surface Areas a^{R}_{SULF}

Introduction

An attempt was made to more accurately (avoiding the spherical pyrite particle assumption used for deriving a^{R}_{SULF} from rapid-scan measurements) estimate the surface area of disseminated pyrite morphologies contained within a host Illinois #6 coal matrix.

A gas adsorption technique, combined with BET calculations, was used to obtain surface areas for specially prepared pyrite samples.*

Sample Preparation

The finely disseminated pyrite found in Illinois #6 coal has a characteristic spongy texture and very irregular surface features. This material, for practical purposes, is impossible to selectively remove from the host coal matrix in a unaltered condition. Selected macroscopic occurrences (1 cm bands) of a pyrite that resembled the finely disseminated pyrite microscopically was separated from the coal matrix, crushed with a mortar and pestle, and sieve-sized into two fractions for surface area determination. Photomicrographs that compare the morphology of pyrite in the prepared samples with that found in situ in the host coal appear in Figure . Although the prepared coal pyrite has a larger diameter range than the disseminated pyrite, the spongy texture and irregular surface features are the same for both sample types.

To compare the results of pyrite surface area measurements with earlier reports that coal pyrite has a surface area approximately an order of magnitude greater than similarly sized museum grade material (Clark, 1966; Smith

*L. E. Eary prepared the pyrite samples, performed the gas adsorption analyses, and kindly supplied the author with results of the BET S.A. calculations.

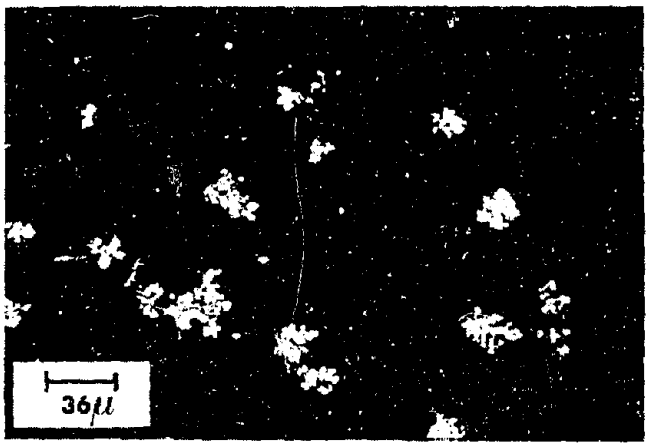

Disseminated aggregates of pyrite in Illinois #6 coal for which an estimate of a^{R}_{SULF} was desired.

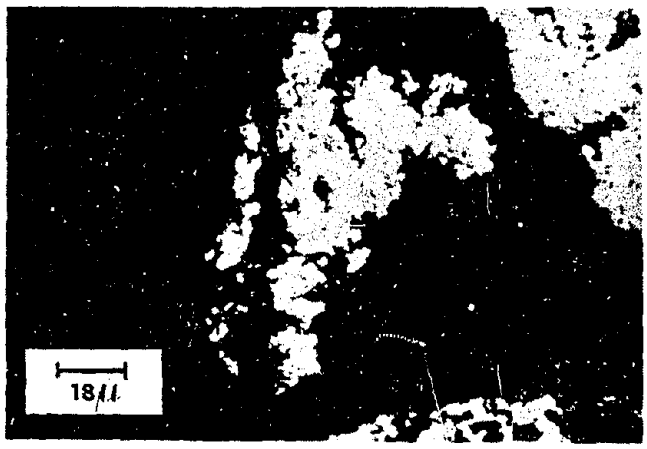

Pyrite material (+125μ-180μ size) isolated from macroscopic bands in Illinois #6 coal. Gas adsorption/BET surface areas of this material used to approximate a^{R}_{SULF} for finely disseminated pyrite.

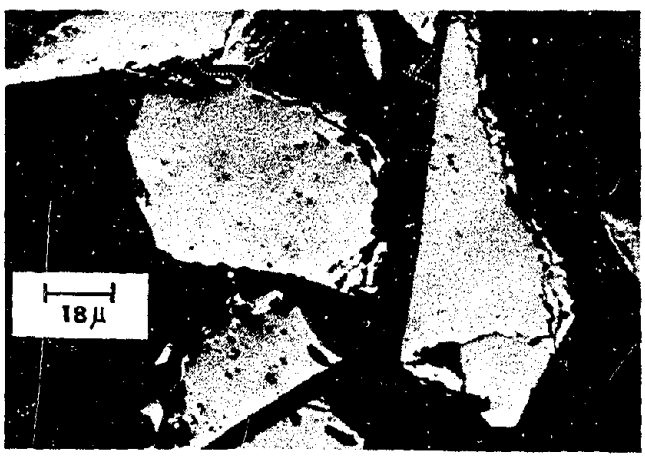

Museum-grade pyrite after crushing (+106μ-125μ) that was used for gas adsorption surface area comparison to coal pyrite material.

Figure B-1

and Shumate, 1970). Museum grade pyrite was obtained** and crushed in a similar manner to a size range comparable to the coal pyrite. A photomicrograph of the museum-grade pyrite is also included in Figure B-1. Texturally, the museum-grade pyrite differs from the coal pyrite in the homogeneity of the crystals themselves, and in the very regular crystal faces exhibited by the museum-grade material.

Results

The results of the BET calculations are listed in Table B-3, along with selected surface area values reported in the literature.

Table B-3

Pyrite Surface Areas as Determined by Gas Adsorption/Bet Techniques

Sample Origin and Size Fraction	Surface Area cm^2/g	Reference
coal pyrite +125μ -180μ	8144	This study
coal pyrite +180μ -250μ	6043	This study
coal pyrite +106μ -250μ	11200 ± 200	Smith and Shumate, 1970
museum grade pyrite +125μ -180μ	238	This study
museum grade pyrite +106μ -125μ	281	This study
museum grade pyrite	1200 ± 100	Smith and Shumate, 1970

** M. A. McKibben supplied the pyrite sample, which originated from the Ward Mine, Glendon, N.C. (a metamorphic mineral).

Derivation of a^R_{SULF}

$$a^R_{SULF}\ \left(\frac{cm^2 FeS_2}{cm^3\ coal}\right) = S.A. \times \rho \times \frac{G_{py}}{100}$$

ρ is the coal bulk density and equals 1.6 g/cm^3 coal. G_{py} is the wt % pyrite in the coal sample (2.1%).

($G_{py}/100$ = 0.021 g FeS_2/g coal)

Using 7000 cm^2/g FeS_2 as an example S.A., we calculate an a^R_{SULF} = 235 cm^{-1}.

APPENDIX B References

Clark, C. S., 1966, Oxidation of coal mine pyrite. J. Sanitary Engng., Proc. of the ASCE, 127-145.

Kuehn, K. W., 1979, An automated microscopical method for the characterization of pyrite in coal. Unpublished M.S. paper, The Pennsylvania State University, University Park, PA.

Smith, E. E. and Shumate, K. S., 1970, The sulfide to sulfate reaction. Water Pollution Control Research Series 14010, FPS 02/70, U.S. Dept. of Interior, Federal Water Quality Adm., 115 p.

APPENDIX C Determination of D_E

A. Measurement of coal connected porosity to water using a vacuum water imbibition weight gain technique:

1. Use a coal wafer of thickness preferably less than 5mm.

2. Transfer the wafer to a shallow pan and cover the wafer with distilled deionized water.

3. Place the pan and wafer in a vacuum jar, attach the jar to a water aspirator, and put under vacuum. At one hour intervals purge the vacuum to force water into the coal pores.

4. Release vacuum and remove wafer, wipe off excess surface water droplets with a Kim-wipe, and immediately weigh the coal wafer.

5. Place the wafer back under vacuum in the solution pan and repeat step 4 until a constant wafer weight is established.

6. Dry the wafer at 105°C for two hours, separate the coal from the epoxy ring and immediately weigh the dry coal and epoxy ring individually.

7. The difference between wet and dry coal weights may be converted to a percent porosity of the coal to water by the equations:

wet weight − ring weight = wet coal weight (WCW)

(WCW − dry coal weight) x 100/WCW = % porosity

8. Water weight gain was found to increase rapidly during the first ten hours of imbibition. Weight became nearly constant after 20 hours. This is consistent with the water imbibition behavior of Pittsburgh Seam coal reported by Dabbous, et al.(1974).

Results of this procedure are summarized below.

Table C-1

Connected Porosity of Wyoming and Illinois Coal
Measured by Water Imbibition Techniques

Illinois

Sample wafer	Thickness (cm)	Dry Weight, g	Wet Weight, g	Weight Gain, g	ϕ'_R
Pit 3.2#1	0.177	1.6648	1.7590	0.0942	8.7%
Pit 3.2#2	0.211	1.9925	2.0979	0.1054	8.3
Pit 3.2#3	0.335	3.2504	3.3732	0.1228	6.0
Pit 3.2#4	0.211	2.0653	2.1640	0.0987	7.8
Pit 3.3#1	0.211	2.0767	2.1626	0.0859	7.3
Pit 3.3#2	0.210	2.0795	2.1546	0.0751	6.2
Pit 3.3#3	0.333	3.2948	3.4190	0.1242	6.5
Pit 3.3#4	0.335	3.2954	3.4247	0.1293	6.9

Pit 3--Illinois #6 River King Mine 3 Mean = 7.2 $\pm$ 7%

Wyoming (Wyodak)

CP6 #1	0.208	1.7604	2.0205	0.2601	21.2%
CP6 #5	0.206	1.7015	1.9950	0.2935	24.6
CP6 #6	0.208	1.7452	2.0116	0.2664	21.7
CP4 #3	0.203	1.8665	2.1165	0.2500	22.0
JR2 #3	0.208	1.8085	2.0668	0.2583	23.1
JR2 #5	0.203	1.7818	1.9980	0.2162	19.0
JR2 #6	0.213	1.8978	2.1015	0.2037	17.1
JR3 #3	0.079	0.6085	0.7615	0.1530	35.2
JR3 #4	0.216	1.9025	2.1190	0.2165	18.2
JR4 #1	0.465	3.9684	4.5470	0.5786	22.2
JR4 #2	0.467	4.0202	4.5650	0.5448	20.8
JR4 #3	0.602	5.2324	5.9135	0.6811	20.2

mean = 22.1

JR - Jacobs Ranch Mine, Kerr McGee Coal Corporation
CP - Clovis Point Mine, Kerr McGee Coal Corporation

B. A Technique for Measuring the Effective Diffusion Coefficient D_E Using a Garrels-Type Diffusion Cell

1. Theory and Equipment

The work of Garrels, Dreyer, and Howland (1949) was used as an experimental basis for measuring the effective diffusion coefficient. D_E was determined using a diffusion cell technique. Diffusion cell theory is reviewed by Gordon (1945).

A diffusion cell consists of two solution reservoirs separated by a dividing wall having an opening in which to mount a porous sample for which a measure of D_E is desired. A driving force for diffusion is generated by filling one reservoir with a concentrated solution containing a solute with a known diffusion constant. The second reservoir is filled level with the first reservoir by adding a less concentrated or dilute solution containing the same solute. The concentrated solute will begin to diffuse through the porous sample in the direction of lesser concentration (down the concentration gradient) into the dilute cell reservoir.

The change in concentration may be measured as time proceeds. The relationship between the concentrations in the two cell reservoirs and time is given by (Gordon, 1945; Sanni and Hutchison, 1968):

$$-\ln[(C'_f - C''_f)/(C'_o - C''_o)] = (D_E At/L)(1/V' + 1/V'')$$

Where C'_o, V' and C''_o, V'' are the initial concentration (M) of the solute and volume (cm^3) of the solution in the concentrated and dilute reservoir, respectively. C'_f and C''_f denote the final solute concentrations in the concentrated and dilute solution reservoirs. L and A are the thickness (cm) and exposed surface (cm^2), respectively, of the coal wafer under test; t denotes time elapsed in the experiment (sec). Combining the cell concentrations

at the beginning and at time t of a diffusion test with the cell volume and sample size terms, an estimate of D_E may be calculated.

The diffusion cell illustrated in Figure C-1 was used to measure D_E for the Illinois #6 bituminous coal samples. The cell reservoirs ($v' = v'' = 225\ cm^3$) were fabricated from 6.4 cm I.D., 0.64 cm wall Plexiglass tube. KCl served as the diffusing solute, and the concentration changes were measured using a conductivity cell mounted in the dilute solution reservoir. Specific conductivity at 25°C is related to KCl concentration, using a precalibrated linear regression relation. The precision of conductometric concentration determinations was ±2%.

2. Sample Preparation and Experimental Procedure

Wafers of the coal samples to be used for the diffusion tests were prepared in the same manner as described for the effective water porosity determinations (see Section III in this appendix). The exposed surface of the coal wafer (A) was measured with a planimeter. Wafer thickness (L) was measured with a micrometer caliper. An attempt was made to prepare diffusion wafers both parallel and perpendicular to the lithologic banding in Illinois #6 bituminous and Wyoming subbituminous coal. Freshly prepared coal wafers were then mounted in the diffusion cell partition and tested for leakage from a solution-filled reservoir attached to the partition sample holder. Differences in the physical properties between the Illinois and Wyoming coal became apparent in the leakage tests. Fractures in the Illinois coal that were not apparent macroscopically became readily visible, as evidenced by beads of solution appearing on the exposed surface of the coal wafer. Leakage was most commonly observed on samples prepared parallel to lithologic banding. The planes between lith-type bands were particularly susceptible zones of leakage. All of the Illinois coal samples prepared parallel to banding (50 samples total) developed leaks,

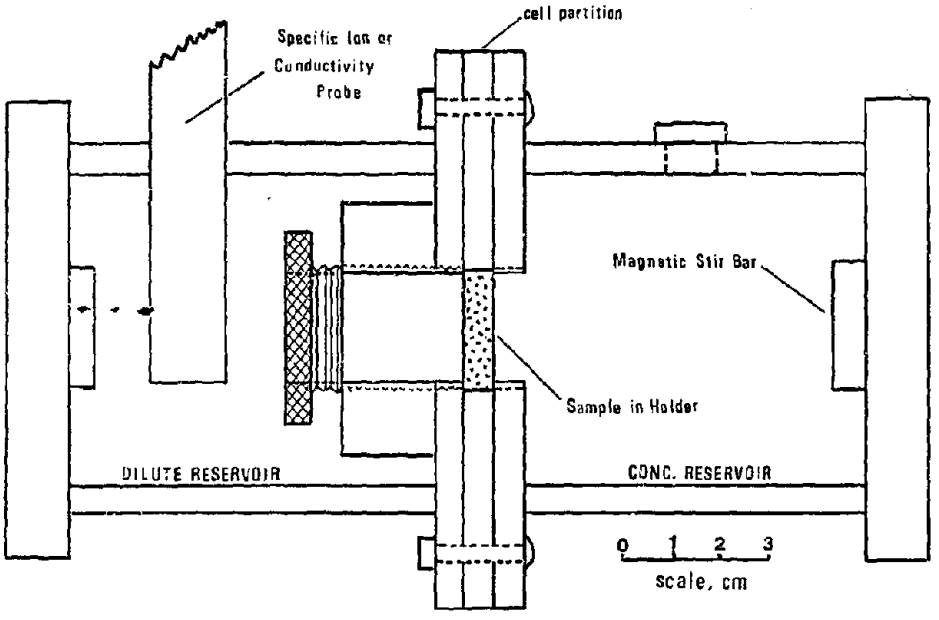

Figure C-1 Diffusion Cell (Garrels-Type) for determination of the effective diffusion coefficient D_E

and the attempt to assess D_E parallel to banding was abandoned. The relative homogeneity of the individual lithotype bands allowed measurements of D_E perpendicular to banding to be made without any visible or analytical evidence of leakage. The Wyoming coal showed no evidence of leakage from microcracks and fractures. Wyoming samples were, however, very prone to form shrinkage cracks due to drying. As a result, the coal had to be prepared and stored under water-saturated conditions. The delicate nature of the coal wafers required that mounting in the cell holder be performed with extreme care.

Once a prospective wafer was mounted and found free of leaks, the wafer was vacuum impregnated with the more concentrated KCl solution. The three-piece Plexiglass diffusion cell was bolted together, reservoirs filled, and the concentration monitoring process begun. The solution within each reservoir was stirred by air or water-driven magnetic stir motors mounted on the ends of the diffusion cell. The temperature of the entire cell assembly was maintained constant by suspending the cell in a water bath kept at $25.0 \pm 0.2°C$.

Upon completion of a diffusion run, the cell was dismantled, and again the wafer was checked for leakage. If leakage was apparent, the data was discarded. After a successful (leak-free) diffusion measurement, selected sample wafers were mounted in epoxy, sectioned, polished, and examined microscopically for microcracks or fractures. Maceral point count analyses for two of the successful diffusion runs showed the Illinois coal wafers to be essentially mono-maceralic in vitrinite. Finely-disseminated pyrite was also present in the wafer samples. The presence of water-soluble mineral matter in the wafers was checked on wafers that failed the leakage test. The wafers were placed in a beaker of distilled water, and the conductivity of the water monitored with time. Water-soluble salts present in the coal contributed a negligible

amount to the conductivity changes observed in the dilute cell reservoir during actual diffusion runs.

3. Results

Fifty diffusion measurements were attempted on Illinois coal wafers prepared perpendicular to sample banding. Data from three of these measurements appears in Table C-2. This data is for both macroscopically and analytically leak-free samples. The values of D_E computed from the cell data are: 9.8×10^{-7}, 7.5×10^{-8}, and 5.6×10^{-8} cm^2/sec. The reproducibility of the diffusion results was estimated as $\pm 10\%$ from duplicate experimental runs.

The success rate for measurements on the Wyoming coal was markedly better. Twenty diffusion wafers were prepared in total. Ten were prepared parallel and ten perpendicular to lithologic banding. Useful diffusion data were obtained from fourteen of the samples. The results of the measurements of D_E appear in Table , where the lithologic orientation of the sample is noted. The experimental data used to calculate D_E appears in Table . The mean value of D_E for perpendicular samples is 1.0×10^{-7} cm^2/sec, and for parallel samples equals 4.6×10^{-7} cm^2/sec. Considering the magnitude of the standard deviations, the two mean values are the same. It is not valid therefore to assign different D_E values for diffusion perpendicular and parallel to lithologic banding. The mean of all fourteen measurements is 2.1×10^{-7} cm^2/sec.

As a check on the measured values, D_E can be calculated from the relation $D_E = \phi'_c D'_{ox}/T$ ($D'_{ox} = 5.2 \times 10^{-6}$ cm^2/sec, $\phi'_c = 0.221$ for Wyoming coal, and assume $T = 5$), which gives a value for D_E of 2.3×10^{-7} cm^2/sec. This is in good agreement with measured values.

Table C-2

KCl Concentration versus Time Data from Effective Diffusion Coefficient Measurements at 25°C

Illinois #6 coal; A = 5.07 cm^2

River King Mine 3 Perpendicular Sample #24

L = wafer thickness = 0.476 cm; $C_o' = 0.111$ M

time, hrs.	KCl Conc., M ****Correlation=99.6%
0.0	3.9×10^{-5}
0.4	5.8×10^{-5}
1.2	8.1×10^{-5}
4.5	1.7×10^{-4}
6.0	1.9×10^{-4}
20.0	5.2×10^{-4}
41.3	9.3×10^{-4}
47.3	1.0×10^{-3}
51.8	1.1×10^{-3}
65.8	1.3×10^{-3}
91.3	1.7×10^{-3}

River King Mine 3 Perpendicular Sample #25

L = 0.335 cm; $C_o' = 1.00$ M

time, hrs.	KCl Conc., M ****Correlation=99.5%
0.0	2.0×10^{-5}
4.0	2.4×10^{-4}
15.5	5.6×10^{-4}
18.0	6.2×10^{-4}
23.5	7.6×10^{-4}
76.5	1.6×10^{-3}
88.0	1.8×10^{-3}
91.0	1.9×10^{-3}
96.0	2.0×10^{-3}
101.0	2.1×10^{-3}
112.0	2.2×10^{-3}
117.0	2.3×10^{-3}
127.0	2.4×10^{-3}
136.0	2.5×10^{-3}
144.0	2.7×10^{-3}
149.0	2.8×10^{-3}
160.0	2.9×10^{-3}

River King Mine 3 Perpendicular Sample #26

L = 0.210 cm; $C_o' = 1.00$ M

time, hrs.	KCl Conc., M ****Correlation=99.7%
0.0	5.2×10^{-5}
4.0	3.0×10^{-4}
15.5	7.3×10^{-4}
18.0	8.0×10^{-4}
23.5	9.4×10^{-4}
76.5	1.9×10^{-3}
88.0	2.1×10^{-3}
91.0	2.2×10^{-3}
96.0	2.3×10^{-3}
101.0	2.4×10^{-3}
112.0	2.6×10^{-3}
117.0	2.7×10^{-3}
127.0	2.9×10^{-3}
136.0	3.1×10^{-3}
144.0	3.3×10^{-3}
149.0	3.4×10^{-3}
160.0	3.6×10^{-3}

Table C-2 continued

Wyoming Coal (Wyodak Seam); A = 5.8 cm^2

Sample # JR1536 L = 0.146 cm, $C_o' = 1.00$ M

time, hrs.	KCl Conc., M
	****Correlation=99.9%
0.0	1.4×10^{-5}
2.0	1.8×10^{-5}
7.0	2.4×10^{-4}
20.0	1.2×10^{-3}
25.5	1.6×10^{-3}
46.5	2.9×10^{-3}
55.5	3.6×10^{-3}
71.5	4.7×10^{-3}
95.0	6.2×10^{-3}
103.5	6.7×10^{-3}
114.5	7.3×10^{-3}
128.0	8.2×10^{-3}
137.0	8.9×10^{-3}

Sample # JR1532 L - 0.146 cm, $C_o' = 1.00$ M

time, hrs.	KCL Conc., M
	****Correlation=99.9%
0.0	6.6×10^{-6}
1.0	8.1×10^{-6}
10.5	1.9×10^{-4}
34.5	8.0×10^{-4}
46.5	1.1×10^{-3}
52.5	1.3×10^{-3}
61.0	1.5×10^{-3}
71.0	1.7×10^{-3}
83.0	7.0×10^{-3}
94.5	2.3×10^{-3}
106.5	2.5×10^{-3}
119.5	2.9×10^{-3}
135.0	3.4×10^{-3}
142.5	3.5×10^{-3}
150.0	3.6×10^{-3}
166.5	4.1×10^{-3}

Table C-2 continued

Sample #JR356 L = 0.348 cm, C_o' = 1.00 M

time, hrs.	KCl Conc., M
	****Correlation=97.1%
0.0	7.0×10^{-6}
1.0	1.0×10^{-5}
5.5	3.4×10^{-5}
11.5	9.3×10^{-5}
29.0	3.6×10^{-4}
45.5	6.6×10^{-4}
50.5	7.8×10^{-4}
57.0	9.0×10^{-4}
71.0	1.3×10^{-3}
74.0	1.4×10^{-3}
84.0	1.8×10^{-3}
93.5	2.2×10^{-3}
97.5	2.4×10^{-3}
101.0	2.6×10^{-3}
105.5	2.8×10^{-3}
117.5	3.2×10^{-3}
124.5	3.6×10^{-3}
131.5	3.9×10^{-3}
147.0	4.8×10^{-3}
155.0	5.3×10^{-3}
165.0	5.9×10^{-3}

Sample #JR1512 L = 0.210 cm, C_o' = 1.00 M

time, hrs.	KCl Conc., M
	****Correlation=99.8%
0.0	2.3×10^{-5}
4.0	2.6×10^{-5}
9.0	5.0×10^{-4}
22.0	2.6×10^{-4}
27.5	3.0×10^{-4}
48.5	7.6×10^{-4}
57.5	9.6×10^{-3}
73.5	1.3×10^{-3}
97.0	1.7×10^{-3}
105.5	1.9×10^{-3}
116.5	2.1×10^{-3}
130.0	2.4×10^{-3}
139.0	2.5×10^{-3}

Table C-2 continued

Sample #JR1522 L = 0.210 cm, $C_o' = 1.00$ M

time, hrs.	KCl Conc., M
0.0	6.7×10^{-6}
1.0	8.2×10^{-6}
10.5	8.5×10^{-5}
34.5	5.1×10^{-4}
46.5	7.4×10^{-4}
52.5	8.6×10^{-4}
61.0	1.0×10^{-3}
71.0	1.2×10^{-3}
83.0	1.4×10^{-3}
94.5	1.6×10^{-3}
106.5	1.9×10^{-3}
119.5	2.1×10^{-3}
135.0	2.4×10^{-3}
142.5	2.5×10^{-3}
150.0	2.6×10^{-3}
166.5	2.9×10^{-3}

****Correlation=99.9%

Sample #JR252 L = 0.211 cm, $C_o' = 1.00$ M

time, hrs.	KCl Conc., M
0.0	7.0×10^{-6}
6.0	6.1×10^{-5}
22.5	6.6×10^{-4}
30.0	9.4×10^{-4}
36.0	1.1×10^{-3}
48.5	1.5×10^{-3}
52.0	1.6×10^{-3}
59.5	1.9×10^{-2}
70.0	2.3×10^{-3}
73.5	2.4×10^{-3}
83.5	2.7×10^{-3}
93.0	3.0×10^{-3}
99.0	3.5×10^{-3}
105.5	4.0×10^{-3}
130.0	5.5×10^{-3}
142.0	6.1×10^{-3}
154.0	6.8×10^{-3}
165.5	7.4×10^{-3}

****Correlation=98.7%

Table C-2 continued

Sample #JR154 L = 0.88 cm, C_o' = 1.00 M

time, hrs.	KCl Conc., M
	****Correlation=99.9%
0.0	7.0×10^{-6}
6.0	2.7×10^{-5}
22.5	2.7×10^{-4}
30.0	4.2×10^{-4}
36.0	5.5×10^{-4}
48.5	8.1×10^{-4}
52.0	8.7×10^{-4}
59.5	1.0×10^{-3}
70.0	1.2×10^{-3}
73.5	1.3×10^{-3}
83.5	1.5×10^{-3}
93.0	1.7×10^{-3}
99.0	1.8×10^{-3}
105.5	1.9×10^{-3}
170.0	2.4×10^{-3}
142.0	2.6×10^{-3}
154.0	2.8×10^{-3}
165.5	3.1×10^{-3}

Sample #JRAPP42 L = 0.462 cm, C_o' = 0.111 M

time, hrs.	KCl Conc., M
	****Correlation=93.6%
0.0	3.6×10^{-4}
0.5	4.0×10^{-4}
27.5	8.0×10^{-4}
30.0	8.2×10^{-4}
46.0	9.2×10^{-4}
51.0	9.5×10^{-4}
71.0	1.0×10^{-3}
77.5	1.1×10^{-3}
85.0	1.1×10^{-3}
93.5	1.1×10^{-3}
118.5	1.2×10^{-3}
145.5	1.3×10^{-3}

Table C-2 continued

Sample #JRAPP54 L = 0.335 cm, C_o' = 0.111 M

time, hrs.	KCl Conc., M
	****Correlation=99.2%
0.0	3.3×10^{-4}
0.5	3.8×10^{-4}
27.5	4.8×10^{-4}
30.0	4.9×10^{-4}
46.0	5.4×10^{-4}
51.0	5.6×10^{-4}
71.0	6.2×10^{-4}
77.5	6.4×10^{-4}
85.0	6.6×10^{-4}
93.5	7.0×10^{-4}
118.5	7.7×10^{-4}
145.5	8.5×10^{-4}

Sample #CP453 L = 0.203 cm, C_o' = 1.00 M

time, hrs.	KCl Conc., M
	****Correlation=99.6%
0.0	2.1×10^{-5}
4.5	3.6×10^{-4}
15.5	1.6×10^{-3}
19.0	2.0×10^{-3}
24.0	2.3×10^{-3}
39.5	3.7×10^{-3}
48.0	4.3×10^{-3}
63.5	5.3×10^{-3}
69.0	5.7×10^{-3}
78.0	6.3×10^{-3}
87.0	7.0×10^{-3}
96.0	7.5×10^{-3}
113.0	9.1×10^{-3}
123.0	9.2×10^{-3}
145.0	1.1×10^{-2}
159.0	1.1×10^{-2}

Table C-2 continued

Sample #JRBPL21 L = 0.333 cm, $C_o' = 0.111$ M

time, hrs.	KCl Conc., M
	****Correlation=92.1%
0.0	1.9×10^{-4}
7.5	9.7×10^{-4}
24.5	1.6×10^{-3}
31.5	1.7×10^{-3}
52.0	2.0×10^{-3}
61.5	2.1×10^{-3}
75.5	2.3×10^{-3}
80.0	2.4×10^{-3}
96.0	2.4×10^{-3}

Sample #JRCPL11 L = 0.203 cm, $C_o' = 0.111$ M

time, hrs.	KCl Conc., M
	****Correlation=97.6%
0.0	5.4×10^{-4}
7.5	1.3×10^{-3}
24.5	1.9×10^{-3}
31.5	2.0×10^{-3}
52.0	2.5×10^{-3}
61.5	2.7×10^{-3}
75.5	3.0×10^{-3}
80.0	3.2×10^{-3}
96.0	3.5×10^{-3}

Table C-2 continued

Sample #JRBPL11 L = 0.213 cm, C_o' = 0.112 M

time, hrs.	KCl Conc., M
	****Correlation=92.6%
0.0	7.7×10^{-5}
6.0	5.9×10^{-4}
26.0	1.4×10^{-3}
32.0	1.5×10^{-3}
48.0	1.8×10^{-3}
56.0	1.9×10^{-3}
72.0	2.1×10^{-3}
107.0	2.4×10^{-3}
146.0	2.7×10^{-3}
151.5	2.8×10^{-3}
166.5	2.8×10^{-3}

Sample #JRBPL31 L = 0.462 cm, C_o' = 0.112 M

time, hrs.	KCl Conc., M
	****Correlation=98.7%
0.0	4.7×10^{-5}
6.0	3.5×10^{-4}
26.0	7.6×10^{-4}
32.0	8.5×10^{-4}
48.0	1.1×10^{-3}
56.0	1.2×10^{-3}
72.0	1.3×10^{-3}
107.0	1.7×10^{-3}
146.0	2.1×10^{-3}
151.5	2.2×10^{-3}
166.5	2.4×10^{-3}

Table C-3

Effective Diffusion Coefficients Determined for
Wyoming Subbituminous Coal (Wyodak)

Perpendicular to Lithologic Banding

Sample I.D.	D_E (cm^2/sec)
JR1536	1.0×10^{-7}
JR1532	3.9×10^{-8}
JR356	1.4×10^{-7}
JR1521	4.0×15^{-8}
JR1522	3.9×10^{-8}
JR252	1.0×10^{-7}
JR154	3.8×10^{-8}
JRAPP42	3.0×10^{-7}
JRAPP54	1.1×10^{-7}
CP453	1.5×10^{-7}
	mean = 1.0×10^{-7}
	std.dev. = $.8 \times 10^{-7}$

Parallel to Lithologic Banding

JRBPL21	7.6×10^{-7}
JRCPL11	6.3×10^{-7}
JRBPL11	1.3×10^{-7}
JRBPL31	3.1×10^{-7}
	mean = 4.6×10^{-7}
	std.dev. = 2.9×10^{-7}

4. Preparation Procedure for coal wafers used in water imbibition and diffusion experiments:

1. Coat the outside of a 2 x 2 inch or larger coal block in APCO[1] epoxy resin to prevent breakage during cutting; allow the epoxy to set.

   APCO epoxy resin preparation: Using a Dixie cup graduated in ounces, pour 1 oz. of R-313 resin. Add to the resin three full eye droppers (3.5ml) of hardener B. Stir until thoroughly mixed.

2. Using a water cooled circular cutting saw, cut the coal block into a roughly 1.5 inch square cube.

3. Note and record the sample orientation (parallel or perpendicular to lithologic banding).

4. Round off the cube edges on a belt sander to form a cylinder one inch in diameter, retaining the 1.5 inch height.

5. Using compressed air, remove excess dust from the surface of the cylinder.

6. Place cylinder in Buehler[2] #20-8180 Sampl-Kup Mold previously coated with a releasing agent[3].

7. Prepare epoxy resin as described above, after mixing transfer from Dixie cup to a disposable glass vial and centrifuge for ~5 min. to remove air bubbles.

8. Pour centrifuged epoxy mix into mold around coal cylinder slowly to avoid trapping air bubbles and fill until cylinder is covered; allow epoxy to set.

9. Remove cylinder from mold and mount on a clean dry glass slide with adhesive.

10. Cut the coal cylinder into wafers of desired thickness on a Buehler Isomet #11-1180 Low Speed Saw.

[1]Applied Plastics Co. Inc.
612 E. Franklin Ave.
El Segundo, Calif. 90245

[2]Buehler Ltd.
2120 Greenwood St.
Evanston, IL 60204 312-475-2500

[3]MS-122 Release Agent Dry Lubricant
Miller-Stephenson Chemical Co. Inc.
6348 Oakton St.
Morton Grove, IL

APPENDIX C References

Dabbous, M. K., Reznik, A. A., Taber, J. J., and Fulton, P. F., 1974, The permeability of coal to gas and water. Soc. of Pet. Engs. J., Dec., 563-572.

Garrels, R. M., Dreyer, R. M., and Howland, A. L., 1949, Diffusion of ions through intergranular spaces in water-saturated rocks, Geol. Soc. Am. Bull. 60, 1809-1828.

Gordon, A. R., 1945, The diaphragm cell method of studying diffusion, N.Y. Acad. Sci., Ann., 46, 285-308.

Sanni, S. A. and Hutchison, H. P., 1968, The diaphragm cell method for diffusion measurements at temperatures up to 60°C. J. Sci. Instr. (J. Phys., E) 1, series 2, 1101-1104.

Appendix D : Experimental Kettle Leaching of Coal*

(Control of Eh and pH to Evaluate the Rate of Pyrite Oxidation by Ferric Ion)

* This appendix is the manuscript of a paper submitted to the Graduate School of The Pennsylvania State University in partial fulfillment of the requirements for the Degree of Master of Science in Geochemistry and Mineralogy, November 1982, by Kevin John Breen. Minor textual changes have been made for incorporation as an appendix to the final technical report.

ABSTRACT

Ferric ion is an effective oxidant for chemically removing pyrite from coal and other geologic materials. The rate of reaction between ferric ion and pyrite is important because the reaction is utilized for coal desulfurization, solution mining, and dump or heap leaching processes. The severity of the acid mine drainage problem resulting from surface and underground mining of coal and sulfide ores also depends, in part, on the rate at which ferric ion attacks pyrite.

An experimental technique is developed to measure the rate at which the following reaction of pyrite and ferric ion takes place:

$$FeS_2 + (2+12X)Fe^{3+} + (8X)H_2O \longrightarrow (3+12X)Fe^{2+} + (14X)H^+ + (2X)HSO_4^- + 2(1-X)S^o \quad .$$

Redox potential measurement is combined with redox-stat titration; this involves titrating the H_2O_2 required to exactly offset emf changes produced when ferric ion is reduced to ferrous ion by reacting with pyrite. The study determines the lower Fe(II), Fe(III), and H^+ concentration limits required for valid application of the redox potential technique and a threshold level below which dissolved organic carbon does not interfere with the H_2O_2 titration. The technique has the sensitivity to detect a 2 ppm change in the concentration of ferrous ion in a bulk solution containing >2000 ppm total iron. This sensitivity allows interpretation of stoichiometric and kinetic data in systems where conventional solution analyses cannot detect small changes in reactant and product concentration. In addition, the technique permits uninterrupted, automated, data

collection in experimental kinetic studies of extended duration. The usefulness of this technique is illustrated in a system where finely disseminated pyrite, constituting a fraction (~2 wt. %) of a host bituminous coal matrix, is oxidized by ferric ion.

TABLE OF CONTENTS

ACKNOWLEDGEMENTS

The author wishes to express his gratitude to all those who have contributed to the preparation of this paper.

I am especially grateful to Dr. L. M. Cathles for offering valuable suggestions, support, and constructive criticism during the course of this research. Special thanks are extended to Dr. R. L. Barnes, Dr. A. W. Rose, and Prof. Norman H. Suhr for their critical reviews of this manuscript. I would also like to thank Dr. Alan Davis for granting permission to use the facilities of the Coal Research Section and for his review of an early draft of this paper. Dr. John A. Campbell kindly supplied the coal sample used in this study. The professional and technical staffs of the Coal Research Section and Mineral Constitution Laboratory provided expert assistance in sample preparation and analysis. Boku Takano and Doug Vonada assisted the author with analytical and electronics problems, respectively. Discussions with L. E. Eary and K. Applin regarding experimental design and aqueous solution chemistry proved most helpful. Lastly, I extend a sincere note of appreciation to my parents for their enduring support throughout my academic training.

This research was supported by the U.S. Department of the Interior, Office of Surface Mining under Grant G-5115427, entitled "Removal of Pyrite from Coal by Heap Leaching" to the Pennsylvania MMRRI and also, in part, by the Mineral Conservation Section of the Pennsylvania State University.

INTRODUCTION

Conventional mechanical desulfurization procedures are unable to remove the finely disseminated fraction of the pyritic sulfur present in coal (Gluskoter, 1968; McCartney et al., 1969). Recent studies by Hamersma and his coworkers (Hamersma et al., 1977; Van Nice et al., 1977) have demonstrated the feasibility of removing finely disseminated pyritic sulfur from coal by chemical methods that utilize ferric ion. Ferric ion has also been proposed for use in desulfurization processes that use microorganisms to lower the pyritic sulfur level of coal (Ford et al., 1977; Detz and Barvinchak, 1979). Ferric sulfate is a particularly desirable oxidant because it selectively attacks the iron-sulfide minerals in coal and does not contaminate the coal matrix (Meyers, 1977).

The reaction between finely disseminated pyrite and ferric ion is not only of interest in coal desulfurization. Geidel and Caruccio (1977) suggest that the finely disseminated pyrite present in coal and its associated strata, when oxidized by ferric ion, is also a cause of acid mine drainage, and Kleinmann et al. (1981) emphasize the role that ferric ion plays in the production of acid mine drainage.

Moreover, the ferric ion is used as a leaching agent and oxidant in the fields of hydrometallurgy and metals extraction (Dutrizac and MacDonald, 1974). A hydrometallurgical application that has received considerable attention, and involves the reaction of finely disseminated chalcopyrite and pyrite with ferric ion, is the deliberate industrial leaching of copper from low-grade porphyry copper waste dumps (Cathles and Apps, 1975; Murr, 1980). These

examples illustrate the importance of the reaction between ferric ion and pyrite disseminated throughout various geologic matrix materials.

Because of the widespread interest in pyrite oxidation by ferric ion, extensive research on the chemistry of the reaction appears in the literature. The following reaction summarizes the overall stoichiometry of pyrite leaching by ferric sulfate:

$$FeS_2 + (2+12X)Fe(III) + (8X)H_2O \rightarrow (3+12X)Fe(II) + (14X)H^+ + (2X)HSO_4^- + 2(1-X)S^o \quad . \quad (D-1)$$

The notation used in Eq.(D-1) accounts for the production of both elemental sulfur (S^o) and bisulfate ion (HSO_4^-), and in effect, combines the following two reactions:

$$FeS_2 + 2Fe(III) \rightarrow 3Fe(II) + 2S^o \quad (D-1a)$$

$$FeS_2 + 14Fe(III) + 8H_2O \rightarrow 15Fe(II) + 14H^+ + 2HSO_4^- \quad . \quad (D-1b)$$

Equations (D-1) and (D-1b) are written with HSO_4^- as a reaction product because the majority of leaching has been performed below pH 2.0 ($pK(25^oC) = 1.97$ for the reaction $HSO_4^- \rightarrow H^+ + SO_4^{2-}$; Barnes et al., 1966). S^o is a metastable product of pyrite oxidation by ferric ion. The conversion of S^o to fully oxidized HSO_4^- involves a complex kinetic pathway. The sulfur oxyanions involved in the kinetic pathway are not known at low pH (< 4.0) because the rate of oxidative conversion of intermediate sulfur species to HSO_4^- is too rapid to detect within current analytical time frames (Goldhaber, 1980). Fe(III) and Fe(II) will be used in this paper to represent the total ferric and total ferrous ion concentrations, respectively. The total

species concentrations may include complexed iron species such as ferric and ferrous bisulfate or sulfate, as well as the free ion species. It is more correct to write the reactions in terms of the dominant species present in solution under a specified set of leaching conditions. To write the reactions using dominant aqueous species, the distribution of aqueous species in solution must be known. Calculation of the species distribution is discussed in more detail in the experimental section of this paper. The stoichiometric X coefficient is reported to vary between zero (all S^o product) and one (all HSO_4^- product), depending upon the leaching conditions. The values for X reported in the literature appear in Table D-1.

A large number of studies have addressed the problem of pyrite oxidation by ferric ion with no enclosing matrix material present (Tab.D-1). The oxidation of pyrite disseminated within a host matrix by ferric ion has received little attention outside of work related to low-grade porphyry copper leaching (Murr, 1980). The reason is that the study of the reaction between in situ finely disseminated pyrite and ferric ion in the laboratory is extremely difficult, and conventional analytical methods of measuring reaction progress are pressed to the limits of their sensitivity. Concentrated ($\geq$0.02 M) ferric bisulfate is commonly used as a leaching medium. One would like to detect changes in reactant (Fe(III)) and product (Fe(II), HSO_4^-) concentrations (5-10 ppm) that are hundreds of times less than their concentration in a bulk solution (1000-2000 ppm). Finely disseminated pyrite constitutes a small fraction ($\sim$<2.0 wt. %) of the matrix material within which it is enclosed. Therefore, little

TABLE D-1

Compilation of Stoichiometric X Coefficients for the Reaction:

$$FeS_2 + (2+12X)Fe(III) + (8X)H_2O \rightarrow (3+12X)Fe(II) + (14X)H^+ + (2X)HSO_4^- + 2(1-X)S^o$$

(enclosing matrix material absent)

X	Temp °C	pH	Fe(III), M	anions	comments	reference
1.0	33	0-2.0	10^{-4}	HSO_4^-	emf ≥250mv (ore pyrite)	Garrels and Thompson(1960)
0.0	33	0-2.0	10^{-7}	HSO_4^-	emf <250mv	Garrels and Thompson(1960)
1.0	30-70	0-1.5	0.02	HSO_4^-	coal pyrite	Mathews and Robins(1972)
1.0?	20?	0.2-2.0	0.002-0.2	Cl^-,HSO_4^-	coal and ore pyrite	Smith and Shumate(1970)
1.0?	25	0.5-4.0	0.002-0.45	Cl^-,HSO_4^-	" " "	Sasmojo(1969)
0.6	102	2.0	1.0	Cl^-,HSO_4^-	coal system (-200 mesh)	Hamersma et al.(1973)
0.3	102	2.0	1.0	Cl^-,HSO_4^-	ore pyrite	Hamersma et al.(1973)
1.0	25	1.0	10^{-4}	?		Singer and Stumm(1970)
0.2	40	?	0.1	Cl^-	marcasite?	King and Perlmutter(1977)
0.4	50	?	0.1	Cl^-	"	" " "
0.6	60	?	0.1	Cl^-	"	" " "
0.6	70	?	0.1	Cl^-	"	" " "
0.5	80	?	0.1	Cl^-	"	" " "
0.2	80,100	0.7	0.1-0.5	HSO_4^-		King and Lewis(1980)
0.5	40-80	1.0	?	HSO_4^-	ore pyrite	Mishra(1973)
0.34	100	0.0	0.05	HSO_4^-		Yurovskii(1974)
0.7	100	0.0	0.10	HSO_4^-		"
0.76	100	0.0	0.50	HSO_4^-	ore pyrite??	"
1.0	100	0.0	1.2	HSO_4^-		"
1.0	40-104	0-2.0?	0.01-1.0	HSO_4^-	coal system (-20, -200 mesh)	Betancourt and Hancock(1978)

pyritic material is available for reaction per unit mass of matrix, and additions of reaction products to the solution are accordingly minute.

The analytical problem has dictated changes in experimental design so that the reaction can be studied by standard analytical methods. Commonly, either (1) the disseminated pyrite is separated from the host matrix, then reacted; (2) the experimental conditions are modified to speed the reaction rate by increasing the temperature, pressure, and concentration of reactants, or by decreasing the ratio of the volume of the aqueous phase to the mass of solid phase; or, (3) the matrix material and associated sulfides are pulverized extensively to expose sulfides to the leach solution. These procedures allow one to measure changes in reactant and product concentrations analytically as the oxidation of pyrite by ferric ion proceeds, but the sample preparation and experimental conditions inhibit a direct understanding of the mechanism by which finely disseminated pyrite is leached from various geologic matrix materials.

Column leach studies are useful for discerning the overall leaching characteristics of a sulfide containing matrix under conditions of practical hydrometallurgical interest (Murr, 1980). However, the heterogeneity of the column charge, which must be large for the reasons already discussed, keeps the basic factors controlling the leaching process from being directly studied. For example, the iron and sulfate products from the oxidation of pyrite are difficult to discriminate from iron and sulfate ions leached from such acid soluble phases as gypsum, anhydrite, jarosite, and melanterite. These

phases are common to complex host matrices like coal and felsic rocks (Davis, 1982; Bladh, 1982). Also, column experiments usually contain a range of matrix fragment sizes and the nature of pyrite in different fragments can vary from finely disseminated to pure "chunk" pyrite. These fragments may leach quite differently, and it is difficult to deduce the leaching characteristics of the component pyrite morphologies from the bulk leaching characteristics of the column sample as a whole.

This paper reports the development of an experimental technique with the sensitivity to measure the oxidation rate of <u>in situ</u> finely disseminated pyrite directly from carefully selected samples. This new technique permits direct experimental measurements of the leaching kinetics of the iron sulfides disseminated in a complex natural matrix. This paper not only introduces the technique, but it also illustrates its applicability to a specific leaching problem. The technique is reported in a separate short article because it may be of general hydrometallurgical interest.

EXPERIMENTAL METHODOLOGY

Redox Potential Measurements: An Historical Perspective

Garrels and Thompson (1960) introduced redox potential (Eh) measurements using a platinum electrode as a way to study the rate at which dilute (<0.02 M) ferric sulfate reacts with pyrite. These researchers recognized that the reaction rate was proportional to the total ferrous and total ferric ion concentrations. They utilized the Nernst equation, which they wrote in a form that relates Eh to the formal solution potential (E_f^o) and to the total solution concentration of ferric and ferrous ion:

$$Eh = E^o_f + \frac{RT}{F} \ln \frac{C_{Fe(III)}}{C_{Fe(II)}} \quad . \qquad (D\text{-}2)$$

At a constant absolute temperature, T, Eh changes reflect changes in the ratio of $C_{Fe(III)}$ to $C_{Fe(II)}$ and changes in E^o_f. R, the universal gas constant, and F, Faraday's constant, are both constants in (D-2). The formal potential of the solution depends on the nature of the solution (anions, cations, complexation, pH, concentration, and temperature) and is generally determined by titration methods (Garrels and Thompson, 1960). The uncertainty in measured values of E^o_f and concern with the problem of multiple redox couples contributing to mixed potentials at the platinum electrode surface have caused most workers to regard Eh as only a qualitative measure of reaction progress.

Smith and Shumate (1970) used Eh in a kinetic study of the oxidation of pure pyritic materials (no matrix) by ferric ion. They did not relate Eh directly to a reaction rate. Instead, they kept Eh constant by titrating with a concentrated ferric ion or $KMnO_4$ solution, and they related the amount of titrant required to keep Eh constant to the rate at which ferric ion reacted with pyrite. Their study left unresolved the question of whether the platinum electrode measured only the redox couple of interest (Fe(II)-Fe(III)) or a combination of potentials from other electroactive species such as dissolved oxygen.

Natarajan and Iwasaki (1970) addressed the problem of measuring redox potential in a variety of hydrometallurgical plant practices involving, for example, the acid leaching of uranium ores and flotation circuits. They noted that mixed potentials at the Pt electrode were a problem in oxygenated ferric sulfate. Subsequently, Natarajan and Iwasaki (1974a, 1974b) showed that the problem of mixed potentials for the redox couple between ferric and ferrous ion at the Pt electrode in oxygenated and deoxygenated solutions of 1 M H_2SO_4 was eliminated if the concentration of ferric and ferrous ions was each $>10^{-2}$ M. In earlier work, Natarajan and Iwasaki (1970) had concluded that the redox couple between ferric and ferrous ion behaves reversibly at a Pt electrode in solutions of pH <3.0. In summary, if pH <3.0, total ferric ion concentration $>10^{-2}$ M, and total ferrous ion concentration $>10^{-2}$ M, then potentials measured in iron sulfate solutions with a Pt electrode are controlled by the Fe(III)-Fe(II)

redox couple.

No significant work appears, however, to have been done using constant Eh techniques since the investigations of Natarajan and Iwasaki validated the use of the Pt electrode in iron sulfate solutions. Moreover, the significance of their work for monitoring chemical solution changes with Eh measurements does not appear to be generally appreciated.

Nevertheless, their work, and that of Smith and Shumate, provide a basis for the use of Eh measurements to study the oxidation of pyrite disseminated within a matrix of bituminous coal by concentrated ($\geq$0.02 M) ferric sulfate. This study uses a titration technique similar in principle to the one described by Smith and Shumate (1970), to measure quantitatively the rate at which ferric ion is reduced by pyrite disseminated in a coal matrix. The study determines the bounds of the valid application of the technique, and it shows that organic carbon derived from the coal matrix does not interfere with the H_2O_2 titration technique.

Experimental Equipment: Design and Materials

The study required an experimental reaction system designed to control the temperature, Eh, and pH of a leach solution within a reaction vessel. The reaction vessel (Fig. D-1) had a double walled Pyrex glass jacket[1] through which water could be circulated from a constant temperature bath[2]. The temperature of both the bath and

---

[1]Commercially available from Ace Glass Inc. P.O. Box 688 Vineland, NJ.
[2]Tecam Model TE-7.

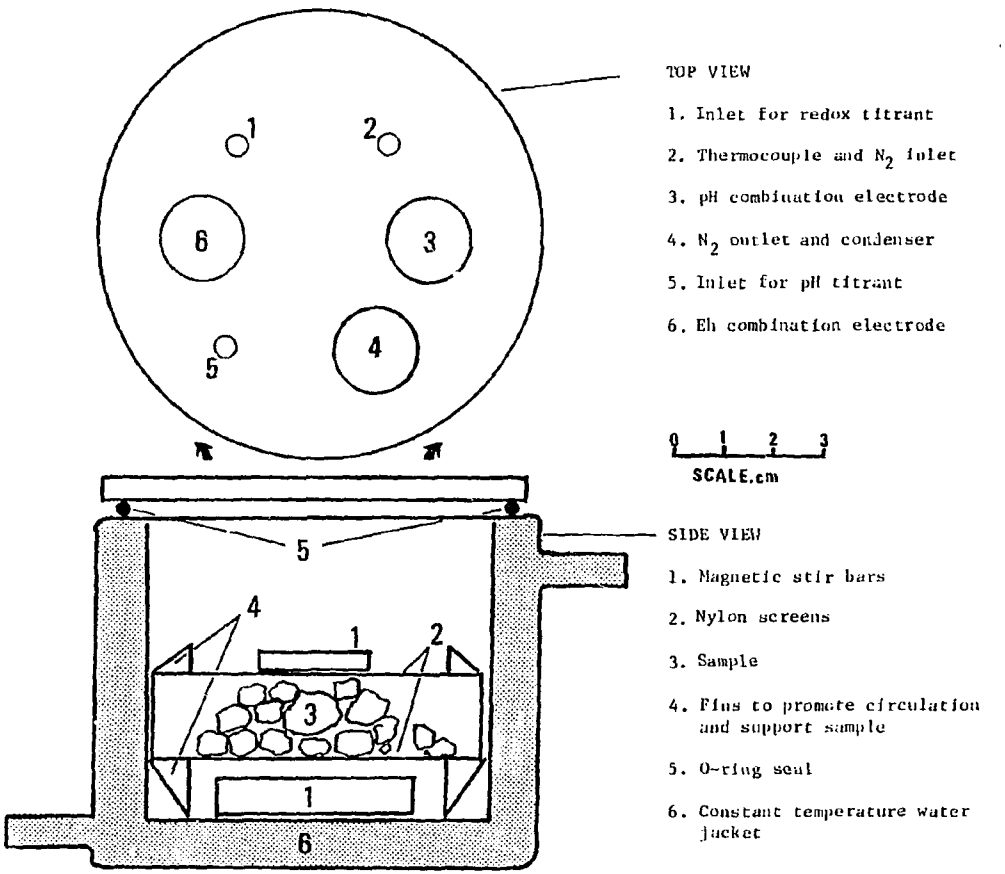

Figure D-1 Reaction Vessel

reaction vessel were thus held constant to a tolerance of $\pm 0.2^{\circ}C$. The advantage of using a remote bath for temperature control is that an electric magnetic stirrer[3] can be placed directly below the vessel to stir the leach solutions. Electrically powered stirrers permit better control over the rate of stirring than models driven by air or water. The stir motor rpm setting was calibrated to the actual stir bar rpm using a strobe light (see calibration data at the end of this appendix). An inert atmosphere could be maintained within the reaction vessel more easily because the stir bars required no access port.

The reaction vessel was sealed airtight by placing a rubber O-ring between the top rim of the vessel and the reaction vessel cover. The top cover had six ports designed to hold the electrodes, thermocouple, and inlet-outlet tubing. The top view of Fig. D-1 the vessel cover.

Inside the vessel, a support platform made of plexiglass held a sample between two 100-mesh nylon screens[4]. The screens served to prevent the flotation of sample particles and also minimized particle decrepitation and abrasion from direct contact with the stir bars. Below the support platform, a 3.8-cm magnetic stir bar rested on the vessel bottom. A second 2.3-cm magnetic stir bar rested on the upper screen. The supporting plexiglass legs of the sample platform were designed to promote fluid circulation within the vessel (Fournier, 1973). A distinct vortex was apparent in the leach solutions at stir rates >400 rpm regardless of whether a sample was present in the

---

[3]Manufactured by Lapine Scientific Co. Chicago, IL.
[4]Commercially available from Spex Industries, Metuchen, NJ.

holder.

A non-oxidizing atmosphere was maintained by passing nitrogen into the vessel at ~0.2 kg/cm^2 pressure. Prior to introducing the gas into the vessel, the gas was scrubbed of CO_2 using Ascarite and of O_2 using a solution of vanadous chloride. The gas then entered a scrubber containing distilled water to eliminate any traces of the vanadous chloride solution. Finally, the gas passed into a bubbling tube containing distilled water. This tube was maintained at the experimental temperature to equilibrate the temperature of the gas and to saturate it with water before it entered the reaction vessel. Outflowing nitrogen first passed through a water-cooled condenser and then through a trap containing mineral oil to monitor gas outflow and prevent any air from entering the reaction system.

The reaction progress was monitored with the equipment shown in Fig.D-2. A pH-millivolt (mv) meter and a combination pH-reference (Ag-AgCl) electrode monitored the pH of the leach solution. A solenoid controlled auto-titrator[5], operating a standard burette, controlled the pH. This titrator would dispense either an acid or a base, as required, to maintain the desired solution pH.

The redox potential was monitored with a digital millivolt meter[6] connected to the leach solution in the vessel by a combination platinum-reference electrode[7]. The gel-filled electrode had a slow rate of electrolyte leakage (1 µl/day) which resulted in the addition of only a minimal amount of saturated KCl to the leach solution. For

---

[5]Fisher Scientific Titrimeter Model 26.
[6] Kiethley Instruments Model 177.
[7]Chemtrix Inc. model P-189 (gel filled, Ag-AgCl reference).

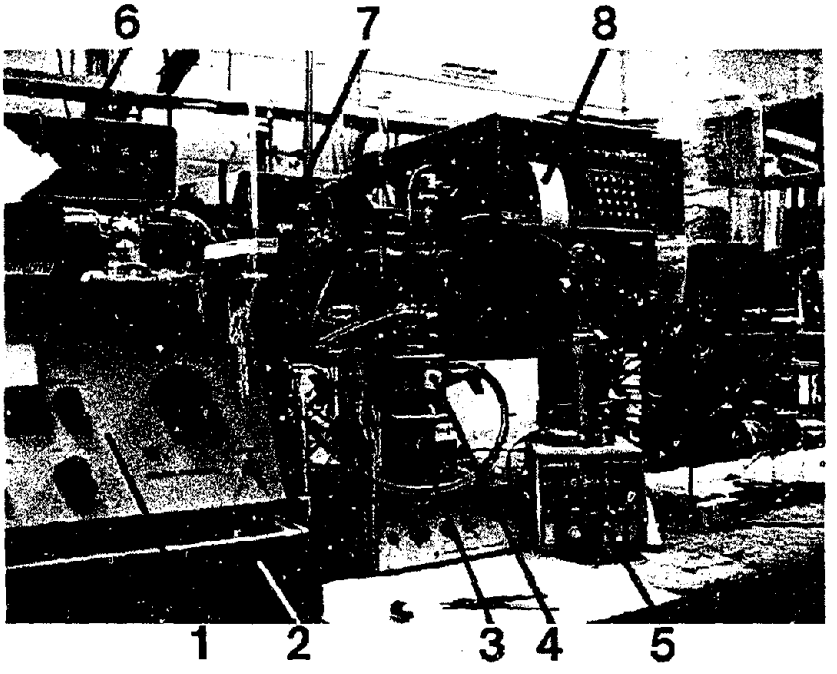

1. pH Stat Titrator
2. Eh Stat Titrator
3. Magnetic Stirrer
4. Reaction Vessel
5. Auto-burette (redox titrant)
6. pH Meter
7. Millivolt multimeter (redox potential)
8. Data Logger

Figure D-2 . Experimental Equipment Layout

comparison, typical rates of electrolyte leackage for asbestos fiber and ceramic plug junction reference cells are 1 ml/day (Langmuir, 1971). The redox potential was controlled with an automatic titrator[8] set to the desired potential. The titrator controlled a digital auto-burette[8] which dispensed oxidant into the reaction vessel.

The voltage output from the digital auto-burette, proportional to the amount of titrant dispensed, entered a multi-channel data logger[9] programmed with a pre-calibrated linear conversion to convert that voltage input to milliliters of titrant consumed. Accordingly, the milliliters (ml) of titrant consumed as a function of time were recorded on a paper tape at programmed sampling intervals, one hour for the work reported here. Simultaneously, using the logger's multi-channel capability, redox potential, temperature, and pH were recorded at hourly intervals on the same paper tape in a similar fashion. The pH reading represented simply a check on the ability of the auto-titrator to keep pH constant. A more desirable and quantitative approach would incorporate an auto-burette similar to the type used for redox titration to perform the pH maintenance. The data logger provided uninterrupted, automated data collection at one hour intervals during runs of extended duration.

Buffers were used to calibrate the pH meter to $\pm$0.05 pH units at 25°C, and matching the buffer temperature with the vessel temperature ensured a proper pH calibration at higher temperatures. Frequent (twice daily) pH electrode calibration was necessary to compensate for drift of the pH electrode unrelated to the leaching reaction. At pH

---

[8] Manufactured by Metrohm Herisau Inc.
[9] Monitor Labs model 9300.

values below 1.5, the magnitude of the electrode drift was typically between -0.05 and -0.10 pH units during a 12-hour period.

Zobell's solution (Langmuir, 1971) was used as a redox potential buffer to check the Eh electrode system for proper response at different temperatures. The emf of Zobell's solution measured with a platinum electrode referenced against a saturated KCl/Ag-AgCl electrode varied with temperature (in the range 8-85°C) according to Nordstrom's equation (1977):

$$emf_{Zob}(T) = 0.23145 - 1.522\times10^{-3}(T-25) - 2.245\times10^{-6}(T-25)^2. \quad (D-3)$$

In (D-3), T is in degrees Celsius and emf is measured in volts. In the temperature range 25-50°C, potentials measured with the combination Eh electrode were less than the potentials calculated from (D-3) by a constant value of 0.012 V. The reproducibility of emf readings proved to be $\pm$ 0.001 V.

The Eh of a leach solution at a particular temperature (Eh(T)) is related to the emf measured with a platinum electrode and a saturated KCl/Ag-AgCl reference cell ($emf_{obs}(T)$) by the following equation (Wood, 1976):

$$Eh(T) = emf_{obs}(T) - emf_{Zob}(T) + Eh_{Zob}(T) \quad (D-4)$$

The potentials must have consistent units (volts). $Eh_{Zob}(T)$ is the emf (in volts) of Zobell's solution relative to the standard hydrogen electrode, and it has a temperature dependence (8-85°C) given by the following equation (Nordstrom, 1977):

$$Eh_{Zob}(T) = 0.43028 - 2.5157\times10^{-3}(T-25) - 3.7979\times10^{-6}(T-25)^2. \quad (D-5)$$

Using Eq.(D-4), one can now convert measured emf values to Eh. The Eh units in Eqs. (D-3), (D-4), and (D-5) are consistent with the Eh units required by Eq.(D-2). Thus, the Eh calculated from thermodynamic theory, an assumption of equilibrium, and the distribution of aqueous species in the leach solution can be compared to emf values measured in the laboratory with the Pt electrode, and vice versa. This comparison is discussed further in the next section.

ILLUSTRATIVE LEACHING EXPERIMENTS

Selection and Preparation of the Coal Sample

The samples for the leaching experiments were carefully selected to provide information on the leaching of pyrite finely disseminated in a coal matrix. The coal came from the Illinois Herrin #6 coal seam of Peabody Coal's River King #3 mine. As-received, the coal contained macroscopic massive (x.0-1x.0 cm) pyrite fragments. A microscopic examination revealed four morphologic types of pyrite disseminated throughout the coal: (1) coarse, anhedral, 50 to 100 μm diameter pyrite blebs; (2) 50 μm or larger mossy or dendritic aggregates of micron-sized pyrite particles; (3) cell infillings of pyrite in fusinite macerals; and (4) finely disseminated pyrite grains (5-10 μm diam.). Gluskoter (1968) has described and photographed the latter three pyrite morphologies. All the pyrite except that with a finely disseminated morphology can be removed by conventional mechanical coal cleaning processes. Chemical pyrite leaching, therefore, has its greatest potential applicability in removing finely disseminated pyrite. Consequently, the discussion here describes the procedure used to isolate samples that contain finely disseminated pyrite.

The samples for analysis and leaching were sieve-sized into five fractions, and the fractions were subjected to a 2.8 g/cm^3 specific-gravity liquid[10] float-sink separation. The coal particles with a bulk density <2.8 g/cm^3 comprised the float material. Pyrite-rich particles with a bulk density >2.8 g/cm^3 were removed from the samples

---

[10]Certigrav flotation medium.

as the sink fraction. The float fraction consisted of coal particles that contained disseminated pyrite and was retained for experimental study. This procedure failed to reject the pyrite occurring as fusinite cell infillings. Discrete particles of fusinite, identified through a binocular microscope, were removed from the leach samples with fine forceps or tweezers. Post-preparation microscopy revealed that some dendritic aggregates of pyrite and coarsely disseminated pyrite remained after preparation. But, using a combination of conventional and Rapid-Scan (Kuehn, 1979) reflected light microscopy, their combined contribution to the total disseminated pyrite was estimated to be less than 5 percent. Ninety-five percent of the remaining pyrite had a finely disseminated morphology, which, from a comparison of the forms-of-sulfur analyses of the prepared and as-received coals, comprised about 45 percent of the total pyrite in the as-received Illinois #6 coal sample.

The float-sink separation was not designed to remove carbonate phases associated with the coal. However, carbonates are undesirable phases because they react with H^+ and the net effect is to increase the pH of the leach solution. Consequently, carbonates were removed by soaking the coal in 1 M HCl for 15 minutes, at which time $CO_2(g)$ production (fizzing) ceased. The coal was then washed with distilled water until no Cl^- was detected in the effluent water (i.e., the addition of $AgNO_3$ produced no milky AgCl precipitate indicating the presence of Cl^-). The coal was then air dried at 30°C for 24 hours. A detailed preparation flow chart for both the experimental and analytical splits of the five size fractions appears with a summary table of the analytical data in Appendix .

One size fraction (+3.2mm -9.5mm) was chosen to illustrate the technique reported here. The elemental, proximate, and forms of

sulfur analyses of this size fraction appear in Table D-2.

Ten-gram samples of coal were leached in the batch reactor. Fresh solutions were added to the reactor at the beginning of each batch experiment (every 24 hours) to prevent a significant build-up of reaction products in solution. A discussion of the reproducibility of measurements obtained on replicate 10-gram samples of the +3.2 -9.5mm coal appears in a later section of this paper.

It should be emphasized again that samples were carefully selected to be of one type, and that the objective was to illustrate a technique to measure, and ultimately to understand, the leaching of finely disseminated pyrite from a natural matrix. The objective was not to characterize the leaching of a natural coal sample consisting of a mixture of many types and sizes of coal fragments, but to measure the leaching of one carefully selected type and size of fragment within which finely disseminated pyrite predominated.

Composition of the Leach Solution

Stock leach solutions were prepared using reagent grade chemicals. Ferrous sulfate ($FeSO_4 \cdot 7H_2O$) was used to prepare the leach solution because the compound has a well-defined hydration state as compared to ferric sulfate ($Fe_2(SO_4)_3 \cdot nH_2O$). The ferrous sulfate solution could then be oxidized to the appropriate ferric ion concentration. Ferrous sulfate was dissolved in distilled, deionized, degassed water acidified to pH 1.5 with concentrated H_2SO_4. The stock leach solution, prepared in four-liter batches, was standardized for

Table D-2. Analytical Data for Prepared Illinois #6 Coal
(+3.2mm, -9.5mm size fraction)

ELEMENTAL ANALYSIS (dry wt. % Basis)

Carbon	Hydrogen	Nitrogen
63.9	4.55	1.34

PROXIMATE ANALYSIS (dry wt. % basis, except moisture)

moisture	volatiles	ash	fixed carbon
3.06	39.18	11.12	49.70

FORMS OF SULFUR ANALYSIS (dry wt. % basis)

pyritic S	sulfate S	organic S	total S
1.15	0.21	2.19	3.55

total iron by EDTA titration. The total initial iron concentration of the leach solution was 2.08 g/l throughout this study. A 100-ml aliquot of stock solution was used for each experimental run. Once the aliquot reached a constant run temperature, the desired redox potential and pH were attained by adding drops of concentrated H_2O_2 (30% solution) and H_2SO_4 (18.0 M), respectively. Total solution required for Eh adjustment of the 100-ml starting solution was approximately 0.2 ml and adjustment of pH required 0.7 ml.

The equilibrium distribution of aqueous species in the leach solution under the selected run conditions was computed by a successive approximation-continued fraction iterative method similar to the WATEQF solution scheme (Plummer et al., 1976). A flow chart of the computational algorithm and the APL computer code written to perform the speciation calculations appears in Addendum 2. The thermodynamic data for the calculations appear in T ble D-3 with the appropriate references. A summary of the solution composition and run conditions used for the experiments discussed in this paper appears in Table D-4.

Titrant Selection

pH Titrant

A pH titrant was required to compensate for the hydrogen ion produced in Eq. (D-1), and in effect, to maintain pH constant. NaOH was selected as a pH titrant because only Na^+ ion and water resulted as neutralization products:

Table D-3 Equilibrium Reactions and Thermodynamic Data for Speciation Calculations (25°C and 1 atm total pressure)

	Reaction and appropriate vector location ( ) in DISTRIB	ΔH_r^o, kcal/mol	Log K_{eq}	Debye-Huckel $\mathring{a}$ for charged ion pair $10^8 a$(cm)[d]	notes and references
(1)	$H^+ + SO_4^{2-} = HSO_4^-$	5.40[b]	1.97	9(H^+) 4(SO_4^{2-}) 4(HSO_4^-)	$\Delta G_f^o(SO_4^{2-})$ = -177.9; Parker et al. (1976) combined with $\Delta G_f^o(HSO_4^-)$ from Wagman et al. (1968)
(2)	$Fe^{2+} + SO_4^{2-} = FeSO_4^o$	1.60[b]	2.20	6(Fe^{2+}) 0($FeSO_4^o$)	Smith and Martell (1976)
(3)	$Fe^{2+} + HSO_4^- = FeHSO_4^+$	0.0[c]	1.10	5	Wiersma (1982) est'd
(4)	$Fe^{3+} + SO_4^{2-} = FeSO_4^+$	6.0[b]	3.96	9(Fe^{3+}) 5($FeSO_4^+$)	Smith and Martell (1976)
(5)	$Fe^{3+} + 2SO_4^{2-} = Fe(SO_4)_2^-$	4.60[a]	5.38	7[e]	Wagman et al. (1969)
(6)	$Fe^{3+} + HSO_4^- = FeHSO_4^{2+}$	0.0[c]	0.6	7[e]	Sapieszko et al. (1977)
(7)	$Fe^{2+} + H_2O = FeOH^+ + H^+$	13.20[a]	-9.48	5	Tremaine et al. (1977)
(8)	$Fe^{3+} + H_2O = FeOH^{2+} + H^+$	10.40[a]	-2.19	5	Baes and Mesmer (1976); Smith and Martell (1976)
(9)	$Fe^{2+} + 2H_2O = Fe(OH)_2^o + 2H^+$	28.56[a]	-20.6	0	Baes and Mesmer (1976); Smith and Martell (1976)
(10)	$Fe^{3+} + 2H_2O = Fe(OH)_2^+ + 2H^+$	0.0(?)	-5.67	5.4	Baes and Mesmer (1976); Smith and Martell (1976)
(11)	$2Fe^{3+} + 2H_2O = Fe_2(OH)_2^{4+} + 2H^+$	13.5	-2.95	11	Baes and Mesmer (1976); Smith and Martell (1976)

[a] Ball et al. (1980)

[b] Smith and Martell (1976)

[c] est'd from data of Sapieszko et al. (1977); for Van't Hoff eqn. enthalpy set = 0.0, since Keq = const. for 25-80°C.

[d] Kielland (1937)

[e] est'd

Table D-4. Run Conditions and the Corresponding Distribution* of Aqueous Species in the Ferric-Ferrous Sulfate Leach Solution.

Run Conditions:

Temperature = 40°C

pH = 1.25 Eh = 0.708 V

Ionic Strength = 0.11

Total iron, molal = 0.0358

Total sulfate, molal = 0.0754

Distribution of Aqueous Species:

Species	molality	% of total iron
Fe^{2+}	0.00774	21.62
Fe^{3+}	0.00201	5.60
$FeSO_4^{\circ}$	0.00178	4.96
$FeSO_4^{+}$	0.02095	58.53
$Fe(SO_4)_2^{-}$	0.00165	4.61
$FeHSO_4^{+}$	0.00134	3.73
$FeHSO_4^{2+}$	0.00009	0.26
$FeOH^{+}$	0.00000	0.00
$FeOH^{2+}$	0.00024	0.68
$Fe(OH)_2^{\circ}$	0.00000	0.00
$Fe(OH)_2^{+}$	0.00000	0.00
$Fe_2(OH)_2^{4+}$	0.00000	0.00
H^{+}	0.06812	
HSO_4^{-}	0.03774	
SO_4^{2-}	0.01016	

Total Fe(III), molal = 0.02495

Total Fe(II), molal = 0.01085

Total Non-Hydroxide Fe(III). molal = 0.024702

*An APL computer program using WATEQ iterative techniques (Plummer at al., 1976) was written to calculate the solution species distribution, (see flow chart and computer code at the end of this appendix).

$$NaOH + H^+ \rightarrow Na^+ + H_2O \quad . \qquad (D\text{-}6)$$

Eh Titrant

The object of introducing a redox titrant into the reaction vessel is to maintain Eh constant. The reaction between pyrite and ferric ion produces ferrous ion as a product. The addition of ferrous ion to solution tends to lower the measured emf and the calculated Eh. A titrant is required that will quantitatively oxidize each mole of ferrous ion produced back to ferric ion. The rate of ferric ion replenishment provides a measure of the rate at which pyrite reacts with ferric ion.

Hydrogen peroxide (H_2O_2) served as a redox titrant because of its well defined overall oxidation-reduction stoichiometry with the ferric-ferrous ion couple. H_2O_2 reacts with ferrous ion in the following series of elementary reactions (Burkin, 1966):

initiation:

$$Fe^{2+} + H_2O_2 \rightarrow Fe^{3+} + {}^{\cdot}OH + OH^- \qquad (D\text{-}7a)$$

chain propagation:

$$^{\cdot}OH + H_2O \rightarrow H_2O_2 + {}^{\cdot}HO_2 \qquad (D\text{-}7b)$$

$$^{\cdot}HO_2 + H_2O_2 \rightarrow O_2 + H_2O + {}^{\cdot}OH \qquad (D\text{-}7c)$$

termination:

$$^{\cdot}OH + Fe^{2+} \rightarrow Fe^{3+} + OH^- \qquad (D\text{-}7d)$$

$$^{\cdot}OH + {}^{\cdot}HO_2 \rightarrow O_2 + H_2O \qquad (D\text{-}7e)$$

Free radicals ($^{\cdot}OH$) are formed as H_2O_2 is reduced and the free radicals, in turn, oxidize ferrous ion. This reaction mechanism

yields an overall stoichiometry of 2 moles of ferrous ion oxidized per mole of H_2O_2, provided H_2O_2 and $^{\cdot}OH$ react only with ferrous ion. Schumb et al. (1955) pointed out that the 2 mole ferrous ion per one mole H_2O_2 stoichiometry is quantitative when ferrous ion is present in excess of H_2O_2. The concurrent decomposition of hydrogen peroxide, the evolution of dissolved oxygen, and the oxidation of ferrous ion will occur if H_2O_2 is more concentrated than ferrous ion. The experimental technique presented here was designed so that ferrous ion would be more concentrated than hydrogen peroxide. This makes hydrogen peroxide a particularly desirable titrant because only water and ferric ion are overall reaction products. H_2O_2 is also a milder consumer of acid (H^+) than such other oxidizing agents as MnO_4^- and $Cr_2O_7^{2-}$ (Weast, 1978).

A redox titrant must be reasonably resistant to decomposition caused by internal chemical interactions and external effects from the storage environment. H_2O_2 is not a particularly stable compound (Mortimer, 1971); therefore, its stability had to be checked under laboratory conditions (25°C) during its storage in the light resistant auto-burette. The following procedure was used to check the stability of the H_2O_2.

Reagent grade $KMnO_4$ was standardized against oxalic acid (Vogel, 1961). The $KMnO_4$, in turn, was used to standardize reagent grade 3% H_2O_2 (Vogel, 1961). Both standardizations were by volumetric titration. Aliquots of the standardized H_2O_2 were taken from the auto-burette and restandardized to check for any decomposition of the H_2O_2. No decomposition was noted during the one-week periods planned

for the experimental runs. Frequent (weekly) restandardization is recommended as a precaution.

In addition to the quantitative stoichiometry relationship and the need for the Eh titrant to be stable, the titrant selected for redox potential adjustment of acidic ferric sulfate used to leach coal requires two other attributes: (1) rapid reaction with ferrous ion upon introduction into the leach solution; and (2) selective reaction with ferrous ion in the presence of dissolved organic carbon.

The rate at which Eq. (D-7a) proceeds is a function of the amount of ferrous ion present in solution (Benson, 1960). This kinetic rate dependence on ferrous ion concentration has only a minor implication in the context of this study. The rate of reaction between H_2O_2 and ferrous ion at pH 1.25 became sluggish at Fe(II) concentrations less than 5×10^{-3} M. This sluggish reaction rate caused an over-titration of the desired redox potential. No over-titration problem was encountered if the concentration of ferrous ion required for the valid use of the Pt electrode (10^{-2} M) was maintained. At concentrations above 5×10^{-3} M Fe(II), the H_2O_2-ferrous ion reaction was found to be complete within seconds after H_2O_2 was added to the leach solution. The time necessary for the reaction to proceed to completion was evidenced by a redox potential increase and stabilization in stirred solutions.

When the overall stoichiometry of Eqs. (D-7a)-(D-7e) must be used quantitatively, the selectivity of H_2O_2 and $^{\cdot}OH$ to ferrous ion is critical if organic carbon is in solution. Free radicals are known to be reactive species and may interact with organic species in solution

(Turney, 1965).

An experiment was designed to test the selectivity of H_2O_2 to ferrous ion in the presence of dissolved organic carbon. The Total Organic Carbon (TOC) added by coal fragments was measured for (1) batch addition of ferric sulfate and no Eh control, (2) batch additions with Eh control by H_2O_2, and (3) batch additions with Eh control by permanganate titrant. Ten-gram sample splits of coal were used in each case and each split was subjected to five batches of leach solution. $KMnO_4$ was compared with H_2O_2 because $KMnO_4$ reacts readily with organic carbon to produce $CO_2(aq)$ (Vogel, 1961). This reaction is used in analytical chemistry to standardize $KMnO_4$ solutions under acid conditions.

The results (with corrections for titrant volume additions) appear in Figure D-3. The cumulative TOC addition to solution for the sample subjected to no Eh control was found to be linear with time to 80 hours, as was the sample subject to Eh control by peroxide titration. As expected, the run solutions subject to Eh control by permanganate titration showed a reduction of TOC levels attributable to the reaction of the dissolved organic carbon with the $KMnO_4$ titrant. The analyses were performed by Penn Environmental Consultants of Pittsburgh on samples filtered through 0.45μ membrane filters. No statistically rigorous error estimate was obtained for the TOC analyses; however, organic carbon standards and sample replicates submitted for analysis with the batch run solutions indicated accuracy and precision of $\pm$ 2%.

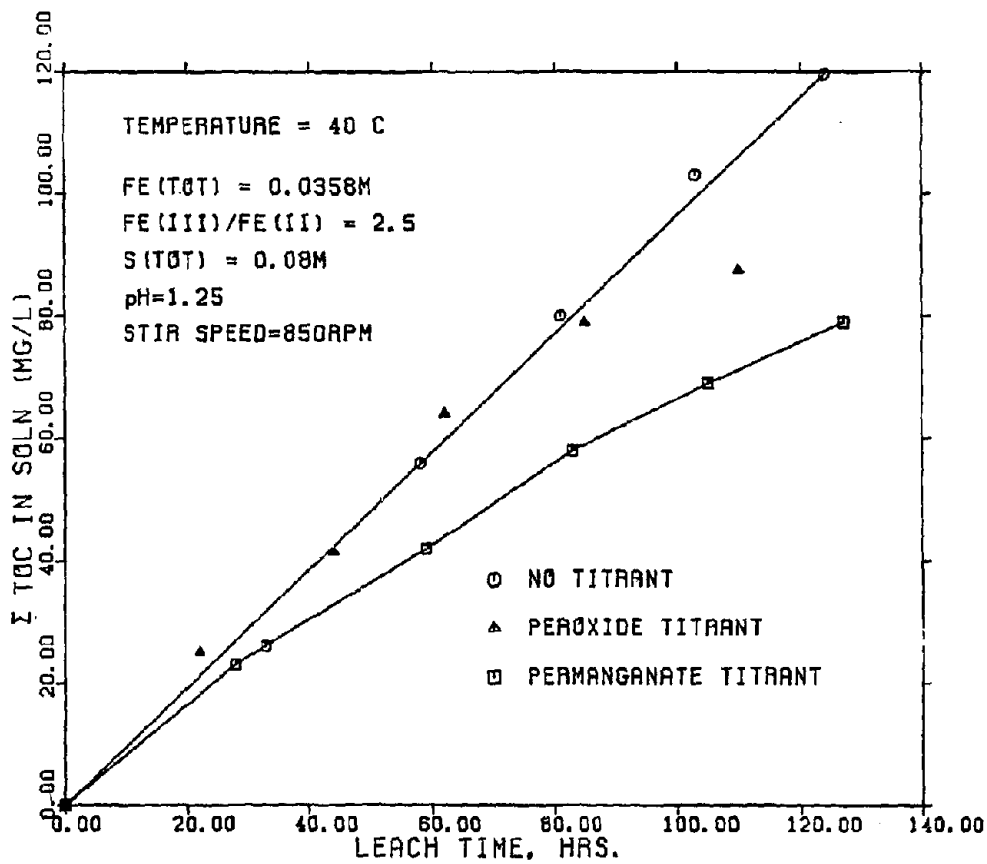

Figure D-3 . Total Organic Carbon (TOC) levels in three separate multi-batch experiments.

A second experiment tested further the selectivity of peroxide for the oxidation of ferrous ion in the presence of dissolved organic carbon. Potassium biphthalate (KHP) was chosen as a source compound of organic carbon because it is comprised of a benzene ring and two carboxylic acid functional groups. Both these organic compounds are likely to be associated with organic coal material and may serve to represent the organic carbon derived from coal leaching. Also, KHP is recommended for use as a dissolved organic carbon standard (ASTM proc. D2579-78).

Ten aliquots of the leach solution were titrated with H_2O_2. Prior to the titrations, organic carbon (32±2 ppm) was added to five of the ten solution aliquots. The other five contained no organic carbon. Each of the ten aliquots was then titrated to an Eh of 0.690 V at 25°C. The same amount (within 0.04 ml) of H_2O_2 was required to titrate the samples containing organic carbon as those without organic carbon. Two days after the H_2O_2 titrations, CO_2 coulometric titration was used to determine the TOC content of each of the ten samples. The samples containing organic carbon retained their pre-titration organic carbon content (32±2 ppm). These findings at 25°C support the results obtained from the TOC experiment performed at 40°C, and provides additional evidence that the organic carbon was not oxidized to $CO_2(aq)$ by the H_2O_2.

As a final check, the validity of the overall stoichiometry of 2 moles ferrous ion oxidized per mole H_2O_2 was tested by performing redox titrations as Walling (1975) suggested. Solutions of ferrous sulfate that contained organic carbon (32±2 ppm) and others with no

organic carbon were titrated with 1.5 and 3.0% H_2O_2. A known quantity of H_2O_2 was found to cause similar redox potential shifts in the organic-containing and the organic-free solutions. By analyzing the solutions for ferrous ion (dichromate titration) before and after H_2O_2 addition, the mole ratio of ferrous ion oxidized to ferric ion per mole of H_2O_2 was determined. The results of the titrations performed on the solutions containing organic carbon agreed with those performed on the organic-free solutions and the 2:1 (ferrous:peroxide) stoichiometry was verified to within 0.1 moles of ferrous ion oxidized per mole of H_2O_2. A TOC threshold for the valid application of the 2:1 overall stoichiometry was determined to be 60 ± 5 ppm TOC. Above this level, the 2:1 overall stoichiometry broke down so that less of the ferrous ion was oxidized to ferric ion per mole of peroxide. At a TOC level of approximately 900 ppm, the stoichiometry of Eq. (D-7a) effectively described the moles of ferrous ion oxidized per mole of H_2O_2. An explanation for the observed behavior is that above 60 ± 5 ppm TOC the free radicals began to react with organic carbon instead of ferrous ion, thereby lessening the selectivity of peroxide for ferrous ion.

To confirm that the H_2O_2 reacting with ferrous ion was completely consumed, colorimetric analyses (Eisenberg, 1943) were performed on aliquots of leach solution extracted from the vessel within minutes after redox potential adjustment and stabilization had occurred. These analyses revealed no residual H_2O_2 above a detection limit of 10^{-5} M.

Hydrogen peroxide met the four requirements for use as a redox titrant:

(1) a quantitative stoichiometry with the ferrous-ferric ion redox couple;

(2) stability during burette storage (~1 week periods);

(3) a rapid reaction with ferrous ion with its addition to the leach solution (provided $C_{Fe(II)} > 5 \times 10^{-3}$ M); and

(4) a selective reaction with ferrous ion in the presence of dissolved organic carbon (provided TOC $< 60 \pm 5$ ppm).

The 0.448 M (1.5%) H_2O_2 concentration proved to be an acceptable compromise. Too concentrated a solution (0.9M), would cause overshoot of the desired redox potential; too dilute a solution (0.1M), caused use of H_2O_2 volumes in excess of 5% of reaction vessel volume.

Approximately 0.05 ml of H_2O_2 (0.448 M) was necessary to shift the redox potential of the 100-ml leach solution by 0.002 V. In the well stirred leach solution, the 0.05 ml H_2O_2 addition was diluted effectively to 2.24×10^{-4} M. Therefore, peroxide decomposition concurrent with ferrous ion oxidation was avoided because the requirement that the peroxide concentration be less than the ferrous ion concentration (0.01085 M) was satisfied.

Experimental Sensitivity

Equation (D-2), combined with the stoichiometry from Eq. (D-1b), for example, may be used to estimate the sensitivity of Eh in terms of changes in the ratio of total ferric ion to the total ferrous ion

concentration. Every milligram (mg) of ferrous ion added per liter of the leach solution (that is, every ppm of iron addition from pyrite leaching) should decrease the emf (and Eh) by approximately one millivolt. A two millivolt change in Eh can be detected and corrected for by automatic titration. Thus, for the leach solution used in this study (2.08 g/l total iron), and for concentrated iron lixiviants in general, redox potential is more sensitive than analytical techniques for detecting small (2 ppm) additions of iron to solution. This sensitivity is largely achieved by the stoichiometric constraints of the leach reaction (Eq. (D-1)). A relatively large amount ((3+12X) moles) of ferrous ion is produced and ferric ion reduced ((2+12X) moles) for every mole increase in the total iron concentration of the bulk solution. For this reason, Eh, which reflects the concentration ratio of total ferric to ferrous ion, when defined in terms of a formal potential, is a particularly sensitive measure of reaction progress.

The problem of pH electrode drift discussed previously made pH measurements insensitive as a measure of reaction progress. The pH-stat titrator was able to detect and compensate for a 0.05 unit change in pH. At pH values below 1.50, reaction related pH changes during a 24-hour batch run fell within the error in pH calibration. In addition, H_2O_2 serves partially as a pH titrant as it adjusts the Eh of the leach solution. Two moles of acid are consumed for every two moles of ferrous ion oxidized to ferric ion by H_2O_2. The dual effect of peroxide in altering the Eh and pH of the leach solution complicates the use of pH titrant consumption as a measure of reaction progress.

Eh Drift Versus Eh Stat Experimental Runs

In an Eh drift experiment, the Eh of the leach solution changes in response to reaction progress. An Eh-stat experiment uses H_2O_2 as a titrant to keep the Eh constant (STATic or STATionary). Initially, a relatively simple Eh drift experiment was used to examine the sensitivity of redox potential measurements.

A 10-gram coal sample was leached with five successive batches of ferric sulfate, and for each batch the redox potential was allowed to shift in response to the progress of the reaction. The results of these runs appear in Fig. D-4a as a plot of emf versus run time. These data show that changes in redox potential were measured within hours (h) of the initiation of the experiment. The resulting decrease in redox potential with time was non-linear, and each of the five batch runs behaved similarly. The magnitude of the decrease in redox potential was largest for batch-1 and became less for each subsequent batch. The Eh drift experiment proved that redox potential shifts are large enough to be useful in studying the reaction between pyrite disseminated within a host coal matrix and ferric ion.

Figure D-4b shows the consumption of H_2O_2 titrant as a function of run time for five successive batch leach runs with emf maintained constant at 0.518 V. The experiment was performed on a second 10-gram coal sample. A linear relationship between peroxide consumption and time with a positive slope was obtained. The slope of the line is largest for the initial batches and diminishes for subsequent batches. This trend is similar to the one observed in the Eh drift experiment

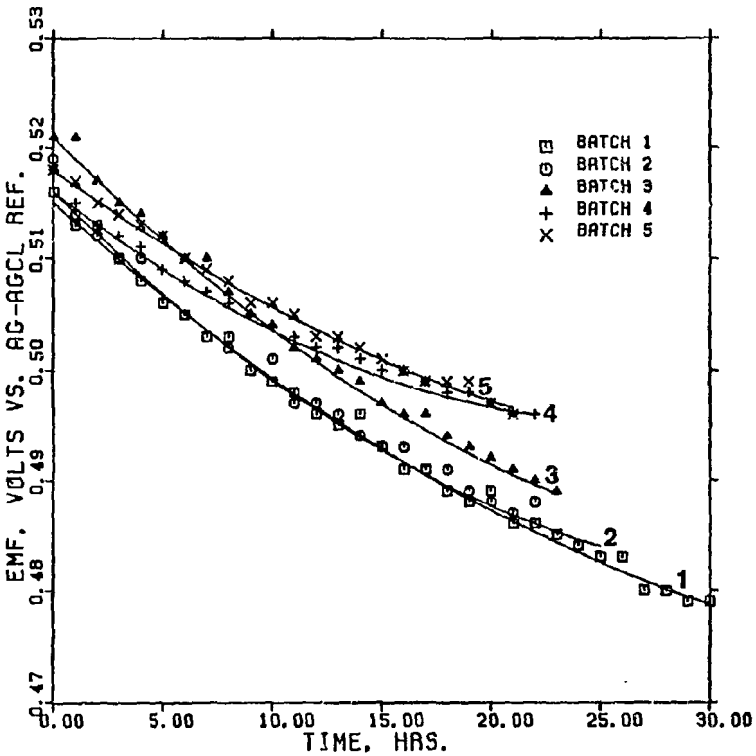

Figure D-4a. Eh drift experimental results for redox potential (EMF) as a function of time in five successive batches of ferric sulfate used to leach a 10-gram Illinois #6 coal sample.

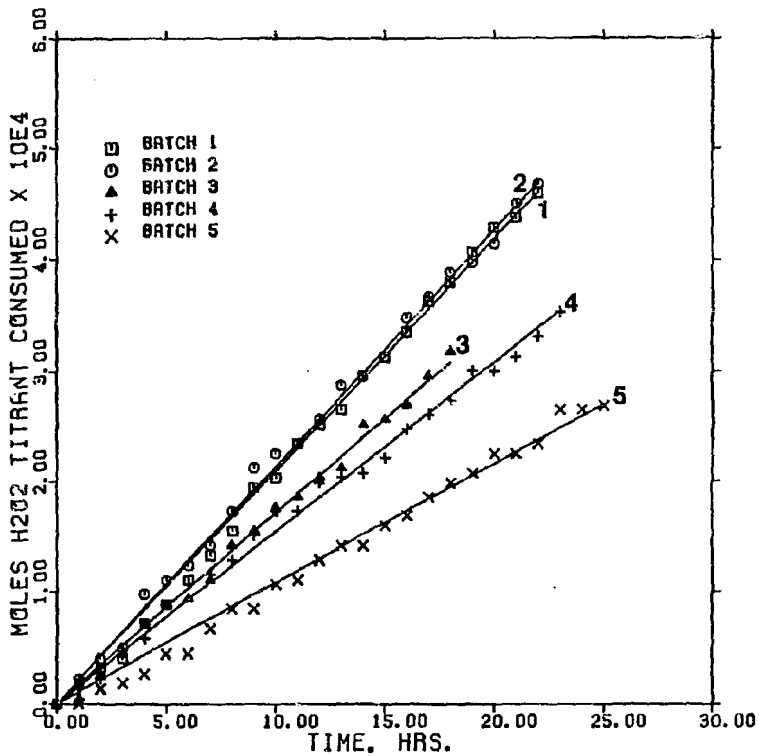

Figure D-4b. Eh Stat experimental results showing the consumption of H_2O_2 titrant with increasing run time for five successive batches of ferric sulfate used to leach a second 10-gram Illinois #6 coal sample.

where the emf decrease in initial runs was greater than it was in later runs.

Interpretation of the data is simplified in the Eh-stat case where the concentration of Fe(III) species in solution is held approximately constant. With a constant Fe(III) concentration, the rate of leaching is, for theoretical reasons, expected to depend only on temperature and time.

The slope of the relationship between peroxide consumption and run time (moles H_2O_2/h) is related to the rate at which pyrite reacts. Equations (D-7a) and (D-7d) indicate that one mole of H_2O_2 oxidizes two moles of ferrous ion to ferric ion through the free radical reaction mechanism. Equation (D-1) indicates that (2+12X) moles of ferric ion are required to oxidize one mole of pyrite. These stoichiometric relations yield the following equation:

$$\text{moles pyrite oxi./h} = [2/(2+12X)] \text{ moles } H_2O_2 \text{ consumed/h.} \quad \text{(D-8)}$$

To use (D-8) in complex leaching systems, ferric ion must be reduced only by reacting with pyrite. In systems containing coal, Meyers (1977) has found that ferric ion is reduced by reacting with coal (-100 or -200 mesh) at 100°C and that the magnitude of the coal-related ferric ion reduction becomes greater for coals of lower rank. The Eh stat technique may be used to estimate the magnitude of this extraneous reaction by ferric ion. Forms-of-sulfur data for the coal sample before and after leaching may be compared with the total H_2O_2 consumed to produce two estimates of the stoichiometric X coefficient in Eq. (D-1).

Reproducibility of Rate Measurements

The technique introduced in this paper measures the reaction rate of pyrite disseminated within coal fragments having a relatively coarse size distribution. Because of the coarse coal particle size and the small sample (10-grams) being tested, it is useful to assess the reproducibility of the measured rate of H_2O_2 consumption.

Six 10-gram coal samples were tested under the same run conditions as those listed in Table D-4. Each sample contained approximately 25 individual fragments of coal. The H_2O_2 consumption rate over the initial 21 hours of leaching was compared. This comparison appears in Table D-5 where the rate data are listed along with the summary statistics. A standard deviation of 29-percent about the mean of six rate measurements was determined. The maximum absolute error attributable to the rate measurement technique itself is between two and four-percent. Therefore, the magnitude of the observed standard deviation reflects variability in the nature of the coarsely-sized coal samples being leached. It is useful to compare the 29-percent variability in the rate of peroxide consumption between fresh samples and the observed rate change in the leaching history of a single sample.

Table D-5 . H_2O_2 Consumption Rate Data from Replicate Leaching Experiments

Run I.D.	Time, h.	H_2O_2 consumption rate (moles/h) x 10^{-5} $\pm$ 1 s.d.
SF18381	21	2.09 $\pm$ 0.02
SF18382	21	2.13 $\pm$ 0.01
T40F1	21	1.89 $\pm$ 0.03
T40F2	21	2.83 $\pm$ 0.02
T40F3	21	3.63 $\pm$ 0.02
T40F4	21	3.63 $\pm$ 0.06

mean = 2.70×10^{-5}

Std. Dev. = 0.79×10^{-5}

Std. error of mean = 0.32×10^{-5}

Coefficient of variation = 29%

Fig. D-4b shows nearly a 50-percent drop in the rate of leaching after 110 hours of total leach time (i.e., batch-1 = 2.13×10^{-4} moles H_2O_2/h and batch-5 = 1.08×10^{-4} moles H_2O_2/h). The 29-percent variation in the initial rate of leaching between fresh coal samples is less than the decrease in rate for a single sample after only 110 hours of leaching.

SUMMARY

Redox potential measurement and H_2O_2 titration are combined in an experimental technique to measure the rate at which the following reaction of pyrite with ferric ion or, for example, its dominant aqueous complex in acid sulfate media takes place:

$$FeS_2 + 14FeSO_4^+ + 8H_2O = 15FeSO_4^o + HSO_4^- + 15H^+$$

The technique is very sensitive ($\pm$ 2 ppm iron added to solution by pyrite leaching) and can be used to study systems of realistic hydrometallurgical complexity where the following limitations restrict using standard analytical measures of reaction progress:

(1) the lixiviant is concentrated (>1000 ppm) in the species consumed and produced in the reaction between pyrite and ferric ion;

(2) the pyrite is enclosed in a matrix of coarse particle size containing iron and sulfate impurities that leach during the pyrite reaction; and

(3) the pyrite is of a fine grained, disseminated morphology that constitutes a small fraction (<2.0 wt.%) of the matrix.

The measurement of redox potential with a Pt electrode in solutions of iron sulfate is valid when pH <3.0 and the concentration of ferric and ferrous ions is each $>10^{-2}$ M.

H_2O_2 is used as a redox titrant to maintain the ratio of total ferric ion to total ferrous ion in the leach solution. H_2O_2 reacts

rapidly and selectively with ferrous ion if the ferrous ion concentration constraint for Pt electrode use is met and the leach solution has an organic carbon content <60±5 ppm. Under these conditions the reaction of H_2O_2 and ferrous ion is described by the overall reaction:

$$H_2O_2 + 2Fe^{2+} + 2H^+ \dashrightarrow 2Fe^{3+} + 2H_2O \quad .$$

The rate of consumption of redox titrant is used to follow reaction progress, and H_2O_2 consumption rate may be interpreted quantitatively in terms of the rate at which ferric ion is reduced by reacting with pyrite.

The Eh-stat technique, used in combination with standard forms-of-sulfur analyses of the coal, provides a way to test hypotheses concerning (1) the selectivity of ferric ion to pyrite within a reactive matrix, and (2) stoichiometry of the ferric ion-pyrite reaction. This technique permits a direct determination of the effect of the matrix material on the kinetics of pyrite oxidation by ferric ion. The technique has possible applications in other fields of hydrometallurgy where one would undertake an analysis of the kinetics of iron sulfide oxidation by lixiviants containing ferric ion.

Appendix D- REFERENCES

Baes, C. F., Jr., and Mesmer, R. E. (1976) The Hydrolysis of Cations, John Wiley Co., New York, 226-236.

Ball, J.W., Nordstrom, D.K., and Jenne, E.A. (1980) Additional and revised thermochemical data and computer code for WATEQ2--a computerized chemical model for trace and major element speciation and mineral equilibria of natural waters: U.S. Geological Survey Water Resources Investigations (WRI), 78-116.

Barnes, H.L., Helgeson, H.C., and Ellis, A.J. (1966) Ionization constants in aqueous solutions. In Handbook of Physical Constants revised edition. Clark, S.P. (editor), Geological Society of America Memoir 97, 402-413.

Betancourt, T. and Hancock, H.A. (1978) Chemical desulfurization of Cape Breton coal by ferric sulfate leaching. Proceedings of the coal and coke sessions--28th Canadian Chemical Engineering Conference, Halifax, Nova Scotia; October 22-25, 1978, Hancock, H.A. (ed.) Canadien Soc. for Chem. Engineering, 157-167.

Benson, S.W. (1960) The Foundations of Chemical Kinetics , McGraw-Hill Co., New York, 596-597.

Bladh, K.W. (1982) The formation of goethite, jarosite, and alunite during the weathering of sulfide-bearing felsic rocks. Econ. Geol. 77, 176-184.

Burkin, A.R. (1966) The Chemistry of Hydrometallurgy Processes , Van Nostrand Co., New York, 80-83.

Cathles, L.M. and Apps, J.A. (1975) A model of the dump leaching process that incorporates oxygen balance, heat balance, and air convection. Metallurgical Transactions B. 6B, 617-624.

Davis, A. (1982) Sulfur in coal. Earth and Mineral Sciences, 51 #2, 13-21.

Detz, C.M. and Barvinchak, G. (1979) Microbial desulfurization of coal. Mining Congress Journal, 65 #7, 75-86.

Dutrizac, J.E. and MacDonald, R.J.C. (1974) Ferric ion as a leaching medium. Minerals Science and Engineering, 6 #2, 59-100.

Eisenberg, G.M. (1943) Colorimetric determination of hydrogen peroxide. Ind. Eng. Chem., Anal. Ed. 15, 327-328.

Ford, W.H., Beimborn, W.A., and Roffman, H.K. (1977) Bacterial removal of sulfur from coal. Combustion, 49 #2, 36-38.

Fournier, R.O. (1973) Silica in thermal waters: laboratory and field investigations. In Proceedings of International Symposium on Hydrogeochemistry and Biogeochemistry, Japan, 1970, Vol.1, Hydrogeochemistry, Washington, D.C.: J.W. Clark, 122-139.

Garrels, R.M. and Thompson, M.E. (1960) Oxidation of pyrite by iron sulfate solutions. Am. J. Sci. 258A, 57-67.

Geidel, G. and Caruccio, F.T. (1977) Time as a factor in acid mine drainage pollution. In Seventh Symposium on Coal Mine Drainage Research Louisville, Kentucky, 41-50.

Gluskoter, H.J. (1968) Forms of sulfur. In Coal Preparation , Leonard, J.W. and Mitchell, J.R. (eds.), AIME Inc., New York, 1-44.

Hamersma, J.W., Kraft, M.L., Koutsoukos, E.P., and Meyers, R.A. (1973) Chemical removal of pyritic sulfur from coal. In Advances in Chemistry Series , No. 127, American Chemical Society, Washington D.C., 68-80.

Hamersma, J.W., Kraft, M.L., and Meyers, R.A. (1977) Applicability of the Meyers process for desulfurization of U.S. coal (a survey of 35 coals). Chapter 11, In Coal Desulfurization: Chemical and Physical Methods , ACS Symposium Series 64 American Chemical Soc. Washington, D.C. 143-152.

King, W.E., Jr. and Lewis, J.A. (1980) Simultaneous effects of oxygen and ferric iron on pyrite oxidation in an aqueous slurry. Ind. Eng. Chem. Process Des. Dev. 19, 719-722.

King, W.E., Jr. and Perlmutter, D.D. (1977) Pyrite oxidation in aqueous ferric chloride. AIChE Journal, 23 #5, 679-685.

Kielland, J. (1937) Individual activity coefficients of ions in aqueous solutions. Am. Chem. Soc. Jour., 59, 1675-1678.

Kleinmann, R.L.P., Crerar, D.A., and Pacelli, R.R. (1981) Biogeochemistry of acid mine drainage and a method to control acid formation. Mining Engineering, March, 300-305.

Kuehn, K.W. (1979) An automated microscopical method for the characterization of pyrite in coal. Unpublished M.S. paper, The Pennsylvania State University, University Park, PA.

Langmuir, D. (1971) Eh-pH determinations. In Procedures in Sedimentary Petrology , Carver, R.E. (ed.), Chapter 26, 597-635.

Mathews, C.T. and Robins, R.G. (1972) The oxidation of iron disulfide by ferric sulfate. Aust. Chem. Eng., August, 21-25.

McCartney, J.T., O'Donnell, H.J., and Ergun, S. (1969) Pyrite size distribution and coal-pyrite particle association in steam coals - correlation with pyrite removal by float-sink methods. Bureau of Mines Rept. of Investigations 7231, 18p.

Meyers, R.A. (1977) Coal Desulfurization , Marcel Dekker Inc., New York, 254p.

Mishra, R.K. (1973) Low temperature surface reactions in leaching of chalcopyrite and pyrite. Unpublished Ph.D. Thesis, Univ. of Utah.

Mortimer, C.E. (1971) Chemistry: A Conceptual Approach , Van Nostrand Reinhold Company, New York, 257-258.

Murr, L.E. (1980) Theory and practice of copper sulfide leaching in dumps and in-situ. Minerals Science and Engineering, 12 #3, 121-189.

Natarajan, K.A. and Iwasaki, I. (1970) Behavior of platinum electrodes as redox potential indicators in some systems of hydrometallurgical interest. AIME Transactions 247, 317-324.

Natarajan, K.A. and Iwasaki, I. (1974a) Eh measurements in hydrometallurgical systems. Minerals Science and Engineering, 6 #1, 35-44.

Natarajan, K.A. and Iwasaki, I. (1974b) Significance of mixed potentials in Eh measurements with platinum electrodes. AIME Transactions 255, 82-86.

Nordstrom, D.K. (1977) Thermochemical redox equilibria of Zobell's solution. Geochimica et Cosmochimica Acta, 41, 1835-1841.

Parker, V.B., Wagman, D.D., and Garvin, D. (1976) Selected thermochemical data compatible with the CODATA recommendations. NBSIR 75-968, Interim Report, Office of Std. Ref. Data, Natl. Bur. Stds., Washington, DC.

Plummer, L.N., Jones, B.F., and Truesdall, A.H. (1976) WATEQF-- a Fortran IV version of WATEQ, a computer program for calculating chemical equilibrium of natural waters. USGS Water Resources Investigations 76-13, 63p.

Sapieszko, R. S., Patel, R. C., and Matijevic, E. (1977) Ferric hydrous oxide sols. 2. Thermodynamics of aqueous hydroxo and sulfato ferric complexes. Jour. of Phys. Chem., 81, #11, 1061-1068.

Sasmojo, S. (1969) Oxidation kinetics of pyritic materials in aqueous media. Unpublished Ph.D. Thesis, Ohio State Univ.

Schumb, W.C., Satterfield, C.N., and Wentworth, R.L. (1955) Hydrogen Peroxide , American Chemical Society Monograph Series, Reinhold Publishing Corp., New York, 490-500.

Singer, S.W. and Stumm, W. (1970) Acidic mine drainage: The rate determining step. Science, 167, 1121-1123.

Smith, E.E. and Shumate, K.S. (1970) The sulfide to sulfate reaction. Water Pollution Control Research Series 14010 FPS 02/70 U.S. Dept. of the Interior, Federal Water Quality Administration, 115p.

Smith, R.M. and Martell, A.E. (1976) Critical stability constants, V.4; in Inorganic Complexes . Plenum Press, New York, 257p.

Tremaine, P.R., Von Massow, R., and Shierman, G.R. (1977) A calculation of Gibbs free energies for ferrous ions and the solubility of magnetite in H_2O and D_2O to 300°C. Thermochim. Acta, 19, 287-300.

Turney, T.A. (1965) Oxidation Mechanisms , Butterworths and Co., Washington, 208p.

Van Nice, L.J., Santy, M.J., Koutsoukos, E.P., Orsini, R.A., and Meyers, R.A. (1977) Coal desulfurization test plant status - July 1977. Chapter 12, In Coal Desulfurization: Chemical and Physical Methods , ACS Symposium Series 64, American Chemical Society, Washington, D.C., 153-163.

Vogel, A.I. (1961) Quantitative Inorganic Analysis , Wiley and Sons, New York, 280-300.

Wagman, D.D., Evans, W.H., Parker, V.B., Halow, I., Bailey, S.M., and Schumm, R.H. (1968) Selected values of chemical thermodynamic properties. Natl. Bur. Stds. Tech. Note 270-3.

Wagman, D.D., Evans, W.H., Parker, V.B., Halow, I., Bailey, S.M., and Schumm, R.H. (1969) Selected values of chemical thermodynamic properties. Natl. Bur. Stds. Tech. Note 270-4.

Walling, C. (1975) Fenton's reagent revisited. Accounts of Chemical Research, 8, 125-133.

Weast, R.C. (1978) Electrochemical Series. In CRC Handbook of Chemistry and Physics , CRC Press, Boca Raton, Florida, D193-195.

Wiersma, C. L. (1982) Relative rates of reaction of pyrite with ferric iron at low pH. Unpublished M.S. thesis, Virginia Polytechnic Institute and State University.

Wood, W.W. (1976) Guidelines for collection and field analysis of ground-water samples for selected unstable constituents. Techniques of Water Resources Investigations, Book 1, Chap. D2, 24p.

Yurovskii, A.Z. (1974) Desulfurization methods based on the use of ferric sulfate. Chap. 18 In Sulfur in Coals , trans. from Russian by Indian National Scientific Documentation Centre, NTIS, 385-408.

Addendum 1: rpm calibration data for magnetic stirrer

Lapine Scientific Model 384-05 Stir Speed Setting	rpm, Measured by Strobe Light	rpm, Measured by Fluke Instr. Digital Line Counter	rpm Used for Experiments
0	--	--	--
1.0	--	--	--
1.5	--	--	--
2.0	--	100	100
2.5	--	200	200
3.0	245 ± 30	264	250
3.5	320 ± 30	370	350
4.0	380 ± 30	426	400
4.5	--	540	500
5.0	695 ± 30	630	650
5.5	790 ± 30	715	750
6.0	900 ± 30	840	850
6.5	985 ± 30	936	950
7.0	1115 ± 30	1074	1050
7.5	1280 ± 30	1224	1250
8.0	1410 ± 30	1380	1350

Addendum 2 : Flow chart and APL computer code for calculating the distribution of aqueous species in acidic iron sulfate solutions

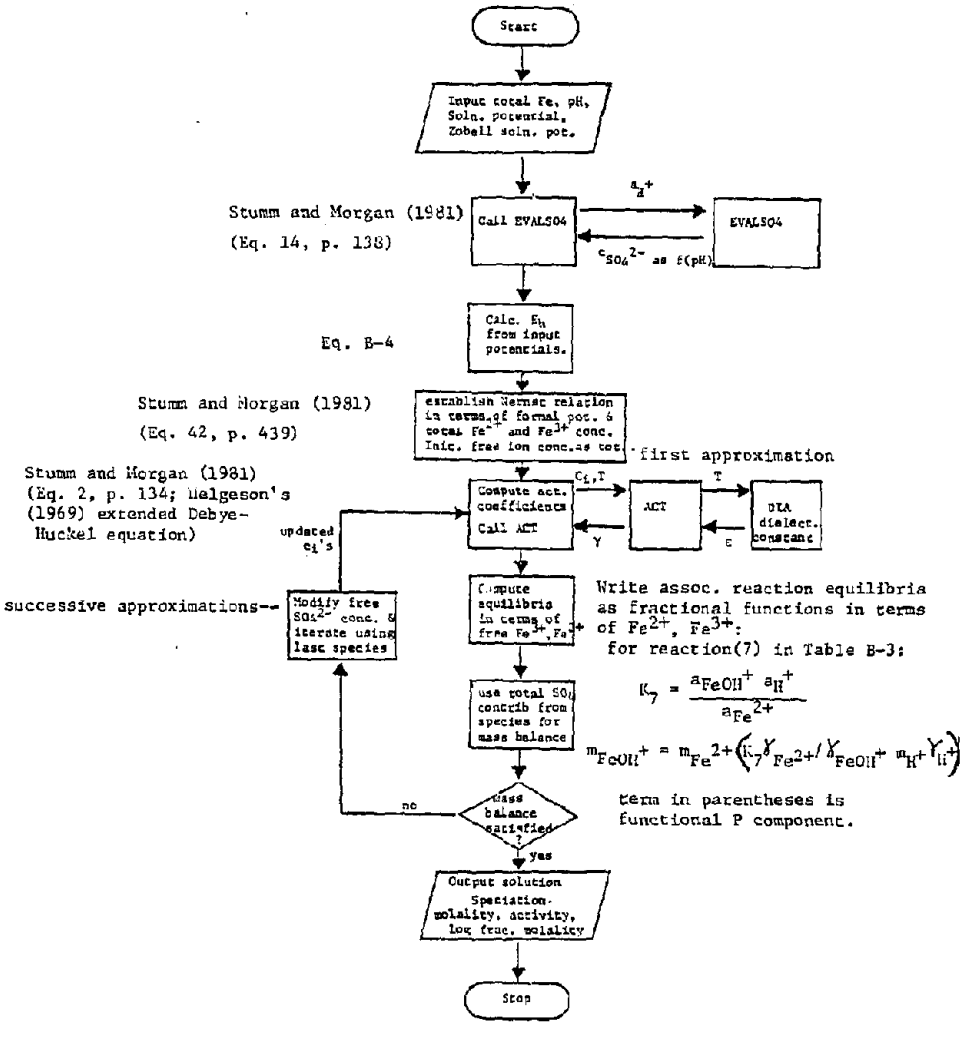

Flow Chart of APL Function DISTRIB

(successive approximation-continued fraction method)

```
      ∇FDISTRIB[□]∇
      ∇ FDISTRIB
[1]   ⍝ APL FUNCTION DISTRIB  KEVIN J BREEN 4/25/81
[2]   ⍝                       L. M. CATHLES AND L. E. EARY
[3]   ⍝                       DEPT. OF GEOCHEMISTRY
[4]   ⍝                       THE PENNSYLVANIA STATE UNIV.
[5]   ⍝ THIS FUNCTION CALCULATES REDOX EQUILIBRIA AND SPECIATION
[6]   ⍝ IN THE FE-SULFATE-H2O SYSTEM AS A FUNCTION OF PH, REDOX
[7]   ⍝ POTENTIAL, TOTAL ANALYTICAL IRON CONC., TOTAL ANALYTICAL
[8]   ⍝ SULFATE CONC., AND TEMPERATURE.
[9]   ⍝ THE FUNCTION IS DESIGNED AS AN AID IN INTERPRETATION OF
[10]  ⍝ EXPERIMENTAL EH AND PH MEASUREMENTS IN AQUEOUS
[11]  ⍝ SOLUTIONS OF FERRIC AND FERROUS SULFATE.
[12]  ⍝
[13]  ⍝   INPUT TO THE PROGRAM CONSISTS OF FIVE LAB MEASUREMENTS:
[14]  ⍝      1.  TOTAL IRON CONC., MOLAR
[15]  ⍝      2.  SOLUTION PH
[16]  ⍝      3.  MEASURED SOLN. POT., V VS SCE OR AG-AGCL REF.
[17]  ⍝      4.  MEASURED ZOBELL SOLN. POT., V VS SCE OR AG-AGCL REF.
[18]  ⍝      5.  SOLUTION TEMPERATURE, °C
[19]  ⍝ THE FUNCTION CORRECTS FOR IONIC STRENGTH RELATED ACTIVITY
[20]  ⍝ EFFECTS USING EXTENDED DEBYE-HUCKEL THEORY WITH THE EXTERNAL
[21]  ⍝ FUNCTIONS ACT (ACTIVITY COEFF) AND DIA (DIELECTRIC CONS.).
[22]  ⍝ EQUILIBRIUM CONSTANTS ARE EXTENDED TO HIGHER TEMPS ASSUMING
[23]  ⍝ ENTHALPY CONSTANT (25-70°C) USING THE VAN'T HOFF EQUATION.
[24]  ⍝
[25]  ⍝
[26]   'ENTER TOTAL FE (MOLAR)):'
[27]   INIT←□
[28]   'ENTER SOLUTION PH,REDOX POT.(V VS REF), ZOBELL SOLN POT. (V VS REF):'
[29]   INIT←INIT,□
[30]   'ENTER SOLUTION TEMP. °C:'
[31]   INIT←INIT,□
[32]   (8 5 ▼FETOT←INIT[1]),(5 2 ▼PH←INIT[2]),(6 3 ▼VVSREF←INIT[3]),(6 3 ▼EZOB←INIT[4]), 5 1 ▼T←INIT[5]
[33]   '↑↑↑THIS INPUT USED BY FDISTRIB'
[34]  ⍝
[35]  ⍝ SET NO. OF SIGNIFICANT DIGITS
[36]   □PP←5
[37]  ⍝
[38]  ⍝    INITIALIZE THERMO DATA VECTORS WITH LOG EQUIL. CONSTS. AND ENTHALPIES
[39]   LOGK25← 2 2.2 1.1 3.96 5.38 0.6 ¯9.48 ¯2.19 ¯20.6 ¯5.67 ¯2.95
[40]   H25← 5.24 1.6 0 6 4.6 0 13.2 10.4 28.56 0 13.5
[41]  ⍝ SET-UP SPECIES NAME VECTOR
[42]   ID←'FE2+      FE3+      H+        HSO4-     SO4-2     FESO4+    FESO4+    '
[43]   ID←ID,'FE(SO4)2- FEHSO4+   FEHSO4+2  FEOH+     FEOH+2    FE(OH)2+  '
[44]   ID←ID,'FE(OH)2+  FE2(OH)2+4'
[45]   IDLIST←(15,10)⍴ID
[46]  ⍝ ASSIGN CHARGE FOR EACH AQUEOUS SPECIE
[47]   CH← 2 3 1 ¯1 ¯2 0 1 ¯1 1 2 1 2 0 1 4
[48]  ⍝ SQUARE CHARGE VECTOR FOR IONIC STRENGTH CALCULATIONS
[49]   ZZ←CH*2
[50]  ⍝ ASSIGN VALUES FOR A-ZERO TERM FOR EACH AQ. SPECIE
[51]  ⍝ A-ZERO IS ''DISTANCE OF CLOSEST APPROACH OF IONS'' AND IS
[52]  ⍝ USED IN DEBYE-HUCKEL EQN IN FUNCT. ACT
[53]   AO← 6 9 9 4 4 0 5 5 7 7 5 5 0 5.4 11
[54]  ⍝ EST. TOTAL SO4 FROM HYD. ION ACT. (H2SO4 ACIDIFICATION AND STOICHIO.
[55]  ⍝ CONTRIB. FROM FESO4 REAGENT.
[56]   ACTH←(10*(-PH))
[57]   ACTHT←ACTH,T
[58]   SO4TOT←FETOT←(EVALSO4 ACTHT)
[59]  ⍝ TAKEN FROM NORDSTROM, D.K. (1977), GCA,41,1835-1841.
[60]  ⍝ STD. POT. OF ZOBELL SOLN. VS H ELECTRODE AS F(T)
[61]   EHZOBT←0.43-(0.0025×(T-25))
[62]  ⍝ COMPUTE EH FROM MEASURED POTENTIALS
```

```
[63]  EH←(VVSREF-EZOB)+EHZOBT
[64] ⍝ FORMAL SOLUTION POTENTIAL(VOLTS) AS F(T)
[65]  EFORMAL←((0.0⌹147×(273+T))-0.11226)-5.111E¯6×((273+T)*2)
[66] ⍝ FERRIC TO FERROUS IRON RATIO
[67]  CONST←10*((EH-EFORMAL)÷(2.303×0.001987×(273.15+T)÷23.06))
[68]  FE2TOT←FETOT÷(1+CONST)
[69]  FE3TOT←FETOT-FE2TOT
[70]  CHG←15⍴0
[71] ⍝ VAN'T HOFF EQN. FOR K(T)
[72]  LOGK←LOGK25+(H25÷(2.303×0.001987))×((÷298)-(÷(T+273)))
[73]  K←10*LOGK
[74]  I←0
[75] ⍝ INITIALIZE MOLALITY AND FUNCTIONAL VECTORS
[76]  X←15⍴0
[77]  P←15⍴0
[78]  X[5]←SO4TOT
[79]  X[1]←FE2TOT
[80]  X[2]←FE3TOT
[81] ⍝ ITERATE TO SATISFY SULFATE MASS BALANCE
[82] ONE:G←ACT T
[83]  X[3]←((10*(-PH))÷G[3])
[84]  P[1]←1
[85]  P[2]←1
[86]  P[6]←K[2]×G[1]×X[5]×G[5]÷G[6]
[87]  P[7]←K[4]×G[2]×X[5]×G[5]÷G[7]
[88]  P[8]←K[5]×G[2]×((G[5]*2)×(X[5]*2))÷G[8]
[89]  P[9]←K[3]×G[1]×K[1]×X[3]×G[3]×X[5]×G[5]÷G[9]
[90]  P[10]←K[6]×G[2]×K[1]×X[3]×G[3]×X[5]×G[5]÷G[10]
[91]  P[11]←K[7]×G[1]÷(X[3]×G[3]×G[11])
[92]  P[12]←K[8]×G[2]÷(X[3]×G[3]×G[12])
[93]  P[13]←K[9]×G[1]÷((X[3]*2)×(G[3]*2)×G[13])
[94]  P[14]←K[10]×G[2]÷((X[3]*2)×(G[3]*2)×G[14])
[95]  P[15]←K[11]×(G[2]*2)×X[2]÷(G[15]×(X[3]*2)×(G[3]*2))
[96] ⍝ COMPUTE MOLALITIES USING EQUIL. FUNCTIONS, P VECTOR
[97]  X[1]←FE2TOT÷(P[1]+P[6]+P[9]+P[11]+P[13])
[98]  X[2]←FE3TOT÷(P[2]+P[7]+P[8]+P[10]+P[12]+P[14]+P[15])
[99]  X[4]←K[1]×X[3]×G[3]×G[5]×X[5]÷G[4]
[100]  X[6]←P[6]×X[1]
[101]  X[7]←P[7]×X[2]
[102]  X[8]←P[8]×X[2]
[103]  X[9]←P[9]×X[1]
[104]  X[10]←P[10]×X[2]
[105]  X[11]←P[11]×X[1]
[106]  X[12]←P[12]×X[2]
[107]  X[13]←P[13]×X[1]
[108]  X[14]←P[14]×X[2]
[109]  X[15]←P[14]×X[2]
[110] ⍝ A SUM FOR SULFATE MASS BALANCE
[111]  SO4TST←X[4]+X[5]+(X[1]×(P[6]+P[9]))+(X[2]×(P[7]+(2×P[8])+P[10]))
[112]  I←I+1
[113] ⍝ SULFATE BALANCE CONVERGENCE TEST
[114]  →((|(SO4TOT-SO4TST))<1E¯6)/TWO
[115] ⍝ RESET SULFATE AND ENTER RECALC. LOOP
[116]  X[5]←X[5]×(1-(0.5×((SO4TST-SO4TOT)÷SO4TST)))
[117]  →ONE
[118] ⍝ OUTPUT SOLUTION CHARACTERISTICS
[119] TWO:'NO. OF ITERATIONS=    ',▼I
[120]  J← 1 2 6 7 8 9 10 11 12 13 14
[121]  XTOT←(+/X[J])+(2×X[15])
[122]  ACTOT←(+/(X[J]×G[J]))+(2×(X[15]×G[15]))
[123]  J← 2 7 8 10
[124]  SOLFE3←(+/X[J])
[125] ⍝ SET UP FRACTIONAL FE OUTPUT
[126]  XTEMP←X
[127]  XTEMP[3]←0
[128]  XTEMP[4]←0
```

```
[129]  XTEMP[5]←0
[130]  '  '
[131]  'SPECIES DISTRIB-------------'
[132]  '            MOLAL      LOG(FRAC FE TOT)   PCT TOTAL IRON   ACTIVITY   ACT COEF'
[133]  '                          (MOLAL)'
[134]  L←1
[135]  OUT:(▼IDLIST[L;⍳10]),(7 5 ▼X[L]),(14 4 ▼(10*(X[L]÷XTOT))),(18 3 ▼(100×XTEMP[L]÷XTOT)),(16 6 ▼G[L]×X[L]),(11 3 ▼G[L])
[136]  L←L+1
[137]  →(L<16)/OUT
[138]  '  '
[139]  'PH=    ',▼-10*(X[3]×G[3])
[140]  'CALC. EH=    ',▼EH
[141]  'IONIC STRENGTH=     ',▼IOH*2
[142]  'TOTAL IRON,MOLAL:  ',(▼XTOT),'  TOTAL IRON ACTIVITY:  ',▼ACTOT
[143]  'TOTAL NON-HYDRXDE FE3+ SPEC,MOLAL:    ',(▼SOLFE3),'  LOG(FRAC TOT FE):',▼(10*(SOLFE3÷XTOT))
[144]  'TOTAL FE3+ SPECIES, MOLAL:     ',▼SOLFE3+X[12]+X[14]+X[15]
[145]  'TOTAL FE2+ SPECIES, MOLAL:     ',▼XTOT-(SOLFE3+X[12]+X[14]+X[15])
[146]  '                  ANION BALANCE ON SULFATE '
[147]  'TOTAL SO4,MOLAL:    ',▼(2×X[8])+X[10]+X[9]+X[7]+X[6]+X[5]+X[4]
[148]  'TOTAL SO4 FROM EVALSO4:    ',▼(EVALSO4 ACTHT)
[149]  'TOTAL SO4 FROM PESO4 REAG:  ',▼FETOT
      ∇
```

Accessory functions for function DISTRIB:

```
      ∇EVALSO4(
              [□]∇
      ∇ ACIDSO4←EVALSO4 ACTHT
[1]   ⍝ GIVEN INPUT HYDROGEN ION ACTIVITY AND SOLN TEMP EVALSO4
[2]   ⍝  RETURNS SULFATE CONC. RESULTING FROM H2SO4
[3]   ⍝  ACIDIFICATION ONLY.  THIS MUST BE ADDED TO
[4]   ⍝  STOICHIOMETRIC CONTRIB. FROM FESO4 REAG.
[5]   ⍝
[6]   ⍝ A LINEAR RELATION EXISTS BETWEEN TEMP (0-50 C) AND LOG K FOR WATER
[7]   ⍝  ALSO A LINEAR RELATION BETWEEN TEMP AND LOG K(DISSOC) FOR HSO4¯
[8]   ⍝ THESE WERE FIT FROM DATA PRESENTED BY BARNES AND HELGESON, 1966.
[9]   ⍝  K(DISSOC) FOR H2SO4 CALC FROM ΔG(RXN)=-6.67 KCAL/MOL AND
[10]  ⍝    K = 10*(ΔG÷(-R×(T+273)×2.303))
[11]  ⍝
[12]  ⍝  THE EXPRESSION FOR SULFATE CONC. AS A F(HYD. ION ACT) WAS
[13]  ⍝  TAKEN FROM STUMM AND MORGAN (1981,P. 138).
[14]  ⍝  DIPROTIC ACID EQUATION USED
[15]  ⍝
[16]   TKW←  0 10 20 30 40 50
[17]   LOGKW← ¯14.95 ¯14.53 ¯14.16 ¯13.83 ¯13.53 ¯13.26
[18]   FITW←LOGKW⌹TKW∘.* 0 1
[19]   LOGKWT←(ACTHT[2]∘.* 0 1)+.×FITW
[20]   TKHSO4← 0 15 18 25 35 45 50
[21]   LOGKHSO4← ¯1.68 ¯1.8 ¯1.9 ¯1.97 ¯2.09 ¯2.22 ¯2.3
[22]   FITHSO4←LOGKHSO4⌹TKHSO4∘.* 0 1
[23]   LOGKHSO4T←(ACTHT[2]∘.* 0 1)+.×FITHSO4
[24]   KW←10*LOGKWT
[25]   KHSO4←10*LOGKHSO4T
[26]   K1←10*(-6.57÷(-0.001987×(ACTHT[2]+273)×2.303))
[27]   K2←KHSO4
[28]   A←((2×K2)+ACTHT[1])
[29]   B1←((ACTHT[1]*3)÷(K1×A))
[30]   B2←((ACTHT[1]*2)÷A)
[31]   B3←((ACTHT[1]×KW)÷(K1×A))
[32]   B4←((ACTHT[1]×K2)÷A)
[33]   B5←((K2×KW)÷(ACTHT[1]×A))
[34]   B6←(KW÷A)
[35]   ACIDSO4←B1+B2-B3+B4-B5-B6
       ∇
```

Temperature dependent dielectric constant for water:

```
      ∇DIA[□]∇
      ∇ Y←DIA T
[1]   Y←87.74+((T*2)×(0.000939))-(((T*3)×(1.415¯6))+(0.4008×T))
      ∇
```

Extended Debye-Huckel equation:

```
      ∇ACT[□]∇
      ∇ G←ACT T
[1]   A←1824600÷(((DIA T)×(273+T))*1.5)
[2]   B←50.29÷(((DIA T)×(273+T))*0.5)
[3]   IOH←(0.5×(+/(X×(CH*2))))*0.5
[4]   G←10*((-A×ZZ×IOH÷(1+A0×B×IOH))+0.041×(IOH*2))
      ∇
```

Note: Statement [35] of Function EVALSO4 should read ACIDSO4←(B1+B2+B4)-(B3+B5+B6)

Example input and output-

```
      FDISTRIB
ENTER TOTAL FE (MOLAR)):
□:
      .0358
ENTER SOLUTION PH,REDOX POT.(V VS REF), ZOBELL SOLN POT. (V VS REF):
□:
      1.25 .518 .203
ENTER SOLUTION TEMP. °C:
□:
      40
  .03580 1.25  .518  .203 40.0
+++THIS INPUT USED BY FDISTRIB
NO. OF ITERATIONS=    31

SPECIES DISTRIB-------------
              MOLAL      LOG(FRAC FE TOT)    PCT TOTAL IRON    ACTIVITY    ACT COEF
                            (MOLAL)
FE2+          .00774          -.6652            21.617          .002964        .383
FE3+          .00201         -1.2517             5.601          .000328        .164
H+            .06812           .2794              .000          .056234        .825
HSO4-         .03774           .0230              .000          .028834        .764
SO4-2         .01016          -.5469              .000          .003355        .330
FESO4°        .00178         -1.3045             4.961          .001794       1.010
FESO4+        .02095          -.2326            58.530          .016329        .779
FE(SO4)2-     .00165         -1.3361             4.612          .001287        .779
FEHSO4+       .00134         -1.4278             3.734          .001076        .805
FEHSO4+2      .00009         -2.5871              .259          .000038        .407
FEOH+         .00000         -8.7397              .000          .000000        .779
FEOH+2        .00024         -2.1653              .683          .000087        .358
FE(OH)2°      .00000        -18.1826              .000          .000000       1.010
FE(OH)2+      .00000         -5.1024              .001          .000000        .785
FE2(OH)2+4    .00000         -5.1024              .001          .000000        .055

PH=   1.25
CALC. ER=   0.7075
IONIC STRENGTH=    0.1104
TOTAL IRON,MOLAL:  0.035798  TOTAL IRON ACTIVITY:  0.023905
TOTAL NON-HYDRXDE FE3+ SPEC,MOLAL:   0.024702  LOG(FRAC TOT FE):-0.16114
TOTAL FE3+ SPECIES, MOLAL:    0.024947
TOTAL FE2+ SPECIES, MOLAL:    0.010852
                ANION BALANCE ON SULFATE
TOTAL SO4,MOLAL:   0.075365
TOTAL SO4 FROM EVALSO4:   0.039564
TOTAL SO4 FROM FESO4 REAG:  0.0358
```

APPENDIX E Experimental Column Leaching of Coal

A. Leach Column Design and Materials

Many variations in column design are reported in the hydrometallurgical literature. In general, the column apparatus is designed to provide as inert a container as possible so that the leaching chemistry of interest may be studied without contamination from the column or accessory hardware. Plastics appear to be best suited for laboratory-scale column leaching applications, both Plexiglass(R) and PVC(R) have been used successfully (Brimhall and Wadsworth, 1973; Bruynesteyn and Vizsoly, 1981). Stainless steel columns have been used in one large-scale leaching experiment (Murr, 1980).

Solution flow within the column is a critical operating parameter and to avoid undue wall effects the column diameter (I.D.) should be four times the largest particle diameter in the aggregate of particles being leached (Potter, 1981). Column length is used to size the experiment to handle the desired mass of material. Four leaching columns, identical to the scale drawing in Figure E-1 were constructed using clear acrylic plastic (Plexiglass) tube. The reader is referred to Figure E-1 for dimensions and other details regarding the construction materials. A photograph of the column apparatus and accessory hardware appears in Figure E-2. The clear column allowed visual checks to be made on solution flow, sample compaction, and solution ponding in the bottom of the column. PVC end fittings (pipe clean-outs) were attached (using PVC cement) to the top and bottom of the

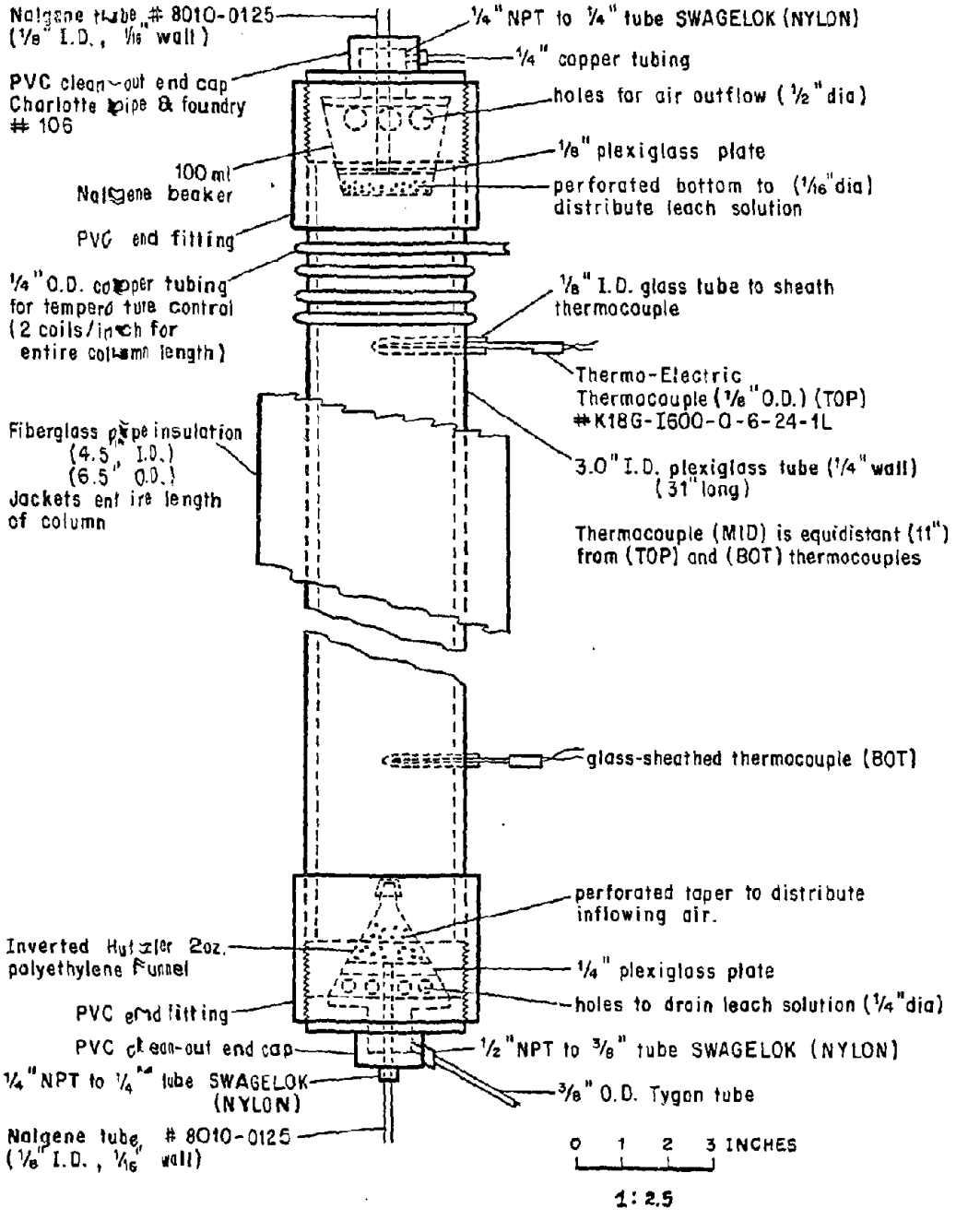

Figure E-1 Design and Construction Materials of the Leaching Column Apparatus (to scale)

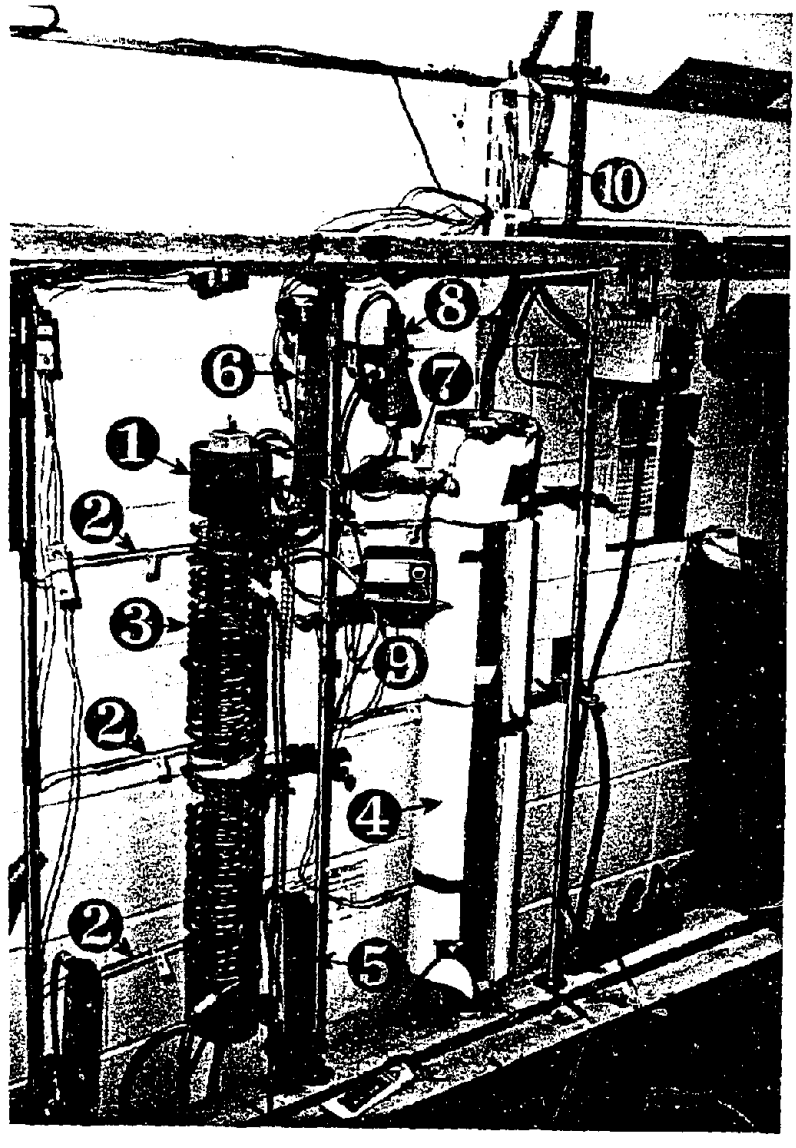

Key:

1. PVC end fittings and caps
2. Thermocouples (TOP, MID, BOTTOM)
3. Copper tubing for temperature control
4. Fiberglass insulation jacket
5. Rotameter for inflow air
6. Rotameter for outflow air
7. Drying tube with desiccant
8. O_2 measurement flask and O_2 probe
9. Oxygen meter
10. Reservoir for leach solution

Figure E-2 The Column Leaching Apparatus and Accessory Hardware

Plexiglass tube. The screw-type inserts (PVC end caps) for the end fittings were modified to hold the inlet and outlet tubing and a solution distribution and collection system.

The top-end cap was drilled to accept an inlet tube for leach solution and an outlet tube for effluent air. Nylon Swagelok(R) compression fittings and Nalgene(R) tubing were used throughout to maintain an air-tight seal and also prevent corrosion. A 100-ml Nalgene beaker was designed and fit to the top-end cap as a leach solution applicator. Thus, the leach solution was sprinkled evenly at the top of the bed of particles within the column. In a similar fashion, the bottom-end cap was drilled for an inlet air tube and a drainage tube for effluent leachate. An inverted polyethylene funnel was designed and fit to the bottom-end cap. The funnel served to 1) support the sample charge in the column, 2) distribute the air inflow evenly in the column, 3) prevent clogging of the solution outflow with particulates while allowing drainage of effluent solution, and 4) prevent leach solution from collecting in the inflow air line.

The column apparatus was designed so that a constant temperature could be maintained throughout the interior of the column. Copper tube was tightly coiled around the column with a spacing of approximately two coils/inch of column. Distilled deionized water could then be circulated from a constant temperature bath.[1] The temperature of the bath was held constant to a tolerance of $\pm 0.2^{\circ}C$. Temperatures up to $65^{\circ}C$ were envisioned for column experimentation and this necessitated using a submersible pump

[1] Tecam model TE-7

unit[2] for water circulation that was thermally insulated and constructed of a plastic material to prevent corrosion at the high operating temperatures. Fiberglass pipe insulation was used to jacket the column and prevent heat loss.

Temperature in the column was monitored with three glass-sheathed type-K thermocouples. Three holes were drilled in the column and the thermocouples were sealed in place with epoxy cement so that the end of the probe rested in the center of the column. Temperatures at the three thermocouple ports were monitored continuously by incorporating a multi-channel data logger.[3] Twelve data channels (3 for each column) were thus dedicated to monitor temperature. Compressed air from a standard laboratory bench outlet was used as a source of air for the column experiments. The bench outlet was modified to accept a compressed air filter[4] and an air line regulator/pressure gage[5]. The compressed air was metered to a predetermined flow rate of 0.003-0.004 std. liters/min. (or a Darcy air flow rate of 0.0011-0.0015 cm/s) with a rotameter[6]. Prior to introducing the air in the column it passed into a bubbling tube containing distilled water. This tube was maintained at the experimental temperature to equilibrate the temperature of the gas and to saturate it with water.

---

[2]Little Giant Pump Co. model NK-1 #526003

[3]Monitor Labs model 9300

[4]Model M-20, Motor Guard Corp., Box 1834, San Leandro, CA 94577

[5]Model 282.16036, Sears Roebuck and Co.

[6]Model #1355CC1B1BAA with a R-2-15-AAA tube, Brooks Instrument Div., Emerson Electric Co., Hatfield, PA 19440

Outflowing air first passed through a drying bottle that contained a desiccant[7] and then into a flask (250 ml Nalgene erlenmeyer) which housed a polarographic probe[8]. The effluent air then passed through a rotameter similar to the one used to meter air inflow. The second (or outflow) rotameter reading could be compared to the inflow rotameter reading to check for air leaks in the column apparatus. Finally, the effluent air passed through a trap containing mineral oil to monitor air outflow qualitatively and prevent back diffusion of air into the O_2 measurement flask or the leaching column.

Measuring the O_2 concentration in the effluent gas stream provided a means of tracking the oxidation reactions taking place between the oxygen in air and the water-saturated coal and pyrite within the column. The polarographic probe responds electrochemically to the oxygen content in the air sample. The current produced by reduction of oxygen at the cathode was input to an oxygen meter[8] which, in turn, produced a voltage proportional to the oxygen concentration in the effluent gas stream. The oxygen analyzer system had to be calibrated and this involved removing the probe from the measurement flask, allowing it to equilibrate with air in the laboratory, and then the meter was adjusted to read 21% O_2. Meter calibration was checked twice each day and adjusted if necessary. Meter fluctuation due to battery discharge was eliminated by incorporating two 120V AC to 9V DC converters. Thus, the meter could be operated on a continuous basis. The voltage

---

[7] Drierite (Anhydrous $CaSO_4$)

[8] Edmont Oxygen Analyzer System, model 60-620, Energetics Science Div. of Becton Dickinson and Co., Elmsford, NY 10523

output from the oxygen meter entered a multi-channel data logger programmed with a pre-calibrated linear conversion from voltage input to percent oxygen.

The data logger produced a record on paper tape at programmed sampling intervals (typically six hours) of the percent oxygen in the air leaving the column. The oxygen probe was rotated between each of the four leach columns every several days.

Leach solution entered the leaching column by gravity flow from a storage reservoir. The solution was applied at predetermined intervals by simply flushing the solution in the reservoir through the packed bed of coal and then collecting the effluent as it drained from the base of the column. Leach solution composition and application rate will be discussed in the section on experimental conditions.

B. Sample Preparation and Analysis

Four column experiments were planned in this study and the coal samples were prepared to provide information on the leaching of pyrite finely disseminated in a coal matrix. Three of the four column experiments were conducted using the Illinois #6 bituminous coal described in Appendix-B. A fourth column experiment was conducted with a Wyoming subbituminous coal. In addition to distinct physical property differences, the greater tendency for subbituminous coal to self-heat and oxidize provided an excellent comparison in leach behavior to the Hi-vol bituminous coal from Illinois.

The leach columns were designed to hold approximately 2.5 kilograms of coal and sample preparation was accordingly less detailed than the procedure for 10-gram samples that appears in Figure 4 of the text. The Wyoming coal did not contain extraneous rock material and therefore was prepared without special hand-picking or float-sink separations. The as-received coal was

crushed to 3/4 inch top size in a chipmunk jaw crusher and the -20 mesh fines removed by sieving. The +20 mesh -3/4 inch size fraction was used for experimentation.

Two 10 kg splits of Illinois coal were taken from the as-received coal. This material contained fragments of clay, shale, and massive pyrite. The macroscopic fragments were removed by hand and the coal was crushed to 3/4 inch top size in a chipmunk jaw crusher. The crushing procedure liberated more massive pyrite from the coal matrix which was again removed by hand. Effort was also placed upon removing the pyrite-enriched fusinite macerals that were characterized by a distinctive bronze coloration and charcoal-like texture. The -20 mesh fines were then removed by sieving. One of the 10 kg splits was used for experimentation at the +20 mesh -3/4 inch size and the other was crushed to 1/4 inch top size. Crushing to 1/4 inch top size again liberated massive pyritic material that was removed by hand. The -20 mesh fines that resulted from the 1/4 inch top size crushing step were removed by sieving, yielding a +20 mesh -1/4 inch coal sample. Sample preparation for analysis is identical to the analytical flowchart that appears in Figure 4 of the text. Selected chemical and physical properties of the coal samples used for the column leaching experiments appear in Table E-1.

Table E-1. Selected Chemical and Physical Characteristics of Coal Used in Column Leach Studies (Before Leaching)

Column Experiment No.	Coal I.D. and (size fraction)	%* Moisture	% Ash (HTA)	Forms of Sulfur Analysis (%) Pyritic S	Sulfate S	Organic S	Total S	Percent Iron in Coal Calc. from % Fe_2O_3 in HTA	Percent Pyrite Calc. from % Iron in Coal	Percent Pyrite Calc. from % Pyritic S	Calorific Value Btu/lb Dry Basis	Mmmf Btu/lb**	dmmf Btu/lb***
1	Wyoming Subbit. (+20 mesh - 3/4 in.)	21.80	5.48	0.13	0.02	0.48	0.63	0.3	0.7	0.24	11955	9805	12674
2	Illinois #6 (+20 mesh - 3/4 in.)	2.93	13.85	0.85	0.40	2.42	3.67	1.7	3.6	1.6	12086	13213	14336
3	Illinois #6 (+20 mesh - 3/4 in.)	2.93	13.85	0.85	0.40	2.42	3.67	1.7	3.6	1.6	12086	13213	14336
4	Illinois #6 (+20 mesh - 1/4 in.)	3.74	11.53	0.79	0.37	2.43	3.59	1.4	3.0	1.5	12190	12830	14035

ASH ANALYSIS

Wt. Percent

	SiO_2	Al_2O_3	TiO_2	Fe_2O_3	MgO	CaO	MnO	Na_2O	K_2O	P_2O_5	SO_3	Totals
Illinois #6	52.8	21.1	0.93	17.3	1.16	1.97	0.025	0.81	2.15			98.25
Wyoming	26.6	14.3	1.20	8.05	4.49	25.1	0.029	0.42	0.30	0.50	19.5	100.49

ppm in Ash

	Ba	Be	Cr	Cu	Ni	Rb	Sr	V	Zn	Zr
Illinois #6	410		170	70	95		200	170	210	160
Wyoming	3150	7	5	160	90	10	2050	210	570	220

*All percents by weight on a dry basis (except moisture)

**Mmmf = [Btu/lb moist coal - 50 (g total S/100 g moist coal)] ÷ [100 - (1.08 (g ash/100 g moist coal) + 0.55 (g total S/100 g moist coal))] x 100

***dmmf = [Btu/lb dry coal -50(g total S/100 g dry coal)] ÷ [100-(1.08(g ash/100 g dry coal) + 0.55 (g total S/100 g dry coal))] x 100

Leaching Conditions:

1. Initial Composition of the Leach Solution and Effluent Solution Analysis

The composition of the leach solution was kept simple and free of iron initially so that effluent iron concentration could be used as a measure of the amount of pyrite solubilized. Distilled water was acidified to a pH of 1.5 with concentrated HCl or H_2SO_4. The acid pH was needed to prevent the hydrolysis of ferric ion and the subsequent precipitation of ferrihydrite (Fe(III)-hydroxide) inside the column apparatus. The leach solutions were stored at room temperature and were added to reservoirs mounted above the column. In this manner, a known volume of leach solution could flow (gravity-flow) into the leach column at pre-determined flushing intervals.

The chemical composition of the effluent leachate was monitored for total iron by atomic absorption spectrometry. The pH of the effluent solutions was also monitored periodically. The results of the total iron analyses are tabulated at the end of this appendix.

2. Bacterial Innoculation

Iron-oxidizing bacteria are known to catalyze the oxidation of pyrite in aqueous media (Lacey and Lawson, 1970). It is therefore desirable to have iron-oxidizing bacteria present and viable in the column experiments. No effort was made to sterilize or treat the coal samples to kill the naturally occurring bacteria associated with coal and coal pyrite. The two column experiments with sulfuric acid lixiviant were innoculated with an active culture of Thiobacillus ferrooxidans. This was accomplished by adding 10 ml of an aqueous growth media containing the bacteria to the column before

starting the regular percolation leaching. No tests were performed to ascertain whether bacterial cells were present in the effluent leachate. Therefore it is not known whether iron-oxidizing bacteria were active during the column experiments. The columns incorporating the HCl lixiviant were not innoculated with the iron-oxidizing bacteria.

3. Column Operating Parameters

The temperature, the solution flush rate, and air inflow rate were the three experimental parameters subject to adjustment during column leaching. Temperatures of 35 and 50°C were chosen for experimentation because:

(1) The activity of non-thermophilic iron-oxidizing bacteria is known to be reduced at temperatures above 50°C (Murr, 1980).

(2) The reaction rate of pyrite and the coal matrix would be at a maximum in this temperature range (relative to temperatures below 35°C). As a result, experiment duration could be lessened and changes to the effluent solution and air chemistry (reflecting the relatively rapid reaction rate) would be more pronounced and easier to measure analytically.

The amount of leach solution used to flush the columns was determined by the practical problems encountered in the manual flush procedure. Leach solutions were applied twice each day and solution volume was determined by the chemical composition of the effluent leachate (i.e., leach rate of the pyrite in the column). The lower temperature column experiments showed low levels of iron in the effluent and a 500 ml/day solution volume was used to flush out the dissolved pyritic iron. Conversely, the effluent solutions from the 50°C column experiments were more concentrated in iron and therefore were flushed with a greater volume of solution each day (1000 ml/day).

To ensure the complete saturation of the coal particles, the column apparatus was flooded with leachate initially. The volume of solution required to fill the column was used to estimate the interblock porosity within the column. The interblock porosity was also computed using coal density. The values agree well and appear in Table E-2. The columns were filled with leachate periodically during the course of the leach experiment to maintain the saturated conditions.

An inflow rate of 0.003 - 0.004 std. liters/min. was selected for metering air into the base of the leaching columns. This flow rate could be measured easily and was slow enough to allow the oxygen concentration in the gas phase to be reduced a measurable amount as it passed through the packed coal bed.

The four column experiments were operated under the conditions that appear in Table E-2.

Table E-2

OPERATIONAL PARAMETERS FOR COLUMN LEACHING EXPERIMENTS

Column Experiment #	^{O}C Temperature	Total Leach Time (days)	Leachate Composition/pH	Coal Mass (Kg)	Solution Flush Rate ml/day	Darcy Air Flow Rate (cm/s)	Interblock Porosity**
1	35	365	HCl/1.5	2.18	500	0.0011-0.0015	--
2	35	422	HCl/1.5	2.46	500	0.0011-0.0015	57%
3	50	376	*H_2SO_4/1.5	2.66	1000	0.0011-0.0015	56%
4	50	379	*H_2SO_4/1.5	2.61	1000	0.0011-0.0015	56%

*Bacterial innoculation with Thiobacillus ferrooxidans ATCC #13661. (Supplied by Prof. R.W. Stone, Microbiology Dept., Penn State University.)

**Interblock porosity = $1 - \left[\left(\frac{\text{mass coal}}{\rho \text{ coal}}\right) \div \text{column volume}\right]$; column volume = 3600 cm^3

D. Experimental Results

Four extended-duration column leaching experiments were conducted in this study. Column 1 and column 2 were leached for 419 days and 427 days, respectively. Column 3 and column 4 were both operated for 374 days. The results of the analyses for total iron in the effluent leachate along with the percent O_2 in the effluent air stream and temperatures measured at the three temperature ports along each column appear in Table E-3. The total iron in the effluent leachate and the fractional O_2 depletion in the effluent air, relative to the influent air, are summarized graphically for the columns that contained Illinois bituminous coal in Figure E-3.

Table E-3

COLUMN LEACHING DATA

NOTES:

Day = Days elapsed in experiment.

Fe_{TOT} = Total iron in effluent leachate (mg/l). (2 sample daily average)

Temperature = Type K thermocouple temperatures (^{o}C) at the top (TOP), middle (MID), and bottom (BOT) of leaching column, see column schematic for exact thermocouple placement. (4 sample daily average)

% O_2 eff. = Percent oxygen in effluent air as measured with a polarographic probe and monitor. (4 sample daily average)

(oxygen content of inflow air = 21%)

-- A zero value (with or without decimal point) represents missing data.

Column 1

Page 1 of 3

Table E-3 (continued)

Line No.	Day	Fe_{TOT}	Temperature TOP	Temperature MID	Temperature BOT	% O_2 Eff
1.	1.0	4.7	.0	.0	.0	14.3
2.	2.0	3.9	.0	.0	.0	11.8
3.	3.0	4.0	.0	.0	.0	11.8
4.	4.0	4.7	.0	.0	.0	11.5
5.	5.0	5.0	.0	.0	.0	10.7
6.	6.0	5.3	.0	.0	.0	12.2
7.	7.0	5.2	.0	.0	.0	16.1
8.	8.0	6.2	.0	.0	.0	19.6
9.	9.0	1.2	.0	.0	.0	.0
10.	12.0	3.7	.0	.0	.0	15.1
11.	13.0	6.0	.0	.0	.0	14.8
12.	14.0	7.4	.0	.0	.0	14.5
13.	15.0	8.4	.0	.0	.0	13.6
14.	18.0	6.3	.0	.0	.0	14.9
15.	19.0	7.6	.0	.0	.0	15.2
16.	20.0	6.7	.0	.0	.0	17.0
17.	21.0	10.8	.0	.0	.0	15.8
18.	22.0	12.8	.0	.0	.0	14.6
19.	23.0	12.1	.0	.0	.0	15.0
20.	25.0	11.4	.0	.0	.0	15.6
21.	26.0	12.2	.0	.0	.0	15.8
22.	28.0	15.0	.0	.0	.0	15.1
23.	29.0	19.2	.0	.0	.0	14.8
24.	30.0	23.5	.0	.0	.0	14.8
25.	31.0	19.9	.0	.0	.0	14.2
26.	32.0	21.2	.0	.0	.0	14.9
27.	33.0	28.9	.0	.0	.0	14.8
28.	34.0	28.3	.0	.0	.0	16.1
29.	43.0	8.0	.0	.0	.0	17.0
30.	48.0	15.3	.0	.0	.0	16.8
31.	49.0	22.8	.0	.0	.0	17.3
32.	53.0	12.6	.0	.0	.0	17.6
33.	54.0	14.3	.0	.0	.0	16.7
34.	55.0	22.9	.0	.0	.0	17.8
35.	56.0	26.3	.0	.0	.0	17.2
36.	57.0	30.7	.0	.0	.0	17.7
37.	59.0	31.4	.0	.0	.0	14.0
38.	60.0	36.1	.0	.0	.0	17.0
39.	61.0	39.2	.0	.0	.0	16.1
40.	62.0	44.8	.0	.0	.0	16.2
41.	63.0	43.6	.0	.0	.0	15.9
42.	64.0	47.0	.0	.0	.0	16.0
43.	67.0	48.6	.0	.0	.0	.0
44.	68.0	52.7	.0	.0	.0	.0
45.	69.0	51.7	.0	.0	.0	.0
46.	75.0	48.2	.0	.0	.0	.0
47.	76.0	50.6	.0	.0	.0	.0
48.	78.0	62.4	.0	.0	.0	.0
49.	80.0	49.4	.0	.0	.0	.0
50.	81.0	44.6	.0	.0	.0	.0
51.	82.0	47.6	.0	.0	.0	.0
52.	84.0	36.8	.0	.0	.0	.0
53.	85.0	35.6	.0	.0	.0	.0
54.	86.0	37.7	.0	.0	.0	.0
55.	87.0	39.5	.0	.0	.0	.0
56.	88.0	39.3	.0	.0	.0	.0
57.	89.0	33.6	.0	.0	.0	.0
58.	90.0	32.7	.0	.0	.0	.0
59.	91.0	34.6	.0	.0	.0	.0
60.	92.0	42.8	.0	.0	.0	.0
61.	93.0	45.3	.0	.0	.0	.0
62.	96.0	42.6	.0	.0	.0	.0
63.	98.0	45.9	.0	.0	.0	.0
64.	99.0	47.4	.0	.0	.0	.0
65.	101.0	46.4	.0	.0	.0	.0
66.	102.0	41.8	.0	.0	.0	.0
67.	103.0	42.6	.0	.0	.0	.0
68.	104.0	33.2	.0	.0	.0	.0
69.	105.0	31.9	.0	.0	.0	.0
70.	107.0	29.8	.0	.0	.0	.0
71.	108.0	33.9	.0	.0	.0	.0
72.	109.0	35.8	.0	.0	.0	.0
73.	112.0	36.0	.0	.0	.0	.0
74.	113.0	36.2	.0	.0	.0	.0
75.	115.0	38.3	.0	.0	.0	.0
76.	117.0	35.5	.0	.0	.0	.0
77.	123.0	32.8	.0	.0	.0	.0
78.	126.0	26.2	.0	.0	.0	.0
79.	135.0	34.3	.0	.0	.0	.0
80.	136.0	37.2	.0	.0	.0	.0
81.	137.0	32.7	.0	.0	.0	.0
82.	138.0	33.8	.0	.0	.0	.0
83.	139.0	40.4	.0	.0	.0	.0
84.	140.0	45.8	.0	.0	.0	.0
85.	142.0	42.9	.0	.0	.0	.0
86.	143.0	39.5	.0	.0	.0	.0
87.	144.0	38.7	.0	.0	.0	.0
88.	145.0	40.4	.0	.0	.0	.0
89.	146.0	40.0	.0	.0	.0	.0
90.	147.0	42.1	.0	.0	.0	.0
91.	148.0	42.5	.0	.0	.0	.0
92.	149.0	42.8	.0	.0	.0	.0
93.	150.0	41.6	.0	.0	.0	.0
94.	151.0	37.6	.0	.0	.0	.0
95.	152.0	36.4	.0	.0	.0	.0
96.	153.0	37.7	.0	.0	.0	.0
97.	154.0	35.3	.0	.0	.0	.0
98.	155.0	38.3	.0	.0	.0	.0
99.	156.0	44.4	.0	.0	.0	.0
100.	157.0	41.4	.0	.0	.0	.0
101.	158.0	35.2	.0	.0	.0	.0
102.	159.0	35.8	.0	.0	.0	18.0
103.	160.0	36.6	.0	.0	.0	18.0
104.	161.0	32.8	.0	.0	.0	18.0
105.	162.0	37.9	.0	.0	.0	18.0
106.	163.0	35.6	.0	.0	.0	18.0
107.	168.0	30.5	.0	.0	.0	18.0
108.	169.0	32.2	.0	.0	.0	18.0
109.	172.0	27.8	.0	.0	.0	18.0
110.	173.0	28.3	.0	.0	.0	18.0
111.	174.0	28.9	.0	.0	.0	18.0
112.	175.0	26.7	.0	.0	.0	17.0
113.	176.0	25.9	.0	.0	.0	17.0
114.	177.0	27.4	.0	.0	.0	16.0
115.	178.0	27.7	.0	.0	.0	17.0
116.	179.0	27.0	.0	.0	.0	16.0
117.	180.0	26.5	.0	.0	.0	16.5
118.	181.0	26.3	.0	.0	.0	17.0
119.	182.0	26.1	.0	.0	.0	17.0
120.	183.0	26.2	.0	.0	.0	16.5
121.	184.0	30.0	.0	.0	.0	16.5
122.	185.0	28.0	.0	.0	.0	17.0

Column 1
Page 2 of 3

Table E-3 (continued)

Line No.	Day	Fe_{TOT}	Temperature TOP	Temperature MID	Temperature BOT	% O_2 Eff	Line No.	Day	Fe_{TOT}	Temperature TOP	Temperature MID	Temperature BOT	% O_2 Eff
183.	186.0	27.6	33.6	35.4	38.3	17.4	184.	247.0	26.4	37.6	36.1	40.4	.0
184.	187.0	28.6	34.1	32.2	37.0	.0	185.	248.0	27.1	37.7	36.7	41.0	.0
185.	188.0	28.5	34.8	33.0	37.0	.0	186.	249.0	29.0	38.1	36.9	41.2	.0
186.	189.0	28.8	35.7	33.9	38.6	.0	187.	250.0	30.5	36.7	37.3	41.8	.0
187.	190.0	28.0	35.9	34.1	39.0	.0	188.	251.0	.0	39.5	37.8	42.2	.0
188.	191.0	27.2	36.9	35.0	39.9	.0	189.	252.0	32.2	39.8	38.1	42.6	.0
189.	192.0	.0	36.5	34.2	38.7	.0	190.	253.0	.0	39.9	38.3	42.5	.0
190.	193.0	27.9	37.3	34.9	39.7	.0	191.	254.0	.0	39.4	37.8	42.0	.0
191.	194.0	28.3	37.7	36.0	41.2	.0	192.	255.0	.0	39.0	37.6	41.7	.0
192.	195.0	29.5	38.3	36.4	41.5	.0	193.	256.0	33.7	38.0	37.1	41.2	.0
193.	196.0	30.7	38.7	36.9	41.9	.0	194.	257.0	28.7	37.6	36.8	40.8	.0
194.	197.0	30.3	38.6	36.8	41.8	18.2	195.	258.0	29.1	37.7	36.9	40.8	.0
195.	198.0	29.7	37.2	36.4	41.5	18.3	196.	259.0	29.5	37.8	36.8	40.9	.0
196.	199.0	30.3	39.1	37.3	42.4	17.9	197.	260.0	29.6	37.7	36.8	41.2	.0
197.	200.0	30.8	39.4	37.8	42.6	17.9	198.	262.0	31.7	38.8	37.3	41.7	.0
198.	201.0	34.1	37.8	36.6	40.8	18.2	199.	262.0	27.7	39.7	38.0	42.5	.0
199.	202.0	33.4	37.1	35.6	39.7	.0	200.	263.0	25.3	39.0	37.6	42.2	.0
200.	203.0	32.8	37.8	36.6	40.9	.0	201.	264.0	24.0	37.9	36.9	41.3	.0
201.	204.0	34.9	39.7	38.0	42.6	.0	202.	265.0	24.9	38.6	37.4	41.8	.0
202.	205.0	34.3	39.3	37.7	42.0	.0	203.	266.0	23.5	36.7	36.5	40.5	.0
203.	206.0	.0	39.8	37.8	42.0	.0	204.	267.0	22.0	36.4	35.3	39.3	.0
204.	207.0	34.0	40.0	38.1	42.2	.0	205.	268.0	21.5	35.4	34.9	38.9	.0
205.	208.0	34.2	38.1	36.1	40.7	.0	206.	269.0	21.2	36.0	34.8	38.8	.0
206.	209.0	32.5	36.2	36.7	40.7	.0	207.	270.0	21.8	35.6	34.9	39.0	.0
207.	210.0	32.1	37.5	36.2	40.0	.0	208.	271.0	20.9	36.5	35.5	39.9	.0
208.	211.0	31.3	37.1	35.9	39.7	.0	209.	272.0	21.0	36.9	36.0	40.1	.0
209.	212.0	29.8	35.7	34.7	37.8	.0	210.	273.0	20.7	37.0	35.9	40.1	.0
210.	213.0	.0	39.8	37.6	41.4	.0	211.	274.0	20.6	36.9	35.8	39.4	.0
211.	214.0	.0	38.1	35.9	39.3	.0	212.	275.0	21.1	36.8	35.4	39.5	.0
212.	215.0	.0	38.0	35.8	39.2	.0	213.	276.0	21.6	36.6	35.9	40.2	.0
213.	216.0	28.2	36.7	34.4	37.6	.0	214.	277.0	18.1	35.3	35.3	39.5	.0
214.	217.0	27.8	35.9	34.9	38.4	.0	215.	278.0	15.7	36.1	35.3	39.4	.0
215.	218.0	29.6	37.7	37.3	40.9	.0	216.	279.0	17.2	35.8	34.8	38.8	.0
216.	219.0	30.2	39.7	38.0	41.5	.0	217.	280.0	16.4	34.7	35.8	39.7	.0
217.	220.0	35.2	37.2	36.7	40.0	.0	218.	281.0	17.2	37.6	36.3	40.7	.0
218.	221.0	28.8	37.9	35.9	39.1	.0	219.	282.0	17.0	37.7	36.3	40.8	.0
219.	222.0	30.8	39.2	37.3	40.8	.0	220.	283.0	16.9	36.7	35.1	39.4	.0
220.	223.0	28.3	32.5	32.0	33.6	.0	221.	284.0	16.5	35.8	34.3	39.0	.0
221.	224.0	29.6	38.2	37.4	41.4	.0	222.	285.0	16.6	35.5	34.2	38.9	.0
222.	225.0	28.0	37.5	36.8	40.7	.0	223.	286.0	15.8	36.2	35.2	40.0	.0
223.	226.0	28.6	38.5	36.6	39.8	.0	224.	287.0	16.4	36.2	35.7	40.2	.0
224.	227.0	28.4	36.8	35.1	38.5	.0	225.	288.0	15.9	36.6	35.8	40.1	.0
225.	228.0	27.8	37.2	35.1	38.5	.0	226.	289.0	16.1	36.6	35.6	40.0	.0
226.	229.0	28.1	37.3	36.8	40.4	.0	227.	290.0	16.5	37.2	35.7	40.0	.0
227.	230.0	29.4	38.9	37.3	41.0	.0	228.	291.0	16.0	35.8	35.0	39.5	.0
228.	231.0	32.3	39.3	38.1	42.1	.0	229.	292.0	15.8	35.3	35.0	39.6	.0
229.	232.0	29.4	37.7	36.5	40.3	.0	230.	293.0	14.6	36.7	35.6	40.2	.0
230.	233.0	30.0	35.7	35.9	39.5	.0	231.	294.0	15.9	37.5	36.4	41.1	.0
231.	234.0	26.8	38.1	36.1	39.5	.0	232.	295.0	16.2	37.1	36.1	42.6	.0
232.	235.0	27.9	36.3	36.6	40.3	20.3	233.	296.0	15.6	35.5	36.0	39.9	.0
233.	236.0	28.9	36.7	36.7	40.2	.0	234.	297.0	14.8	34.5	35.0	38.6	.0
234.	237.0	27.4	38.4	37.2	40.8	.0	235.	298.0	15.3	33.7	34.5	38.4	.0
235.	238.0	27.4	37.5	36.0	39.7	.0	236.	299.0	15.2	34.7	34.9	39.0	.0
236.	239.0	27.5	37.9	36.4	40.1	.0	237.	300.0	15.4	34.9	35.2	39.2	.0
237.	240.0	28.6	39.2	37.4	41.0	.0	238.	301.0	14.8	32.9	34.3	38.6	.0
238.	241.0	27.2	38.0	36.8	40.3	.0	239.	302.0	14.7	34.2	34.3	38.4	.0
239.	242.0	26.6	37.6	35.9	39.6	.0	240.	303.0	14.1	32.3	32.5	36.4	.0
240.	243.0	25.5	36.0	35.8	39.4	.0	241.	304.0	13.9	34.2	33.5	37.5	.0
241.	244.0	32.4	36.3	35.6	39.0	.0	242.	305.0	14.6	34.0	34.1	37.8	.0
242.	245.0	25.5	36.8	35.0	38.6	.0	243.	306.0	16.2	35.6	34.8	38.8	.0
243.	246.0	25.1	37.2	35.3	38.7	.0	244.	307.0	16.1	35.0	35.1	39.6	.0

Column 1
Page 3 of 3

Table E-3 (continued)

Line No.	Day	Fe_{TOT}	Temperature TOP	Temperature MID	Temperature BOT	% O_2 Eff
245.	308.0	17.1	34.9	34.4	38.6	.0
246.	309.0	13.6	33.6	33.5	37.6	.0
247.	310.0	.0	30.4	30.1	30.2	.0
248.	311.0	.0	25.0	24.6	25.6	.0
249.	312.0	.0	32.6	32.2	35.6	.0
250.	313.0	.0	37.0	37.0	37.0	.0
251.	314.0	85.7	36.5	36.0	37.8	.0
252.	315.0	30.1	34.7	34.1	37.7	.0
253.	316.0	30.9	34.0	33.4	37.3	.0
254.	317.0	30.1	34.3	33.5	37.5	.0
255.	318.0	24.8	32.5	33.2	37.3	.0
256.	319.0	21.2	32.4	33.4	37.6	.0
257.	320.0	23.9	34.2	34.0	38.4	.0
258.	321.0	24.8	34.5	34.4	36.9	.0
259.	322.0	27.4	35.8	35.1	39.4	.0
260.	323.0	23.8	33.3	34.1	38.3	.0
261.	324.0	.0	34.9	34.1	37.8	.0
262.	325.0	.0	35.7	35.1	38.8	.0
263.	326.0	.0	35.0	34.7	38.2	.0
264.	327.0	26.5	34.9	34.4	37.8	.0
265.	328.0	24.6	34.7	34.4	38.3	.0
266.	329.0	24.6	34.8	34.5	38.3	.0
267.	330.0	21.1	35.7	34.9	39.0	.0
268.	331.0	18.6	35.8	35.4	39.6	.0
269.	332.0	19.3	36.2	35.7	39.8	.0
270.	333.0	18.6	35.9	35.5	39.6	.0
271.	334.0	17.6	35.1	34.5	38.5	.0
272.	335.0	16.9	34.9	34.1	38.3	.0
273.	336.0	17.1	34.5	34.1	38.4	.0
274.	337.0	16.9	35.0	34.4	38.6	.0
275.	338.0	17.2	35.2	34.5	38.7	.0
276.	339.0	16.7	34.2	34.0	38.2	.0
277.	340.0	16.8	35.0	33.9	38.0	.0
278.	341.0	16.3	34.0	33.9	38.3	.0
279.	342.0	16.6	34.9	34.1	38.4	.0
280.	343.0	16.9	34.8	34.1	38.4	.0
281.	344.0	16.3	35.1	34.4	38.5	.0
282.	345.0	17.0	35.3	34.8	38.9	.0
283.	346.0	17.2	32.5	33.1	36.9	.0
284.	347.0	18.1	35.3	34.7	38.9	.0
285.	348.0	18.1	35.1	35.1	39.1	.0
286.	349.0	17.7	35.3	35.1	39.1	.0
287.	350.0	17.5	34.9	34.4	38.3	.0
288.	351.0	16.8	34.5	34.1	37.8	.0
289.	352.0	15.3	34.2	33.7	37.6	.0
290.	353.0	15.3	34.1	33.7	37.4	.0
291.	354.0	15.0	34.4	33.7	37.6	.0
292.	355.0	15.4	34.9	34.1	37.9	.0
293.	356.0	15.3	34.4	33.9	38.0	.0
294.	357.0	15.5	34.4	34.4	38.4	.0
295.	358.0	15.8	35.1	34.2	37.9	.0
296.	359.0	15.9	36.4	35.4	39.5	.0
297.	360.0	17.0	37.3	36.7	40.8	.0
298.	361.0	.0	37.9	37.5	41.3	.0
299.	362.0	19.9	38.7	38.1	42.0	.0
300.	363.0	21.1	38.8	38.7	42.6	.0
301.	364.0	23.4	38.8	38.5	42.7	.0
302.	365.0	22.0	38.8	38.4	42.4	.0
303.	366.0	22.3	38.9	38.0	42.1	.0
304.	367.0	21.7	38.0	37.3	41.5	.0
305.	368.0	21.4	37.5	36.7	40.8	.0
306.	369.0	20.6	37.7	36.7	40.9	.0
307.	370.0	21.1	36.9	37.0	41.3	.0
308.	371.0	20.3	37.7	36.6	40.8	.0
309.	372.0	20.8	35.2	34.5	37.2	.0
310.	373.0	15.0	24.1	24.1	25.0	.0
311.	374.0	18.9	36.1	35.0	39.0	.0
312.	375.0	19.9	37.3	36.6	40.6	.0
313.	376.0	16.9	37.4	36.6	40.6	.0
314.	377.0	18.8	37.7	36.4	40.4	.0
315.	378.0	19.3	37.5	36.4	40.4	.0
316.	379.0	21.7	39.4	38.5	42.7	.0
317.	380.0	21.9	38.7	38.0	41.9	.0
318.	381.0	21.4	38.2	37.4	41.2	.0
319.	382.0	21.4	37.6	37.1	40.9	.0
320.	383.0	21.1	38.2	37.5	41.3	.0
321.	384.0	21.9	39.0	38.5	42.3	.0
322.	385.0	20.9	38.2	38.2	42.2	.0
323.	386.0	20.7	38.3	37.8	41.9	.0
324.	387.0	19.6	37.5	37.1	41.1	.0
325.	388.0	19.1	37.2	36.8	40.7	.0
326.	389.0	.0	38.0	36.8	40.6	.0
327.	390.0	18.9	38.1	36.6	40.4	.0
328.	391.0	17.2	37.5	36.5	39.9	.0
329.	392.0	16.9	35.4	33.9	37.0	.0
330.	393.0	16.3	35.4	33.9	37.0	.0
331.	394.0	15.6	35.3	34.9	38.4	20.1
332.	395.0	15.6	33.9	33.4	36.6	20.0
333.	396.0	.0	34.7	33.3	36.3	19.8
334.	397.0	14.9	34.3	32.8	35.8	19.9
335.	398.0	14.3	33.7	32.6	36.2	20.3
336.	399.0	14.8	37.3	36.2	40.3	20.1
337.	400.0	15.3	37.5	37.0	41.2	20.4
338.	401.0	15.3	37.8	36.7	40.3	.0
339.	402.0	14.9	36.9	35.8	39.8	.0
340.	403.0	14.9	36.8	35.6	39.5	.0
341.	404.0	15.1	37.4	36.1	40.2	.0
342.	405.0	14.6	37.2	36.6	40.6	.0
343.	406.0	14.4	37.4	36.2	40.1	.0
344.	407.0	14.1	36.0	35.3	39.0	.0
345.	408.0	13.3	36.4	35.4	39.2	.0
346.	409.0	.0	36.6	35.4	36.7	.0
347.	410.0	14.9	36.3	35.3	39.1	.0
348.	411.0	14.8	36.5	36.0	40.0	.0
349.	412.0	14.4	37.5	36.4	40.0	.0
350.	413.0	13.3	37.1	35.9	39.7	.0
351.	414.0	13.2	37.3	36.0	39.6	.0
352.	415.0	12.7	37.8	36.4	39.8	.0
353.	416.0	9.5	36.1	35.2	38.3	.0
354.	417.0	6.3	36.7	35.4	38.5	.0
355.	418.0	4.8	36.7	35.6	38.8	.0
356.	419.0	3.7	34.0	34.1	37.2	.0

Table E-3 (continued)

Column 2
Page 1 of 4

Line No.	Day	Fe_{TOT}	Temperature TOP	Temperature MID	Temperature BOT	% O_2 Eff
2.	0	260.0	00.0	00.0	00.0	00.0
3.	1	270	.0	.0	.0	.0
4.	2	264.0	30.0	.0	.0	19.0
5.	3	238.3	33.0	.0	.0	19.0
6.	4	219.3	39.0	.0	.0	17.5
7.	5	481.4	41.0	.0	.0	15.0
8.	7	682.9	39.0	.0	.0	15.0
9.	8	623.7	38.0	.0	.0	16.0
10.	9	695.6	38.0	.0	.0	16.5
11.	10	634.8	37.0	.0	.0	16.5
12.	11	524.4	37.5	.0	.0	14.3
13.	12	500.8	39.0	.0	.0	12.5
14.	13	580.0	39.5	.0	.0	11.5
15.	14	633.6	37.0	.0	.0	15.5
16.	15	655.0	34.5	.0	.0	16.5
17.	16	647.9	34.5	.0	.0	17.5
18.	17	525.3	37.0	.0	.0	15.3
19.	18	515.0	37.0	.0	.0	14.5
20.	19	450.0	25.0	.0	.0	17.5
21.	20	426.2	35.0	.0	.0	16.0
22.	21	371.5	35.0	.0	.0	16.0
23.	22	391.4	35.0	.0	.0	.0
24.	23	485.7	35.0	.0	.0	.0
25.	24	495.0	35.0	.0	.0	.0
26.	25	474.6	35.0	.0	.0	.0
27.	26	425.5	35.0	.0	.0	.0
28.	27	420.7	35.0	.0	.0	.0
29.	28	396.1	36.0	.0	.0	.0
30.	33	624.3	36.0	.0	.0	.0
31.	34	653.4	35.5	.0	.0	.0
32.	37	636.1	35.0	.0	.0	.0
33.	38	536.9	36.0	.0	.0	.0
34.	39	367.9	36.0	.0	.0	.0
35.	40	290.6	36.0	.0	.0	.0
36.	41	241.5	36.0	.0	.0	.0
37.	42	248.0	36.0	.0	.0	.0
38.	43	207.0	37.0	.0	.0	.0
39.	44	217.1	37.0	.0	.0	.0
40.	45	202.1	.0	.0	.0	.0
41.	46	204.7	.0	.0	.0	.0
42.	47	197.1	.0	.0	.0	.0
43.	48	177.3	.0	.0	.0	.0
44.	49	190.9	.0	.0	.0	.0
45.	50	137.3	.0	.0	.0	.0
46.	51	137.3	35.5	34.7	35.4	19.3
47.	52	110.0	36.5	35.0	36.1	18.8
48.	53	141.1	37.0	36.5	36.7	18.5
49.	54	147.4	38.4	37.4	37.8	18.6
50.	55	151.8	37.2	37.3	37.8	18.5
51.	56	152.7	39.2	38.0	39.2	18.2
52.	57	0.0	38.8	37.8	37.9	18.4
53.	58	169.4	39.9	38.8	38.9	17.7
54.	59	192.2	39.9	39.7	40.3	17.4
55.	60	177.0	40.7	40.0	40.6	17.7
56.	61	172.2	41.8	40.7	41.0	17.8
57.	62	168.6	41.6	40.7	40.9	17.8
58.	63	154.6	39.2	39.1	40.4	0.0
59.	64	154.1	42.4	41.4	41.5	0.0
60.	65	154.1	41.5	41.1	41.6	0.0
61.	66	148.0	40.6	39.4	40.0	0.0
62.	67	160.0	39.6	38.5	38.9	0.0
63.	68	150.0	40.3	39.6	40.2	0.0
64.	69	0.0	41.7	41.1	41.7	0.0
65.	70	169	41.6	40.7	41.1	0.0
66.	71	0	42.2	41.1	41.3	0.0
67.	72	220	42.4	41.2	41.3	0.0
68.	73	236	40.6	39.4	39.7	0.0
69.	74	193	40.2	39.3	39.8	0.0
70.	75	166	39.8	38.6	39.1	0.0
71.	76	145	39.8	38.6	38.9	0.0
72.	77	138	37.2	37.1	37.3	0.0
73.	78	0	41.1	40.8	40.6	0.0
74.	79	0	39.7	38.7	38.6	0.0
75.	80	0	39.6	38.6	38.5	0.0
76.	81	191	38.2	38.9	37.0	0.0
77.	82	244	38.4	37.6	37.9	0.0
78.	83	181	40.7	40.2	40.4	0.0
79.	84	149	42.0	41.1	41.0	0.0
80.	85	124	38.2	38.3	39.3	0.0
81.	86	126	40.0	38.8	38.7	0.0
82.	87	128	41.4	40.3	40.3	0.0
83.	88	126	37.4	37.4	37.5	0.0
84.	89	118	40.4	40.3	40.7	0.0
85.	90	105	39.3	39.2	40.0	0.0
86.	91	103	40.4	39.3	39.3	0.0
87.	92	111	38.8	37.9	37.9	20.1
88.	93	111	39.1	38.0	38.1	20.3
89.	94	111	38.4	39.0	39.9	0.0
90.	95	105	40.6	40.2	40.6	0.0
91.	96	105	42.2	41.5	41.6	0.0
92.	97	111	40.4	39.6	39.7	0.0
93.	98	0	38.5	38.2	38.9	0.0
94.	99	130	40.3	39.3	39.2	0.0
95.	100	124	38.5	38.8	39.6	0.0
96.	101	107	37.8	38.5	39.7	0.0
97.	102	107	39.7	39.6	40.4	0.0
98.	103	97	39.6	38.9	39.2	0.0
99.	104	99	40.2	39.6	39.8	0.0
100.	105	92	41.0	40.4	40.6	0.0
101.	106	105	39.4	39.2	39.7	0.0
102.	107	0	40.2	39.3	39.2	0.0
103.	108	97	40.0	39.2	39.0	0.0
104.	109	0	37.3	37.6	38.4	0.0
105.	110	90	39.2	38.1	38.1	0.0
106.	111	93	39.4	38.4	38.3	0.0
107.	112	84	40.6	39.6	39.4	0.0
108.	113	86	39.9	39.4	39.9	0.0
109.	114	99	40.8	40.0	40.2	0.0
110.	115	86	39.1	39.1	40.7	0.0
111.	116	0	42.2	41.3	41.2	19.3
112.	117	0	42.6	41.6	41.5	19.2
113.	118	0	42.5	41.6	41.3	19.0
114.	119	0	42.0	41.0	40.8	19.0
115.	120	0	41.6	40.7	40.4	18.9
116.	121	170	39.8	39.6	40.1	19.3
117.	122	134	39.7	39.2	39.6	20.2
118.	123	113	40.1	39.4	39.7	20.2
119.	124	101	40.1	39.5	39.8	0.0
120.	125	92	40.5	39.8	40.1	0.0
121.	126	91	40.6	40.1	40.5	0.0
122.	127	91	42.4	41.5	41.6	0.0

Table E-3 (continued)

Column 2
Page 2 of 4

Line No.	Day	Fe_{TOT}	Temperature TOP	Temperature MID	Temperature BOT	% O_2 Eff
123.	128	79	41.6	40.8	41.1	0.0
124.	129	86	40.0	39.7	40.1	0.0
125.	130	80	41.0	40.4	40.7	0.0
126.	131	0	39.0	38.8	39.4	0.0
127.	132	73	39.5	38.3	38.6	0.0
128.	133	82	39.1	37.9	37.7	0.0
129.	134	81	39.0	37.7	37.7	0.0
130.	135	73	37.9	37.3	37.9	0.0
131.	136	72	39.4	38.5	38.7	0.0
132.	137	71	39.1	38.5	38.9	0.0
133.	138	44	39.6	38.7	38.9	0.0
134.	139	63	39.5	38.4	38.3	0.0
135.	140	76	39.3	38.4	38.4	0.0
136.	141	66	39.8	39.1	39.1	0.0
137.	142	75	38.6	37.4	38.2	0.0
138.	143	69	39.4	38.6	38.5	0.0
139.	144	74	38.1	37.5	37.4	0.0
140.	145	65	37.6	37.9	38.6	0.0
141.	146	64	40.3	39.5	39.6	0.0
142.	147	63	40.7	39.5	39.6	0.0
143.	148	64	39.8	38.3	38.3	0.0
144.	149	64	39.0	37.7	37.7	0.0
145.	150	63	38.5	37.4	37.7	0.0
146.	151	62	39.8	38.6	38.8	0.0
147.	152	64	38.8	38.3	38.9	0.0
148.	153	57	39.4	38.4	38.9	0.0
149.	154	58	39.4	38.3	38.9	0.0
150.	155	53	40.0	38.8	38.8	0.0
151.	156	54	39.3	38.1	38.4	0.0
152.	157	56	38.5	37.9	38.3	0.0
153.	158	56	39.1	38.4	38.9	0.0
154.	159	56	39.9	39.3	39.8	0.0
155.	160	55	41.3	40.5	41.2	0.0
156.	161	56	38.9	37.9	38.3	0.0
157.	162	55	38.7	37.8	37.8	0.0
158.	163	60	37.6	36.3	36.8	0.0
159.	164	45	38.4	37.3	37.4	0.0
160.	165	40	38.2	37.3	37.6	0.0
161.	166	44	36.8	36.4	36.8	0.0
162.	167	37	37.9	36.7	36.7	0.0
163.	168	32	32.9	33.4	34.3	0.0
164.	169	33	35.9	35.6	35.7	0.0
165.	170	47	36.8	35.8	36.1	0.0
166.	171	49	38.0	37.6	37.4	0.0
167.	172	51	37.5	37.6	37.9	0.0
168.	173	59	37.1	36.8	37.3	0.0
169.	174	56	30.7	31.7	29.0	0.0
170.	175	0	25.0	25.0	25.0	0.0
171.	176	0	25.2	25.1	25.1	0.0
172.	177	0	37.2	37.1	35.5	0.0
173.	178	145	37.9	37.7	37.0	0.0
174.	179	67	36.5	36.3	36.7	0.0
175.	180	49	35.9	35.6	36.7	0.0
176.	181	48	35.3	35.1	36.0	0.0
177.	182	47	35.8	35.6	36.5	0.0
178.	183	49	34.2	34.8	36.1	0.0
179.	184	48	34.7	35.1	36.3	0.0
180.	185	51	35.7	35.9	37.0	0.0
181.	186	44	35.7	36.1	37.4	0.0
182.	187	47	37.5	37.5	38.2	0.0
183.	188	49	33.4	35.8	37.2	0.0

Line No.	Day	Fe_{TOT}	Temperature TOP	Temperature MID	Temperature BOT	% O_2 Eff
184.	189	0	36.4	36.3	36.7	0.0
185.	190	0	37.4	37.4	37.7	0.0
186.	191	0	36.9	36.6	36.9	0.0
187.	192	59	36.6	36.4	36.5	0.0
188.	193	62	36.7	36.5	37.0	0.0
189.	194	58	36.6	36.5	37.0	0.0
190.	195	55	37.5	37.3	37.8	0.0
191.	196	50	37.6	37.6	38.1	0.0
192.	197	40	38.0	37.9	38.5	0.0
193.	198	45	37.9	37.7	38.3	0.0
194.	199	48	36.9	36.4	37.3	0.0
195.	200	48	36.7	36.2	37.0	0.0
196.	201	47	36.0	35.9	37.6	0.0
197.	202	52	36.9	36.5	37.3	0.0
198.	203	44	37.0	36.6	37.4	0.0
199.	204	0	36.0	35.7	36.9	0.0
200.	205	56	37.0	36.2	36.6	0.0
201.	206	52	35.5	35.7	37.0	0.0
202.	207	50	36.7	36.1	37.1	0.0
203.	208	46	36.7	36.1	37.1	0.0
204.	209	47	37.2	36.5	37.3	0.0
205.	210	48	37.2	36.7	37.6	0.0
206.	211	38	34.7	34.7	35.7	0.0
207.	212	47	37.8	37.2	38.0	0.0
208.	213	46	36.9	36.8	38.2	0.0
209.	214	44	37.0	36.9	38.1	0.0
210.	215	47	36.7	36.3	37.4	0.0
211.	216	44	36.2	35.8	36.9	0.0
212.	217	43	36.0	35.6	36.8	0.0
213.	218	44	35.9	35.4	36.5	0.0
214.	219	42	36.2	35.7	36.6	0.0
215.	220	43	36.9	36.2	37.0	0.0
216.	221	45	36.3	35.9	37.0	0.0
217.	222	40	36.8	36.4	37.5	0.0
218.	223	41	37.0	36.3	37.1	0.0
219.	224	40	38.4	37.8	38.6	0.0
220.	225	41	39.6	39.2	40.0	0.0
221.	226	0	40.4	39.9	40.6	0.0
222.	227	51	41.1	40.6	41.2	0.0
223.	228	53	41.4	41.1	41.8	0.0
224.	229	39	41.3	41.0	41.7	0.0
225.	230	49	41.0	40.6	41.5	0.0
226.	231	46	40.8	40.5	41.1	0.0
227.	232	44	40.2	40.0	40.4	0.0
228.	233	42	39.5	39.4	40.0	0.0
229.	234	41	39.8	39.5	40.0	0.0
230.	235	42	38.3	38.9	40.2	0.0
231.	236	40	39.9	39.4	39.9	0.0
232.	237	0	37.1	36.5	36.1	0.0
233.	238	40	25.1	25.1	25.0	0.0
234.	239	45	38.4	37.9	38.3	0.0
235.	240	43	39.5	39.2	39.7	0.0
236.	241	51	39.6	39.2	39.8	0.0
237.	242	40	39.4	39.1	39.5	0.0
238.	243	43	39.5	39.2	39.5	0.0
239.	244	41	41.2	41.3	41.9	0.0
240.	245	46	40.3	40.2	41.0	0.0
241.	246	40	39.9	39.9	40.3	0.0
242.	247	42	39.5	39.4	39.9	0.0
243.	248	42	39.7	39.6	40.4	0.0
244.	249	43	40.6	40.7	41.5	0.0

Table E-3 (continued)

Column 2
Page 3 of 4

Line No.	Day	Fe_{TOT}	Temperature TOP	Temperature MID	Temperature BOT	% O_2 Eff
245.	250	43	40.3	40.3	41.3	0.0
246.	251	41	39.8	39.9	41.1	0.0
247.	252	40	38.5	38.9	40.2	0.0
248.	253	38	38.5	38.5	39.7	0.0
249.	254	0	39.4	39.0	39.6	0.0
250.	255	42	39.3	39.0	39.4	20.4
251.	256	45	39.2	38.5	39.2	20.5
252.	257	43	36.4	36.2	36.4	20.3
253.	258	38	36.5	36.4	36.6	20.2
254.	259	39	35.6	36.7	37.9	20.2
255.	260	35	34.2	35.1	36.0	0.0
256.	261	0	35.8	35.8	35.9	0.0
257.	262	41	35.3	35.1	35.5	0.0
258.	263	33	34.6	34.6	34.5	0.0
259.	264	34	38.4	38.3	39.3	0.0
260.	265	40	38.8	38.9	40.1	0.0
261.	266	40	39.1	38.7	39.5	0.0
262.	267	39	38.0	37.8	38.8	0.0
263.	268	39	38.8	38.2	39.1	0.0
264.	269	39	38.8	39.2	39.5	0.0
265.	270	46	38.2	39.2	39.5	0.0
266.	271	36	38.4	38.6	39.3	0.0
267.	272	39	38.8	38.7	37.9	0.0
268.	273	0	37.6	37.2	38.2	0.0
269.	274	0	37.7	37.2	37.7	0.0
270.	275	45	37.4	37.1	38.0	0.0
271.	276	44	37.1	37.5	38.8	0.0
272.	277	46	38.8	38.6	39.1	0.0
273.	278	44	37.9	37.9	38.7	0.0
274.	279	41	38.4	38.1	38.6	0.0
275.	280	39	38.7	38.5	39.1	0.0
276.	281	41	37.1	36.9	37.9	0.0
277.	282	35	37.6	37.3	37.9	0.0
278.	283	38	37.9	37.6	38.2	0.0
279.	284	35	35.1	35.1	36.1	0.0
280.	285	34	34.2	34.6	35.7	0.0
281.	286	33	35.4	35.2	35.8	0.0
282.	287	32	35.3	35.3	36.2	20.7
283.	288	33	35.2	35.2	36.0	20.5
284.	289	32	35.7	35.6	36.2	20.4
285.	290	35	35.2	35.2	36.2	20.5
286.	291	33	35.5	35.5	36.2	20.6
287.	292	33	35.0	35.0	36.2	0.0
288.	293	33	35.8	35.4	36.2	0.0
289.	294	29	35.1	34.7	36.1	0.0
290.	295	35	34.9	35.1	36.2	0.0
291.	296	35	35.0	35.1	36.2	0.0
292.	297	34	35.8	35.6	36.2	0.0
293.	298	32	35.0	35.2	36.2	0.0
294.	299	32	35.0	35.2	36.2	0.0
295.	300	30	35.5	35.4	36.1	0.0
296.	301	24	35.3	35.2	35.9	0.0
297.	302	27	35.3	35.2	35.9	0.0
298.	303	25	35.4	35.1	35.8	0.0
299.	304	27	35.3	35.2	35.9	0.0
300.	305	26	33.3	34.4	35.7	0.0
301.	306	24	35.4	35.4	36.1	0.0
302.	307	27	34.7	35.0	36.1	0.0
303.	308	30	35.6	35.5	36.2	0.0
304.	309	30	34.0	34.7	36.0	0.0
305.	310	28	35.3	35.1	35.8	0.0
306.	311	30	35.2	35.2	36.0	0.0
307.	312	28	35.5	35.6	36.0	0.0
308.	313	26	34.8	35.2	36.3	0.0
309.	314	28	35.9	36.1	36.5	0.0
310.	315	26	34.6	35.3	36.3	0.0
311.	316	0	35.6	35.6	36.0	0.0
312.	317	31	35.7	35.6	36.1	0.0
313.	318	32	34.4	35.2	36.2	0.0
314.	319	31	35.5	35.6	36.3	0.0
315.	320	32	35.2	35.3	36.0	0.0
316.	321	26	35.3	35.6	36.5	0.0
317.	322	30	35.9	36.1	36.5	0.0
318.	323	31	36.0	36.1	36.5	0.0
319.	324	30	35.2	35.7	36.4	0.0
320.	325	29	35.6	35.8	36.5	0.0
321.	326	28	35.9	35.7	36.4	0.0
322.	327	29	35.2	35.1	36.0	0.0
323.	328	27	33.4	34.2	35.8	0.0
324.	329	27	35.4	34.9	35.5	0.0
325.	330	26	34.4	34.7	35.9	0.0
326.	331	26	35.0	34.8	35.7	0.0
327.	332	26	35.3	34.8	35.4	0.0
328.	333	26	34.5	34.1	35.2	0.0
329.	334	30	35.5	35.1	35.7	0.0
330.	335	28	32.9	32.7	32.9	0.0
331.	336	0	20.8	20.7	20.3	0.0
332.	337	0	22.5	21.9	22.2	19.5
333.	338	0	35.6	35.1	35.5	19.6
334.	339	32	35.5	35.0	35.6	19.1
335.	340	33	35.3	35.1	35.9	20.0
336.	341	31	35.3	35.2	36.2	20.3
337.	342	30	35.6	35.5	36.1	19.6
338.	343	26	35.8	35.8	36.5	20.3
339.	344	29	35.9	35.5	36.2	20.2
340.	345	28	35.4	35.6	36.1	20.5
341.	346	27	35.7	35.8	36.2	20.6
342.	347	27	34.3	35.0	36.1	20.8
343.	348	28	35.8	35.9	36.2	20.3
344.	349	30	35.2	35.6	36.2	20.5
345.	350	26	35.0	35.4	36.2	20.8
346.	351	25	35.4	35.7	36.2	20.5
347.	352	25	35.5	35.7	36.1	20.7
348.	353	25	35.6	35.7	36.1	20.5
349.	354	23	34.1	34.8	36.1	0.0
350.	355	25	35.5	35.7	36.0	0.0
351.	356	25	35.8	35.6	36.0	0.0
352.	357	26	35.2	35.3	36.0	0.0
353.	358	26	35.2	35.6	36.2	0.0
354.	359	27	35.6	35.7	36.1	0.0
355.	360	26	35.0	34.9	35.6	0.0
356.	361	26	35.9	35.7	36.0	0.0
357.	362	26	35.4	35.3	36.0	0.0
358.	363	25	35.7	35.4	36.0	0.0
359.	364	25	36.0	35.7	36.0	0.0
360.	365	23	35.6	35.3	35.7	0.0
361.	366	0	35.3	35.2	35.4	0.0
362.	367	28	35.4	35.2	35.6	0.0
363.	368	0	35.7	35.6	36.1	0.0
364.	369	32	35.5	35.4	35.7	0.0
365.	370	30	34.7	34.9	35.7	0.0
366.	371	31	35.1	35.5	36.4	0.0

Table E-3 (continued)

Column 2
Page 4 of 4

Line No.	Day	Fe_{TOT}	Temperature TOP	Temperature MID	Temperature BOT	% O_2 Eff	Line No.	Day	Fe_{TOT}	Temperature TOP	Temperature MID	Temperature BOT	% O_2 Eff
367.	372	0	35.9	35.8	36.2	0.0							
368.	373	32	35.8	35.8	36.5	0.0							
369.	374	29	36.1	36.0	36.3	0.0							
370.	375	32	35.6	35.7	36.0	0.0							
371.	376	28	35.6	35.6	36.4	0.0							
372.	377	27	35.9	35.8	36.4	0.0							
373.	378	25	36.1	36.0	36.4	0.0							
374.	379	26	35.7	35.7	36.4	0.0							
375.	380	25	35.9	36.0	36.2	0.0							
376.	381	26	35.8	35.8	36.1	0.0							
377.	382	26	35.9	36.2	36.4	0.0							
378.	383	25	35.3	35.4	36.1	0.0							
379.	384	23	35.9	35.8	36.3	0.0							
380.	385	22	35.4	35.5	36.1	0.0							
381.	386	21	35.8	35.6	36.0	0.0							
382.	387	24	35.7	35.6	36.1	0.0							
383.	388	25	35.8	35.6	36.0	0.0							
384.	389	19	35.1	35.2	36.1	0.0							
385.	390	23	35.4	35.2	36.2	0.0							
386.	391	24	35.7	35.5	36.4	0.0							
387.	392	23	36.4	36.1	36.4	0.0							
388.	393	22	35.7	35.6	36.3	0.0							
389.	394	22	36.0	35.8	36.3	0.0							
390.	395	23	36.3	36.0	36.3	0.0							
391.	396	24	35.9	35.7	36.0	0.0							
392.	397	23	36.2	35.6	36.4	0.0							
393.	398	23	36.3	35.9	36.5	0.0							
394.	399	22	35.6	35.7	36.1	0.0							
395.	400	21	36.1	35.8	36.2	0.0							
396.	401	0	35.8	35.7	35.9	0.0							
397.	402	26	35.5	35.6	36.5	0.0							
398.	403	27	35.5	35.7	36.5	0.0							
399.	404	26	35.4	35.6	36.4	0.0							
400.	405	21	35.5	35.6	36.0	0.0							
401.	406	24	35.8	36.0	36.2	0.0							
402.	407	24	35.6	35.9	36.2	0.0							
403.	408	23	35.8	36.0	36.2	0.0							
404.	409	21	35.8	36.0	36.0	0.0							
405.	410	23	35.4	36.4	36.0	0.0							
406.	411	23	34.0	35.1	36.0	0.0							
407.	412	23	35.7	35.7	36.2	0.0							
408.	413	23	34.5	35.2	36.2	0.0							
409.	414	21	35.8	35.7	35.9	0.0							
410.	415	0	35.9	35.8	36.0	0.0							
411.	416	23	35.8	35.8	36.0	0.0							
412.	417	25	35.6	35.7	36.1	0.0							
413.	418	25	36.0	36.0	36.2	0.0							
414.	419	23	36.0	36.0	36.2	0.0							
415.	420	23	35.9	36.0	36.2	0.0							
416.	421	24	35.9	35.9	36.2	0.0							
417.	422	21	34.1	35.1	36.3	0.0							
418.	423	10	35.9	35.9	36.2	0.0							
419.	424	9	33.8	34.1	34.7	0.0							
420.	425	9	27.3	28.0	29.0	0.0							
421.	426	8	27.6	28.3	29.3	0.0							
422.	427	7	26.8	27.6	28.8	0.0							

Table E-3 (continued)

Column 3
Page 1 of 4

Line No.	Day	Fe_{TOT}	Temperature TOP	Temperature MID	Temperature BOT	% O_2 Eff
2.	0	1934	41.1	37.2	36.7	0.0
3.	1	1129	44.8	39.5	38.3	0.0
4.	2	742	47.6	43.5	44.0	0.0
5.	3	577	47.9	42.8	42.9	0.0
6.	4	0	46.8	40.9	39.7	0.0
7.	5	536	47.0	41.7	40.7	0.0
8.	6	608	47.1	42.9	43.0	0.0
9.	7	640	48.7	43.9	43.3	0.0
10.	8	677	50.1	44.8	43.9	0.0
11.	9	707	50.4	44.8	45.2	0.0
12.	10	671	47.2	43.8	44.5	0.0
13.	11	563	49.2	44.5	43.5	0.0
14.	12	706	49.0	44.5	43.5	0.0
15.	13	535	49.0	44.5	43.5	12.0
16.	14	540	51.6	46.8	45.5	12.7
17.	15	567	50.9	46.8	46.3	12.9
18.	16	0	47.4	45.3	47.2	13.0
19.	17	520	49.9	46.2	45.0	13.4
20.	18	0	46.3	42.8	42.0	14.5
21.	19	670	46.2	42.6	41.6	14.6
22.	20	640	45.5	41.4	40.7	15.5
23.	21	586	45.3	41.5	41.0	15.8
24.	22	472	45.2	40.9	40.0	16.8
25.	23	443	45.4	41.3	40.4	16.9
26.	24	396	45.1	41.5	41.2	16.5
27.	25	0	46.4	43.0	41.9	0.0
28.	26	0	45.7	41.4	40.3	0.0
29.	27	0	45.8	41.5	40.4	0.0
30.	28	592	47.0	41.8	40.6	0.0
31.	29	664	48.4	43.5	42.8	0.0
32.	30	546	48.4	44.2	43.8	0.0
33.	31	460	49.2	44.6	43.5	0.0
34.	32	366	46.1	42.7	43.2	0.0
35.	33	347	49.1	44.2	42.8	0.0
36.	34	401	49.2	44.7	43.6	0.0
37.	35	393	48.3	44.4	44.0	0.0
38.	36	347	48.2	44.8	44.5	0.0
39.	37	336	47.3	43.5	44.0	0.0
40.	38	330	49.1	44.2	43.1	0.0
41.	39	351	49.1	44.2	43.0	0.0
42.	40	351	49.4	44.7	43.4	0.0
43.	41	374	46.4	45.2	45.3	18.2
44.	42	338	49.1	45.8	45.2	17.3
45.	43	357	49.7	45.8	45.1	16.6
46.	44	368	49.3	44.9	43.9	17.0
47.	45	0	47.4	44.0	43.8	17.8
48.	46	397	49.9	45.6	44.0	16.5
49.	47	393	46.6	44.8	44.5	0.0
50.	48	395	45.0	44.4	44.5	0.0
51.	49	359	47.7	44.7	44.8	0.0
52.	50	338	48.7	44.5	43.8	0.0
53.	51	359	48.9	45.1	44.2	0.0
54.	52	376	49.3	45.6	44.7	0.0
55.	53	307	47.8	44.5	44.0	0.0
56.	54	0	49.5	45.0	43.5	0.0
57.	55	340	49.3	44.8	43.4	0.0
58.	56	0	45.7	44.0	43.8	17.4
59.	57	318	49.1	44.6	43.1	17.2
60.	58	318	49.1	44.6	43.1	17.2
61.	59	378	49.1	45.1	43.5	16.7
62.	60	319	47.6	44.7	43.9	17.0
63.	61	296	48.4	44.7	43.7	16.7
64.	62	298	45.1	44.0	43.7	17.4
65.	63	0	48.4	44.6	43.0	16.7
66.	64	0	48.3	44.4	42.7	0.0
67.	65	0	48.9	45.0	43.5	0.0
68.	66	468	46.0	44.1	43.9	0.0
69.	67	0	49.4	46.8	45.7	0.0
70.	68	524	48.0	45.9	45.8	0.0
71.	69	403	42.8	41.5	39.9	0.0
72.	70	338	45.6	42.3	41.3	17.7
73.	71	313	42.9	38.6	36.8	18.6
74.	72	296	46.8	42.9	41.7	17.3
75.	73	253	45.8	42.0	40.5	17.7
76.	74	293	47.0	42.8	40.7	17.2
77.	75	237	44.5	41.5	40.2	18.1
78.	76	241	48.0	46.1	45.1	0.0
79.	77	237	47.9	44.3	43.2	0.0
80.	78	0	46.4	43.0	42.2	0.0
81.	79	218	48.2	43.2	41.3	0.0
82.	80	238	48.3	43.2	40.8	0.0
83.	81	230	48.1	43.1	40.5	0.0
84.	82	284	4538	42.2	40.4	0.0
85.	83	222	47.5	43.1	41.5	0.0
86.	84	216	47.2	42.6	41.6	0.0
87.	85	219	48.1	43.1	41.7	0.0
88.	86	208	49.9	44.8	43.1	0.0
89.	87	205	49.7	44.6	43.2	0.0
90.	88	225	48.1	43.2	41.6	0.0
91.	89	187	41.7	40.0	39.0	0.0
92.	90	238	48.8	43.9	42.1	0.0
93.	91	202	46.3	41.8	40.5	0.0
94.	92	225	48.2	43.5	43.7	0.0
95.	93	211	47.9	43.8	43.6	0.0
96.	94	212	47.8	42.9	42.5	0.0
97.	95	215	47.7	42.5	41.8	0.0
98.	96	215	47.1	41.9	41.7	0.0
99.	97	177	46.6	41.7	41.7	0.0
100.	98	170	46.1	41.0	40.3	0.0
101.	99	189	45.6	42.0	42.3	0.0
102.	100	181	47.5	43.1	43.0	0.0
103.	101	148	48.1	43.1	43.6	0.0
104.	102	171	49.3	44.0	43.2	0.0
105.	103	180	48.9	43.6	43.2	0.0
106.	104	190	48.2	43.4	43.4	18.4
107.	105	177	47.9	43.6	43.4	18.7
108.	106	186	48.5	44.3	44.2	18.5
109.	107	187	47.9	44.5	44.6	18.5
110.	108	178	50.7	45.9	45.2	18.9
111.	109	181	54.6	48.3	46.9	17.7
112.	110	160	53.3	47.5	46.7	17.9
113.	111	145	53.8	47.8	46.8	18.4
114.	112	171	49.8	44.1	43.0	18.4
115.	113	158	52.1	47.1	47.0	18.3
116.	114	163	54.3	47.7	46.7	18.0
117.	115	138	51.0	46.6	46.8	18.5
118.	116	145	51.3	44.3	42.6	18.8
119.	117	136	50.2	43.5	42.9	19.3
120.	118	183	53.3	47.1	47.1	18.7
121.	119	174	50.0	45.8	45.8	0.0
122.	120	165	53.3	49.0	49.4	0.0

Table E-3 (continued)

Column 3
Page 2 of 4

Line No.	Day	Fe_{TOT}	Temperature TOP	Temperature MID	Temperature BOT	% O_2 Eff
123.	121	0	37.3	33.6	33.1	0.0
124.	122	0	25.6	25.0	25.0	0.0
125.	123	0	29.8	29.4	29.5	0.0
126.	124	0	49.4	49.5	47.3	0.0
127.	125	264	33.0	31.2	29.2	0.0
128.	126	0	35.5	32.1	30.4	0.0
129.	127	0	20.9	21.1	21.2	0.0
130.	128	0	28.2	26.5	26.2	0.0
131.	129	173	53.2	48.2	46.9	0.0
132.	130	143	49.9	46.5	46.9	0.0
133.	131	121	50.4	47.7	48.1	0.0
134.	132	108	51.9	48.1	48.4	0.0
135.	133	95	51.1	48.2	46.3	0.0
136.	134	112	53.4	49.1	48.4	0.0
137.	135	106	43.7	40.9	41.1	0.0
138.	136	0	29.7	29.0	29.5	0.0
139.	137	0	41.6	39.0	38.7	0.0
140.	138	0	28.4	28.0	27.6	0.0
141.	139	0	21.3	21.3	21.5	0.0
142.	140	0	21.8	21.6	21.4	0.0
143.	141	0	21.7	21.6	21.5	0.0
144.	142	445	49.8	44.1	44.5	0.0
145.	143	185	52.3	47.3	48.2	0.0
146.	144	140	52.4	47.3	46.0	0.0
147.	145	129	52.7	47.3	48.1	0.0
148.	146	115	52.4	47.3	48.0	0.0
149.	147	121	53.4	47.4	48.2	0.0
150.	148	118	52.3	47.0	48.1	0.0
151.	149	130	53.0	47.2	48.0	0.0
152.	150	122	53.1	47.3	47.9	0.0
153.	151	0	51.7	46.8	47.8	0.0
154.	152	147	53.2	47.5	47.6	0.0
155.	153	140	51.2	46.6	47.9	0.0
156.	154	119	52.6	47.2	47.9	0.0
157.	155	122	53.0	47.0	47.7	0.0
158.	156	116	53.3	47.3	47.9	0.0
159.	157	125	53.1	47.4	48.0	0.0
160.	158	106	52.5	47.1	48.1	0.0
161.	159	105	53.6	47.7	48.2	0.0
162.	160	114	52.0	47.2	48.1	0.0
163.	161	108	52.5	47.1	47.9	0.0
164.	162	108	53.4	47.4	47.8	0.0
165.	163	95	53.2	47.2	47.4	0.0
166.	164	91	53.0	46.9	47.2	0.0
167.	165	90	53.2	46.9	47.2	0.0
168.	166	93	53.5	47.3	47.2	0.0
169.	167	93	53.5	47.3	47.2	0.0
170.	168	91	52.7	47.0	47.3	0.0
171.	169	88	53.2	47.4	47.7	0.0
172.	170	101	53.5	47.6	47.1	0.0
173.	171	98	53.4	48.2	48.2	0.0
174.	172	93	52.7	48.7	49.0	0.0
175.	173	0	53.6	48.3	47.7	0.0
176.	174	128	47.5	45.8	45.2	0.0
177.	175	114	47.7	46.0	45.9	0.0
178.	176	106	48.0	45.8	45.5	0.0
179.	177	106	46.2	45.7	45.4	0.0
180.	178	103	49.3	45.7	45.0	0.0
181.	179	98	49.3	45.3	44.8	0.0
182.	180	94	49.2	45.2	45.0	0.0
183.	181	94	49.2	45.2	45.0	0.0
184.	182	98	47.3	44.5	44.6	0.0
185.	183	78	49.6	45.2	45.4	0.0
186.	184	88	49.4	45.1	44.1	0.0
187.	185	90	49.2	44.8	44.1	0.0
188.	186	92	49.1	45.1	43.9	0.0
189.	187	92	48.9	45.3	44.1	0.0
190.	188	84	49.2	45.4	44.4	0.0
191.	189	85	49.4	45.1	44.2	0.0
192.	190	88	49.3	45.3	44.4	20.1
193.	191	82	49.0	46.1	45.8	19.5
194.	192	83	49.0	45.5	45.0	19.8
195.	193	86	49.1	45.2	44.9	19.9
196.	194	85	49.1	45.2	45.0	19.4
197.	195	77	49.0	45.4	45.3	19.3
198.	196	77	48.3	45.4	45.8	19.4
199.	197	85	48.7	45.3	45.6	19.6
200.	198	85	48.6	45.1	45.3	19.5
201.	199	88	47.7	44.6	45.0	19.7
202.	200	79	48.1	44.5	44.7	19.6
203.	201	0	49.1	45.0	44.4	19.5
204.	202	93	49.3	45.1	44.0	19.4
205.	203	90	49.0	44.7	43.9	0.0
206.	204	88	50.2	44.7	42.7	0.0
207.	205	83	51.1	45.5	43.2	0.0
208.	206	76	48.0	44.1	43.1	0.0
209.	207	61	48.8	44.6	42.9	0.0
210.	208	0	51.0	45.6	42.7	0.0
211.	209	73	50.9	45.2	42.8	0.0
212.	210	68	49.8	44.7	44.2	0.0
213.	211	73	50.3	45.8	45.8	0.0
214.	212	69	49.9	45.7	45.7	0.0
215.	213	67	50.7	46.1	45.2	0.0
216.	214	72	50.0	45.3	45.1	0.0
217.	215	69	50.5	45.5	45.1	0.0
218.	216	69	50.7	45.8	45.3	0.0
219.	217	68	49.7	45.6	45.5	0.0
220.	218	68	50.5	45.6	45.0	0.0
221.	219	67	49.6	44.9	44.5	19.4
222.	220	0	50.4	45.3	44.8	19.7
223.	221	0	50.8	45.5	44.4	19.3
224.	222	86	50.5	45.2	44.9	19.2
225.	223	75	49.1	44.9	45.0	19.2
226.	224	81	51.1	45.9	44.8	19.4
227.	225	72	50.5	45.4	44.9	19.7
228.	226	70	50.9	45.7	44.6	19.5
229.	227	69	51.0	45.7	44.6	19.7
230.	228	67	48.5	43.5	42.3	20.3
231.	229	79	51.2	45.7	44.7	19.8
232.	230	67	51.1	45.8	44.8	19.8
233.	231	70	46.5	42.3	41.4	20.2
234.	232	68	54.7	48.9	48.1	19.0
235.	233	67	50.8	45.4	44.3	19.7
236.	234	64	50.4	45.4	45.0	0.0
237.	235	59	50.5	45.4	44.9	0.0
238.	236	64	53.8	48.2	47.3	0.0
239.	237	61	51.9	46.8	46.3	0.0
240.	238	67	52.7	47.1	46.2	0.0
241.	239	63	51.7	46.8	46.2	0.0
242.	240	67	48.5	43.7	42.9	0.0
243.	241	65	48.0	44.3	44.2	0.0
244.	242	66	52.9	47.5	47.0	0.0

Table E-3 (continued)

Column 3
Page 3 of 4

Line No.	Day	Fe_{TOT}	Temperature TOP	Temperature MID	Temperature BOT	% O_2 Eff
245.	243	67	55.4	49.5	49.0	0.0
246.	244	68	56.1	49.7	48.1	0.0
247.	245	70	54.0	48.1	47.4	0.0
248.	246	66	52.6	47.2	46.8	0.0
249.	247	67	50.6	45.3	44.7	0.0
250.	248	62	50.8	45.4	44.6	0.0
251.	249	70	50.8	45.3	44.3	0.0
252.	250	66	51.1	45.5	44.6	0.0
253.	251	64	51.5	45.6	44.8	0.0
254.	252	61	47.8	44.8	44.7	0.0
255.	253	70	51.0	45.5	44.6	0.0
256.	254	66	54.4	48.6	48.0	0.0
257.	255	69	55.8	49.4	47.9	0.0
258.	256	67	51.2	47.3	47.1	0.0
259.	257	67	50.5	44.7	43.9	0.0
260.	258	59	54.6	48.3	47.4	0.0
261.	259	59	56.2	49.6	48.1	18.9
262.	260	57	54.2	48.3	47.9	19.6
263.	261	60	55.8	49.9	48.8	19.5
264.	262	54	53.1	48.4	48.3	19.8
265.	263	0	55.2	49.0	47.8	19.9
266.	264	75	55.0	48.9	48.0	19.9
267.	265	58	52.3	48.3	47.8	19.6
268.	266	56	54.9	48.9	48.0	18.6
269.	267	54	54.8	48.5	47.5	17.7
270.	268	48	54.9	49.1	48.9	18.9
271.	269	52	54.8	49.1	47.5	19.3
272.	270	51	53.8	48.2	47.4	19.3
273.	271	48	52.6	47.6	47.6	19.6
274.	272	54	53.4	48.2	47.0	19.2
275.	273	53	53.6	47.7	46.8	19.4
276.	274	47	52.5	46.8	46.2	19.6
277.	275	46	49.3	46.5	46.5	19.9
278.	276	51	53.6	47.0	45.5	19.5
279.	277	43	51.1	46.5	47.0	19.7
280.	278	41	53.0	46.8	46.3	19.4
281.	279	49	53.6	47.0	45.7	19.8
282.	280	41	52.3	46.1	45.4	20.1
283.	281	56	53.3	47.1	46.7	19.4
284.	282	46	45.8	41.8	41.6	19.6
285.	283	0	20.2	20.2	20.2	21.0
286.	284	0	20.2	24.2	24.1	21.0
287.	285	0	53.6	47.6	46.2	0.0
288.	286	72	53.8	47.6	46.0	0.0
289.	287	61	53.1	47.3	46.2	0.0
290.	288	56	53.0	47.9	46.4	0.0
291.	289	53	53.7	47.7	46.1	0.0
292.	290	52	53.5	48.2	46.9	0.0
293.	291	54	53.7	48.1	46.3	0.0
294.	292	51	53.4	47.6	46.5	0.0
295.	293	51	53.4	47.6	46.1	0.0
296.	294	44	51.8	46.9	46.2	0.0
297.	295	48	53.8	48.2	46.2	0.0
298.	296	49	53.0	47.8	46.2	0.0
299.	297	49	52.5	47.4	46.1	0.0
300.	298	48	52.4	47.2	45.3	0.0
301.	299	48	52.8	47.2	45.3	0.0
302.	300	49	53.4	47.8	46.1	0.0
303.	301	44	51.3	46.9	46.3	0.0
304.	302	45	53.4	47.8	45.8	0.0
305.	303	47	53.7	48.1	45.6	0.0
306.	304	47	53.0	47.4	45.8	0.0
307.	305	49	52.9	47.7	46.3	0.0
308.	306	48	53.6	48.3	45.9	0.0
309.	307	48	52.4	47.0	45.8	0.0
310.	308	48	53.6	47.8	45.7	0.0
311.	309	46	52.9	47.4	45.8	0.0
312.	310	45	53.5	47.8	45.9	0.0
313.	311	47	53.8	48.2	45.9	0.0
314.	312	41	50.4	45.5	43.6	0.0
315.	313	0	42.9	38.9	37.2	0.0
316.	314	53	49.4	44.2	42.2	0.0
317.	315	0	54.6	49.2	46.8	0.0
318.	316	56	52.3	47.0	44.7	0.0
319.	317	50	51.3	46.8	44.8	0.0
320.	318	42	52.3	47.8	46.1	0.0
321.	319	0	53.1	48.0	45.3	0.0
322.	320	53	52.8	47.6	46.1	0.0
323.	321	49	54.8	49.1	46.4	0.0
324.	322	45	54.4	48.9	46.2	0.0
325.	323	44	54.0	48.6	46.7	0.0
326.	324	42	54.7	49.0	46.6	0.0
327.	325	43	55.0	49.0	46.9	0.0
328.	326	39	54.5	48.7	46.8	0.0
329.	327	38	54.7	49.0	46.4	0.0
330.	328	39	54.3	48.7	46.1	0.0
331.	329	43	54.9	49.4	46.9	0.0
332.	330	38	54.3	48.9	46.7	0.0
333.	331	37	55.0	49.3	46.7	0.0
334.	332	34	54.2	48.5	46.5	0.0
335.	333	36	54.8	49.1	46.1	0.0
336.	334	41	53.7	47.9	45.0	0.0
337.	335	41	55.0	49.1	46.4	0.0
338.	336	41	53.8	48.8	46.6	19.4
339.	337	41	53.9	48.8	46.8	19.9
340.	338	43	53.1	47.7	45.7	20.2
341.	339	42	53.6	47.7	45.1	19.9
342.	340	39	53.9	47.9	46.3	19.8
343.	341	41	54.6	49.1	46.7	19.6
344.	342	42	54.2	48.6	45.9	19.5
345.	343	41	53.5	47.6	45.0	19.8
346.	344	39	54.5	48.8	46.7	19.9
347.	345	47	54.7	48.9	46.5	19.7
348.	346	46	54.0	48.3	46.4	19.8
349.	347	44	54.0	48.5	45.8	19.8
350.	348	0	53.7	48.0	45.0	19.5
351.	349	54	54.1	49.0	47.1	19.7
352.	350	52	53.8	48.4	46.5	19.7
353.	351	48	54.0	48.6	46.7	19.7
354.	352	45	54.1	48.4	46.4	19.6
355.	353	44	54.7	49.0	46.7	19.6
356.	354	44	53.6	48.1	45.8	19.8
357.	355	43	54.6	48.9	46.7	19.8
358.	356	37	54.6	48.7	46.1	19.7
359.	357	54	53.5	48.5	45.4	19.8
360.	358	47	50.2	47.0	45.3	20.1
361.	359	47	54.3	48.7	46.3	19.7
362.	360	47	52.3	48.2	47.0	19.9
363.	361	40	54.7	48.9	46.2	19.7
364.	362	0	54.7	49.3	46.4	19.7
365.	363	51	54.7	48.9	46.4	19.8
366.	364	40	54.4	48.7	46.3	19.8

Table E-3 (continued)

Column 3
Page 4 of 4

Line No.	Day	Fe_{TOT}	Temperature TOP	Temperature MID	Temperature BOT	% O_2 Eff	Line No.	Day	Fe_{TOT}	Temperature TOP	Temperature MID	Temperature BOT	% O_2 Eff
367.	365	40	54.7	49.1	46.4	19.8							
368.	366	34	54.6	49.2	47.0	19.5							
369.	367	29	54.6	48.9	46.4	19.5							
370.	368	33	54.6	48.7	46.7	0.0							
371.	369	31	51.1	47.0	46.1	0.0							
372.	370	20	55.2	48.6	46.7	0.0							
373.	371	14	35.4	33.5	32.4	0.0							
374.	372	16	22.9	22.6	22.5	0.0							
375.	373	11	23.1	23.0	22.7	0.0							
376.	374	10	23.0	22.7	22.5	0.0							

Table E-3 (continued)

Column 4
Page 1 of 4

Line No.	Day	Fe_{TOT}	Temperature TOP	Temperature MID	Temperature BOT	% O_2 Eff
5.	0	1827	0	0	0.0	0.0
6.	1	1267	48.4	45.4	44.5	0.0
7.	2	618	48.3	47.9	47.8	0.0
8.	3	823	49.9	48.2	47.5	0.0
9.	4	0	51.1	49.0	47.5	0.0
10.	5	607	51.6	50.2	48.4	0.0
11.	6	840	50.0	49.4	48.3	0.0
12.	7	0	50.3	49.3	48.1	0.0
13.	8	1092	51.2	49.7	47.8	0.0
14.	9	0	51.8	51.0	49.1	0.0
15.	10	1642	49.1	48.0	47.7	0.0
16.	11	1346	51.9	49.9	48.4	0.0
17.	12	901	51.0	50.0	48.0	0.0
18.	13	703	51.	50.	48.	0.0
19.	14	740	51.3	48.3	46.4	0.0
20.	15	735	50.6	48.5	47.3	0.0
21.	16	0	45.5	46.3	48.4	0.0
22.	17	718	49.5	46.9	45.7	0.0
23.	18	0	45.8	43.4	42.4	0.0
24.	19	949	45.1	43.0	42.0	0.0
25.	20	0	44.0	42.0	41.6	0.0
26.	21	0	43.7	42.0	41.8	0.0
27.	22	666	44.1	41.8	41.4	0.0
28.	23	603	44.7	42.3	41.6	0.0
29.	24	693	44.0	42.3	42.0	16.5
30.	25	0	46.5	43.9	42.4	17.0
31.	26	0	44.4	42.1	40.2	17.4
32.	27	0	44.7	42.1	40.9	17.3
33.	28	1092	45.6	42.9	41.9	17.0
34.	29	911	46.9	44.7	44.5	10.8
35.	30	827	47.5	45.5	45.4	9.0
36.	31	613	48.2	45.9	44.9	8.8
37.	32	536	43.4	44.4	45.5	11.4
38.	33	546	48.3	45.5	44.6	9.5
39.	34	526	48.7	46.2	45.4	9.4
40.	35	456	47.5	45.6	48.3	10.6
41.	36	422	47.7	46.2	46.1	11.4
42.	37	307	45.8	45.1	46.0	12.2
43.	38	403	48.1	45.7	44.9	11.0
44.	39	420	48.3	45.6	44.6	0.0
45.	40	406	48.9	46.0	44.9	0.0
46.	41	412	45.2	47.0	46.9	0.0
47.	42	373	49.1	47.5	46.4	0.0
48.	43	405	50.0	47.9	46.6	0.0
49.	44	424	49.4	47.2	46.1	0.0
50.	45	0	46.4	46.0	45.9	0.0
51.	46	569	50.6	47.6	45.9	0.0
52.	47	525	45.9	47.0	46.6	7.2
53.	48	452	44.9	47.1	47.1	8.8
54.	49	410	47.9	46.7	46.7	9.9
55.	50	414	48.7	46.7	45.7	9.3
56.	51	483	49.5	47.4	46.3	7.3
57.	52	410	50.1	48.2	46.5	8.1
58.	53	414	48.1	46.7	45.9	8.9
59.	54	0	50.6	47.4	45.5	7.5
60.	55	440	50.2	47.2	45.6	7.5
61.	56	0	50.4	46.4	45.9	0.0
62.	57	389	50.6	47.2	45.2	0.0
63.	58	372	50.3	47.7	45.3	0.0
64.	59	309	50.4	48.6	46.0	0.0
65.	60	317	47.9	47.3	45.8	0.0
66.	61	376	50.0	48.2	46.1	0.0
67.	62	353	50.2	48.8	46.2	0.0
68.	63	0	50.0	48.0	45.9	0.0
69.	64	0	50.1	48.4	45.8	0.0
70.	65	0	50.1	48.3	45.8	0.0
71.	66	622	45.4	48.7	45.9	0.0
72.	67	0	49.7	48.1	45.6	0.0
73.	68	467	47.6	47.0	45.8	0.0
74.	69	399	48.4	47.0	45.5	0.0
75.	70	433	49.1	48.9	45.2	0.0
76.	71	445	48.9	48.9	45.5	0.0
77.	72	376	49.0	47.7	46.0	0.0
78.	73	363	48.3	47.4	45.9	0.0
79.	74	353	49.9	48.3	46.0	0.0
80.	75	328	49.2	47.6	45.7	10.9
81.	76	374	48.2	47.3	46.0	11.5
82.	77	387	48.9	47.3	46.1	10.5
83.	78	0	47.1	45.5	45.3	10.3
84.	79	349	49.9	46.4	44.3	9.6
85.	80	386	49.9	46.4	44.5	9.4
86.	81	406	49.9	46.1	44.2	9.1
87.	82	340	47.6	45.5	44.6	11.7
88.	83	333	49.5	46.2	44.8	11.0
89.	84	325	48.9	45.9	45.1	10.7
90.	85	265	50.0	46.6	45.0	13.1
91.	86	277	50.5	46.8	44.5	12.4
92.	87	331	50.3	46.4	44.4	10.2
93.	88	409	50.1	47.4	45.0	10.5
94.	89	364	44.9	45.3	45.2	17.5
95.	90	361	50.3	47.6	45.4	14.1
96.	91	355	48.5	46.2	44.7	14.2
97.	92	313	45.6	45.3	45.7	14.4
98.	93	314	49.6	46.9	45.3	14.3
99.	94	310	49.8	46.8	44.6	14.3
100.	95	311	50.0	46.4	43.5	19.5
101.	96	305	49.6	46.2	43.9	18.0
102.	97	260	48.8	45.9	43.6	17.0
103.	98	268	49.5	46.5	44.2	17.2
104.	99	307	45.8	45.3	45.2	16.9
105.	100	254	46.8	44.9	44.4	17.8
106.	101	224	47.3	45.0	44.5	17.6
107.	102	234	49.0	45.9	43.5	16.3
108.	103	232	48.6	45.5	43.6	16.7
109.	104	276	47.2	45.1	43.8	18.8
110.	105	266	47.5	45.4	44.1	0.0
111.	106	271	48.5	46.3	45.4	0.0
112.	107	267	46.4	45.9	45.7	0.0
113.	108	283	48.3	47.2	46.2	0.0
114.	109	305	52.0	50.2	47.6	0.0
115.	110	243	49.2	49.4	48.2	0.0
116.	111	180	51.8	49.9	48.0	0.0
117.	112	176	50.4	49.4	48.0	0.0
118.	113	149	49.0	48.7	47.8	0.0
119.	114	195	51.6	49.6	47.5	0.0
120.	115	148	48.0	48.2	47.8	0.0
121.	116	126	51.5	49.7	47.6	0.0
122.	117	182	51.0	49.2	47.6	0.0
123.	118	242	52.6	50.7	47.5	14.5
124.	119	265	51.0	49.8	48.1	15.6
125.	120	230	50.5	49.3	47.6	15.7

Table E-3 (continued)

Column 4
Page 2 of 4

Line No.	Day	Fe_{TOT}	Temperature TOP	Temperature MID	Temperature BOT	% O_2 Eff	Line No.	Day	Fe_{TOT}	Temperature TOP	Temperature MID	Temperature BOT	% O_2 Eff
126.	121	197	50.1	49.4	47.4	16.4	187.	182	144	46.2	47.3	45.6	17.9
127.	122	0	53.9	50.7	47.2	16.0	188.	183	143	50.2	49.2	45.2	17.0
128.	123	200	53.3	50.7	47.5	15.9	189.	184	144	50.0	48.8	45.1	17.1
129.	124	0	48.8	49.1	48.8	15.4	190.	185	137	49.1	48.4	45.1	17.2
130.	125	0	49.6	51.8	47.6	16.5	191.	186	148	48.6	48.5	44.9	16.3
131.	126	426	50.6	50.7	47.8	17.0	192.	187	144	48.2	48.8	45.4	17.5
132.	127	196	51.8	49.5	46.7	17.9	193.	188	142	49.3	49.1	46.2	17.6
133.	128	205	50.9	48.6	46.7	18.1	194.	189	146	49.9	49.5	47.8	17.0
134.	129	203	50.8	48.8	45.7	18.7	195.	190	146	49.7	49.5	47.9	17.3
135.	130	189	47.6	46.3	46.6	18.8	196.	191	147	49.4	49.9	48.5	0.0
136.	131	162	48.6	48.2	46.6	18.5	197.	192	147	49.2	49.5	48.1	0.0
137.	132	164	50.3	48.9	47.2	14.8	198.	193	148	49.4	49.7	47.4	0.0
138.	133	166	48.6	48.5	47.2	15.2	199.	194	125	49.3	49.6	47.4	0.0
139.	134	163	52.4	49.6	46.7	16.1	200.	195	122	49.2	49.6	47.8	0.0
140.	135	133	50.1	48.7	47.3	16.7	201.	196	127	49.0	49.5	47.9	0.0
141.	136	0	53.0	50.1	46.2	16.2	202.	197	123	48.8	49.2	47.8	0.0
142.	137	0	48.9	47.0	43.0	16.3	203.	198	116	48.5	48.9	47.8	0.0
143.	138	0	52.9	50.3	46.3	15.4	204.	199	120	47.5	48.1	47.6	0.0
144.	139	0	42.3	41.2	37.6	16.3	205.	200	110	48.0	48.5	47.6	0.0
145.	140	0	21.5	22.2	21.4	21.8	206.	201	0	50.1	49.5	47.2	0.0
146.	141	0	21.5	22.1	21.4	20.0	207.	202	152	50.2	49.4	47.1	0.0
147.	142	216	48.4	45.7	42.9	17.8	208.	203	143	49.2	48.4	47.2	0.0
148.	143	379	52.1	49.9	47.0	18.1	209.	204	136	50.7	48.8	47.1	0.0
149.	144	329	52.0	49.9	47.2	13.0	210.	205	130	51.8	49.8	47.9	0.0
150.	145	290	52.8	50.0	46.6	18.6	211.	206	102	47.4	48.4	48.8	0.0
151.	146	241	53.7	50.6	47.4	14.9	212.	207	90	48.3	47.2	47.1	0.0
152.	147	217	54.6	52.5	48.0	14.4	213.	208	0	52.1	49.8	47.6	0.0
153.	148	188	54.9	51.4	48.2	14.9	214.	209	122	51.8	49.8	47.4	0.0
154.	149	171	53.5	51.8	47.4	14.7	215.	210	111	49.8	48.8	47.9	0.0
155.	150	188	53.2	50.9	47.3	14.7	216.	211	110	50.3	49.8	48.5	0.0
156.	151	0	51.4	49.5	47.3	15.7	217.	212	101	49.4	49.3	48.6	20.5
157.	152	233	53.7	50.8	46.5	14.5	218.	213	95	50.0	49.4	47.9	20.5
158.	153	204	50.4	49.3	47.6	15.6	219.	214	88	48.9	48.9	48.4	20.4
159.	154	184	53.5	50.4	47.2	15.2	220.	215	87	50.5	49.7	48.6	20.3
160.	155	173	53.7	50.3	47.2	15.3	221.	216	86	50.4	49.5	48.5	20.5
161.	156	170	53.7	50.5	47.1	15.4	222.	217	87	48.4	48.8	48.7	20.4
162.	157	160	53.6	50.6	47.3	15.4	223.	218	103	48.6	48.3	48.3	20.3
163.	158	151	52.4	50.2	47.6	16.0	224.	219	105	46.8	47.3	47.6	20.4
164.	159	165	54.2	50.9	47.5	15.6	225.	220	0	48.9	48.1	48.0	0.0
165.	160	171	51.8	49.6	47.7	16.5	226.	221	0	50.3	49.1	47.4	0.0
166.	161	152	52.4	49.8	47.3	16.0	227.	222	134	49.7	49.1	47.7	0.0
167.	162	143	51.6	50.2	46.9	15.7	228.	223	109	47.8	48.1	48.1	0.0
168.	163	156	53.3	49.9	46.6	16.0	229.	224	110	50.2	49.2	47.5	0.0
169.	164	153	53.4	49.7	46.3	15.9	230.	225	96	49.2	48.5	47.8	0.0
170.	165	159	53.4	49.7	46.0	15.8	231.	226	94	49.9	48.9	47.7	0.0
171.	166	156	53.5	49.7	45.6	15.7	232.	227	90	49.5	48.5	47.5	0.0
172.	167	151	55.4	53.7	47.7	15.3	233.	228	90	47.3	46.5	45.2	0.0
173.	168	146	53.4	51.8	47.9	14.9	234.	229	65	50.6	49.6	48.0	0.0
174.	169	150	54.0	51.8	48.2	15.3	235.	230	85	50.0	49.2	47.9	0.0
175.	170	175	54.2	51.7	47.8	15.1	236.	231	84	44.9	44.3	44.2	0.0
176.	171	190	54.3	52.5	48.3	15.6	237.	232	90	52.5	51.9	49.3	0.0
177.	172	130	53.6	53.5	49.1	17.1	238.	233	79	49.5	48.7	46.8	0.0
178.	173	0	51.6	52.8	47.9	15.3	239.	234	77	49.8	49.0	47.8	0.0
179.	174	196	48.3	49.6	45.4	15.3	240.	235	79	49.8	49.2	47.6	0.0
180.	175	184	48.1	49.8	45.9	18.8	241.	236	71	53.8	52.7	50.4	0.0
181.	176	179	48.7	49.3	45.8	17.2	242.	237	73	50.9	50.3	49.9	0.0
182.	177	163	48.6	49.0	45.7	17.2	243.	238	80	51.7	50.7	49.4	20.2
183.	178	169	45.6	48.6	45.6	16.9	244.	239	76	49.8	50.0	49.6	20.3
184.	179	161	49.1	48.5	45.2	17.2	245.	240	75	47.5	48.9	45.9	20.4
185.	180	160	48.2	48.5	45.3	17.2	246.	241	69	47.	48.8	47.2	20.3
186.	181	146	49.2	48.3	44.9	17.5	247.	242	72	51.6	51.4	50.8	19.8

Table E-3 (continued)

Column 4
Page 3 of 4

Line No.	Day	Fe_{TOT}	Temperature TOP	MID	BOT	% O_2 Eff
248.	243	77	54.5	54.0	53.1	19.6
249.	244	76	55.5	53.8	52.2	19.7
250.	245	75	54.2	52.7	50.9	20.1
251.	246	69	51.5	51.1	50.2	20.4
252.	247	66	50.0	49.1	47.6	20.6
253.	248	63	50.2	49.2	47.6	20.1
254.	249	64	50.2	49.1	47.4	20.1
255.	250	63	50.4	49.3	47.7	20.0
256.	251	66	50.7	49.7	48.0	20.0
257.	252	65	45.2	47.4	47.7	20.3
258.	253	66	49.9	49.0	47.0	20.0
259.	254	70	53.0	52.4	51.3	19.7
260.	255	69	55.0	53.2	51.0	19.7
261.	256	64	49.7	50.9	50.2	20.0
262.	257	57	49.5	48.3	45.5	20.4
263.	258	59	53.2	52.8	50.6	19.8
264.	259	60	55.0	54.1	51.2	19.9
265.	260	54	53.0	52.9	52.0	0.0
266.	261	51	55.9	54.5	51.9	0.0
267.	262	46	51.1	52.3	51.9	0.0
268.	263	0	54.5	53.6	51.1	0.0
269.	264	66	54.7	53.7	51.1	0.0
270.	265	63	49.8	51.6	51.3	0.0
271.	266	59	54.2	53.0	51.1	0.0
272.	267	52	52.9	52.4	51.0	0.0
273.	268	50	54.3	53.7	52.5	0.0
274.	269	53	54.4	52.9	51.0	0.0
275.	270	54	54.1	52.6	50.7	0.0
276.	271	51	52.0	51.8	50.6	0.0
277.	272	50	53.7	52.4	50.9	0.0
278.	273	51	52.1	51.5	50.0	0.0
279.	274	49	51.3	51.1	50.0	0.0
280.	275	46	46.7	49.4	50.2	0.0
281.	276	51	52.2	51.2	49.4	0.0
282.	277	46	50.1	51.0	50.7	0.0
283.	278	48	51.8	51.2	50.2	0.0
284.	279	52	52.9	51.6	49.6	0.0
285.	280	53	51.1	50.6	49.7	0.0
286.	281	57	53.8	52.2	50.4	0.0
287.	282	54	46.1	49.2	45.0	0.0
288.	283	0	20.1	21.1	20.6	0.0
289.	284	0	26.0	25.1	24.6	0.0
290.	285	0	53.3	52.4	49.6	0.0
291.	286	71	52.9	51.8	49.3	0.0
292.	287	59	51.8	51.0	50.1	0.0
293.	288	56	51.9	51.3	50.5	0.0
294.	289	55	51.9	50.7	49.7	0.0
295.	290	55	53.7	51.9	50.4	0.0
296.	291	56	53.1	51.1	49.9	0.0
297.	292	52	52.4	51.0	49.8	0.0
298.	293	54	52.5	51.0	49.5	0.0
299.	294	51	49.2	49.3	49.8	0.0
300.	295	53	52.8	50.8	49.5	0.0
301.	296	55	50.9	49.6	49.5	0.0
302.	297	52	50.5	49.6	49.5	0.0
303.	298	51	52.1	50.3	49.6	0.0
304.	299	54	52.8	51.0	49.7	0.0
305.	300	57	52.4	50.6	49.5	19.9
306.	301	50	49.2	49.5	49.9	20.1
307.	302	50	51.7	50.2	49.2	20.3
308.	303	55	52.8	50.5	49.1	20.1
309.	304	48	50.9	49.4	49.2	20.4
310.	305	50	52.3	50.5	49.6	20.0
311.	306	53	53.0	51.0	49.2	20.4
312.	307	49	50.1	49.0	49.4	20.3
313.	308	52	52.1	50.1	49.1	20.3
314.	309	49	51.1	49.8	49.4	20.2
315.	310	48	51.8	49.9	49.2	20.4
316.	311	50	52.3	50.5	49.1	20.1
317.	312	43	49.8	48.7	47.1	20.4
318.	313	0	41.7	40.9	39.6	20.2
319.	314	57	49.0	47.1	44.9	19.4
320.	315	0	54.7	53.0	50.3	20.1
321.	316	56	51.4	50.0	47.8	20.2
322.	317	52	49.6	49.1	47.9	20.3
323.	318	46	51.8	50.8	49.4	20.1
324.	319	0	54.0	51.3	48.2	20.2
325.	320	55	53.9	51.2	48.7	20.3
326.	321	52	54.2	51.6	49.3	20.1
327.	322	45	52.3	50.9	49.0	19.9
328.	323	45	53.5	51.3	49.7	20.3
329.	324	44	53.8	51.2	49.4	20.3
330.	325	45	54.6	51.5	49.5	20.3
331.	326	43	53.1	51.0	49.6	20.2
332.	327	46	54.0	52.0	49.1	20.0
333.	328	43	53.5	51.8	49.4	20.0
334.	329	43	53.7	52.1	49.6	20.2
335.	330	43	53.1	51.5	49.3	20.1
336.	331	42	53.9	51.8	49.4	20.2
337.	332	40	51.3	50.4	49.2	20.0
338.	333	45	53.4	51.8	49.1	19.9
339.	334	45	52.8	51.5	49.1	20.1
340.	335	46	53.8	51.7	49.2	20.1
341.	336	46	52.3	51.5	49.8	20.1
342.	337	44	52.8	51.5	50.1	0.0
343.	338	44	52.6	51.0	49.8	0.0
344.	339	43	53.9	51.3	49.4	0.0
345.	340	43	52.0	50.1	49.2	0.0
346.	341	44	54.0	51.7	49.4	0.0
347.	342	46	53.0	50.8	47.9	0.0
348.	343	45	51.0	49.3	46.7	0.0
349.	344	44	53.4	50.8	48.9	0.0
350.	345	42	53.2	49.7	48.4	0.0
351.	346	39	50.5	49.3	47.7	0.0
352.	347	38	53.1	50.3	47.0	0.0
353.	348	0	52.2	49.7	46.5	0.0
354.	349	48	54.5	52.2	48.9	0.0
355.	350	46	52.8	50.6	48.3	0.0
356.	351	43	52.4	50.4	48.3	0.0
357.	352	42	50.9	49.7	47.4	0.0
358.	353	42	51.8	50.1	47.8	0.0
359.	354	39	51.1	49.5	46.6	0.0
360.	355	61	53.0	51.0	47.6	0.0
361.	356	46	51.6	49.7	46.5	0.0
362.	357	46	50.0	48.5	45.9	0.0
363.	358	39	46.8	48.0	46.1	0.0
364.	359	41	52.1	50.1	47.7	0.0
365.	360	37	48.9	49.9	48.6	0.0
366.	361	34	52.3	50.4	47.0	0.0
367.	362	0	53.9	51.4	47.2	0.0
368.	363	42	52.7	50.8	47.7	0.0
369.	364	45	47.6	46.5	43.2	0.0

Table E-3 (continued)

Column 4
Page 4 of 4

Line No.	Day	Fe_{TOT}	Temperature TOP	Temperature MID	Temperature BOT	% O_2 Eff	Line No.	Day	Fe_{TOT}	Temperature TOP	Temperature MID	Temperature BOT	% O_2 Eff
370.	365	44	54.0	52.0	49.0	0.0							
371.	366	43	52.8	50.0	48.0	0.0							
372.	367	43	49.3	47.7	43.6	0.0							
373.	368	35	22.3	23.2	22.3	0.0							
374.	369	30	22.7	23.0	22.3	0.0							
375.	370	16	21.8	22.2	21.4	0.0							
376.	371	9	22.7	23.2	22.3	0.0							
377.	372	8	22.6	23.1	22.2	0.0							
378.	373	5	22.7	23.3	22.4	0.0							
379.	374	5	22.7	23.2	22.3	0.0							

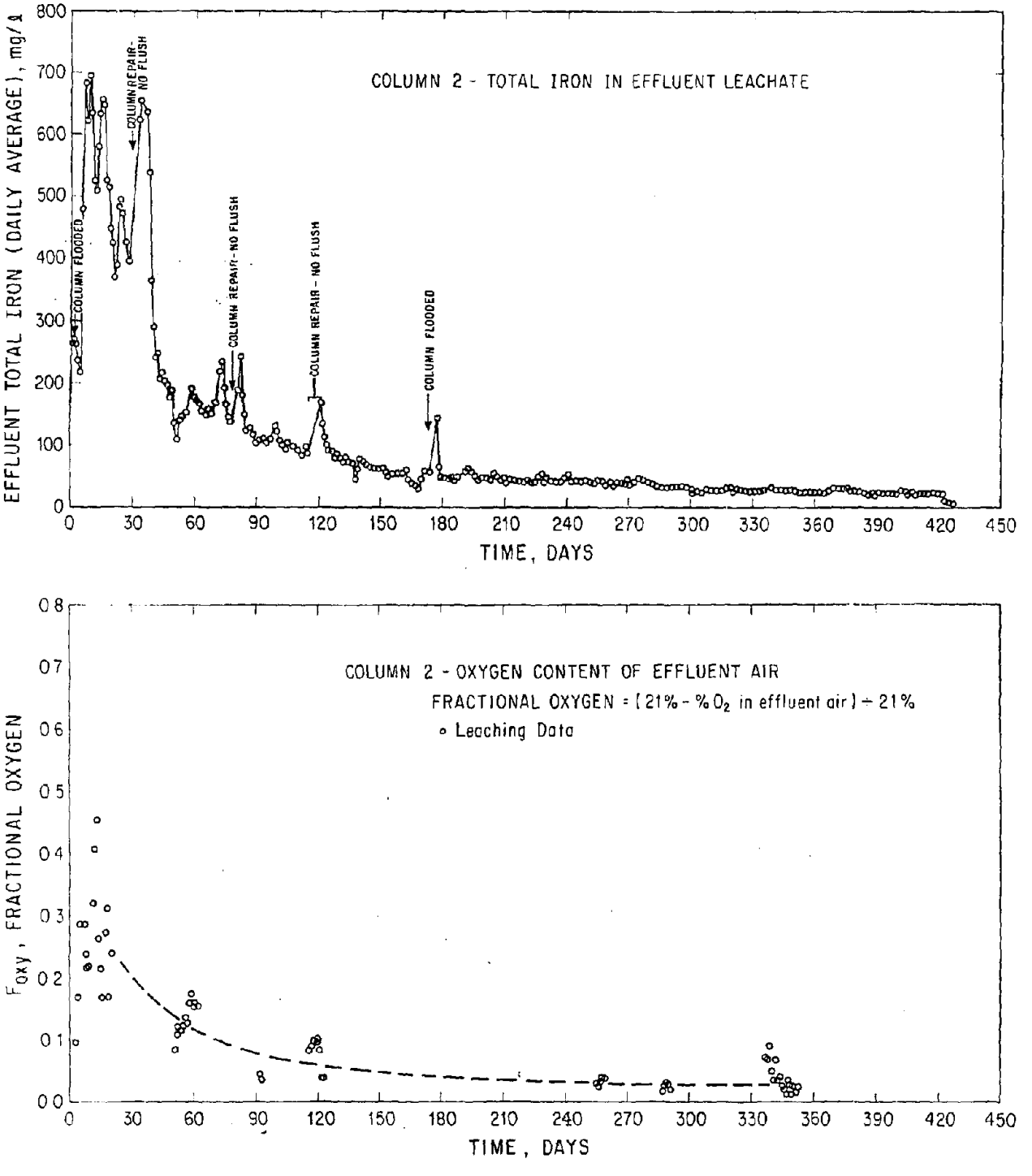

Figure E-3 Effluent Iron and Oxygen Data for Column Leach Experiments with Illinois Bituminous Coal. See Table E-2 for Experimental Conditions.

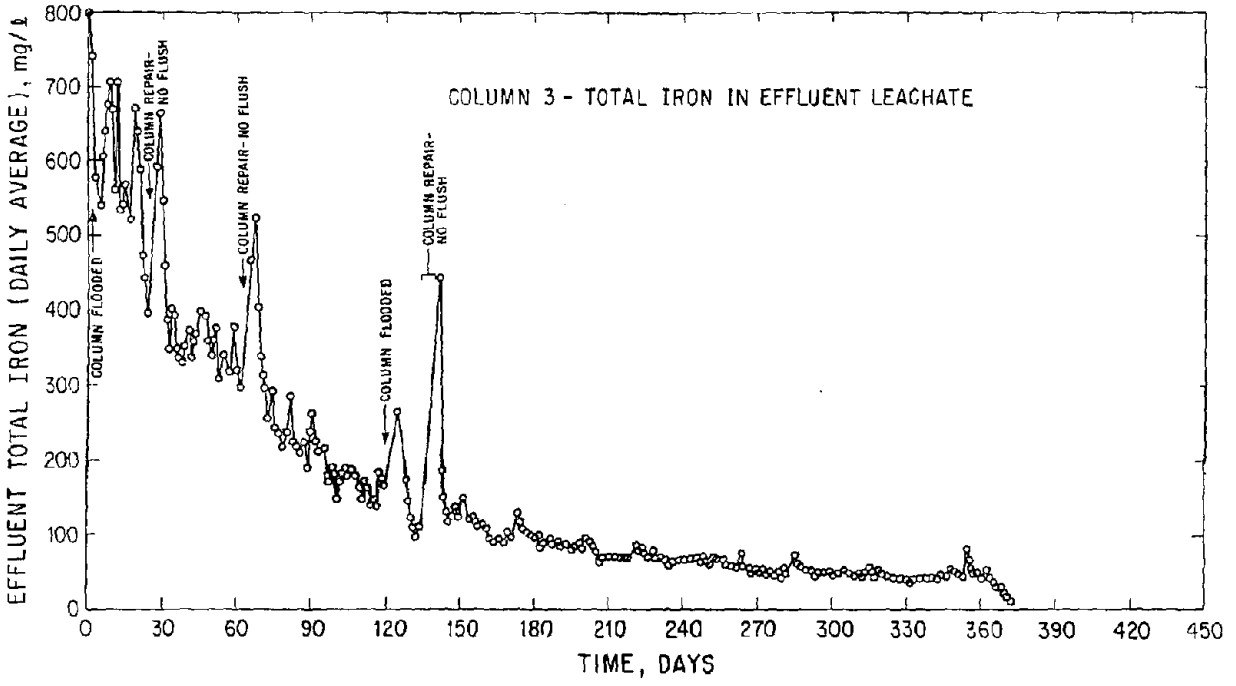

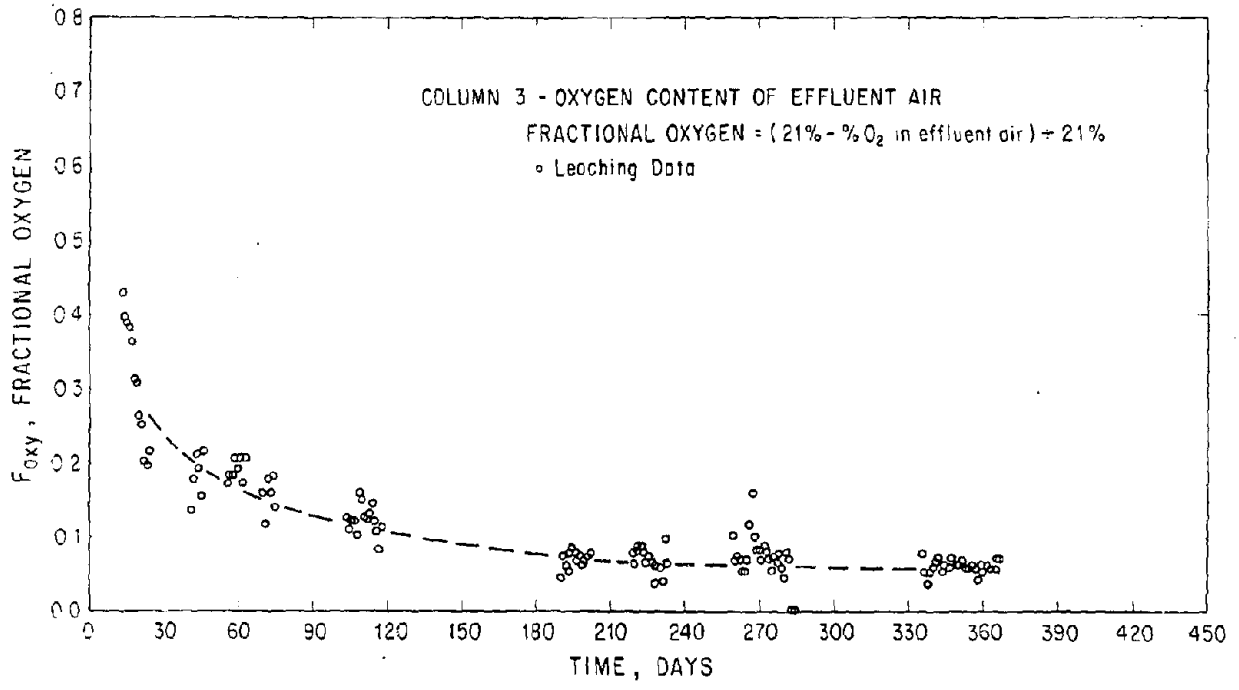

Figure E-3 (continued)

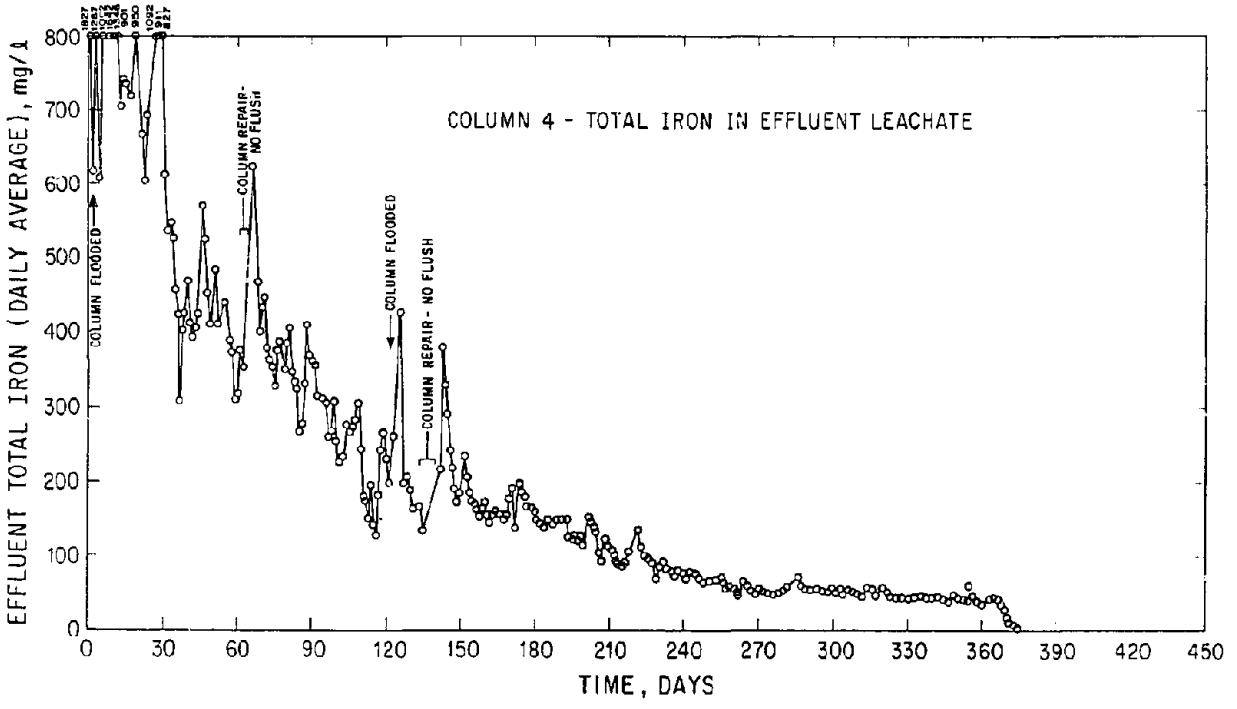

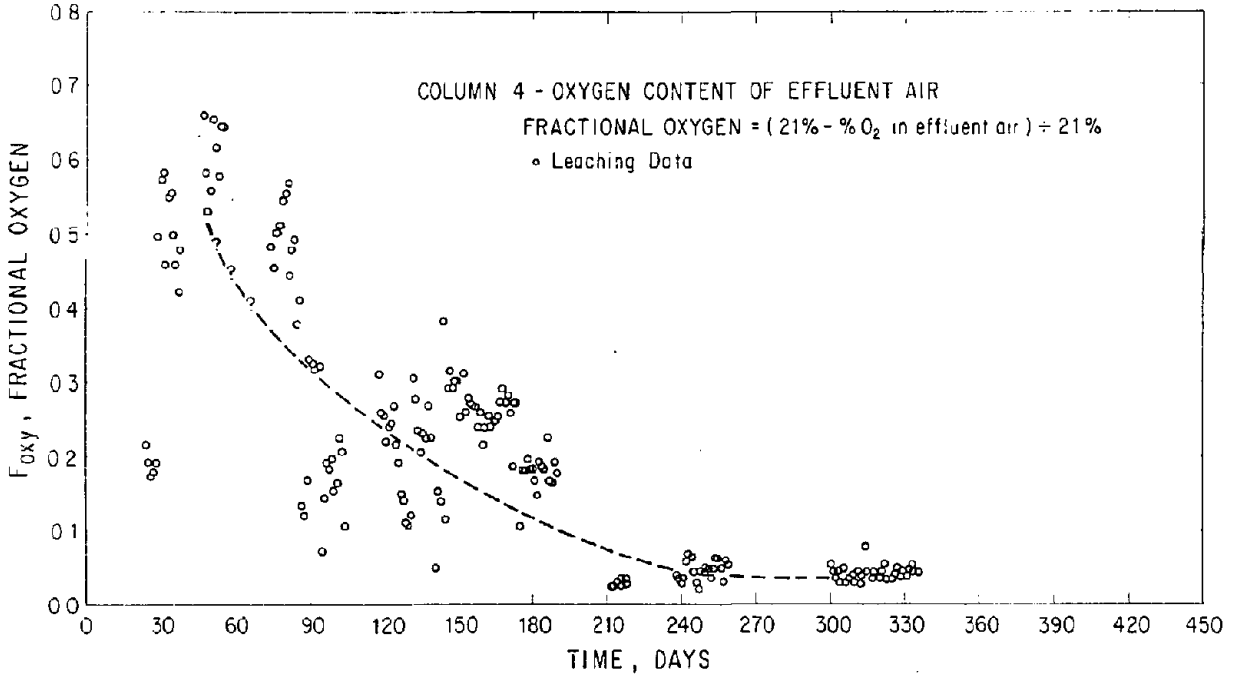

Figure E-3 (continued)

APPENDIX E References

Brimhall, D. B. and Wadsworth, M. E., 1973, Oxygen consumption in dump leaching. AIME Transactions 254, 68-75.

Bruynesteyn, A. and Vizsolyi, A., 1981, The effect of pH and Eh on the chemical and biological leaching of a pyritic uranium ore. AIME-SME preprint No. 81-370, Littleton, CO.

Lacey, D. T. and Lawson, F., 1970, Kinetics of the liquid phase oxidation of acid ferrous sulfate by the bacterium Thiobacillus ferrooxidans. Biotechnol. Bioengng. 12, 29-38.

Murr, L. E., 1980, Theory and practice of copper sulphide leaching in dumps and in situ. Minerals Sci. Engng. 12, 121-189.

Potter, G. M., 1981, Design factors for heap leaching operation. Mining Engineering 33, 277-281.

Appendix F Description of the Finite Difference Computer Model of Coal Heap Leaching

The program is listed in part 3 of this appendix. We first briefly describe the use of the program and the kind of output it gives, then discuss the nature of the finite difference approximation in enough detail that the program code should be intelligible to the really determined, and finally give a listing of the program.

1. Description of the program

The program is simply an implementation of the mathematical model given in Section II-B of the text. To implement it, the program must be given the parameters listed in Tables 1, 6 and 18 and such information as the height of the heap (or column), the average rate of irrigation of the heap, ambient temperature at the location of the heap or column, etc. Input to the program is made through namelist statements. The program first reads a master file to get the base values of the various parameters. This file is called NMEXDAD. The program then reads an update file in which the user can change the values of particular parameters to suit his particular situation. This is done through a file called BLNKDAD. The program then executes. Full description of the parameters in each of the three NAMELIST statements together with the values usually used is given in Tables F-1 through F-3.

The program calculates the leach history of the heap or column at time intervals DELT long (usually 2 days). At each iteration the program lists the maximum rate of pyrite and coal oxidation (RTMX and RCMX), the air velocity up through the column or heap (VA in cm/sec), the maximum temperature in the heap, the fraction pyrite leached, the fraction coal oxidized, the iron added to the effluent (in ppm), the concentration of oxygen in the effluent air (fraction of atmospheric), and the average rate of pyrite oxidation. Every NKOL timesteps a plot is given showing the oxygen, rate of leaching (*) and temperature profiles through the heap. At the end of each heap calculation a plot is given showing the ambient temperature (*), the maximum heap temperature (T), the effluent oxygen content (O), and the cumulative fraction pyrite leached (X). If a series

of heaps of different height are computed, a plot is output at the end of the series giving the maximum heap temperature attained and the fraction pyrite leached as a function of heap height. All output is on a standard printer.

Figure F-1 gives a flow chart of the program.

Table F-1 Description of parameters for computer model;

NAMELIST PAR

Parameter	Typical Value	Dimensions	Definition
N	150	--	Number of heap layers
HGT	10-75	ft	Heap height; ignored if NHGT ≠ 0
EXD	5000	cal/mol	Diffusional activation energy, E^*_D
EXK	20000	cal/mol	Chemical activation energy, E^*_C
EACTC	12000	cal/mol	Activation energy for coal oxid., E^*
PHI	0.2	--	Interblock porosity of heap, ϕ
TAUC	.0	months	Disseminated pyrite chemical leach time; if <.01, value of TAUC and TAUD calculated internally
TAUD	.0	months	Disseminated pyrite diffusional leach time
GPY	0.027	--	Weight fraction pyrite in coal, G_{py}
ASULFR	30	cm^{-1}	Surface area of pyrite per unit volume of coal; a^R_{SULF}
NB	0	--	Number of layers in heap pad (if=0, ignor)
TMXM	65	^oC	Maximum temperature at which pyrite oxid. occurs, T_{kill}
NHGT	5	--	Number of heaps of height HGTL(I); ≤ 40
HGTL	10,15,20,30	ft	Heap height
FRACT	0	--	Fraction water saturation of incoming air
RORD	0.	--	Order of oxygen uptake, $([O_2])^{RORD}$
ITPL	1	--	(=1), Advection at I=N set equal to zero
TSIK	55	^oC	Temperature at which bacteria become sick, T_{sick}
TMSCL	2	mo/inch	Time scale for plots of leach history
NMBSE	0	--	
XSTRT	1.	--	Pyrite fraction present initially

Table F-2 Description of parameters for computer model;

NAMELIST OPER

Parameter	Typical Value	Dimensions	Definition
	column/heap		
VAIR	0 0	cm/sec	Darcy velocity of air; =0 compute using RACL and Blake-Kozeny Eqn.
VWAT	.01	gal/ft^2-hr	Average irrigation rate
NDELT	360	--	Number of timesteps in calculation
DELT	.0645	months	Time increment each timestep
NTOT	2	--	No. of increments in cycle, irrelevant if NRES = 0
NRES	0	--	No. of increments when water not applied
PCTAC	.001		Fraction convergence required in calc.
AO	0 0		Insulating boundary condition at base of column or heap
BO	1 1		
GO	0 0		
AN	0 1		Insulating boundary condition at top of column. Top of heap set at ambient temp.
BN	1 0		
GN	0 TAMB		
NKOL	--	--	Profiles through heap output every NKOL timesteps
NXOUT	--	--	Profile layers NXOUT, 2NXOUT, 3NXOUT output
NTOUT	--	--	Time frequency of output on time evolution plot
NSW	not applicable		
VWAT2	na		
VAIR2	na		
NREST2	na		
RTCT	0.34	cal/cm^3-^{o}C	Density times the heat capacity of heap
AKT	5.28 x 10^{-3}	cal/cm-s-^{o}C	Thermal conductivity of heap

Table F-3 Description of parameters for computer model;

NAMELIST ANSF

Parameter	Typical Value	Dimensions	Definition
	column/heap		
COALS	2.87×10^{-7}	mo^{-1}	Initial coal oxidation rate; fraction oxidized per month
XCOLO	1.13×10^{-4}	--	Initial fractional oxidation of coal
RACL	.315, .635	cm	Radius of coal fragments
OXCL	2.67	-->	grams O_2 consumed per gram coal oxidized
ACOAL	6440	cal/g	Calories liberated per gram coal oxidized
AMOSTR	6	--	Month of year leaching started
TCAV	10.22	^oC	Average temperature of heap surface
SDTA	11.9	^oC	Amplitude of seasonal temperature variation of heap surface
TCAVA	10.22	^oC	Average ambient temperature
TSTR	20.1	^oC	Starting temperature of heap
NCUT	2	--	Output every NCUT timesteps; if NCUT=NDELT no NAMELIST data output
IOUT			Output device number
DX(250)			Point spacing; Internally set if N=NQ
DXPL	2		Variable point spacing parameter; "
DXMN	1.3		" " " " "
NQ	0		Code; if N=NQ point spacing is automatic
CONDK	0.	--	Conductive heat leakage of column
IFIXT	1 0		(=1)-constant temp column;≠ 1 calcs T
SDT	11.9		Amplitude of seasonal temperature var.
ICAL	0		
IPSC	1		Plot scaling parameter
IPLT	1		code; enables time evolution plot output
XS	.6		Stoichiometry of pyrite oxidation, "X" in text, =1 all SO_4^{2-}, =0 all S^o.
AO2PY	2900	cal/mol O_2	Calories generated per mole O_2 consumed in pyrite oxidation
AKOX	3.3×10^{-8}	cm/sec	First-order pyrite oxidation rate cons.
DEFF	1.0×10^{-8}	cm^2/sec	Effective diffusion constant for Fe(III) in coal matrix

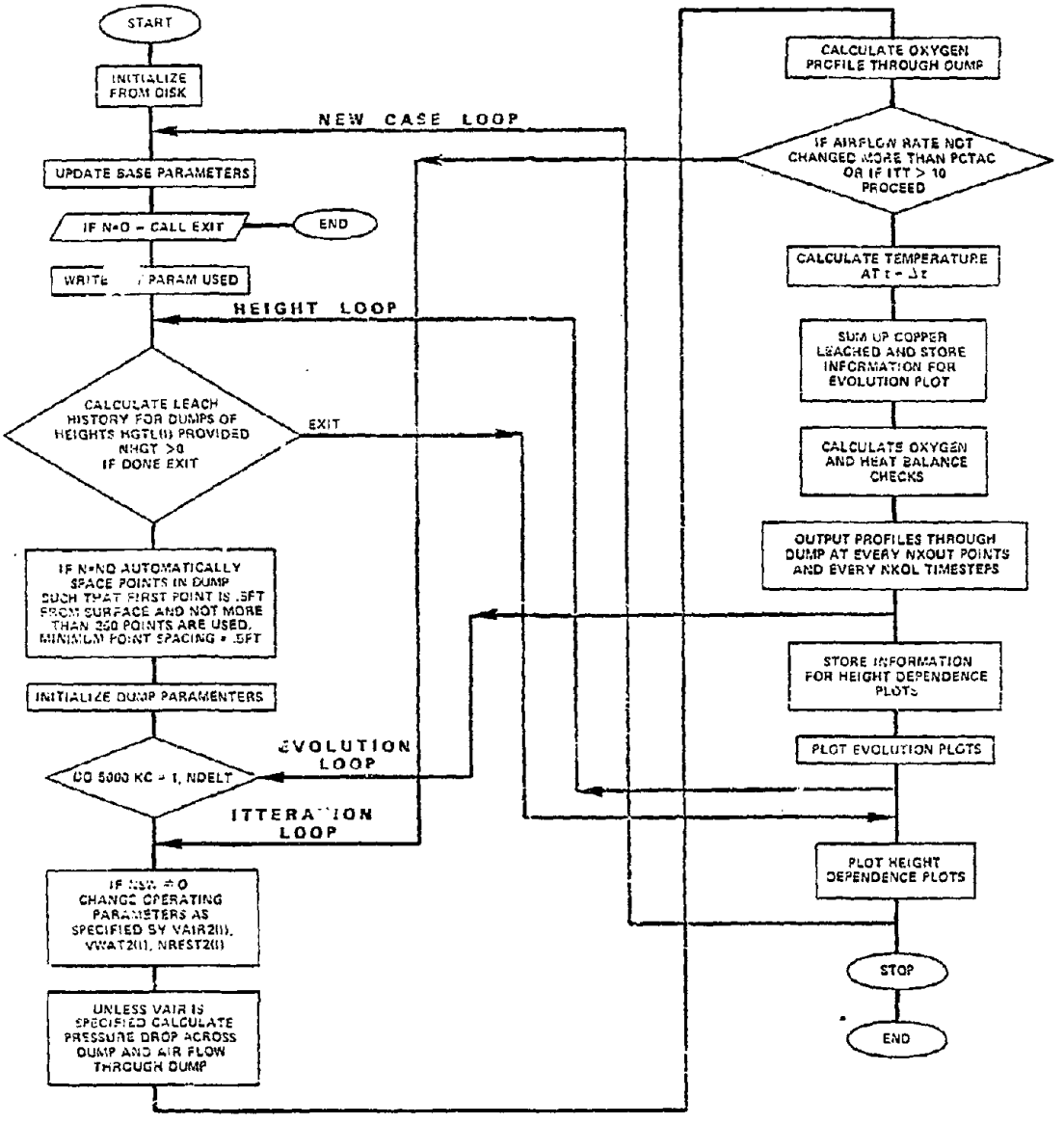

Figure F-1 . Flow Chart for Heap Leach Program

2. Some Programming Details - Solution of the Energy (Heat Balance) Equation

Let t and z be made dimensionless:

$$\text{(F-1)} \qquad \bar{t} = t \frac{K_T}{\rho_T C_T H^2}$$

$$\text{(F-2)} \qquad \bar{z} = Z/H$$

Then the energy (heat balance) equation, eq. 13 of the text becomes

$$\text{(F-3)} \qquad \frac{\partial T}{\partial \bar{t}} = (\rho_\ell C_\ell V_\ell - \rho_g C_g V_g) \frac{\partial T}{\partial \bar{z}} \frac{H}{K_T} + \frac{\mathcal{R}_A H^2}{K_T} + \bar{\nabla}^2 T$$

If point triplets are envisaged -0^+ about the central point (0), (F-3) may be approximated in finite difference form for $\left(\begin{smallmatrix} V > 0 \\ V < 0 \end{smallmatrix}\right)$:

$$\text{(F-4)} \qquad \frac{T^+ - T_o}{\Delta \bar{t}} = \underset{\substack{v<o \\ v<o}}{(ADW-ADG)} \left(\frac{\frac{T_o^* - T_-^*}{\Delta X_{-o}}}{\frac{T_+^* - T_o^*}{\Delta X_{+o}}} \right) \frac{H}{K_T} + \frac{\mathcal{R}_A H^2}{K_T} + \frac{\frac{T_+^* - T_o^*}{\Delta X_{+o}} - \frac{T_o^* - T_-^*}{\Delta X_{-o}}}{\Delta X_{+o-}}$$

Since V_ℓ is always less than zero (solution flow is always downward), ADW always multiplies $\frac{T_+ - T_O^*}{\Delta X_{+O}}$. ADG may multiply either the upper or lower term, but usually the upper term since air flow is generally upward through the heap. The half gradient preserves causality in advection. $ADW = \rho_\ell C_\ell V_\ell$, $ADG = \rho_g C_g V_g$.

Rearranging terms in (F-4):

$$(F\text{-}5)\quad \frac{T_o}{\Delta\bar{t}} + \frac{\mathcal{R}_A H^2}{K_T} = T_-^* \left\{ \begin{pmatrix} \frac{-ADG\cdot H}{\Delta X_{-o} K_T} \\ \\ o \end{pmatrix} - \frac{1}{\Delta X_{-o}\,\Delta X_{+o-}} \right\} + T_+^* \left\{ \begin{pmatrix} o \\ \\ \frac{ADG\cdot H}{\Delta X_{+o} K_T} \end{pmatrix} - \frac{ADW}{\Delta X_{+o}} \frac{H}{K_T} - \frac{1}{\Delta X_{+o}\,\Delta X_{+o-}} \right\} + T_o^* \left\{ \frac{1}{\Delta\bar{t}} + \frac{ADW\cdot H}{\Delta X_{+o} K_T} + \begin{pmatrix} \frac{ADG\cdot H}{\Delta X_{-o} K_T} \\ \\ \frac{-ADG\cdot H}{\Delta X_{+o} K_T} \end{pmatrix} + \frac{\frac{1}{\Delta X_{+o}} + \frac{1}{\Delta X_{-o}}}{\Delta X_{+o-}} \right\}$$

If we change ΔX and $\Delta\bar{t}$ according to (F-6)

$$(F\text{-}6)\qquad \Delta X = \Delta Z \Delta X^* \qquad \lambda = \Delta\bar{t}/(\Delta X^*)^2$$

Such that

$$\Delta X^* \equiv 1/\sum_1^N \Delta Z \ ,$$

multiplying (F-5) through by $(\Delta X^*)^2\ \lambda$ gives:

$$\overbrace{T_o + \frac{\mathcal{R}_A H^2 (\Delta X^*)^2 \lambda}{K_T}}^{D} = T_-^* \left\{ \overbrace{\begin{pmatrix} \frac{-ADG}{\Delta \bar{Z}_o} & \frac{\Delta X^* \lambda H}{K_T} \\ & o \end{pmatrix} - \frac{\lambda}{\Delta \bar{Z}_{-o} \Delta \bar{Z}_{+o-}}}^{A} \right\}$$

$$+ T_+^* \left\{ \overbrace{\begin{pmatrix} o & \\ \frac{ADG}{\Delta \bar{Z}_{+o}} & \frac{H \Delta X^* \lambda}{K_T} \end{pmatrix} - \frac{\lambda}{\Delta \bar{Z}_{+o} \Delta \bar{Z}_{+o-}} - \frac{ADW}{\Delta \bar{Z}_{+o}} \frac{H \Delta X^* \lambda}{K_T}}^{C} \right\} \quad \text{(F-7)}$$

$$+ T_o^* \left\{ \overbrace{1 + \frac{ADW \Delta X^* \lambda H}{\Delta \bar{Z}_{+o} K_T} + \begin{pmatrix} \frac{ADG \Delta X^* \lambda H}{\Delta Z_{-o} K_T} \\ \frac{-ADG \Delta X^* \lambda H}{\Delta Z_{+o} K_T} \end{pmatrix} + \lambda \begin{pmatrix} \frac{1}{\Delta \bar{Z}_{+o}} + \frac{1}{\Delta \bar{Z}_{-o}} \\ \Delta Z_{+o-} \end{pmatrix}}^{B} \right\}$$

(F-7) represents one equation for each point in the heap. Since only neighboring points (up, $^+$, or down, -) from the central point are involved, (F-7) is a tridiagonal matrix and may be inverted by a simple algorithm. In (F-7), A is the upper diagonal, B the principal diagonal, and C the lower diagonal; D is the constant vector and T_i^* the unknowns.

At the end points, boundary conditions must be used to interpret (F-7) since otherwise (F-7) would involve non-existant points. General boundary conditions (Neuman, A = 0; Dirichelet B = 0; mixed $A \neq 0$. $B \neq 0$) may be written:

$$T_B = \frac{\overbrace{G\emptyset}^{D} + \overbrace{B\emptyset\ (T_2/2\Delta X_2)}^{C}}{A\emptyset + B\emptyset/2\Delta X_2}$$

(F-8)

$$T_T = \frac{\overbrace{GN}^{D} + \overbrace{BN\ (T_{N-1}/2\Delta X_N)}^{A}}{AN + BN/2\Delta X_N}$$

As can be seen, (F-8) permits the boundary point to be expressed in terms of points inside the NxN tridiagonal matrix, (F-7). (N is the number of points in the heap). Thus

At I = 1

(F-9)

$$\textcircled{D} = \textcircled{D} - \textcircled{A} \cdot G\emptyset/(A\emptyset + B\emptyset/2\Delta X_2)$$
$$\textcircled{C} = \textcircled{C} + \textcircled{A} \cdot (B\emptyset/2\Delta X_2)/(A\emptyset + B\emptyset/2\Delta X_2)$$

At I = N

(F-10)

$$\textcircled{D} = \textcircled{D} - \textcircled{C} \cdot GN/(AN + BN/2\Delta X_N)$$
$$\textcircled{A} = \textcircled{A} + \textcircled{C} \cdot (BN/2\Delta X_N)/(AN + BN/2\Delta X_N) \quad .$$

Boundary conditions at the base of the heap must also be corrected to account for the thermal effects of water saturation of influent air. The water vapor content of air is given by the expression:

(F-11) $$[wv]^g_{STP} = 953\ e^{-5220.9/T}$$

where T is given in Kelvins. At 30°C, (F-11) gives 3.37×10^{-5} gm wv/cm^3 compared to a table value of 3.13×10^{-5}. At 90°C the comparison is 5.4×10^{-4} (eq. (F-11)) vs 5.2×10^{-4}.

The comparative enthalpy of air can be written as in (F-12), taking into account water vapor and the normal heat capacity of air, c_g = .24 cal/gm.°C, and the heat of vaporization of water → water vapor of 540 cal/gm.

$$\text{(F-12)} \qquad \text{ENTH}(T) = .24\ T + \frac{(540)(953)\ e^{-5220.9/(T+273)}}{\rho_g}$$

The heat capacity of air, including water vapor contribution, may then be written

$$\text{(F-13)} \qquad C_g = \frac{\text{ENTH}\ (T,X)}{T} \equiv CG\ (T)$$

(F-12) & (F-13) are treated as function statements in the program. (F-12) is modified so a certain fraction of water vapor saturation may be requested.

ADW and ADG (in (F-4), (F-5), and (F-6)) may now be written:

$$\text{ADG} = \text{DENG} * CG(T) * VA$$
$$\text{ADW} = \text{RLCL} * VW \ .$$

Further groups of terms in (F-7) may be defined:

$$\text{AMUL1} \equiv \frac{ADW \cdot \Delta X^* \cdot \lambda \cdot H}{K_T}$$

$$\text{(F-14)} \qquad \text{AMUL2} \equiv \frac{\rho_g \cdot VA \cdot H \cdot \Delta X^* \cdot \lambda}{K_T}$$

$$\text{AMUL3} \cdot \frac{\partial X}{\partial \bar{t}} \equiv \frac{\mathcal{R}_A\ H^2\ (\Delta X^*)^2\ \lambda}{K_T} \ .$$

To return to the original question of boundary conditions, water will come in the top of the heap near ambient temperature irregardless of the top surface boundary conditions, and air will come in the bottom undersaturated in water vapor. Thus we want to null out the usual advection terms and force the issue by putting in the advection terms explicitely:

(F-15) $- \frac{H}{K_T} \rho_\ell C_\ell V_\ell \frac{\partial T}{\partial \bar{Z}}$ and $+ \rho_g C_g V_g \frac{H}{K_T} \frac{\partial T}{\partial \bar{Z}}$

[remember advection terms have switched sides of equation between eq. (F-3) and (F-7)]. (F-15) may be converted to source terms:

$$- [(\Delta X^*)^2 \lambda] \left(\frac{H}{K_T} \rho_\ell C_\ell V_\ell \frac{T_{N+} - T_N}{\Delta \bar{Z} \; \Delta X^*}\right) \qquad [(\Delta X^*)^2 \lambda] \left(\frac{H}{K_T} \rho_g V_g \frac{\mathcal{H}_1 - \mathcal{H}_{1-}}{\Delta \bar{Z} \; \Delta X^*}\right)$$

$$- \text{AMUL1} \frac{\text{TAMBS} - T_N}{\Delta \bar{Z}}$$

(D) (B)

Note $\mathcal{H} \equiv$ Enthalpy $\approx$ CG (T)*T

$$+ \text{AMUL2} \frac{\frac{\text{ENTH}(T_1)}{T_1} \cdot T_1^* - \text{ENTH (TAMB)}}{\Delta \bar{Z}}$$

(B) (D)

TAMBS is ambient surface temperature TAMB is ambient temperature

With these comments and Carnahan (1969) the program, with a little effort, should be easily decipherable.

APPENDIX F References

Carnahan, B., Luther, H. A., and Wilkes, J. O., Applied Numerical Methods, John Wiley & Sons, New York, 1969, 604 p.

3. Heap Leach Program Listing

NAMELIST FILES FOR COLUMN SIMULATION RUNS

NMEXDAT

```
1.      &PAR N=150,HGT=3.00,EXD=5000.,EXK=20000.,EACTC=12000.,PHI=.2,TAUC=44.5,
2.       TAUD=22.2,AKAVE=1000.,GPY=.0328,ASULFR=30.,NB=0,TMXM=65.,NHGT=0,
3.       HGTL=10.,20.,40.,80.,36*1.,
4.       FRACT=0.,RORD=0.,ITPL=1,TSIK=55.,TMSCL=.774200,NMBSE=0,XSTRT=1., &END
5.      &OPER VAIR=.0011,VWAT=0.22,NDELT=29,DELT=.03226,NTOT=2,NRES=0,
6.      PCTAC=.001,A0=0.,B0=1.,G0=0.,AN=1.,BN=0.,GN=0.,NKOL=28,NXOUT=3,NTOUT=4,
7.       NSW=0,VAIR2=4*.008,2*.0005,2*.001,3*.002,2*.004,.008,5*0.,
8.       2*.0005,2*.001,2*.002,2*.004,16*.008,4*.016,7*.008,6*.016,
9.      26*.032,16*.023,4*.0114,4*.01,
10.     VWAT2=3*0.,.718,0.,.541,0.,.541,2*0.,.445,0.,.539,0.,.563,.196,
11.     .227,.276,.265,0.,.505,0.,.537,0.,.503,0.,.535,3*0.,.5,0.,.545,
12.     0.,.52,7*0.,.514,6*0.,.509,5*0.,.538,4*0.,.533,6*0.,.555,10*0.,
13.     .576,8*0.,.578,2*0.,.543,14*0.,.576,4*.5,
14.      NREST2=3*7,5,7,5,7,5,2*7,5,7,5,7,5*0,7,5,7,5,7,5,7,5,3*7,
15.      5,7,5,7,5,7*7,3,6*7,5,5*7,5,4*7,3,6*7,5,10*7,5,8*7,5,2*7,
16.     5,14*7,5,4*7,RTCT=.6,AKT=5.E-3,  &END
17.     &ANSF COALS=2.87E-4,XCOL0=1.13E-4,RACL=.3175,AMOSTR=1.45,SDT=11.,
18.       TCAV=1.45,SDTA=11.,TCAVA=14.5,TSTR=40.,NCUT=2,IOUT=6,DX=250*1.0,
19.     DXPL=2.,DXMN=1.3,NQ=0,CONDK=8.E-8,IFIXT=1,OXCL=2.67,DEFF=7.5E-8,
20.     ACOAL=6440.,ICAL=0,IPSC=1,IPLT=1,XS=.6,A02PY=2900.,AKOX=1.E-7, &END
```

BLNKDAT

```
1.      &PAR HGT=3.0,TAUC=00., TAUD=300.,XSTRT=1.0,GPY=1.7E-2, &END
2.      &OPER NDELT=450,DELT=.03226,NKOL=84, &END
3.      &ANSF ICAL=0,OXCL=2.67,RACL=.635,AKOX=.33E-5,DEFF=1.0E-8,TSTR=50.,
4.       COALS=2.87E-7,ACOAL=6440, &END
5.      &PAR  N=0,   &END
```

NAMELIST FILES FOR HEAP SIMULATION RUNS

NMEXDAD

```
 1.      &PAR N=150,HGT=3.00,EXD=5000.,EXK=20000.,EACTC=12000.,PHI=.2,TAUC=44.5,
 2.       TAUD=22.2,GPY=.0328,ASULFR=30.,NB=0,TMXM=65.,NHGT=0,
 3.       HGTL=10.,20.,40.,80.,36*1.,
 4.       FRACT=0.,RORD=0.,ITPL=1,TSIK=55.,TMSCL=.774200,NMBSE=0,XSTRT=1. &END
 5.      &OPER VAIR=.0011,VWAT=0.22,NDELT=29,DELT=.03226,NTOT=2,NRES=0,
 6.      PCTAC=.001,A0=0.,B0=1.,G0=0.,AN=1.,BN=0.,GN=0.,NKOL=28,NXOUT=3,NTOUT=4,
 7.       NSW=0,VAIR2=4*.008,2*.0005,2*.001,3*.002,2*.004,.008,5*0.,
 8.       2*.0005,2*.001,2*.002,2*.004,16*.008,4*.016,7*.008,6*.016,
 9.      26*.032,16*.023,4*.0114,4*.01,
10.      VWAT2=3*0.,.718,0.,.541,0.,.541,2*0.,.445,0.,.539,0.,.563,.196,
11.      .227,.276,.265,0.,.505,0.,.537,0.,.503,0.,.535,3*0.,.5,0.,.545,
12.      0.,.52,7*0.,.514,6*0.,.509,5*0.,.538,4*0.,.533,6*0.,.555,10*0.,
13.      .576,8*0.,.578,2*0.,.543,14*0.,.576,4*.5,
14.       NREST2=3*7,5,7,5,7,5,2*7,5,7,5,7,5*0,7,5,7,5,7,5,7,5,3*7,
15.       5,7,5,7,5,7*7,3,6*7,5,5*7,5,4*7,3,6*7,5,10*7,5,8*7,5,2*7,
16.      5,14*7,5,4*7,RTCT=.6,AKT=5.E-3,  &END
17.      &ANSF COALS=2.87E-4,XCOL0=1.13E-4,RACL=.3175,AMOSTR=1.45,SDT=11.,
18.        TCAV=1.45,SDTA=11.,TCAVA=14.5,TSTR=40.,NCUT=2,IOUT=6,DX=250*1.0,
19.      DXPL=2.,DXMN=1.3,NQ=0,CONDK=8.E-8,IFIXT=1,OXCL=2.67,DEFF=7.5E-8,
20.      ACOAL=6440.,ICAL=0,IPSC=1,IPLT=1,XS=.6,AO2PY=2900.,AKOX=1.E-7, &END
```

BLNKDAD

```
 1.      &PAR HGT=30.,TAUC=00., TAUD=300.,XSTRT=1.0,GPY=1.7E-2,
 2.       NHGT=2,HGTL=15.,20.,TMSCL=2.,  &END
 3.      &OPER NDELT=360,DELT=.06452,NKOL=44,RTCT=.34,AKT=5.28E-4,VWAT=.015,
 4.       VAIR=0.,PCTAC=.01, &END
 5.      &ANSF ICAL=0,OXCL=2.67,RACL=.317,AKOX=.33E-5,DEFF=1.E-8,TSTR=20.11,
 6.       AMOSTR=6.0,CONDK=0.0,IFIXT=0,SDT=11.9,SDTA=11.9,TCAV=10.22,
 7.       TCAVA=10.22,ACOAL=6440.,COALS=.287E-6, &END
 8.      &PAR  N=0,   &END
```

```
//MN2XXXXX JOB
// EXEC RUN,PROG=WTLOG,PARM='1-D  DUMP'
/*JP FULLSKIPS
// EXEC FXCLG,PARM='NOLIST,NOSOURCE'
//SYSIN DD *
C------MODIFIED PSU FORTRAN VERSION OF DUMPS; L M CATHLES
         DIMENSION H(200),V(200),V1(200),V2(200),V3(200)
         DIMENSION V4(200),V5(200),V6(200),V7(200)
         DIMENSION HP(100),VP(100),VP1(100),VP2(100),VP3(100)
         DIMENSION VAIR2(110),VWAT2(110),HPCT(42),VPCT(42),VPCT1(42)
         DIMENSION VC(250),VT(250),VX(250),RNS(250),RT(250),A(250),B(250)
         DIMENSION NREST2(110),TBD(200),TP1(200),TP3(200),COT(200)
        1,D(250),VTS(250),XNS(250),C(250),TB(250),HGTL(40),SCALE(5),DX(250)
         NAMELIST/PAR/N,HGT,EXD,EXK,EACTC,PHI,TAUC,TAUD,GPY,ASULFR,
        1NB,TMXM,NHGT,HGTL,FRACT,RORD,ITPL,TSIK,TMSCL,NMBSE,XSTRT
         NAMELIST/OPER/VAIR,VWAT,NDELT,DELT,NTOT,NRES,PCTAC,A0,B0,G0,
        1AN,BN,GN,NKOL,NXOUT,NTOUT,NSW,VWAT2,VAIR2,NREST2,RTCT,AKT
         NAMELIST/ANSF/COALS,XCOL0,RACL,OXCL,ACOAL,AMOSTR,
        1TCAV,SDTA,TCAVA,TSTR,NCUT,IOUT,DX,DXPL,DXMN,NQ,CONDK,IFIXT,SDT
        1,ICAL,IPSC,IPLT,XS,AO2PY,AKOX,DEFF
         NAMELIST/TBAS/TBD
         NAMELIST/TPORT1/TP1
         NAMELIST/TPORT3/TP3
         NAMELIST/COXYT/COT
         DATA VISC,GRAV,OXC,RLCL/1.9E-4,980.,3.0E-4,1./
         DATA SPMO,DENG,BETA/2.6784E6,1.2E-3,2.83E-2/
         DATA DENCL,FECON/1.8,1.E-3/
         WV(X)=953.*EXP(-5220.9/(273+X))
         ENTH(X,Y)=.24*X+514620.*(Y+1.E-8)*EXP(-5220.9/(X+273.))/DENG
         CG(X)=.24+2.0828E12*EXP(-5220.9/(X+273.))/(X+273.)**2
         ALPHA(X)=3.66E-3*(X-20.)+4.7093E5*EXP(-5220.9/(X+273.))
         CALL CC
         IIN=22
         ITTY=8
         READ(5,PAR)
         READ(5,OPER)
         READ(5,ANSF)
         RCD1=0.
         IOTC=0
1000     CONTINUE
```

```
41.              IHGTX=0
42.              RCD1=RCD1+1.
43.      C       IF(IOUT.EQ.7)WRITE(ITTY,900)
44.              READ(ITTY,PAR)
45.              IF(N.EQ.0)CALL EXIT
46.              READ(ITTY,OPER)
47.              READ(ITTY,ANSF)
48.              IF(NCUT.NE.NDELT)WRITE(IOUT,PAR)
49.              IF(NCUT.NE.NDELT)WRITE(IOUT,OPER)
50.              IF(NCUT.NE.NDELT)WRITE(IOUT,ANSF)
51.              IF(IOUT.GE.20)IOTC=IOTC+1
52.              IHTFL=0
53.              IF(NHGT.NE.0.AND.N.EQ.NQ)IHTFL=1
54.              O2KG=0.
55.              AKAVE=1.0E8*RACL**2*PHI**3/150.*(1.-PHI)**2
56.             EXC=(EXD+EXK)*.5
57.             OXPY=.13333*(1+6*XS)
58.             AFES2=OXPY*AO2PY
59.             IF(TAUC.GT..0001)GO TO 15
60.             DEL=(DEFF/(AKOX*ASULFR))**.5
61.             AKSTOI=6.875*OXPY*GPY*DENCL

62.             TAUC=AKSTOI*RACL/(AKOX*ASULFR*DEL*FECON*SPMO)
63.             TAUD=(RACL**2)*AKSTOI/(6.*FECON*DEFF*SPMO)
64.      15     CONTINUE
65.      1001    CONTINUE
66.              KCX=1
67.      C.......MULTIPLE HEIGHT CALCULATION CONTROL
68.              IF(IHTFL.EQ.1)N=NQ
69.              IF(NHGT.NE.0)IHGTX=IHGTX+1
70.              IF(IHGTX.GT.NHGT.AND.NHGT.NE.0)GO TO 1002
71.              IF(IHGTX.NE.0)HGT=HGTL(IHGTX)
72.              IF(HGT.EQ.0.)HGT=333.
73.      C.......AUTOMATIC VARIABLE POINT SPACING IF N=NQ..............
74.      C       (FOR COLLUMNS HGT<75 FT OR ROCK PAD IS ASSUMED)
75.              IF(N.NE.NQ)GO TO 528
76.              IFLNB=0
77.              IF(HGT/FLOAT(NQ).LE..5)GO TO 521
78.              DX(1)=.5
79.              DX(2)=.5
80.              DX(NQ)=.5
```

```
      DX(NQ-1)=.5
      XLEX=(HGT-2.)/FLOAT(N-4)
      XLED=AMIN1(XLEX,1.)
      DO 531 I=1,9
      DX(NQ-1-I)=XLED
531   CONTINUE
      SUM=1.
      SUM2=1.+9.*XLED
      IPLFG=0
      II=2
      JJ=11
      DO 518 I=1,32
      IF(IPLFG.EQ.0)II=II+1
      JJ=JJ+1
      DX(II)=DX(II-1)*DXPL
      DX(NQ-JJ+1)=DX(NQ-JJ+2)*DXMN
      IF(IPLFG.EQ.0)SUM=SUM+DX(II)
      SUM2=SUM2+DX(NQ-JJ+1)
      DXT1=DX(II)*DXPL
      DXT2=DX(NQ-JJ+1)*DXMN
      DXR=(HGT-SUM-SUM2)/FLOAT(NQ-II-JJ)
      IF(DXT1.GE.DXR)IPLFG=1
      IF(SUM.GE.20..AND.IFLNB.EQ.0)NB=II
      IF(SUM.GE.20..AND.IFLNB.EQ.0)IFLNB=1
      IF(DXT2.GE.DXR)GO TO 519
518   CONTINUE
      WRITE(IOUT,969)
      CALL EXIT
969   FORMAT(' AUT VAR SPG COULD NOT SPAN DUMP HEIGHT')
519   IF(IFLNB.EQ.0)NB=II+1+IFIX((20.-SUM)/DXR)
      IK=IT+1
      MK=NQ-JJ
      DO 520 IX=IK,MK
      DX(IX)=DXR
520   CONTINUE
      DO 529 IQ=1,N
      DX(IQ)=DX(IQ)/DXR
529   CONTINUE
      BASE=SUM+FLOAT(NB-(II))*DXR
      GO TO 523
```

```
      521     CONTINUE
              N=IFIX(2.*HGT)


              DXR=HGT/FLOAT(N)
              IF(NB.NE.0)NB=MIN0(IFIX(FLOAT(N)*20./HGT),249-N)
              IF(NB.NE.0)BASE=FLOAT(NB)*DXR
              DO 522 I=1,N
              DX(I)=1.
      522     CONTINUE
      523     CONTINUE
      968     FORMAT(/' N,N1,N2=',3I5,' NB=',I5,' BASE=',F7.2,' FEET  ICMT=',
           1F7.2,' FEET',/)
              WRITE(IOUT,910)
              WRITE(IOUT,968)N,II,JJ,NB,BASE,DXR
      C.......END AUTOMATIC VARIABLE POINT SPACING.................
      528     CONTINUE
      910     FORMAT(///)
      C     1,NREST2',///)
      C     1///)
      C  INITIALIZATION.....................
              DEN=DENCL*(1.-PHI)
              N2=N/2
              SUM=0.
              DO 6 I=1,N
      6       SUM=SUM+DX(I)
              DELX=1./SUM
              DELX2=2.*DELX
              DELXSQ=DELX*DELX
              GRAMI=DEN
              HT=HGT*30.48
              VW=VWAT*1.13E-3
              IF(VAIR.NE.0)VA=VAIR
              NREST=NRES
              ONE=1.
              TMXXX=0.
              NSX=1
              IPLX=1
              TAVES=TSTR
              TSCL=20.
              IF(IPSC.GE.3)TSCL=10.
              DO 1 I=1,N
```

```
161.              VC(I)=0.5
162.              VT(I)=TSTR
163.              VX(I)=XSTRT
164.              XNS(I)=XCOL0
165.      1       CONTINUE
166.              IF(NB.NE.0)G0=TCAVA
167.              IF(NB.EQ.0)GO TO 314
168.              DO 313 I=1,NB
169.              TB(I)=TCAVA
170.      313     CONTINUE
171.      314     CONTINUE
172.      C.......CONVERT AVE IRRIGATION RATE TO APPLICATION RATE IF NECESS.
173.              IF(NREST.NE.0.)VW=VW*FLOAT(NTOT)/FLOAT(NTOT-NREST)
174.      C..EXECUTION LOOP.....................................
175.              WRITE(IOUT,9111)TAUC,TAUD
176.              WRITE(IOUT,9111)RACL,XCOL0,COALS
177.             WRITE(IOUT,912)VA,VW,AKAVE
178.      912     FORMAT(' VAIR CM/SEC =',E10.3,' VWAR CM/SEC =',E10.3
179.           1 ,' PERM CM**2 =',E10.3)
180.             WRITE(IOUT,913)AKOX,DEFF
181.      913     FORMAT(' AKOX=',E10.3,' DEFF=',E10.3)
182.      C9111    FORMAT(' TCNS=',E10.3,'  MO,  TDNS=',E10.3,'  MO',/)
183.              WRITE(IOUT,972)


184.      9111    FORMAT(' RAD COAL=',F6.2,'CM  INIT FX OXID=',E10.3,
185.           1'  OXID RATE CONST=',E10.3)
186.      972     FORMAT(/,'  KC',1X,' TIME',5X,'RTMX',5X,' RCMX',5X,'  VA',2X,
187.           1'TMAX',2X,'FXPYL',3X,' FXCLOX',2X,'PPMFEEFF',2X,'COUT',2X,'RTAVE')
188.      971     FORMAT(I4,F6.2,3E9.2,F6.1,5E9.2)
189.      C.......EVOLUTION LOOP.....................................
190.              DO 5000 KC=1,NDELT
191.              TIME=FLOAT(KC)*DELT
192.              ALBD=DELT*SPMO*(AKT/(HT**2*RTCT))/DELXSQ
193.              TIMEH=TIME-DELT/2.
194.              TAMBS=TCAV-SDT*COS((TIMEH+AMOSTR-.5)*3.14159/6.)
195.               TAMB=TCAVA-SDTA*COS((TIMEH+AMOSTR-.5)*3.14159/6.)
196.               IF(AMOSTR.NE.0..AND.AN.EQ.1)GN=TAMBS
197.               IF(AMOSTR.NE.0.)G1N=TAMB
198.                IF(AMOSTR.EQ.0.)G1N=TCAVA
199.      C.....,..OXYGEN CONCENTRATION LOOP.................
200.              ITT=0
```

```
      VST=1.
C.....ITTERATION LOOP.....
      IF(NSW.EQ.0)GO TO 201
      IF(MOD(KC,NSW).EQ.1)VA=VA1R2(NSX)/FXL
      VW=0.
      KCM=KC-1
      IDAY=MOD(KCM,NSW)+1
      IF(IDAY.GT.NREST2(NSX))VW=VWAT2(NSX)*1.13E-3/FXL
      IF(IDAY.EQ.7)NSX=NSX+1
201   CONTINUE
200   CONTINUE
      IF(VAIR.NE.0.)GO TO 100
C.....CALCULATE PRESSURE DROP ACROSS DUMP.....
      SUM=0.
      DO 10 I=1,N
      SUM=SUM+(ALPHA(VT(I))-ALPHA(G1N)+BETA*(1.-VC(I)))*DX(I)
10    CONTINUE
      P=SUM*DENG*GRAV*HT*DELX
      VA=AKAVE*1.0E-8*P/(VISC*HT)
100   CONTINUE
C     CALCULATE OXYGEN CONCENTRATION.....
      DO 109 I=1,N
      X13=VX(I)**.3333333333
      X23=VX(I)**.6666666666
      VTSK=VT(I)
      IF(TSIK.GT.0..AND.VT(I).GT.TSIK)VTSK=TSIK
      TNC=TAUC*SPMO/(EXP(.5*EXC*(VTSK-20.)/(293.*(273.+VTSK))))
      TND=TAUD*SPMO/(EXP(.5*EXD*(VTSK-20.)/(293.*(273.+VTSK))))
      RT(I)=3.*X23/(6.*TND*X13*(1.-X13)+TNC)
      IF(VT(I).GT.TSIK.AND.TSIK.GT.0)RT(I)=RT(I)*AMAX1((1-
     1(VT(I)-TSIK)/(TMXM-TSIK)),0.)
      IF(RORD.NE.0..AND.VC(I).GT.0.)RT(I)=RT(I)*VC(I)**RORD
      IF(I.LT.NMBSE)RT(I)=0.
      XNS13=XNS(I)**.333333333333
C  COAL LEACH RATE (EQUATION 4 NOTEBOOK)
      RBAR=EXP(EACTC*.5*((1./298.)-(1./(VT(I)+273.))))
      SBAR=(1.-EXP(-4.34*RACL))*1.09*.5/RACL
      RNS(I)=COALS*((RBAR*SBAR*VC(I))**1.25)/((XNS(I)**.25)*SPMO)
      IF(I.LT.NMBSE)RNS(I)=0.
109   CONTINUE
```

```
241.              AMUL=GRPH1*GPY*OXPY*HT*DELX/((ABS(VA)+1.0E-10)*OXC)
242.             AMULC=GRPHI*OXCL*HT*DELX/((ABS(VA)+1.0E-10)*OXC)
243.              IF(VA)121,122,123
244.      123     CONTINUE


245.              VC(1)=1.-RT(1)*AMUL*DX(1)/2.
246.              VC(1)=VC(1)-AMULC*RNS(1)*DX(1)/2.
247.              IF(VC(1).LE.0.)VC(1)=0.
248.      C        WRITE(6,11)
249.      C  11    FORMAT(/'  DELX',2X,' AMUL',2X,'AMULC')
250.      C        WRITE(6,12)DELX,AMUL,AMULC
251.      C        WRITE(6,14)GRPHI,GPY,OXPY,HT,VA,OXC
252.      C14      FORMAT(6E10.3)
253.      C        WRITE(6,13)
254.      C  13   FORMAT(/' VC(I)',2X,' RT(I)',2X,' RNS(I)',2X,' DX(I)')
255.              DO 111 I=2,N
256.              VC(I)=VC(I-1)-RT(I)*AMUL*(DX(I)+DX(I-1))/2.
257.              VC(I)=VC(I)-AMULC*RNS(I)*(DX(I)+DX(I-1))/2.
258.      C       WRITE(6,12)VC(I),RT(I),RNS(I),DX(I)
259.              IF(VC(I).LT.0.)VC(I)=0.
260.      111     CONTINUE
261.              COUT=VC(N)-RT(N)*AMUL*DX(N)/2.
262.              COUT=COUT-RNS(N)*AMULC*DX(N)/2.
263.      C        WRITE(6,12)COUT
264.      C  12    FORMAT(1X,7E10.3)
265.              IF(COUT.LT.0.)COUT=0.
266.              GO TO 124
267.      122     CONTINUE
268.              DO 131 I=1,N
269.              VC(I)=0.
270.      131     CONTINUE
271.              COUT=0.
272.              GO TO 124
273.      121     CONTINUE
274.              VC(N)=1.-RT(N)*AMUL*.5*DX(N)
275.             VC(N)=VC(N)-RNS(N)*AMULC*DX(N)*.5
276.              IF(VC(N).LE.0.)VC(N)=0.
277.              NM1=N-1
278.              DO 132 I=1,NM1
279.              VC(N-I)=VC(N-I+1)-AMUL*.5*(DX(N-I)+DX(N-I+1))*RT(N-I)
280.             VC(N-I)=VC(N-I)-RNS(N-I)*.5*AMULC*(DX(N-I)+DX(N-I+1))
```

```
281.                IF(VC(N-I).LT.0.)VC(N-I)=0.
282.      132       CONTINUE
283.                COUT=VC(1)
284.      124       TST=1.-ABS(VA/VST)
285.                VST=VA
286.                IF(TST.LE.PCTAC)GO TO 300
287.                ITT=ITT+1
288.                IF(ITT.GT.10)WRITE(IOUT,903)VA,TST
289.      903       FORMAT(' SS VA NOT REACHED IN TEN ITT..VA,TST=',2E10.3,/)
290.                IF(ITT.GT.10)GO TO 300
291.                IF(VAIR.EQ.0.)GO TO 200
292.      300       CONTINUE
293.      C.........END OF ITTERATION LOOP.................................
294.      C........CALCULATE TEMPERATURE
295.                SWA=1.
296.                KCC=KC-1
297.                IF(MOD(KCC,NTOT).LT.NREST)SWA=0.
298.                IF(IFIXT.EQ.1)GO TO 322
299.                NM1=N-1
300.                AMUL1=SWA*ALBD*DELX*HT*RLCL*VW/AKT
301.                AMUL2=ALBD*DELX*HT*DENG*ABS(VA)/AKT
302.                AMUL3=ALBD*DELXSQ*HT**2*GRPHI/AKT
303.                SUM=0.
304.                DO 309 I=1,N
305.                AKIL=1.

306.                IF(VC(I).LE.0.)AKIL=0.
307.                SUM=SUM+RT(I)*AKIL*DX(I)
308.                VTS(I)=VT(I)
309.      309       CONTINUE
310.                HGENC=DELX*SUM*HT*GRPHI*SPMO
311.      308       CONTINUE
312.                DO 310 I=1,N
313.                IF(I.NE.N)DXP=(DX(I+1)+DX(I))/2.
314.                IF(I.EQ.N)DXP=DX(I)
315.                IF(I.NE.1)DXM=(DX(I-1)+DX(I))/2.
316.                IF(I.EQ.1)DXM=DX(I)
317.                IF(I.NE.1.AND.I.NE.N)DXMP=(DX(I+1)+DX(I-1)+2.*DX(I))/4.
318.                IF(I.EQ.1.OR.I.EQ.N)DXMP=DX(I)
319.                IF(VA.GE.0..AND.I.NE.1)CSX=(CG(VT(I))+CG(VT(I-1)))/2.
320.                IF(VA.LT.0..AND.I.NE.N)CSX=(CG(VT(I))+CG(VT(I+1)))/2.
```

```
321.              IF(VA.LT.0..AND.I.EQ.N)CSX=CG(VT(N))
322.              IF(VA.GE.0.AND.I.EQ.1)CSX=0.
323.             CSW=1.
324.             IF(I.EQ.N)CSW=0.
325.              A(I)=-ALBD/(DXM*DXMP)
326.              IF(VA.GE.0.)A(I)=A(I)-AMUL2*CSX/DXM
327.             C(I)=-ALBD/(DXP*DXMP)-AMUL1*CSW/DXP
328.              IF(VA.LT.0.)C(I)=C(I)-AMUL2*CSX/DXP
329.              B(I)=1.+ALBD*(1./DXP+1./DXM)/DXMP
330.              B(I)=B(I)+AMUL1*CSW/DXP+AMUL2*CSX/DXM
331.              IF(VA.LT.0.)B(I)=B(I)-AMUL2*CSX*(1./DXM+1./DXP)
332.              AKIL=1.
333.              IF(VC(I).LE.0.)AKIL=0.
334.              D(I)=VT(I)+AMUL3*AKIL*(AFES2*GPY*RT(I)+ACOAL*RNS(I))
335.              D(I)=D(I)-CONDK*(VT(I)-G1N)*(HT**2)*DELXSQ*ALBD/AKT
336.     310      CONTINUE
337.     C.......EDGE FIXES
338.              DG0=G0/(A0+B0/(DELX2*DX(1)))
339.              DGN=GN/(AN+BN/(DELX2*DX(N)))
340.              CB0=B0/(DELX2*DX(1))/(A0+B0/(DELX2*DX(1)))
341.              ABN=BN/(DELX2*DX(N))/(AN+BN/(DELX2*DX(N)))
342.              IF(NB.NE.0)GO TO 315
343.              C(1)=C(1)+A(1)*CB0
344.              D(1)=D(1)-A(1)*DG0
345.             A(1)=0.
346.     315      CONTINUE
347.               CG1=ENTH(VT(1),1.)/VT(1)
348.             T1S=VT(1)
349.               IF(VA.GE.0.)D(1)=D(1)+AMUL2*ENTH(TAMB,FRACT)/DX(1)
350.              CG1=ENTH(VT(1),ONE)/VT(1)
351.              B(1)=B(1)+AMUL2*CG1/DX(1)
352.             KTST=N/2
353.             TS2=VT(KTST)
354.              IF(ITPL.EQ.1.AND.VA.GE.0.)A(N)=A(N)+AMUL2*CG(VT(N))/DX(N)
355.              IF(ITPL.EQ.1.AND.VA.GE.0.)B(N)=B(N)-AMUL2*CG(VT(N))/DX(N)
356.              A(N)=A(N)-C(N)*ABN
357.              D(N)=D(N)-C(N)*DGN+AMUL1*TAMBS/DX(N)
358.             B(N)=B(N)+AMUL1/DX(N)
359.              C(N)=0.
360.              IF(NB.EQ.0)GO TO 316
```

```
C.......CONDUCTIVE BASE
      DO 311 NJ=1,N
      I=N-NJ+1
      A(NB+I)=A(I)
      B(NB+I)=B(I)
      C(NB+I)=C(I)


      D(NB+I)=D(I)
311   CONTINUE
      DO 312 I=1,NB
      K=NB-I+1
      DXM=(DX(K+1)+DX(K))/2.
      IF(K.NE.1)DXP=(DX(K-1)+DX(K))/2.
      IF(K.EQ.1)DXP=DX(1)
      IF(K.NE.1)DXMP=(DX(K-1)+DX(K+1)+DX(K)*2.)/4.
      IF(K.EQ.1)DXMP=DX(K)
      A(I)=-ALBD/(DXM*DXMP)
      C(I)=-ALBD/(DXP*DXMP)
      B(I)=1.+ALBD*(1./DXM+1./DXP)/DXMP
      D(I)=TB(I)
312   CONTINUE
      C(1)=C(1)+A(1)*(B0/(DELX2*DX(NB)))/(A0+B0/(DELX2*DX(NB)))
      D(1)=D(1)-A(1)*G0/(A0+B0/(DELX2*DX(NB)))
316   CONTINUE
      NIV=N+NB
C
      CALL TRIDAG(1,NIV,A,B,C,D,VT)
C
C.......RESTACK
      IF(NB.EQ.0)GO TO 319
      DO 317 I=1,NB
      IF(VT(I).GT.TMXM.AND.TSIK.EQ.0.)VT(I)=TMXM
      TB(I)=VT(I)
317   CONTINUE
      JM=NB+1
      DO 318 I=JM,NIV
      IF(VT(I).GT.90.0)VT(I)=90.0
      VT(I-NB)=VT(I)
318   CONTINUE
      GO TO 320
319   CONTINUE
```

```
401.              DO 321 I=1,N
402.              IF(VT(I).GT.90.0)VT(I)=90.0
403.      321     CONTINUE
404.      320     CONTINUE
405.      322     CONTINUE
406.      C  322 AVOIDS TEMPERATURE CALCULATION FOR LAB SITUATIONS WHERE
407.      C  COLUMNS ARE HELD AT CONSTANT TEMPERATURE.
408.      C..OUTPUT.....................................
409.              RTSUM=0.
410.             RTMX=0.
411.             RCMX=0.
412.              TMX=0.
413.              XSUM=0.
414.             XSUMC=0.
415.              TAVE=0.
416.      911     FORMAT(' TAUC=',E10.3,'  MO,  TAUD=',E10.3,'  MO')
417.              DO 410 I=1,N
418.              TMX=AMAX1(TMX,VT(I))
419.              TAVE=TAVE+VT(I)*DX(I)
420.              AKIL=1.
421.              IF(VC(I).LE.0.)AKIL=0.
422.              RTMX=AMAX1(RTMX,RT(I)*AKIL)
423.              RCMX=AMAX1(RCMX,RNS(I)*AKIL)
424.             XSUM=XSUM+VX(I)*DX(I)
425.             XSUMC=XSUMC+(XNS(I)-XCOL0)*DX(I)
426.              RTSUM=RTSUM+RT(I)*DX(I)*AKIL
427.              VX(I)=VX(I)-RT(I)*AKIL*SPMO*DELT

428.              IF(VX(I).LT.0.)VX(I)=0.
429.              XNS(I)=XNS(I)+RNS(I)*SPMO*DELT*AKIL
430.      410     CONTINUE
431.             XCAVE=XSUMC*DELX
432.             RTAVE=RTSUM*DELX
433.              IF(TMX.GT.TMXXX)TMXXX=TMX
434.              XAVE=1.-XSUM*DELX
435.              TAVE=DELX*TAVE
436.             PPMFE=RTAVE*GPY*GRPHI*HT*(55.8/120.)*1.E6/VW
437.             TIMDAY=TIME*31.
438.             PCTO2=1.-COUT
439.              IF(MOD(KC,NTOUT).EQ.0)WRITE(14,992)TIMDAY,PPMFE,PCTO2,XAVE,XCAVE
440.      992     FORMAT(5E10.3)
```

```
      250      CONTINUE
      991      FORMAT(8E10.3)
               IF(MOD(KC,NTOUT).NE.0)GO TO 411
               IF(IPLT.EQ.1)H(KCX)=TIME
               IF(IPLT.EQ.1)V1(KCX)=TMX+10.
               IF(IPLT.EQ.1)V2(KCX)=COUT
               IF(IPLT.EQ.1)V3(KCX)=XAVE
               IF(IPLT.EQ.1)V(KCX)=TAMB+10.
               KCX=KCX+1
      411      CONTINUE
               VOLORE=70.1E3
               DENORE=DEN
      C971       FORMAT(I4,F6.2,2F8.4,F6.1,3F8.2,F8.4,F8.1)
                    VWWX=(VW/1.13E-3)*SWA
               IF(MOD(KC,NCUT).EQ.0)WRITE(IOUT,971)KC,
             1TIME,RTMX,RCMX,VA,TMX,XAVE,XCAVE,PPMFE,COUT,RTAVE
               IF(MOD(KC,NKOL).NE.0)GO TO 4999
      C.......PROFILING OF DEPTH DEPENDENT VARIABLES
               WRITE(IOUT,910)
      930      FORMAT(6X,' DEPTH',5X,'O2 CONC',8X,'TEMP',2X,'FRACT LEFT',
             14X,' SL RATE',/)
      931      FORMAT(5E12.3)
               JDX=0
               HPX=HGT*DX(1)*DELX/2.
               NM1=N-1
               DO 420 I=2,N
               HPX=HPX+(DX(I)+DX(I-1))*DELX*.5*HGT
               XOUT=HGT-HPX
               IF(IPLT.NE.1.OR.MOD(I,NXOUT).NE.0)GO TO 419
               JDX=JDX+1
               HP(JDX)=HPX
               VP(JDX)=1.-VX(I)
               VP1(JDX)=VT(I)
               VP2(JDX)=VC(I)
               VP3(JDX)=XNS(I)-XCOL0
      419      CONTINUE
      420      CONTINUE
      C.......PLOT PROFILES THROUGH DUMP AT EACH TIMESTEP
               SCALE(1)=HGT/4.
               SCALE(2)=.1
```

```
481.              SCALE(3)=10.
482.              SCALE(4)=.1
483.              SCALE(5)=.1
484.              IF(IPLT.EQ.1)CALL PLOTC(JDX,4,HP,VP,VP1,VP2,VP3,SCALE,100,IOUT,
485.             1IPLX)
486.              IPLX=IPLX+1
487.              WRITE(IOUT,980)VT(1),GIN,COUT,PPMFE
488.       980   FORMAT(' TBS=',F6.1,' TAMB=',F6.1,' O2EFF=',F5.2,' PPMFEEF=',F9.1)


489.              TMOCC=FLOAT(KC)*DELT
490.              AMONTH=AMOD(AMOSTR+TIME-1.,12.)+1.
491.              IF(IPLT.EQ.1)WRITE(IOUT,963)HGT,XAVE,TMX,AMONTH,TIME
492.       963    FORMAT(' HGT=',F10.1,' XAVE=',E10.3,' TMX=',F6.1,
493.             1'  MONTH=',F6.3,' LCHD=',F6.3)
494.              IF((IPLX+1)*NKOL.GE.NCUT.OR.NCUT.EQ.1)WRITE(IOUT,
495.             1910)
496.              IF((IPLX+1)*NKOL.GE.NCUT.OR.NCUT.EQ.1)WRITE(IOUT,
497.             1972)
498.       4999   CONTINUE
499.       5000   CONTINUE
500.       C.......END EVOLUTION LOOP.....................................
501.       C.......HEIGHT DEPENDANCE STORAGE
502.       C.......DUMP EVOLUTION PLOT
503.              IF(IHGTX.EQ.0.OR.NHGT.EQ.0.OR.IPLT.NE.1)GO TO 858
504.              HPCT(IHGTX)=HGT
505.              VPCT(IHGTX)=XAVE
506.              VPCT1(IHGTX)=TMXXX+10.
507.       858    CONTINUE
508.       957    FORMAT('  HGT,XAVE,TMXXX=',3F10.3)
509.              IF(IPLT.EQ.1)WRITE(IOUT,958)
510.              SCALE(1)=TMSCL
511.              SCALE(2)=10.
512.              SCALE(3)=10.
513.              SCALE(4)=.1
514.              SCALE(5)=.1
515.       156     CONTINUE
516.              KCXM=KCX-1
517.              IF(IPLT.EQ.1)CALL PLOTC(KCXM,4,H,V,V1,V2,V3,SCALE,100,IOUT,1)
518.              IF(IPLT.EQ.1)WRITE(IOUT,966)HGT,XAVE,TMXXX,AMOSTR
519.              IF(IPLT.EQ.1)WRITE(IOUT,958)
520.       966    FORMAT(' HGT=',F8.1,' XAVE=',F10.3,' TMAX=',F6.1,' VERT AXIS AT'
```

```
     1,F7.4,' TH MONTH')
        IF(NHGT.NE.0)GO TO 1001
958     FORMAT(1H1)
1002    CONTINUE
        IF(NHGT.EQ.0.OR.IPLT.NE.1)GO TO 1003
C.......DUMP HEIGHT PLOT
        WRITE(IOUT,958)
        SCALE(1)=20.
        SCALE(2)=.1
        SCALE(3)=10.
        CALL PLOTC(NHGT,2,HPCT,VPCT,VPCT1
     1,VPCT1,VPCT1,SCALE,100,IOUT,1)
        WRITE(IOUT,951)
        DO 953 IOX=1,NHGT
        VPCTX=VPCT1(IOX)-10.
        WRITE(IOUT,952)HPCT(IOX),VPCTX,VPCT(IOX)
953     CONTINUE
951     FORMAT(///,' DMP HGT     TEMP   FXLCHD')
952     FORMAT(2F8.1,F8.3)
        WRITE(IOUT,958)
1003    CONTINUE
        GO TO 1000
3000    CONTINUE
        STOP
        END
        SUBROUTINE PLOTC(NP,NG,H,V,V1,V2,V3,SCALE,IWTH,IOUT,IDX)
        DIMENSION SCALE(5),B(120),C(120),H(1),V(1),V1(1),V2(1),V3(1)
911     FORMAT(1H+,/)
912     FORMAT(1H+)


903     FORMAT(1H ,A3,3X,F5.2,'  UNITS PER INCH')
904     FORMAT(1H ' HR/',F7.2,'  UNITS PER INCH')
905     FORMAT(1H-)
900     FORMAT(1H+,120A1)
991     FORMAT(1H1)
        DATA AM/1H-/,XL/1HI/,HO/1HO/,TM/1HT/,BL/1H /,PL/1H+/,ST/1H*/
        DATA AX/1HX/
C       IWTH            WITH OF PLOT
C       NP              NUMBER OF POINTS
C       NG              NUMBER OF GRAPHS
C       SCALE(5)        HORIZONTAL AND VERITCAL SCALES :UNITS PER INCH
```

```
      IF(IDX.EQ.1)WRITE(IOUT,904)SCALE(1)
      IF(IDX.EQ.1)WRITE(IOUT,903)ST,SCALE(2)
      IF(IDX.EQ.1.AND.NG.GE.2)WRITE(IOUT,903)TM,SCALE(3)
      IF(IDX.EQ.1.AND.NG.GE.3)WRITE(IOUT,903)HO,SCALE(4)
      IF(IDX.EQ.1.AND.NG.GE.4)WRITE(IOUT,903)AX,SCALE(5)
      IF(IDX.EQ.1)WRITE(IOUT,905)
      IWTHP=IWTH+1
      DO 4 I=1,120
      IF(I.LE.IWTHP)B(I)=AM
      IF(I.GT.IWTHP)B(I)=BL
      IF(MOD(I-1,10).EQ.0.AND.I.LE.IWTHP)B(I)=PL
4     CONTINUE
      WRITE(IOUT,900)B
      ALINE=0.
      DO 1 I=1,NP
      DO 2 J=1,120
2     C(J)=BL
      GO TO (111,112,113,114),NG
114   IPL3=INT(V3(I)*10./SCALE(5)+1.5)
      IF(IPL3.GT.IWTHP)IPL3=IWTHP
      C(IPL3)=AX
113   IPL2=INT(V2(I)*10./SCALE(4)+1.5)
      IF(IPL2.GT.IWTHP)IPL2=IWTHP
      C(IPL2)=HO
112   IPL1=INT(V1(I)*10./SCALE(3)+1.5)
      IF(IPL1.GT.IWTHP)IPL1=IWTHP
      C(IPL1)=TM
111   IPL=INT(V(I)*10./SCALE(2)+1.5)
      IF(IPL.GT.IWTHP)IPL=IWTHP
      C(IPL)=ST
      C(1)=XL
      C(IWTH+1)=XL
103   IF((H(I)*6./SCALE(1))-ALINE)101,102,102
102   ALINE=ALINE+1.
      WRITE(IOUT,911)
      GO TO 103
101   IF(AMOD(ALINE,6.).EQ.0.)C(IWTH+1)=PL
      IF(AMOD(ALINE,6.).EQ.0.)C(1)=PL
      WRITE(IOUT,900)C
1     CONTINUE
```

```
601.              WRITE(IOUT,900)B
602.              RETURN
603.              END
604.              SUBROUTINE TRIDAG(IF,L,A,B,C,D,V)
605.              DIMENSION A(1),B(1),C(1),D(1),V(1),BETA(251),GAMMA(251)
606.              BETA(IF)=B(IF)
607.              GAMMA(IF)=D(IF)/BETA(IF)
608.              IFP1=IF+1
609.              DO 1 I=IFP1,L
610.              BETA(I)=B(I)-A(I)*C(I-1)/BETA(I-1)

611.      1       GAMMA(I)=(D(I)-A(I)*GAMMA(I-1))/BETA(I)
612.              V(L)=GAMMA(L)
613.              LAST=L-IF
614.              DO 2 K=1,LAST
615.              I=L-K
616.      2       V(I)=GAMMA(I)-C(I)*V(I+1)/BETA(I)
617.              RETURN
618.              END
619.      //DATA.FT05F001 DD DSN=MEN.U05964.LEE.MOD.NMEXDAD,DISP=(OLD,KEEP),
620.      // DCB=(RECFM=FB,LRECL=80,BLKSIZE=2960),VOL=REF=MEN.U05964.LEE.LIB
621.      //DATA.FT08F001 DD DSN=MEN.U05964.LEE.MOD.BLNKDAD,DISP=(OLD,KEEP),
622.      // DCB=(RECFM=FB,LRECL=80,BLKSIZE=2960),VOL=REF=MEN.U05964.LEE.LIB
623.      //DATA.FT14F001 DD DSN=MEN.U05964.LEE.MOD.NMPLT,DISP=(OLD,KEEP),
624.      // VOL=REF=MEN.U05964.LEE.LIB,SPACE=(TRK,(10,10),RLSE),
625.      // DCB=(RECFM=FB,LRECL=80,BLKSIZE=3120)
626.      // EXEC PGM=UMSG,PARM=(INTERACT,'TO LEE JOB READY'),COND=EVEN
627.      /*
```